Characterisation of human body and environmental effects on the performance of mobile terminal antennas

Ur Rehman, Masood

For additional information about this publication click this link.
https://qmro.qmul.ac.uk/jspui/handle/123456789/385

Characterisation of Human Body and Environmental Effects on the Performance of Mobile Terminal Antennas

Masood Ur Rehman

A thesis submitted to the University of London in partial fulfillment of the requirements for the degree of

Doctor of Philosophy

School of Electronic Engineering and Computer Science
Queen Mary, University of London
London E1 4NS, United Kingdom

November 2010

To My Parents and My Family

Abstract

Provision of efficient services to the user anywhere at anytime is being a centre of research and development in Wireless Personal Area Networks (WPAN) and Wireless Body Area Networks (WBAN). Antenna is the essential part of WPAN/WBAN applications that got affected by two major factors: human body presence and nature of the surrounding environment. The presence of the human body in the proximity of the antenna causes electromagnetic (EM) reflections from the body surface and absorptions in the lossy body tissues resulting in antenna detuning, radiation pattern degradations and impedance mismatch. On the other hand, incident radio waves undergo reflections, diffractions and scattering from the surrounding environment objects including buildings, trees, vehicles and ground, causing multipath fading.

The thesis gives an overview of the main investigations, results and analyses accomplished in a study concerning the commercially available Bluetooth and GPS antennas working in the vicinity of the human body. Detailed numerical modelling process is adopted followed by measurements for validation. The thesis highlights the role of surface waves as a potential transmission medium in an on-body Bluetooth wireless communication link taking into account the effects of antenna-body separations and presence of the surrounding objects blocking the direct communication path. The thesis also presents a novel statistical model to evaluate the performance of GPS mobile terminal antennas in the multipath environment. This model characterises the antenna performance and identifies the key factors that can be used to enhance it, in a real working environment outside an anechoic chamber. The study also deals with presence of the human body in the multipath environment and its effects on the operation of the GPS antennas.

Acknowledgments

It is my greatest pleasure to express sincere appreciation and gratitude to my supervisor Prof. Xiaodong Chen for his beneficial discussions, encouragement, valuable advice and guidance through out the course of this work. I would also like to thank Dr. Zhinong Ying and Dr. Robert Donnan for their positive and constructive comments during my research.

I am also greatly indebted to Dr. Yue Gao, Dr. Yasir Alfadhl and Dr. Zhao Wang for their formative discussions and invaluable advice regarding this work. Special thanks to Mr. John Dupuy for his help in antenna fabrications and measurements. Also, thanks to Prof. Brian Collins and Mr. Shihua Wang for assisting me during the measurements and data processing.

I would also take this opportunity to thank all my friends who encouraged me at each and every step throughout the time. I am grateful to my brothers (Habib Ur Rehman and Waheed Ur Rehman) and sister (Tahera Kalsoom) for their continuous support and encouragement. Above all, I am deeply obliged to my parents (Khalil Ur Rehman and Ilfaz Begum), whose love and upbringing have been instrumental behind every success I achieved in my life.

Last but not the least; all the praises to the God Almighty who bestowed me with His unending blessings and made me reach to this point.

Masood Ur Rehman
London, November 01, 2010

Preface

Most of the research work presented in this thesis has been carried out in the School of Electronic Engineering and Computer Science, Queen Mary, University of London. Some parts, specifically 3-D antenna radiation pattern measurements and data processing, have been done in cooperation of Sony Ericsson Mobile Communications AB, Sweden and Antenova Ltd., Cambridge, UK.

The author's main contributions include the investigation and analysis of on-body transmission mechanism between two body worn antennas in Bluetooth band with an in-sight of radio wave propagation behaviour, statistical modelling of multipath environment for GPS operation, study of mobile terminal GPS antenna performance in the multipath environment using the proposed model and actual measurements and evaluation of working of the GPS antennas in the multipath environment for different body-worn scenarios. These results asses the complexity of portable antenna performance in real working scenarios giving essential information to ensure efficient and reliable radio systems.

Journal and conference papers published by the author include:

Journal Papers

1. **M. Ur Rehman**; Y. Gao; Z. Wang; J. Zhang; Y. Alfadhl; X. Chen; C.G. Parini; Z. Ying; T. Bolin and J.W. Zweers, "Investigation of on-body bluetooth transmis-

sion," *IET Microwaves, Antennas and Propagation*, vol. 4, no. 7, July 2010.

2. **M. Ur Rehman**; Y. Gao; X. Chen; C.G. Parini and Z. Ying, "Environmental effects and system performance characterisation of GPS antennas for mobile terminals," *IET Electronics Letters*, vol. 45, no. 5, February 2009.

Conference Papers

1. **M. Ur Rehman**; Y. Gao; X. Chen; C.G. Parini and Z. Ying, "Impacts of human body on built-in GPS antennas for mobile terminal in multipath environment," *European Conference on Antennas and Propagation (EuCap)*, April 2010, Barcelona, Spain.

2. Y. Gao; O.P. Falada; **M. Ur Rehman**; S. Wang; X. Chen and C.G. Parini, "Study of a miniaturized circular patch diversity antenna for mobile terminals," *European Conference on Antennas and Propagation (EuCap)*, April 2010, Barcelona, Spain.

3. **M. Ur Rehman**; Y. Gao; X. Chen; C.G. Parini and Z. Ying, "Mobile terminal GPS antennas in multipath environment and effects of human body presence," *Loughborough Antennas and Propagation Conference (LAPC)*, November 2009, Loughborough, UK.

4. **Masood Ur Rehman**; Yue Gao; Xiaodong Chen and Clive Parini, "Dual-element diversity antenna for Galileo/GPS receivers," *13th World Congress of International Association of Institutes of Navigation (IAIN)*, October 2009, Stockholm, Sweden.

5. **M. Ur Rehman**; Y. Alfadhl; Z. Wang; X. Chen; J. Tattersall and R.H. Inns, "Study of human body exposure to RF signal at UHF frequencies," *Joint Meeting of Bioelectromagnetics Society and the European Bioelectromagnetics Association (BioEM)*, June 2009, Davos, Switzerland.

6. **M. Ur Rehman**; Y. Gao; X. Chen; C.G. Parini and Z. Ying, "Characterisation of

system performance of GPS antennas in mobile terminals including environmental effects," *European Conference on Antennas and Propagation (EuCap)*, March 2009, Berlin, Germany - (Convened).

7. **M. Ur Rehman**; Y. Gao; X. Chen; C.G. Parini and Z. Ying, "Analysis of GPS antenna performance in a multipath environment," *IEEE Antennas and Propagation Society International Symposium (AP-S)*, July 2008, San Diego, California, USA.

8. **M. Ur Rehman**; Y. Gao; X. Chen; C.G. Parini; Z. Ying; T. Bolin and J.W. Zweers, "On-body bluetooth link budget: Effects of surrounding objects and role of surface waves," *Loughborough Antennas and Propagation Conference (LAPC)*, March 2008, Loughborough, UK.

9. **M. Ur Rehman**; Y. Gao; X. Chen and C.G. Parini, "Effects of human body interference on the performance of a GPS antenna," *European Conference on Antennas and Propagation (EuCap)*, November 2007, Edinborough, UK.

10. L. Guo; **M. Ur Rehman**; J. Liang; X. Chen and C. Parini, "A study of cross ring antenna for UWB applications," *IEEE International Workshop on Antenna Technology (iWAT)*, March 2007, Cambridge, UK.

Project Reports

1. **M. Ur Rehman**; Y. Gao; Z. Wang; J. Zhang and X. Chen, "Bluetooth on-body propagation model," *Final Project Report, Submitted to Sony Ericsson Communications AB*, Sweden, July 2007.

2. **M. Ur Rehman**; Y. Gao and X. Chen, "GPS characterisation, environment and body effects," *Final Project Report, Submitted to Sony Ericsson Communications AB, Sweden*, November 2008.

3. **M. Ur Rehman**; Y. Gao and X. Chen "Enhanced GPS for indoor and urban environments," *ICUK Collaboration Development Fund*, March 2009.

4. Z. Wang; **M. Ur Rehman**; Y. Alfadhl and X. Chen, "Electromagnetic waves interaction with human body and biological tissues," *Final Project Report, Submitted to Dstl, UK*, August 2009.

Table of Contents

List of Figures

xiii

List of Tables

List of Abbreviations

η_c Coverage Efficiency

AoA   Angle of Arrival

AR   Axial Ratio

CE   Coverage Efficiency

CP   Circularly Polarised

DRA   Dielectric Resonant Antenna

dB   Decibel

dBm   Decibels relative to 1 mW

EIRP   Effective Isotropic Radiated Power

EM   Electromagnetic

FCC   Federal Communications Commission

FDTD   Finite Difference Time Domain

FIT   Finite Integral Technique

FR   Frequency Response

FR4   Flame Resistance 4

GHz   Giga Hertz

GNSS   Global Navigation Satellite Systems

GPS   Global Positioning System

ICNIRP   International Commission on Non-Iodising Radiation Protection

IEEE	Institute of Electrical and Electronics Engineers
IET	Institute of Engineering and Technology
IFA	Inverted F Antenna
ISM	Industrial, Scientific and Medical
ITU	International Telecommunication Union
LHCP	Left Hand Circularly Polarised
LOS	Line-of-Sight
MEG	Mean Effective Gain
MEG_{GPS}	GPS Mean Effective Gain
MEO	Middle Earth Orbit
MHz	Mega Hertz
NLOS	Non-Line-of-Sight
PBA	Perfect Boundary Approximation
PC	Personal Computer
PCB	Printed Circuit Board
PDA	Personal Digital Assistant
PIFA	Planar Inverted F Antenna
PND	Personal Navigation Device
RF	Radio Frequency
RHCP	Right Hand Circularly Polarised
SAR	Specific Absorption Rate
SNR	Signal-to-Noise Ratio
UWB	Ultra Wide-Band
VNA	Vector Network Analyser
WBAN	Wireless Body Area Network
WPAN	Wireless Personal Area Network
XPR	Cross Polarisation Ratio

Chapter 1

Introduction

Electronic devices are an essential part of today's life. Evolution of portable devices has brought a revolution in the field of wireless communications both in terms of research and development due to wider approach, mobility and ease of use. The trend of miniaturisation of such devices with ever-growing demand of ease of portability has resulted in the development of a vast variety of hand-held and body-worn applications [1, 2]. These devices provide services ranging from communication to navigation and entertainment to health care. Personal Digital Assistants (PDAs), laptops, Personal Navigation Devices (PNDs), pocket gaming consoles, body-worn health monitors, RFID tags, wireless USB dongles and mobile phones are a few examples [3]. These devices operate in the vicinity of human user forming a personal communication system termed as Wireless Personal Area Networks (WPAN) [4, 5]. Wireless Body Area Networks (WBAN) are a natural progression from the WPAN concept with the human body as the primary focus [6].

This chapter discusses the WPAN/WBAN with brief overview of standardisation issues discussing key features of the WPAN/WBAN applications. The challenges faced by the WPAN/WBAN systems are described highlighting areas with scope of research.

1.1 Wireless Personal Area Networks (WPAN)

Personal communication systems have seen a rapid growth and are now developed worldwide. A WPAN is defined as a network that interconnects devices around an individual person's work space communicating using wireless medium [7]. The WPANs are classified in three major categories based on the targeted application [8]:

- On-body communications

- Off-body communications

- In-body communications

The wireless link between wearable computing devices placed on the user's body is termed as on-body communications. A communication link between a mobile handset placed in the user's pocket and ear-worn Bluetooth headset is an example. Off-body communications describe a wireless link between body-worn devices and a base unit. In this case, most of the communication channel lies in the air, away from the body. Body-worn sensors sending information of a patient's blood pressure to the processing unit forms an off-body communication link. The in-body communications scenario occurs when the radio data transmission takes place between implanted devices and body-worn nodes.

1.1.1 Standardisation of Wireless PAN

From the modest beginnings of land-mobile communications a few decades ago, the WPAN is experiencing an explosive growth today. Increasing demand of the WPAN applications necessitates a standardisation procedure to integrate such applications into wireless wide-area infrastructure. IEEE 802.15 WPAN is an international standards group working on this task [9]. Since, the WPAN typically spans very short distances ranging at 10 m, a new standard based on the Bluetooth technology is proposed. IEEE
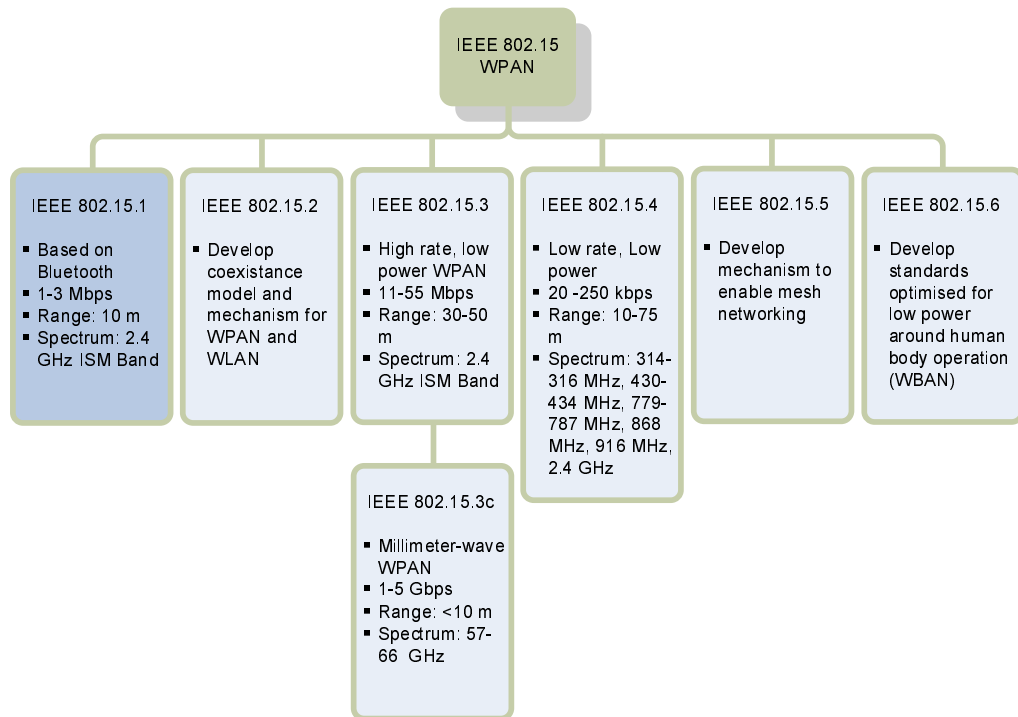
Figure 1.1: Organisational structure of IEEE 802.15 standards working group for WPAN (extracted from [9])

802.15 is divided into six task groups, presented in Figure 1.1, to address various standard issues for the WPAN. Other short-range technologies considered in the WPAN include Ultra-Wide Band (UWB) and Zigbee. Millimetre-wave communications have also got attention in the WPAN [9].

Currently, no specified standard is available that defines the operability of WBAN among other wireless networks. Although, a special task group, IEEE 802.15.6, is set-up to look after the issue but its main focus is on the WBAN for medical devices. The task group for the WBAN has initially concluded that the WBAN should operate in a range of 0.01-2 m near the human body with on, off or inside the body mode of communication. The devices should consume extremely low power (0.1-1 mW) and human body effects with absorptions and health hazards should be considered [10]. However, the WBAN is still in its initial stages and much work is needed to be done to achieve a comprehensive integration with existing and future wireless systems. This study is therefore, mainly

focussed on the Bluetooth technology for the WPAN/WBAN on-body link.

1.1.2 Bluetooth

Bluetooth is a short range wireless technology for data and voice exchange. It supports both point-to-point and point-to-multi-point communications. It is designed to be an inexpensive, low power and always-on radio networking system for all classes of portable devices.

Bluetooth implements a system architecture where units go into low-power modes when not active on the network. It operates on a globally unlicensed 2.4 GHz industrial, scientific and medical (ISM) frequency band. Bluetooth is an open specification for short-range wireless communications ensuring globally available wireless connectivity. Two Bluetooth devices located within a range of 10 m, can achieve a data rate of 1-3 Mbps, depending on the modulation technique used [11].

Bluetooth technology supports three application areas using short-range wireless connectivity [12]:

- **Data/Voice Access Points:** Bluetooth allows portable and stationary communication devices to transmit real-time voice and data by facilitating easy wireless connectivity.

- **Cable Replacement:** Bluetooth removes various types of cable attachments required for the connection of different communication devices. These usually proprietary cables need a fixed infrastructure limiting the flexibility and mobility of user.

- **Ad-hoc Networking:** Ad-hoc networking enables personal devices to automatically exchange information and synchronise with each other when located in close range to each other.
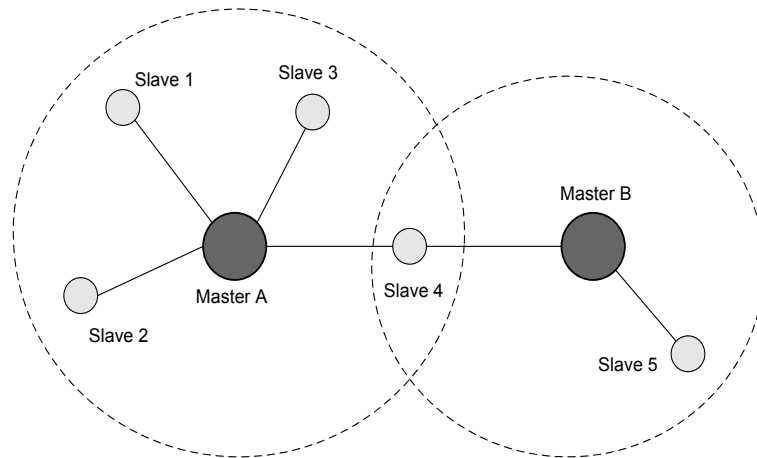
Figure 1.2: Structure of piconets and scatternets in the Bluetooth networking [12]

Bluetooth networks comprise of Piconets and Scatternets. Piconets are small groups of Bluetooth enabled units that communicate to each other. Piconets consist of a master unit and up to seven active slave units. The master starts transmission and the slaves respond to that. This type of Bluetooth network can have only one master unit. The overlapping of several piconets in a physical area causes communication between members of different piconets. It forms a larger network, termed as a scatternet. Any unit can communicate in more than one piconet, however, it can only serve as master for a single piconet at a time [13].

1.2   Features of Wireless PAN/BAN

The WPAN exhibits a number of advantages. Being a continuation of the WPAN, the WBAN inherits all the key features with added benefits. Major advantages include [14]:

- Exclusive frequency band with no requirement of licensing, especially for the medical applications.

- Long time of usage as ultra low power is a requirement. Due to this, increasing battery life is also getting attention in the WPAN/WBAN.

- Extreme miniaturisation leads to few external elements with greater sense of mobility and flexibility.

- Low complexity as most of the units are worn on the body.

- Simple usability in everyday practice.

- Low costs per unit.

These advantages have attracted greater research and development activities in the WPAN/WBAN in recent years. The future WPAN/WBAN systems are aiming to provide reliable data transmission, constant availability, re-configurability and discreteness to make maximum use of the above listed features.

1.2.1 Applications of Wireless PAN/BAN

The idea of WBANs originated from the desire to monitor health aspects of a patient in continuation. However, due to its greater advantages as a subsidiary of the WPAN, the WBANs are set to play an increasingly important role in the applications operating in the vicinity of an individual's personal space. These fields include, but not restricted to, secure data transmission, surveillance and safety, home entertainment and health care [7, 8]. A Few examples of the WPAN/WBAN applications are shown in Figure 1.3 and are listed as follows [3, 15]:

- A number of WBAN applications are currently in use for health monitoring. These applications can measure body parameters including acceleration, temperature, oxygen consumption, blood pressure, glucose level, vision and pulse rate. Other applications include pacemakers, imaging camera pills, systems for epilepsy and depression monitoring and radio treatments for tumours [15–18]. E-health and tele-health concepts (Figure 1.4) are an upcoming front where a patient will be treated by doctors sitting at far distances. The patient's condition will be observed and treatments will be made using the monitored body parameters transmitted and

processed on a remote computer [16, 19, 20].

- Access/identification systems based on recognition of individual parameters or peripheral devices.

- Navigation and positioning support to individual or to vehicle using efficient communication with existing GPS technology.

- Monitoring of athletes body parameters, for example pulse rate, blood pressure, etc. using bio-sensors to enhance their performance.

(a) Blood pressure monitoring watch

(b) Tele-health monitor

(c) WPAN/WBAN entertainment systems

Figure 1.3: Some examples of modern day WBAN/WPAN applications [14]
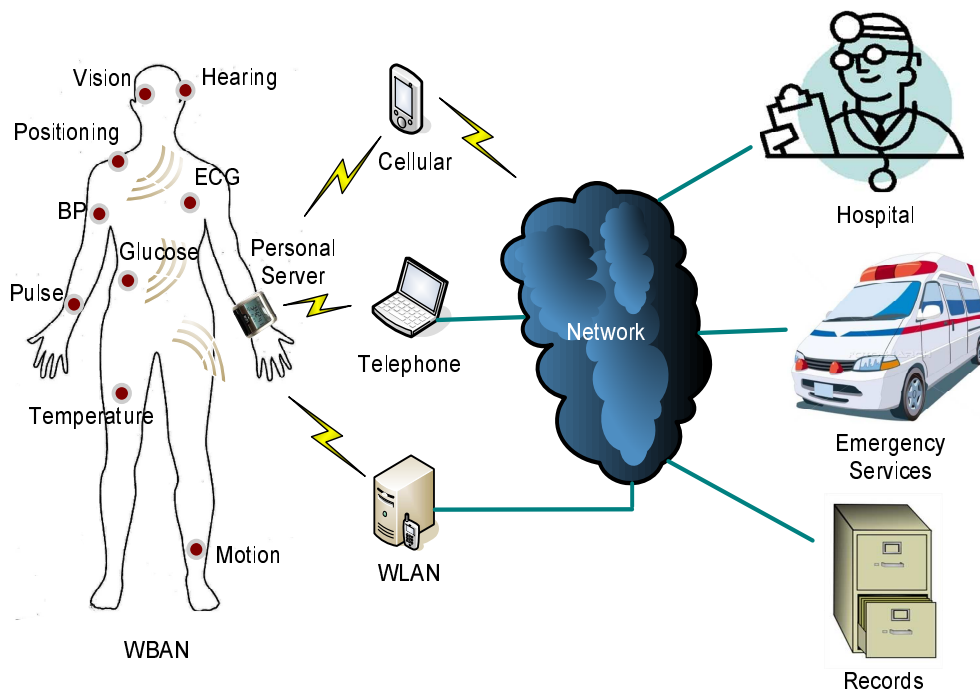
Figure 1.4: Concept of bio-telemetry system for distant health monitoring

- Home entertainment systems and portable gaming consoles including MP3 players, tablet PCs, Wii, PSP and mobile phones.

- Military applications including tracking systems for soldier's location, in-field instant communications and image/video transmission.

- Emergency services and assistance to police, fire fighters and paramedics.

- Industrial automation to enhance the productivity while reducing cost.

- RFID tags for enhanced security measures in retail outlets.

1.3   Challenges in Wireless PAN/BAN

The distinction between the wireless and conventional wired systems is its wireless mode of communication. Being wireless is an apparent challenge for the WPAN/WBAN as this medium of communication is hostile to radio waves causing attenuation, delay and

distortion of the transmitted signal. The WPAN/WBAN systems consist of a number of nodes and units either placed on the human body or working in the close proximity of the human body. As discussed in the previous section, the WPAN/WBAN applications vary from low power, low data rate communication used for health monitoring to high power, high data rate personal entertainment systems.

The human body being an integral part of the WPAN/WBAN by definition, makes antenna design a very complex issue. These antennas not only require to be of small size to guarantee ease of portability and mobility with reliable data transmission but also have to cope with the effects of the presence of the human body. The lossy nature of human body causes the WPAN/WBAN antennas to suffer from reduction in efficiency due to electromagnetic absorption in tissues, degradation of the radiation pattern and variation in the feed point impedance [8, 21–27]. These effects are system specific in nature depending on the operating frequency, physical limitations of the antenna itself and propagation environment [10]. The changing body postures and varying on-body antenna placements affect the transmission behaviour in these networks [28, 29].

The real working environment for the antennas is quite different from the conditions they are tested in the anechoic chamber. The incident communication signal in a radio environment is affected by the reflections, diffractions and scattering from the objects located in the vicinity of the antenna including buildings, vegetation, vehicles and ground plane modifying the antenna free space parameters greatly. These factors result in multipath arrival of the signal at the receiving antenna terminal. Miniaturised WPAN/WBAN devices restrict the antenna size only to a fraction of a wavelength. Typical length of a handset chassis ranges from 80-100 mm. It contains multiple components, for example, camera, loudspeaker, radio that further restricts the size of the antenna. It affects the antenna characteristics of gain, directivity, efficiency and polarisation due to losses caused by input impedance mismatch and circuit absorptions. As a result, these electrically small antennas are more vulnerable to the environmental degradations. It makes the traditional electromagnetic evaluation tools inefficient to predict the overall

behaviour of the WPAN/WBAN antennas in the real multipath scenarios [3, 30–33].

Characterisation of the human body and environment effects is a challenging task. This is due to the fact that the human body consists of a number of inhomogeneous layers with each having different electric properties. Also, the radiated signal took different paths including in-body, on-body and off-body and reflected, scattered and diffracted rays occur from different environmental objects present in the path of the signal before reaching the destination. There are some studies reported in the literature that tried to explore the actual transmission mechanism in an on-body link [8, 24, 34]. However, these efforts are mainly based on individual human body part models (e.g. arm models) rather than the whole body models.

The aspects of the multipath environment and its effects on the WPAN/WBAN antennas are also of greater importance. This issue has also been investigated with a few studies being reported in the literature. However, these investigations are restricted to land mobile radio environments with human head models [35–37]. The studies conducted to evaluate the environment effects in the presence of a complete human body model are very small in number.

1.4   Research Scope and Objectives

The characterisation of human body and environment effects is essential to develop a WPAN/WBAN system with desired levels of mobility and efficiency. Although, a detailed measurement process could be employed to study these effects, it needs extreme care and a longer time to reach the conclusions. Hence, efficient numerical and statistical modelling in accordance to the required system specifications is necessary for better understanding. The proposed techniques should give a clear picture of the performance of the WPAN/WBAN antennas under different practical scenarios.

The aim of the research work presented in this thesis is therefore, to investigate the

effects of the human body and the surrounding environment on different antennas, that are being used in the WPAN/WBAN applications. The main objectives of the work include:

- Study of on-body communication links for better understanding of the degrading effects of the human body on the performance of the WPAN/WBAN antennas using efficient numerical models.

- Investigation of the operation of body-worn antennas with respect to on-body placement, antenna-body separation and body postures.

- Development and application of a statistical model replicating the real multipath environment to study the environmental effects on the performance of the GPS antennas used to provide navigation services in the WPAN/WBAN applications.

- Study and analyse the working of the GPS antennas for WPAN/WBAN mobile terminals operating in close proximity of the human body in the multipath environment using developed statistical models and considering various on-body placements of the antennas with effects of homogeneous and inhomogeneous body models.

1.5   Organisation of Thesis

Following the introductory chapter, the rest of the thesis is organised as follows:

Chapter 2 introduces practical considerations for the WPAN/WBAN reviewing the literature and highlighting main requirements for the antennas, numerical modelling of the human body, GPS and provision of the navigation services. The fundamentals of statistical modelling of the multipath environment are also discussed.

Chapter 3 describes the transmission mechanism in an on-body Bluetooth link between a commercial mobile handset antenna and a Bluetooth headset antenna empha-

sising the role of surface waves in this link. The effects of surrounding objects and effects of handset antenna orientations on the link are also studied numerically.

Chapter 4 details the work carried out to characterise the effects of the multipath environment on the performance of the GPS antennas introducing a novel statistical environment model. The working of the GPS mobile terminal antennas in the multipath environment is analysed highlighting the role of the antenna orientation and performance enhancement using diversity antennas.

Chapter 5 deals with the effects of the human body presence on the operation of a GPS receiver antenna taking into account different body postures, antenna placements and antenna-body separations. It also discusses the performance of the GPS mobile terminal antennas in the multipath environment while operating in the vicinity of the human body taking into account varying on-body placements with effects of homogeneous and inhomogeneous head models.

Chapter 6 provides a summary of the main findings and contributions of the study, concluding the accomplished work and giving aspects of potential future research.

References

[1] K. Siwiak and Y. Bahreini, "Radiowave propagation and antennas for personal communications (3rd edition)," *Artech House, Inc., (USA)*, 2007.

[2] C. Baber, J. Knight, D. Haniff, and L. Cooper, "Ergonomics of wearable computers," *Mobile Networks and Applications*, vol. 4, no. 1, pp. 15–21, March 1999.

[3] Z. N. Chen, "Antennas for portable devices," *John Wiley and Sons, Inc., (UK)*, 2007.

[4] O. Shivers, "Bodytalk and the bodynet: A personal information infrastructure, personal information architecture," *MIT Laboratory for Computer Science, Cambridge, MA*, vol. Personal Information Architecture Note 1, December 1993.

[5] T. G. Zimmerman, "Personal area networks: Near field intra-body communications," *IBM Systems Journal*, vol. 35, no. 3 and 4, pp. 609–617, 1996.

[6] E. Jovanov, A. Milenkovic, C. Otto, P. de Groen, and B. Johnson, "A wireless body

area network of intelligent motion sensors for computer assisted physical rehabilitation," *URL: http://www.pubmedcentral.nih.gov/articlerender.fcgi?artid=552302.*

[7] R. Kraemer and M. Katz, "Short-range wireless communications: Emerging technologies and applications," *John Wiley and Sons, Inc., (UK)*, 2009.

[8] P. S. Hall and Y. Hao, "Antennas and propagation for body-centric wireless networks," *Artech House Inc., (UK)*, 2006.

[9] IEEE802.15, "IEEE 802.15 working group for WPAN," *URL:http://www.ieee802.org/15*.

[10] A. Alomainy, "Antennas and radio propagation for body-centric wireless networks," *PhD Thesis, Queen Mary University of London*, 2007.

[11] "Bluetooth specifications," 2003, *URL:http://www.bluetooth.com/Bluetooth/Learn/Technology*.

[12] L. Harte, "Introduction to Bluetooth (2nd edition)," *Althos Publishing, (USA)*, 2009.

[13] *URL:http://media.wiley.com/product_data/excerpt/75/07645488/0764548875.pdf*.

[14] *URL:http://www.pubmedcentral.nih.gov/articlerender.fcgi?artid=552302*.

[15] *URL:http://www.lifesourceonline.com/and_med.nsf/index*.

[16] *URL:http://www.medeaplus.org/web/downloads/profiles/A109_profile.pdf*.

[17] *URL:http://ftp.cordis.europa.eu/pub/ist/docs/fet/comms-23.pdf*.

[18] J. Kim and Y. Rahmat-Samii, "Implanted antennas inside a human body: Simulations, designs and characterizations," *IEEE Transactions on Microwave Theory and Techniques*, vol. 52, no. 8, pp. 1934–1943, August 2004.

[19] E. Jovanov, A. Milenkovic, C. Otto, P. de Groen, B. Johnson, S. Warren, and G. Taibi, "A WBAN system for ambulatory monitoring of physical activity and health status: Applications and challenges," *IEEE International Conference of Engineering in Medicine and Biology Society (EMBS)*, September 2005.

[20] H. Higgins, "In-body RF communications and the future of healthcare," *COST284 Final Report*, 2005.

[21] Z. Wang, X. Chen, and C. G. Parini, "Effects of the ground and the human body on the performance of a handset antenna," *IEE Proceedings on Microwave and Antenna Propagation*, vol. 151, no. 2, pp. 131–134, April 2004.

[22] J. Ryckaert, P. De Doncker, R. Meys, A. de Le Hoye, and S. Donnay, "Channel model for wireless communication around human body," *IEE Electronics Letters*, vol. 40, no. 9, pp. 543–544, April 2004.

[23] T. Kellomaki, J. Heikkinen, and M. Kivikoski, "Wearable antennas for FM reception," *European Conference on Antenna and Propagation (EuCAP)*, pp. 1–6, November 2006.

[24] K. Fujii, M. Takahashi, K. Ito, K. Hachisuka, Y. Terauchi, K. Y., K. Sasaki, and K. Itao, "Study on the transmission mechanism for wearable device using the human body as a transmission channel," *IEICE Transactions on Communications*, vol. E88-B, no. 6, pp. 2401–2410, 2005.

[25] M. Sanad, "Effect of the human body on microstrip antennas," *IEEE Antennas and Propagation Society International Symposium (AP-S)*, vol. 1, pp. 298–301, June 1994.

[26] J. Wang and O. Fujiwara, "EM interaction between a 5GHz band antenna mounted PC and a realistic human body model," *IEICE Transactions on Communications*, vol. E88-B, no. 6, pp. 2604–260, 2005.

[27] D. Nashaat, H. Alsadek, and H. Ghali, "Investigation of the mutual effect between human head and new shapes of PIFAs used in mobile communication systems," *Microwave and Optical Technology Letters*, vol. 46, no. 3, pp. 243–248, January 2005.

[28] B. Sanz-Izquierdo, J. A. Miller, J. C. Batchelor, and M. I. Sobhy, "Dual-band wearable metallic button antennas and transmission in body area networks," *IET Proceedings on Microwaves, Antennas and Propagation*, vol. 4, no. 2, pp. 182–190, 2010.

[29] G. Conway, S. Cotton, and W. Scanlon, "An antennas and propagation approach to improving physical layer performance in wireless body area networks," *IEEE Journal on Selected Areas in Communications*, vol. 27, no. 1, pp. 27–36, January 2009.

[30] J. B. Andersen and F. Hansen, "Antennas for VHF/UHF personal radio: A theoretical and experimental study of characteristics and performance," *IEEE Transactions on Vehicular Technology*, vol. 26, no. 4, pp. 349–357, November 1977.

[31] T. Taga, "Analysis for mean effective gain of mobile antennas in land mobile radio environments," *IEEE Transactions on Vehicular Technology*, vol. 39, no. 2, pp. 117 – 131, May 1990.

[32] K. Kalliola, K. Sulonen, H. Laitinen, O. Kivekas, J. Krogerus, and P. Vainikainen, "Angular power distribution and mean effective gain of mobile antenna in different propagation environments," *IEEE Transactions on Vehicular Technology*, vol. 51, no. 5, pp. 823–838, September 2002.

[33] P. L. Carro and J. de Mingo, "Mean effective gain of compact WLAN genetic printed dipole antennas in indoor-outdoor scenarios," *International Conference on Personal Wireless Communications (PWC)*, pp. 275–283, September 2006.

[34] G. A. Conway and W. G. Scanlon, "Antennas for over-body-surface communication at 2.45GHz," *IEEE Transactions on Antennas and Propagation*, vol. 57, no. 4, pp. 844–855, April 2009.

[35] J. Krogerus, C. Ichelun, and P. Vainikainen, "Dependence of mean effective gain of mobile terminal antennas on side of head," *European Conference on Wireless Technology (ECWT)*, pp. 467–470, October 2005.

[36] M. G. Douglas, M. Okoniewski, and M. A. Stuchly, "A planar diversity antenna for handheld PCS devices," *IEEE Transactions on Vehicular Technology*, vol. 47, no. 3, pp. 747–754, August 1998.

[37] K. Ogawa and T. Uwanao, "Mean effective gain analysis of a diversity antenna for portable telephones in mobile communication environments," *Electronics and Communication in Japan (Part I: Communications)*, vol. 83, no. 3, pp. 88–96, December 2000.

Chapter 2

Antennas and Propagation in Wireless PAN/BAN

Wireless Personal Area Networks/Wireless Body Area Networks (WPAN/WBAN) is a key area of wireless communication systems that has seen enormous growth in recent years. The antennas used in WPAN/WBAN systems operate close to the human body and have to cope with degrading effects caused by its lossy nature. Also the reliability of the WPAN/WBAN data link strongly depends upon the environment in which these applications work. Multipath arrival of the transmitted radio waves, caused by reflection, diffraction and scattering from the objects around the receiver, tends to undermine the successful data transmission [1].

This chapter discusses the radio propagation in the WPAN/WBAN highlighting antenna specifications. An overview of Global Positioning System (GPS) and navigation services in the WPAN/WBAN is also presented. The main issues regarding on-body propagation mechanism, numerical modelling of the human body and environment effects are discussed with literature review covering recent developments.

2.1 Practical Considerations for Wireless PAN/BAN

The design of body-worn and hand held devices has many aspects to be taken into account including safety for the user, low power requirements, low profile, scalable data rates and low complexity to provide mobility with ease of use and low cost to be affordable for the masses [2, 3]. This area has undergone great research and development activities because of the huge scale of current usage and anticipated future increase in the use of WPAN/WBAN devices [4–6].

The human body is an inherent part of the WPAN/WBAN applications. Being wireless makes these applications vulnerable to electromagnetic distortions caused by the lossy human body tissues. Therefore, the electromagnetic interaction between the human body and antennas has been an important research area [7–14]. It is now a well established fact that the performance of the antennas operating in close proximity of the human body is degraded due to losses caused by varying electric properties of human tissues. As a result, the WPAN/WBAN antenna suffers from distortion in radiation pattern, reduction in radiation efficiency and de-tuning of input impedance [3, 15–18].

The fears for the safety of the human body resulted in standardisation of maximum levels of expositions of human tissues to electromagnetic radiations emitted by the body-worn antennas defined in terms of Specific Absorption Rate (SAR) [19–21]. Many studies have also been reported on the human body interaction with the WPAN/WBAN antennas and their compliance to the SAR standards [22–25]. Human body phantoms (Figure 2.1) are also developed for the experimental investigations of wearable antenna performance [26].

2.1.1 On-Body Transmission Mechanism

The efficient deployment of the WPAN/WBAN systems make it indispensable to evaluate the interaction of the human body with electromagnetic waves radiated by the

Figure 2.1: Realistic human body phantom for on-body measurements [27]

antennas. Wearable antennas use the human body as a transmission channel for on-body communications. Reliable wireless communications require the characterisation of the radio channel with deep understanding of the transmission mechanism. A number of studies has been reported on the on-body communication link using stochastic path loss models [28, 29], concluding that on-body communication channel varies depending not only on the body posture and movement but also on antenna type, placement on-body and orientation as well as local environment [3]. However, there is a lack of information related to the transmission mechanism of the body worn and near body devices in the physical sense to describe the cause of these variations.

A few steps have been taken in this direction now as Fujii et al. [30, 31] studied the transmission mechanism for a short range on-body channel between a hand-held receiver and wrist-worn transmitter. The two devices were placed at a distance of 200 mm and communicate at a frequency of 10 MHz. A simple cube has been used to represent the human arm both numerically and experimentally. For this kind of study, electric and magnetic field distributions give valuable information to characterise the dominant medium of transmission and role of surface waves. Fujii et al. concluded in this study that for this small on-body channel, the dominant medium is surface waves and not the air waves or the penetrating waves.

Conway et al. [32, 33] have demonstrated the importance of the surface waves in a 250 mm on-body channel at 2.45 GHz. The link has been established between two microstrip patch antennas placed on a small cylindrical homogeneous model representing the human body.

The on-body transmission mechanism has also been studied by Hao et al. [17] and See et al. [34]. However, these studies mainly deal with the statistical channel modelling and effects of the human body presence on radiation patterns and input impedance of the antennas giving little information of the transmission mechanism.

The scope of the reported studies is, therefore, limited due to use of small canonical models of human body and very short range on-body channels. Furthermore, the investigated antennas and their on-body placements do not represent a realistic and more commonly used scenario. Also, the operating frequency of 10 MHz, used by Fujii et al. makes the results less relevant to on-body communications using Bluetooth.

The acceptance of the human body as a transmission channel for on-body link is therefore, limited due to a lack of insight into the actual physical mechanism of transmission. This important but mostly neglected aspect of the WPAN/WBAN needs to be explored further to develop a more efficient and reliable on-body communication channel. It necessitates the investigation of larger on-body link between commercially available antennas placed on more realistic positions on a complete human body model. Chapter 3 of this thesis addresses this issue in detail highlighting the role of the surface waves in the on-body link.

2.1.2 Antennas for Wireless PAN/BAN

The optimal performance of a radio system depends greatly on efficient design of the antenna. In addition to the general characteristics of the antennas, the WPAN/WBAN requires high performance antennas with small size, less weight, body-conformal and inexpensive designs. These added requirements are necessary to guarantee maximum

mobility, less complexity and reliability of service.

The presence of the lossy human body in the proximity makes the design of body-worn antennas more critical. These antennas have to exhibit good performance while undergoing efficiency reduction, detuning and radiation pattern distortions caused by the human body. Many studies have presented various miniaturised designs for WPAN/WBAN applications including printed dipoles, planar inverted F antennas (PIFAs), ceramic substrate antennas and dielectric loaded antennas (DRAs) that perform well to cope with the degradations caused by the human body [2, 33, 35].

The concept of integration of the antennas into clothes has realised textile antennas [36, 37]. These antennas however, often face the problem of being bent, wrinkled and sometimes wet in common use scenarios. Sanz-Izquierdo et al. have presented novel designs of a metallic button antenna and belt antenna [38, 39]. These antennas have the appearance and dimensions of standard jeans button and a standard belt buckle, respectively. These designs not only cope well with the bending, wrinkling and being wet effects but also offers good dual band performance at 2.45 GHz and 5 GHz in the on-body scenarios. Various designs of implantable antennas have also been proposed [40] in the literature for medical use, especially for cancer detection and treatment.

2.2 Numerical Modelling of Antenna and Human Body Interaction

The evolution of computer based modelling techniques has brought a revolution in the solution and analysis of electromagnetic problems. Complex electromagnetic problems such as interaction of antennas and the human body and on-body radio propagation, can be solved easily using these numerical simulation tools. These very powerful electromagnetic analysis tools are also capable of providing useful physical insight into the radio propagation mechanism, extending the body modelling to include the surrounding

Table 2-1: Maxwell's Equations in differential and corresponding integral form

EM Law	Differential Form	Integral Form
Gauss's law	$\nabla . D = \rho$	$\int D.ds = \int \rho.dV$
Magnetic field law	$\nabla . B = 0$	$\int B.ds = 0$
Faraday's law	$\nabla \times E = -\dfrac{\partial B}{\partial t}$	$\int E.dl = -\dfrac{\partial d}{\partial t}\int B.ds$
Ampere's Law	$\nabla \times H = J_e + \dfrac{\partial D}{\partial t}$	$\int H.dl = \int J_e.ds + \dfrac{\partial d}{\partial t}\int D.ds$

environment.

The numerical techniques attempt to solve fundamental Maxwell's equations, subject to the boundary constraints posed by the geometry. They usually require greater computational resources.

2.2.1 Full-Wave Numerical Modelling

The core of electromagnetic numerical modelling is based on the relationships and variations of charges, currents and electric and magnetic fields defining the behaviour of electromagnetic waves [41, 42]. In 1873, James Clark Maxwell assembled the laws of Ampere, Faraday, Gauss and the magnetic field law into a set of equations which formed the basis of modern electromagnetic numerical tools. Table 2-1 presents these equations in differential and corresponding integral formulations.

The electromagnetic problems are related to the field behaviour in certain medium.

Following equations are used to describe and relate the Maxwell's equations with the properties of the medium [42, 43]:

$$D = \epsilon E \tag{2.1}$$

$$B = \mu H \tag{2.2}$$

$$J_e = \sigma E \tag{2.3}$$

Where E is the electric field intensity (V/m), D is the electric flux density, H is the magnetic field intensity (A/m) and B is the magnetic flux density (Wb/m^2). Also, J_e is the electric current density (A/m^2) and σ is the electric conductivity (S/m).

The electric permittivity and magnetic permeability of the medium is defined as:

$$\epsilon = \epsilon_r \epsilon_o \tag{2.4}$$

$$\mu = \mu_r \mu_o \tag{2.5}$$

Where $\epsilon_o = 8.854 \times 10^{-12}$ F/m is the permittivity of the free space and $\mu_o = 4\pi \times 10^{-7}$ H/m is the permeability of the free space.

A number of numerical techniques are available with each exhibiting its own strength and limitations. Great care is needed to be exercised in the choice of a modelling technique and simulation parameters including mesh generation, simulation duration and computational domain size to avoid errors [44]. At present, the best numerical method/tool for the design and verification of radio communication on the human body is not yet very clear. However, a COST244 benchmark study of different commercial codes based on various numerical techniques on the same electromagnetic problem has concluded that although, using more computational resources, Finite Difference Time Domain (FDTD) / Finite Integration Technique (FIT) based tools provide highly accurate results with faster computation time [45]. Therefore, Computer Simulation Technology (CST) Microwave Studio$^{\textregistered}$ is used for numerical modelling throughout the thesis.

Appendix A discusses two electromagnetic numerical modelling techniques, FDTD and FIT briefly, highlighting key features of CST Microwave Studio®.

2.2.2 Electric Properties of Human Body

The biological system of the human body is an irregularly shaped dielectric medium with frequency dependent permittivity and conductivity. The electromagnetic interaction of antennas and human body depends upon the body's electric parameters, geometry as well as the frequency and the polarisation of the incident wave. Advanced numerical techniques have made it possible to model the complex electromagnetic problems involving the human body with a choice of high resolution models in a broad frequency range. Therefore, a set of specific parameters defining the electric properties of the human tissues at different frequencies is required to model the electromagnetic fields in and around the body correctly.

The parameters that describe the electric properties of the human tissues include the relative permittivity (ϵ_r) and the conductivity (σ). Many researchers have measured these properties and compiled the results for various body tissues covering a wide frequency range from 10 Hz to 100 GHz [46–49]. The parametric values for different tissues at considered frequencies used in different models in this thesis are indicated in the following chapters.

2.3 Navigation Services in Wireless PAN/BAN

Ever-growing demand of navigation and positioning facilities to be available in portable devices has made the GPS antennas an essential part of the modern WPAN/WBAN applications, especially the mobile phones. The WPAN/WBAN works in collaboration with existing technology of Global Positioning System (GPS) to provide these services. Although, external GPS receivers are available for mobile PCs, portable media players
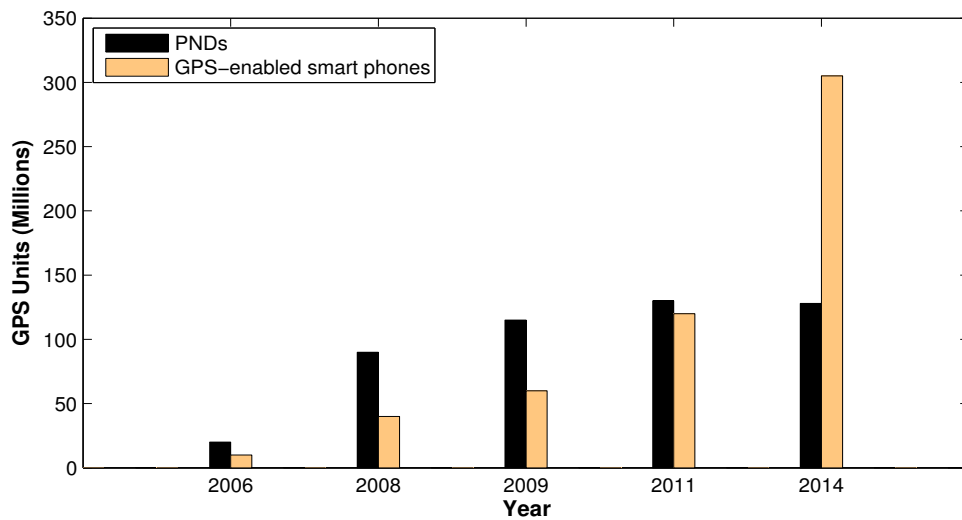
Figure 2.2: Survey and forecast of worldwide PNDs and GPS-enabled smart phones in use (reproduced from [51])

and digital cameras, there is a greater demand of integration of GPS receivers within these products. A Federal Communications Commission (FCC) adoption to enhance the provision of emergency services by tracking a user's location through his mobile also necessitates the integration of the GPS to the cellular phones [50].

The navigation devices are typically divided into two parts, Personal Navigation Devices (PNDs) and GPS enabled mobile handsets. In the past few years, PNDs had dominated the global navigation market. However, introduction of the smart phones has been causing a change in this trend and they are tipped to account for a 70% share of the personal navigation market in 2014. The usage of navigation-enabled smart-phones will rise to 305 million units, exceeding the 128 million PNDs in 2014 (Figure 2.2). The navigation industry is predicted to earn a gross total of £130 billions in 2014 [51, 52].

2.3.1 GPS

Global Positioning System (GPS) delivers the navigation and positioning services worldwide being the only fully functional satellite navigation system at present. The GPS navigation services can be used on land, sea, in the air and even in space.

A number of applications make use of GPS to provide navigation, positioning, monitoring, geographic surveys, natural resource explorations, mapping, weather and atmospheric information, public safety and surveillance. Figure 2.3 shows few examples of GPS enabled WPAN/WBAN devices.

2.3.2 Principle of GPS

The navigation systems are based on a fundamental positioning procedure where knowing the distance from an unknown location to a certain number of known locations, allows finding the coordinates of the unknown position. In the GPS, a number of satellites orbiting the earth provide the known locations while the position of the user on earth

(a) In-vehicle GPS PND   (b) GPS-enabled wrist watch

(c) GPS-enabled smart phone   (d) GPS-enabled mobile handset

Figure 2.3: Examples of portable navigation devices [53–55]

with a receiver is the unknown location [56].

To determine 3-D position of the receiver, time delay between transmission and reception of each GPS radio signal transmitted by the GPS satellites is measured. The distance between the user and the satellite is calculated from this time delay as the speed of signal (equals to the speed of light) is already known. The GPS signals also carry information about the location of the satellites. By determining the position of, and distance to at least three satellites, the GPS receiver can compute its position in terms of latitude, longitude and height. However, a fourth satellite is also required for a timing offset that occurs between the clock in the receiver and those in the satellites due to poor synchronisation. Using the data from the fourth satellite, the receiver can find this timing offset and hence can eliminate it [56–58].

2.3.3 GPS System Architecture

The GPS system comprises of three segments that operate together to provide a functional positioning service namely space segment, control segment and user segment (Figure 2.4).

The space segment consists of 30 satellites placed in six Middle Earth Orbits (MEO) at an altitude of 20,180 km above the surface of the earth. These orbits are inclined at 55° to the equator. This satellite constellation makes at least four satellites visible above the horizon anywhere on the earth, at any time of the day [57, 58]. The space segment transmits navigation message containing satellite time and ephemeris data. The ephemeris data provides information about the precise location of the satellite in the orbit [56].

The control segment consists of a system of monitoring stations spread around the globe. This segment tracks the GPS satellites and generate periodic updates of their position drift and clock skew. The individual satellites then adjust the ephemeris data provided to the user segment based on these updates [56, 58].
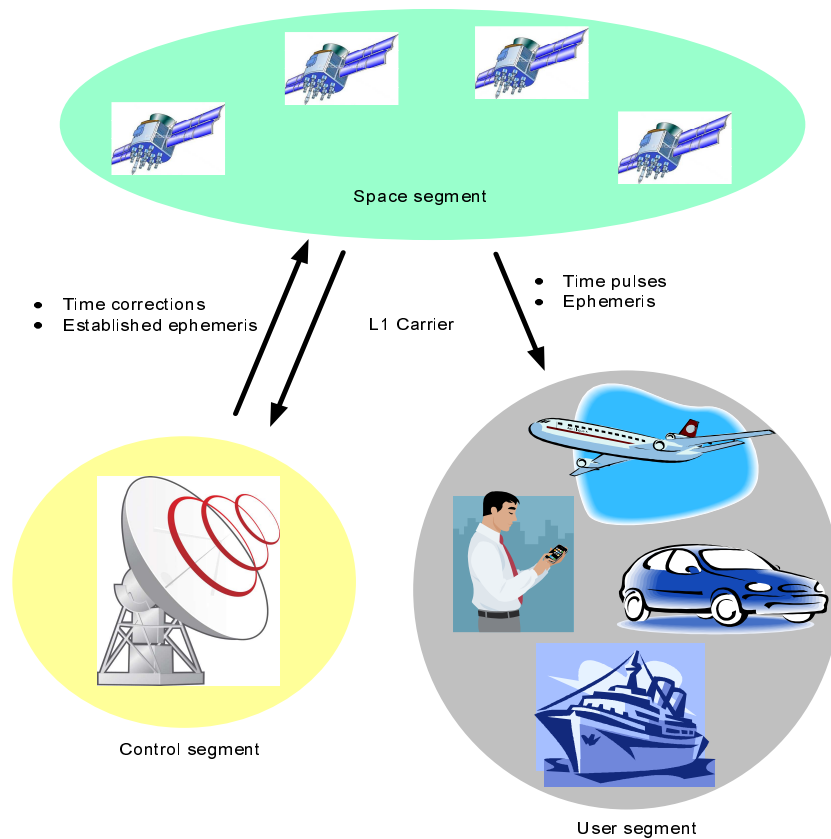
Figure 2.4: GPS system architecture with space, control and user segments

The user segment processes the time and the ephemeris data from the GPS satellites and generates accurate estimates for position, velocity and timing. The user segment typically consists of three components including GPS antenna, processor and display. The antenna receives the GPS signal from the satellites and passes it to the processor that extracts useful information from these signals and determines the navigation solution being relayed to the end user by the display [56, 57].

2.3.4   GPS Satellite Signal

The GPS operation is divided into civilian and military categories. The commercially available civilian GPS operates at a frequency of 1575.42 MHz (L1) while US military uses the GPS frequency of 1227.60 MHz (L2) [57–59].

The GPS assigns a unique Coarse Acquisition Code (C/A code) and a unique Precision Code (P-code) to each satellite. The navigation message is superimposed on both the C/A and the P codes. The phase of the transmitted L1 and L2 carrier signal is shifted by the C/A code, the P-code and the navigation message. Code Division Multiple Access (CDMA) technique is employed by the satellites to use a common carrier frequency while still allowing the receiver to determine which satellite is transmitting [57, 59].

The C/A code is a Pseudo Random Noise (PRN) code that repeats every 1023 bits (one millisecond). This code modulates the L1 carrier signal used for commercial Standard Positioning Service (SPS), spreading the spectrum over a 1 MHz bandwidth [57, 59].

The P-Code is a very long PRN code that repeats every seven days. This code modulates both the L1 and the L2 carrier phases, spreading the spectrum over a 10 MHz bandwidth. The P-Code is further encrypted into another code called the Y-Code. This P(Y)-Code requires special modules that could be used by authorised personnel having the cryptographic keys and is the basis for the US military's Precise Positioning Service (PPS) [59].

The navigation message also modulates the L1-C/A code signal. It is a 50 Hz signal containing the satellite ephemeris data, atmospheric propagation correction data and satellite clock bias [56, 59].

The civilian GPS signal is controlled by the US Department of Defence (DoD) to provide 100 m horizontal accuracy, 156 m vertical accuracy and 340 nsec time accuracy [56, 58]. Many techniques are being employed nowadays to improve the positioning accuracy including Differential GPS and Assisted GPS that are beyond the scope of this thesis.

A number of factors affect the performance of a GPS system including atmospheric effects, clock errors, signal jamming, incorrect positioning, multipath effects and presence of the human operator [56, 57]. The multipath effects occur when the signal from the

satellite is reflected from different objects located near the GPS receiver. This increases travel time of the signal and introduces errors. The electromagnetic absorptions in the human body tissues and reflections from the body surface also detunes the GPS receiver antenna. It reduces the antenna performance introducing impedance mismatch, efficiency drop, resonance shift and radiation pattern fragmentation. These issues are discussed thoroughly in the following chapters of this thesis.

2.3.5   Wireless PAN/BAN Antennas for GPS

Antenna is an important element of a GPS receiver. The basic theoretical requirements for a GPS antenna can be listed as [60–62]:

- Antenna should be capable of handling Circularly Polarised (CP) waves to transfer most of the incoming Right Hand Circularly Polarised (RHCP) GPS signal power to the receiver.

- Uniform radiation pattern over the entire upper hemisphere is required to ensure that all visible satellites can maintain signal lock.

- To eliminate the multipath effects, a good rejection of Left Hand Circular Polarisation (LHCP) and no back lobes are essential.

- The receiving GPS antennas should exhibit a minimum of 2 MHz bandwidth as the modulated GPS signal is spread over 2 MHz bandwidth in L1 band with centre frequency of 1575.42 MHz. However, efficient performance of commercial GPS applications typically require the antennas to achieve -10 dB impedance bandwidth of ± 5 MHz to mitigate the variations caused by transmitting satellite hardware and atmospheric effects [63].

The modern mobile handsets are no longer just cellular phones, but have to support other services including mobile television, Bluetooth, Wi-Fi, FM radio and digital camera applications. This consumer driven market also necessitates provision of these features

in a small form factor at reasonable cost. Integration of the GPS on the same platform also requires miniaturisation of the antenna [50, 63].

An enhanced emergency protocol adopted by the FCC requires the mobile phones to be able to establish a GPS communication link when the user makes a call to emergency services. It helps to track the user's location so that help can be provided in the event of a call drop or user's inability to give information about his whereabouts [50]. The proximity of the user's head and hand in this scenario affects the radiation characteristics of the GPS antennas. Similarly, the mobile phones are not used in a fixed position which means the "up" direction of the antenna changes depending in which orientation the mobile phone is being used. In the talking position, the user's head and hand obstructs the clear view of the sky of the mobile terminal GPS antenna. Also, the reflections of the incident RHCP satellite signal from the objects in the vicinity of the mobile terminal GPS antenna cause change in the signal polarisation.

In the common operating scenarios of cluttered environments, for example indoors and city streets, the line-of-sight satellite signal is obstructed and a limited angular space is available for its arrival while the polarisation of the reflected signal is not defined. Therefore, a wide-beam linearly polarised GPS antenna gives better performance as compared to the conventional circularly polarised antenna types. Hence, these antennas are a preferred choice to acquire signals concurrently from the four GPS satellites for the navigation solution [64, 65].

The current developments and expected future growth of GPS usage in the WPAN/ WBAN devices necessitate a detailed study of the electromagnetic interaction of the human body and the GPS mobile terminal antennas. A number of studies have been reported in the literature covering design aspects of the GPS antennas for hand-held devices [66, 67]. However, effects of the human body presence on these antennas have got little attention. Chapter 5 of this thesis presents detailed investigations of the electromagnetic interaction of the human body and the GPS antennas for the WPAN/WBAN applications.

2.4 Multipath Environment and Wireless PAN/BAN

The hand-held devices in the WPAN/WBAN applications are used freely in different situations and positions. The radio wave propagation in the WPAN/WBAN, therefore, not only depends upon the antenna placements and orientations on-body but also on the near-by environment.

The antenna designers are used to stringent requirements in free space with a single wave incident. However, in an actual working environment, objects surrounding the receiving antenna including vehicles, trees, buildings, ground and even the human body itself cause the incident waves to reflect, diffract and scatter resulting in a multipath scenario. These factors cause the antenna radiation patterns to modify greatly resulting in degradation of antenna performance due to propagation losses. It makes the traditional electromagnetic approaches, based on the free space parameters to evaluate the antenna performance, insufficient [1, 68]. These factors must be characterised in order to design efficient transceivers that provide a better sense of reliability in the wireless communication link.

The analysis of antenna performance in a multipath environment through open-field test suffers from disadvantage of long experimental time. Moreover, the weather conditions, temperature and location hazards make it difficult to control the test environment. It results in decreased accuracy and poor repeatability. The draw-backs of the field test can be avoided using statistical models to replicate the real multipath scenario. It provides an excellent alternative to the field tests predicting the antenna performance with added benefits of controlled test conditions and enhanced accuracy due to faster and repeatable calculations [69, 70].

In recent years, environmental effects on the performance of the antennas in land mobile radio environment are studied by various groups. The environmental factors are usually defined by Angle of Arrival (AoA) distribution and Mean Effective Gain (MEG) of the incoming wave in a land mobile radio environment [1, 69–71].

2.4.1 Mean Effective Gain (MEG)

The Mean Effective Gain is the average gain of the antenna performance in a multipath radio environment. It is a figure of merit for the average performance of an antenna on a mobile terminal taking into account the incident radio waves in the multipath environment and also the gain patterns of the antenna.

In 1977, the ground breaking idea to predict the average performance of an antenna in a multipath environment was proposed by Andersen et al. [69]. They suggested that this prediction can be made by measuring the mean levels of the received power of the test antenna and a reference antenna on a random route in a typical working environment. The MEG of the antenna is then calculated as the ratio of the two measured values. Although, this method is the best evaluation technique due to reliability, it lacks in accuracy because of poor repeatability of the measurement and longer measurement times [1, 70, 72].

The need for a fast computational method for the MEG calculations were fulfilled by Taga [70]. He derived a general expression that can be used to evaluate the MEG of an antenna in a certain environment based on 3-D power gain pattern of the antenna and the average angular distribution of incident plane waves in the environment. The power distribution must be known in both the azimuth and the elevation, and separately for horizontal and vertical polarised field components. The clear benefit of this method is fast and repeatable computations. Furthermore, it enables to characterise the antenna properties of gain and polarisation and directional response of the communications channel separately [1, 72].

The MEG of an antenna in a mobile terminal is defined as the ratio between the mean received power of the antenna, $P_{received}$, over a random route and the total mean incident power, $P_{incident}$, arriving at the antenna [70]:

$$MEG = \frac{P_{received}}{P_{incident}} \tag{2.6}$$

If P_θ is the mean incident power of θ polarised incident waves and P_ϕ is the mean incident power of ϕ polarised incident waves, then $P_\theta + P_\phi$ is the total mean incident power arriving at the antenna.

The ratio between the time averaged mean powers received in θ and ϕ polarisations when the transmitted radio wave is θ polarised is called Cross Polarisation Ratio (XPR) and described as:

$$XPR = \frac{P_\theta}{P_\phi} \tag{2.7}$$

For spherical coordinates, $P_{received}$ can be expressed as [73]:

$$P_{received} = \int_0^{2\pi} \int_0^{\pi} [P_1 G_\theta(\theta,\phi) p_\theta(\theta,\phi) + P_2 G_\phi(\theta,\phi) p_\phi(\theta,\phi)] \sin\theta d\theta d\phi \tag{2.8}$$

Where $G_\theta(\theta,\phi)$ and $G_\phi(\theta,\phi)$ are the θ and ϕ components of the antenna power gain pattern, respectively. $p_\theta(\theta,\phi)$ and $p_\phi(\theta,\phi)$ indicate the components of angular density functions of the incoming waves in the elevation and the azimuth planes, respectively. θ is the angle in the elevation and ϕ is the angle in the azimuth as shown in Figure
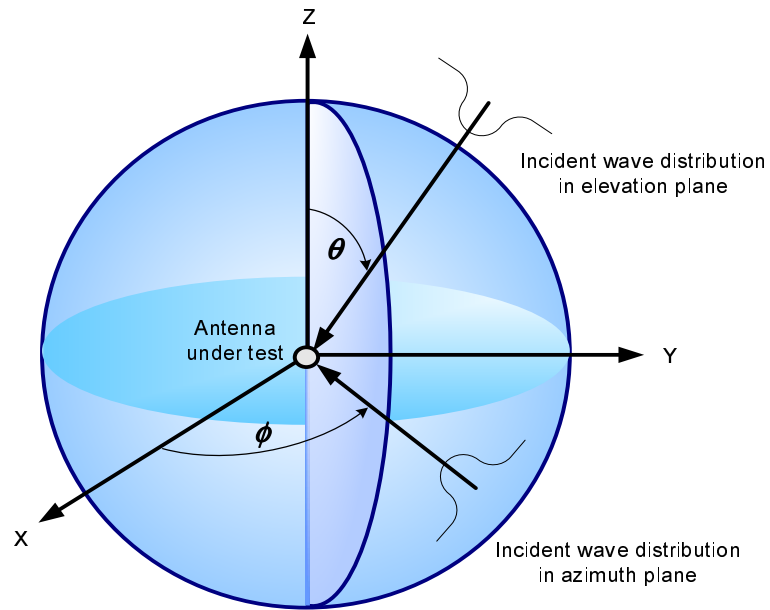
Figure 2.5: Spherical coordinates system and representation of a hypothetical incident wave distribution model

2.5. P_1 represents the mean power that would be received by an isotropic antenna in θ polarisation while P_2 is the mean power received by an isotropic antenna in ϕ polarisation. These functions satisfy the following conditions [1, 70, 72]:

$$\int_0^{2\pi} \int_0^{\pi} [G_\theta(\theta, \phi) + G_\phi(\theta, \phi)] \sin\theta d\theta d\phi = 4\pi \tag{2.9}$$

$$\int_0^{2\pi} \int_0^{\pi} p_\theta(\theta, \phi) \sin\theta d\theta d\phi = \int_0^{2\pi} \int_0^{\pi} p_\phi(\theta, \phi) \sin\theta d\theta d\phi = 1 \tag{2.10}$$

Using Equations 2.7-2.10, the MEG expression can be rearranged to form the following equation:

$$MEG = \int_0^{2\pi} \int_0^{\pi} \left[\frac{XPR}{1 + XPR} G_\theta(\theta, \phi) p_\theta(\theta, \phi) \right.$$
$$\left. + \frac{1}{1 + XPR} G_\phi(\theta, \phi) p_\phi(\theta, \phi) \right] \sin\theta d\theta d\phi \tag{2.11}$$

2.4.2 Statistical Distribution Model of Incident Waves

In a multipath radio environment, the incident plane waves arriving at the mobile terminal have various Angles of Arrival (AoA) and the Cross Polarisation Ratio (XPR). The MEG of the mobile antenna (Equation 2.11) depends upon the XPR and the nature of the multipath environment depicted by the angular density functions $p_\theta(\theta, \phi)$ and $p_\phi(\theta, \phi)$. Those functions describe the AoA distribution of the incident waves. Therefore, it is necessary to study a suitable statistical model of the AoA distribution of the incoming plane waves, similar to an actual working environment to be able to get an account of the antenna performance in real scenarios, outside an anechoic chamber.

Various groups have studied the land mobile terminal antenna performance in multipath environment and reported quite a few statistical models for the AoA distribution of incoming radio waves based on simulations and actual measurements [70, 72, 74]. It is assumed that due to the random movement of the mobile user in any environment, the

radio waves can be incident from any azimuth direction with equal probability resulting in a uniform power density function [1, 68, 70, 72, 74–77]. However, the *AoA* distribution in the elevation is found to follow the Gaussian and Laplacian distribution [70, 77, 78] summarised in Table 2-2. In these equations, m_V and m_H are the mean elevation angles whereas σ_V and σ_H are the standard deviations of the vertical and horizontal polarised wave distributions, respectively. A_θ and A_ϕ are constants determined by Equation 2.10.

Table 2-2: Commonly used statistical *AoA* distributions for the incident radio waves in a land mobile radio environment [1, 72, 78]

Distribution	Mathematical Formulation
Uniform	$p_\theta\left(\theta, \phi\right) = 1 \quad (0 \leq \theta \leq \pi)$ $p_\phi\left(\theta, \phi\right) = 1 \quad (0 \leq \theta \leq \pi)$
Gaussian	$p_\theta\left(\theta, \phi\right) = A_\theta \exp\left[-\dfrac{\left\{\theta - \left[(\pi/2) - m_V\right]\right\}^2}{2\sigma_V^2}\right] \quad (0 \leq \theta \leq \pi)$ $p_\phi\left(\theta, \phi\right) = A_\phi \exp\left[-\dfrac{\left\{\theta - \left[(\pi/2) - m_H\right]\right\}^2}{2\sigma_H^2}\right] \quad (0 \leq \theta \leq \pi)$
Laplacian	$p_\theta\left(\theta, \phi\right) = A_\theta \exp\left[-\dfrac{\sqrt{2}\left|\theta - \left[(\pi/2) - m_V\right]\right|}{\sigma_V}\right] \quad (0 \leq \theta \leq \pi)$ $p_\phi\left(\theta, \phi\right) = A_\phi \exp\left[-\dfrac{\sqrt{2}\left|\theta - \left[(\pi/2) - m_H\right]\right|}{\sigma_H}\right] \quad (0 \leq \theta \leq \pi)$

Studies are also reported with environmental effects on mobile antennas in street

microcells [74] and on diversity antennas [75, 76, 79] in literature. The antenna performance in an indoor multipath environment is also investigated [77]. All these studies are concentric on land mobile environment (900 MHz-5.8 GHz) and no serious effort is made to study the environmental effects on the GPS applications. Chapter 4 of the thesis discusses this relatively unexplored topic thoroughly.

2.4.3   Antennas and Human Body Presence in Multipath Environment

Being an integral part of the WPAN/WBAN applications, the human body influences the performance of the mobile terminal GPS antennas greatly. On the other hand, these antennas operate in the multipath environment and hence, are affected by the two degrading elements (i.e. human body and multipath environment) simultaneously. It necessitates to study the performance of the mobile terminal antennas in the multipath environment while operating in the vicinity of the human body.

Recently, the effects of the presence of a human head beside the mobile handset antennas [68] are studied, however, the GPS antennas have not been studied so far. Chapter 5 of this thesis gives a detailed investigation of the performance of the on-body mobile terminal GPS antennas while operating in the multipath environment.

2.5   Summary

The antenna considerations and importance of the electromagnetic numerical methods in the analysis of the complex problem of radio propagation on and around the human body has been discussed. Use of the GPS technology to provide the navigation services in the WPAN/WBAN applications is highlighted. Antennas operating in real scenarios suffer from the multipath arrival of the transmitted radio waves due to the presence of reflectors and scatterers in the surroundings. The importance of the stochastic models for the multipath environment to characterise the environment degradations and predict

the antenna's actual performance has also been discussed with details of parameters of the Mean Effective Gain and the Angle of Arrival.

The presented review of the open literature on studies regarding the electromagnetic interaction of the human body with the antennas has concluded that efficiency reduction due to power dissipation in tissues, radiation pattern fragmentation and variation in feed point impedance are often associated with the WPAN/WBAN antennas. The presence of reflectors and scatterers in the vicinity causes the multipath arrival of the electromagnetic waves resulting in further degraded performance. A need for a deep insight into the physical mechanism involved in the on-body radio transmission and effective analysis of the multipath environment effects is therefore, pertinent. This will provide the necessary tools and assist to pave the way for the development of reliable and efficient WPAN/WBAN systems.

References

[1] K. Fujimoto and J. R. James, "Mobile antenna systems handbook (2nd edition)," *Artech House Publishers, (USA)*, 2001.

[2] Z. N. Chen, "Antennas for portable devices," *John Wiley and Sons, Inc., (UK)*, 2007.

[3] P. S. Hall and Y. Hao, "Antennas and propagation for body-centric wireless networks," *Artech House Inc., (UK)*, 2006.

[4] E. Jovanov, A. Milenkovic, C. Otto, P. de Groen, and B. Johnson, "A wireless body area network of intelligent motion sensors for computer assisted physical rehabilitation," *URL: http://www.pubmedcentral.nih.gov/articlerender.fcgi?artid=552302*.

[5] J. Bernardhard, P. Nagel, J. Hupp, W. Strauss, and T. Von der Grun, "BAN-body area network for wearable computing," *9th Wireless World Research Forum Meeting*, July 2003.

[6] S. Matsushita, "A headset-based minimized wearable computer," *IEEE Intelligent Systems archive*, vol. 16, no. 3, pp. 28–32, May 2001.

[7] J. Toftgard, S. Hornsleth, and J. B. Anderson, "Effects on portable antennas of the presence of a person," *IEEE Transactions on Antennas and Propagation*, vol. 41, no. 6, pp. 739–746, June 1993.

[8] H. R. Chuang, "Human operator coupling effects on radiation characteristics of a portable communication dipole antenna," *IEEE Transactions on Antennas and Propagation*, vol. 42, no. 4, pp. 556–560, April 1994.

[9] M. A. Jensen and Y. Rahmat-Samii, "EM interaction of handset antennas and human in personal communications," *IEEE Transactions on Antennas and Propagation*, vol. 83, no. 1, pp. 7–17, January 1995.

[10] M. Okoniewski and M. A. Stuchly, "A study of the handset antenna and human body interaction," *IEEE Transactions on Microwave Theory and Techniques*, vol. 44, no. 10, pp. 1855–1864, October 1996.

[11] J. S. Colburn and Y. Rahmat-Samii, "Human proximity effects on circular polarized handset antennas in personal satellite communications," *IEEE Transactions on Antennas and Propagation*, vol. 46, no. 6, pp. 813–820, Junuary 1998.

[12] Z. Wang, X. Chen, and C. G. Parini, "Effects of the ground and the human body on the performance of a handset antenna," *IEE Proceedings on Microwave and Antenna Propagation*, vol. 151, no. 2, pp. 131–134, April 2004.

[13] J. Wang and O. Fujiwara, "EM interaction between a 5GHz band antenna mounted PC and a realistic human body model," *IEICE Transactions on Communications*, vol. E88-B, no. 6, pp. 2604–260, 2005.

[14] J. Guterman, A. A. Moreira, C. Peixeiro, and Y. Rehmat-Samii, "Electromagnetic human interaction with ISM 2.4GHz laptop antennas," *European Conference on Antennas and Propagation (EuCAP)*, November 2007.

[15] P. S. Hall and Y. Hao, "Antennas and propagation for body centric communications," *European Conference on Antennas and Propagation (EuCAP)*, November 2006.

[16] S. Curto and M. J. Ammann, "Electromagnetic interaction between resonant loop antenna and simulated biological tissue," *Microwave and Optical Technology Letters*, vol. 48, no. 12, pp. 2418–2421, September 2006.

[17] Y. Hao, A. Alomainy, P. S. Hall, Y. I. Nechayev, C. G. Parini, and C. C. Constantinou, "Antennas and propagation for body centric wireless communications," *IEEE International Conference on Wireless Communications and Applied Computational Electromagnetics*, pp. 586–589, April 2005.

[18] Z. H. Hu, M. Gallo, Q. Bai, Y. I. Nechayev, P. S. Hall, and M. Bozzetti, "Measurement and simulations for on-body antenna design and propagation studies," *European Conference on Antennas and Propagation (EuCAP)*, November 2007.

[19] "IEEE standard for safety levels with respect to human exposure to radiofrequency electromagnetic fields, 3kHz to 300GHz," *IEEE Standards, C95.1*, 1999.

[20] International Commission on Non-Iodizing Radiation Protection (ICNIRP), "Guidelines for limiting exposure to time-varying electric, magnetic and electromagnetic

fields (up to 300GHz)," *Health Physics*, vol. 74, pp. 494–522, 1998.

[21] "Considerations for the evaluation of human exposure to electromagnetic fields (EMFs) from mobile telecommunication equipment (MTE) in the frequency range from 30MHz-6GHz," *CENELEC, European Specification, Ref. No. ES-59005:1998 E*, 1998.

[22] V. Hombach, K. Meier, M. Burkhardt, E. Kuhn, and N. Kuster, "The dependence of EM energy absorption upon human head modelling," *IEEE Transactions on Microwave Theory and Techniques*, vol. 44, no. 10, pp. 1865–1873, October 1996.

[23] D. Nashaat, H. Alsadek, and H. Ghali, "Investigation of the human head and new shapes of PIFAs used in mobile communication systems," *Microwave and Optical Technology Letters*, vol. 46, no. 3, pp. 243–248, August 2005.

[24] S. E. Troulis, W. G. Scanlon, and N. E. Evans, "Effect of hands-free leads and spectacles on SAR for a 1.8GHz cellular handset," *Physics in Medicine and Biology*, vol. 48, pp. 1675–1684, June 2003.

[25] A. D. Ball, N. E. Evans, S. J. Burgess, and W. G. Scanlon, "Head-SAR dependence on spectacle frame shape for operator of 450MHz personal radio," *IET Electronics Letters*, vol. 43, no. 20, pp. 1063–1065, September 2007.

[26] K. Ito, "Human body phantoms for evaluation of wearable and implantable antennas," *European Conference on Antennas and Propagation (EuCAP)*, November 2007.

[27] *URL:http://ftp.cordis.europa.eu/pub/ist/docs/fet/comms-23.pdf*.

[28] J. Ryckaert, P. De Doncker, R. Meys, A. de Le Hoye, and S. Donnay, "Channel model for wireless communication around human body," *IEE Electronics Letters*, vol. 40, no. 9, pp. 543–544, April 2004.

[29] A. Alomainy, Y. Hao, A. Owadally, C. G. Parini, Y. Nechayev, C. C. Constantinou, and P. S. Hall, "Statistical analysis and performance evaluation for on-body radio propagation with microstrip patch antennas," *IEEE Transactions on Antennas and Propagation*, vol. 55, no. 1, pp. 245–248, 2007.

[30] K. Fujii, M. Takahashi, K. Ito, K. Hachisuka, Y. Terauchi, K. Y., K. Sasaki, and K. Itao, "Study on the transmission mechanism for wearable device using the human body as a transmission channel," *IEICE Transactions on Communications*, vol. E88-B, pp. 2401–2410, 2005.

[31] K. Fujii, M. Takahashi, and K. Ito, "Electric field distributions of wearable devices using the human body as a transmission channel," *IEEE Transactions on Antennas and Propagation*, vol. 55, no. 7, pp. 2080–2087, July 2007.

[32] G. A. Conway, W. G. Scanlon, and D. Linton, "Low-profile microstrip patch antenna for over-body surface communication at 2.45GHz," *IEEE Vehicular Technology Conference*, April 2007.

[33] G. A. Conway and W. G. Scanlon, "Antennas for over-body-surface communication at 2.45GHz," *IEEE Transactions on Antennas and Propagation*, vol. 57, no. 4, pp. 844–855, April 2009.

[34] P. S. P. See, A. Cai, and Z. N. Chen, "Study on the transmission of RF signals on the human body," *IEE Conference on Wideband and Multi-band Antennas and Arrays*, September 2005.

[35] K. Siwiak and Y. Bahreini, "Radiowave propagation and antennas for personal communications (3rd edition)," *Artech House, Inc., (USA)*, 2007.

[36] L. Vallozzi, H. Rogier, and C. Hertleer, "Dual polarized textile patch antenna for integration into protective garments," *IEEE Journal on Selected Areas in Communications*, vol. 7, no. 1, pp. 440–443, January 2008.

[37] P. Salonen and Y. Rahmat-Samii, "Textile antennas: effects of antenna bending on input matching and impedance bandwidth," *IEEE Aerospace and Electronic Systems Magazine*, vol. 22, no. 3, pp. 10–14, December 2007.

[38] B. Sanz-Izquierdo, F. Huang, and J. C. Batchelor, "Covert dual-band wearable button antenna," *IET Electronics Letters*, vol. 42, no. 12, pp. 668–670, 2006.

[39] B. Sanz-Izquierdo, , and J. C. Batchelor, "A dual band belt antenna," *IEEE International Workshop on Antenna Technology (iWAT)*, 2008.

[40] J. Kim and Y. Rahmat-Samii, "Implanted antennas inside a human body: Simulations, designs and characterizations," *IEEE Transactions on Microwave Theory and Techniques*, vol. 52, no. 8, pp. 1934–1943, August 2004.

[41] D. K. Cheng, "Field and wave electromagnetics (2nd edition)," *Addison Wesley, Inc., (USA)*, 1989.

[42] J. D. Kraus and D. A. Fleisch, "Electromagnetics with applications (5th edition)," *McGraw-Hill, Inc., (USA)*, 1997.

[43] U. S. Inan and A. S. Inan, "Electromagnetic waves," *Prentice-Hall, Inc., (USA)*, 1999.

[44] H. ElKamchouchi and G. Abouelseoud, "Automating the electromagnetric simulation procedure and its possible "fatal" consequences," *IEEE Antennas and Propagation Magazine*, vol. 49, no. 2, April 2007.

[45] Z. Wang, "Design of low-SAR antennas for mobile communications devices," *PhD Thesis, Queen Mary University of London*, August 2001.

[46] C. Gabriel, "Compilation of the dielectric properties of body tissues at RF and microwave frequencies," *Brooks Air Force Technical Report, AL/OE-TR-1996-0037*, 1996.

[47] S. Gabriel, R. W. Lau, and C. Gabriel, "The dielectric properties of biological tis-

sues: II. measurements in the frequency range 10Hz to 20GHz," *Physics in Medicine and Biology*, vol. 41, no. 11, pp. 2251–2269, November 1996.

[48] "Body tissue dielectric properties," *Federal Communication Commision (FCC), URL:http://www.fcc.gov/oet/rfsafety/dielectric.html*.

[49] "Caculation of the dielectric properties of body tissues," *Institute of Applied Physics, Italian National Research Council, URL:http://niremf.ifac.cnr.it/tissprop*.

[50] G. Miller, "Adding GPS applications to an existing design," *RF Design*, pp. 50–57, March 1998.

[51] G. J. K. Moernaut and D. Orban, "Smart phones to surpass pnds in navigation market in 2014," September 2009, *URL:http://www.isuppli.com/News/Pages/smart_Phones-to-Surpass-PNDs-in-Navigation-Market-in-2014.aspx*.

[52] "GPS chip market driven by integration into mobile devices," *In-Stat, URL:http://www.instat.com/press.asp?ID=2140\&sku=IN0703846WT*.

[53] *URL:http://www.garmin.com*.

[54] *URL:http://www.tomtom.com*.

[55] *URL:http://www.nokia.co.uk*.

[56] T. Logsdon, "The Navstar Global Positioning System," *Springer*, 1992.

[57] A. El-Rabbany, "Introduction to GPS: the Global Positioning System," *Artech House Inc., (UK)*, 2002.

[58] Z. Jean-Marie, "GPS basics," 2002, *URL: http://geology.isu.edu/geostac/Field-Exercise/GPS/GPS-basics-u-blox-en.pdf*.

[59] J. B. Tsui, "Fundamentals of Global Positioning System receivers: A software approach (2nd edition)," *John Wiley and Sons Inc., (USA)*, 2000.

[60] R. Bancroft, "Microstrip and printed antenna design (2nd edition)," *SciTech Publishing, Inc., (USA)*, 2009.

[61] L. Boccia, G. Amendola, and G. Di Massa, "A dual frequency microstrip patch antenna for high-precision GPS applications," *IEEE Antennas and Wireless Propagation Letters*, vol. 3, pp. 157–160, 2004.

[62] G. J. K. Moernaut and D. Orban, "GNSS antennas," *GPS World*, February 2009, *URL: http://www.gpsworld.com/gnss-system/receiver-design/innovation-gnss-antennas*.

[63] R. B. Langley, "A primer on GPS antennas," *GPS World*, pp. 50–55, July 1998.

[64] S. Kingsley, "GPS antenna design for mobile phones," *URL:http://www.electronicsweekly.com/Articles/2007/04/11/41146/GPS-antenna-design-for-mobile-*

phones.htm.

[65] T. Haddrell, N. Ricquier, and M. Phocas, "Innovation: Mobile-phone GPS antennas: Can they be better?" *GPS World, URL:http://www.gpsworld.com/professional-oem/component-technologies/innovation-mobile-phone-gps-antennas-9457.*

[66] N. Padros, J. I. Ortigosa, J. Baker, M. F. Iskander, and B. Thornberg, "Comparative study of high-performance GPS receiving antenna designs," *IEEE Transactions on Antennas and Propagation*, vol. 45, no. 4, pp. 698–706, April 1997.

[67] C. Hua-Ming, W. Yang-Kai, L. Yi-Fang, L. Che-Yen, and P. Shan-Cheng, "Microstrip-fed circularly polarized square-ring patch antenna for GPS applications," *IEEE Transactions on Antennas and Propagation*, vol. 57, no. 4, pp. 1264–1267, April 2009.

[68] J. O. Nielsen and G. F. Pedersen, "Mobile handset performance evaluation using radiation pattern measurements," *IEEE Transactions on Antennas and Propagation*, vol. 54, no. 7, pp. 2154–2165, July 2006.

[69] J. B. Andersen and F. Hansen, "Antennas for VHF/UHF personal radio: A theoretical and experimental study of characteristics and performance," *IEEE Transactions on Vehicular Technology*, vol. 26, no. 4, pp. 349–357, 1977.

[70] T. Taga, "Analysis for mean effective gain of mobile antennas in land mobile radio environments," *IEEE Transactions on Vehicular Technology*, vol. 39, no. 2, pp. 117 – 131, May 1990.

[71] A. L. Davidson and W. J. Turney, "Mobile antenna gain in multipath environment at 900MHz," *IEEE Transactions on Vehicular Technology*, vol. 26, no. 4, pp. 345–348, November 1977.

[72] K. Kalliola, K. Sulonen, H. Laitinen, O. Kivekas, J. Krogerus, and P. Vainikainen, "Angular power distribution and mean effective gain of mobile antenna in different propagation environments," *IEEE Transactions on Vehicular Technology*, vol. 51, no. 5, pp. 823–838, September 2002.

[73] W. C. Jakes, "Microwave mobile communications," *John Wiley and Sons Inc., (USA)*, 1974.

[74] A. Ando, T. Taga, A. Kondo, K. Kagoshima, and S. Kubota, "Mean effective gain of mobile antennas in line-of-sight street microcells with low base station antennas," *IEEE Transactions on Antennas and Propagation*, vol. 56, no. 11, pp. 3552–3565, November 2008.

[75] K. Ogawa and T. Uwanao, "Mean effective gain analysis of a diversity antenna for portable telephones in mobile communication environments," *Electronics and Communication in Japan (Part I: Communications)*, vol. 83, no. 3, pp. 88–96, December 2000.

[76] T. W. C. Brown, "Antenna diversity for mobile terminals," *PhD Thesis, University*

of Surrey, 2002.

[77] P. L. Carro and J. de Mingo, "Mean effective gain of compact WLAN genetic printed dipole antennas in indoor-outdoor scenarios," *International Conference on Personal Wireless Communications (PWC)*, pp. 275–283, September 2006.

[78] Z. Ying and V. Plicanic, "Characterization of multi-channel antenna performance for mobile terminal by using near field and far field parameters," *COST 273 TD (04) (095)*, June 2004.

[79] M. G. Douglas, M. Okoniewski, and M. A. Stuchly, "A planar diversity antenna for handheld PCS devices," *IEEE Transactions on Vehicular Technology*, vol. 47, no. 3, pp. 747–754, August 1998.

Chapter 3

On-Body Bluetooth Transmission Mechanism

The development of portable devices including mobile phones, Personal Digital Assistants (PDAs), Personal Navigation Devices (PNDs) and laptops has brought a revolution in the field of wireless communications. This rapid growth of research and development has been promoted by the wider approach, mobility and ease of use provided by these devices. It has necessitated the advances of several portable and wearable technologies, such as Bluetooth headsets within Wireless Personal Area Networks (WPAN) and Wireless Body Area Networks (WBAN). Since, the human body is an integral part of the WPAN/WBAN applications, such wearable devices use the human body as a communication channel. Hence, a comprehensive understanding of the transmission mechanism between these devices is vital.

This chapter presents an investigative study to characterise the electromagnetic transmission between a body-mounted Bluetooth headset antenna and a mobile phone handset antenna. Commercially used planar inverted F antennas (PIFA) on the mobile phone handset and a meander line monopole antennas on the headset have been used in this study. Various factors affecting the on-body communication links including handset-to-

body separation, handset antenna orientation and presence of blocking objects have been considered. A thorough numerical modelling, supported by the measurements, has been carried out to demonstrate the importance of surface waves in the on-body Bluetooth transmission.

3.1   Characterisation of On-body Propagation Channel

The electromagnetic interaction between the human body and antennas has been studied for many years [1, 2]. It is now well established fact that the close proximity of the human body degrades the performance of the antennas significantly [1–9]. The very lossy nature of human tissues causes high level of losses over the communication spectrum. The resulting phenomena affects the antenna performance by introducing distortion in the radiation pattern, reduction in radiation efficiency and detuning in antenna input impedance [5–9].

In principle, the human body can be used as a communication channel for different devices that are located within a close proximity as well as body-worn devices. A typical scenario may involve a Bluetooth enabled body-worn mobile handset and a Bluetooth headset forming a similar wireless communication link. Characterisation of such on-body channel has attracted the interest of many researchers around the world. Various characterisation criteria have been taken into account to evaluate this communication channel including path gain, radiation pattern, gain and efficiency of different antennas [4, 7–9]. The influences of varying the body postures and the different antenna types on the on-body communication channel, as well as the on-body channel path gain for a moving human body have also been studied [7, 8].

The on-body wireless communication link involves two mediums for the transfer of signals, the human body and the air. It has been noticed that when there is no line-of-sight and reflecting objects, the transfer of electromagnetic energy between two body-mounted antennas takes place mostly in the form of surface waves [8–10]. These waves are

generated in, and guided by the air-body interface. Studies have also shown that these surface waves may play an important role in UWB communications [6]. However, most of these studies were only concerned with the models of a small part of the human body with shorter on-body channels and generic antennas. In practical scenarios, on-body communication link requires a better insight into the on-body radio wave propagation including effects of antenna orientations and presence of blocking objects so that possible measures can be taken to improve the link budget. Therefore, this study examines the role of these surface waves in practically used larger on-body Bluetooth links involving a complete human body model.

3.2 Antennas for On-body Communication

Two commercially available antennas operating at 2440 MHz are used in this study. The antenna parameters are numerically investigated using CST Microwave Studio®️ and verified through measurements.

3.2.1 Headset Antenna

The headset antenna used in this study is a meander line monopole. The antenna is implemented in one of Sony Ericsson's Bluetooth headsets. The antenna is mounted on one end of the PCB (FR4), as illustrated in Figure 3.1 with a ground plane of 55 mm×12 mm. The headset antenna prototype used in measurements is shown in Figure 3.13(b).

Simulations have been carried out in CST Microwave Studio®️ using a discrete port with 50 Ω impedance to represent the commonly used 50 Ω coaxial port feed. Figures 3.1-3.4 show the antenna performance in free space. It can be seen from Figure 3.2 that the antenna has a very wide coverage over the Bluetooth band. It has a -10 dB bandwidth of 592 MHz, ranging from 2142 MHz to 2734 MHz. The 3-D radiation pattern (Figure 3.4) indicates a typical donut shape with a maximum gain value of 2.7 dBi. It is
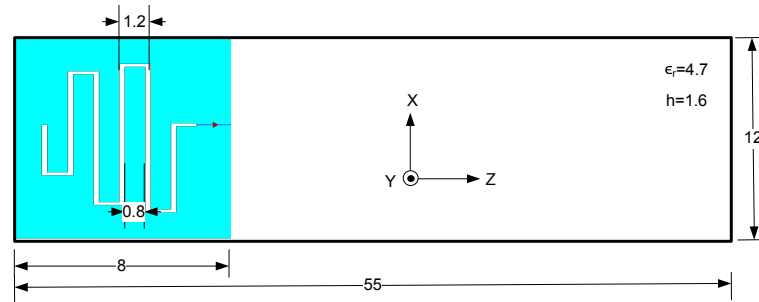
Figure 3.1: Schematic of headset meander line monopole antenna (all lengths are in mm)
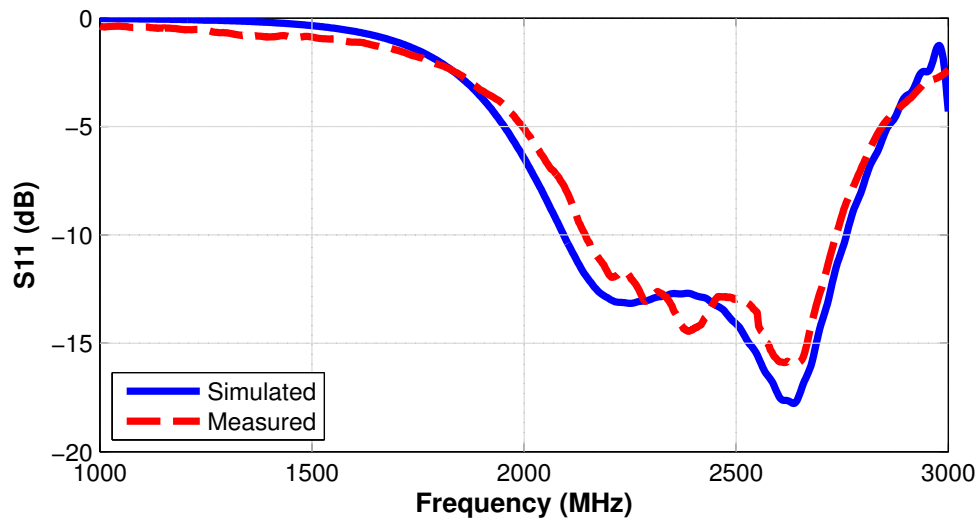
Figure 3.2: Simulated (blue) and measured (red) S11 curves for headset meander line monopole antenna at 2440 MHz

verified in experiments by measuring the 2-D patterns on the XY and YZ planes in an anechoic chamber in Antenna Measurement Lab at QMUL, shown in Figure 3.3. The measurements agree well with the simulated results.

3.2.2 Handset Antenna

A mobile handset (one of Sony Ericsson's mobile phone model K750i) with a PIFA antenna as the radiating element has been modelled in this study. The PIFA is mounted on a ground plane of 100 mm×40 mm and fed by a coaxial port, as shown in Figure 3.5. The handset antenna prototype used in the measurements is shown in Figure 3.13(b).

(a) XY plane   (b) YZ plane
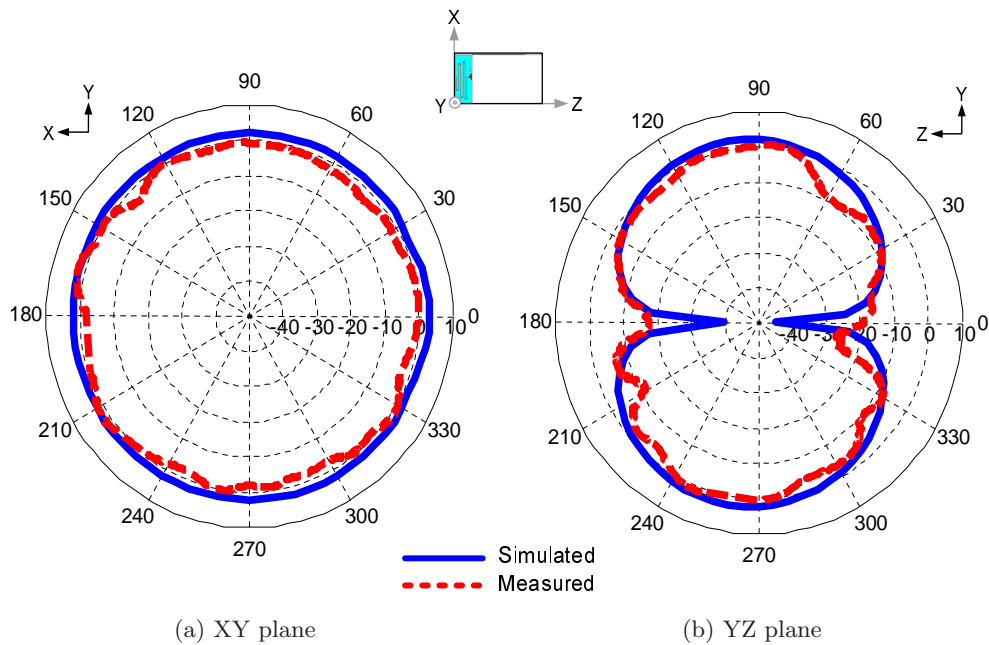
Figure 3.3: Simulated (blue) and measured (red) 2-D radiation patterns of headset meander line monopole antenna at 2440 MHz
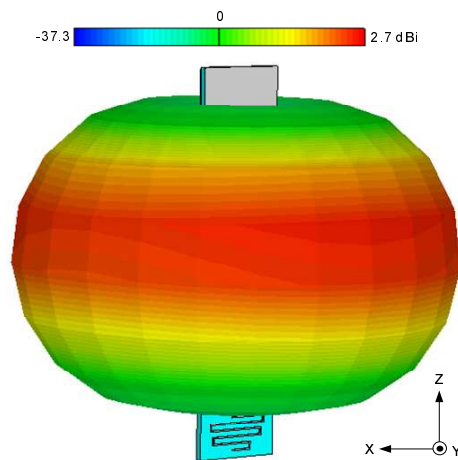
Figure 3.4: Simulated 3-D radiation pattern for headset meander line monopole antenna at 2440 MHz

The antenna itself is not visible as it is covered by the mobile casing.

Figures 3.5-3.8 show the antenna performance illustrating simulated and measured S11 curves, simulated and measured 2-D radiation patterns and simulated 3-D radiation pattern. It is noted that the measured resonance is shifted slightly upwards due to the fact that the antenna is surrounded by other components including LCD, camera and
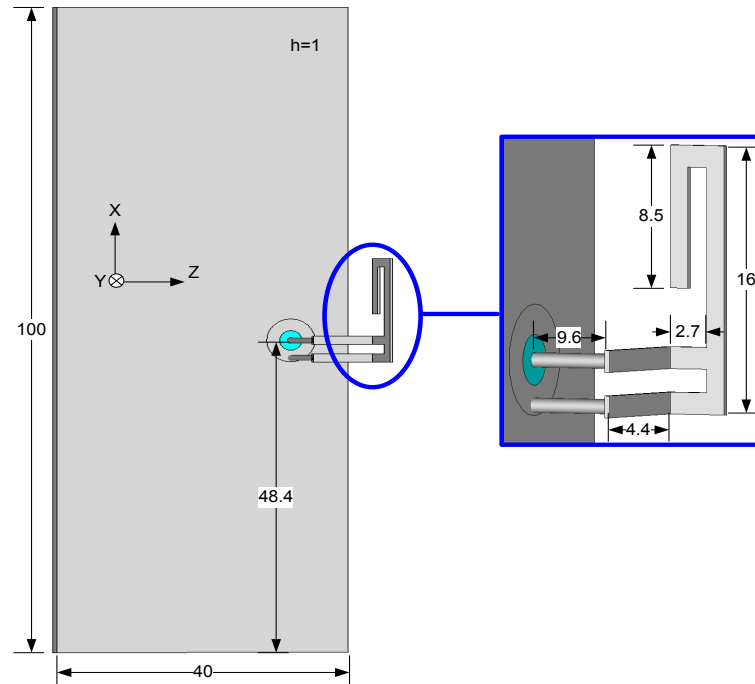
Figure 3.5: Geometrical structure of handset PIFA antenna (all lengths are in mm)
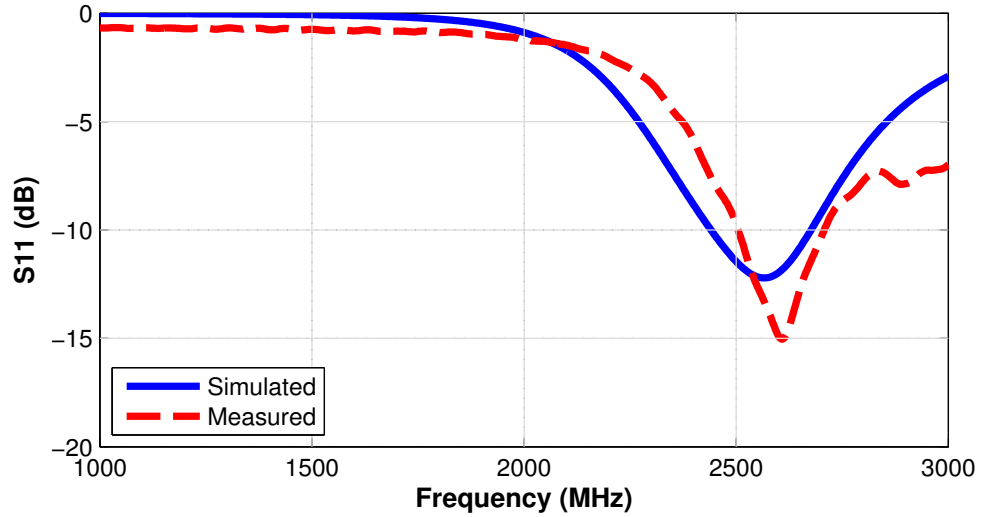
Figure 3.6: Simulated (blue) and measured (red) S11 curves for handset PIFA antenna at 2440 MHz

covered by a chassis, that are not included in the simulated model. Nevertheless, the measured and simulated S11, illustrated in Figure 3.6, both cover the -10 dB bandwidth of 206 MHz in the required frequencies which is sufficient for the Bluetooth applications. Figure 3.8 shows the simulated 3-D radiation pattern with a maximum gain of 4.09 dBi.

(a) XY plane (b) YZ plane
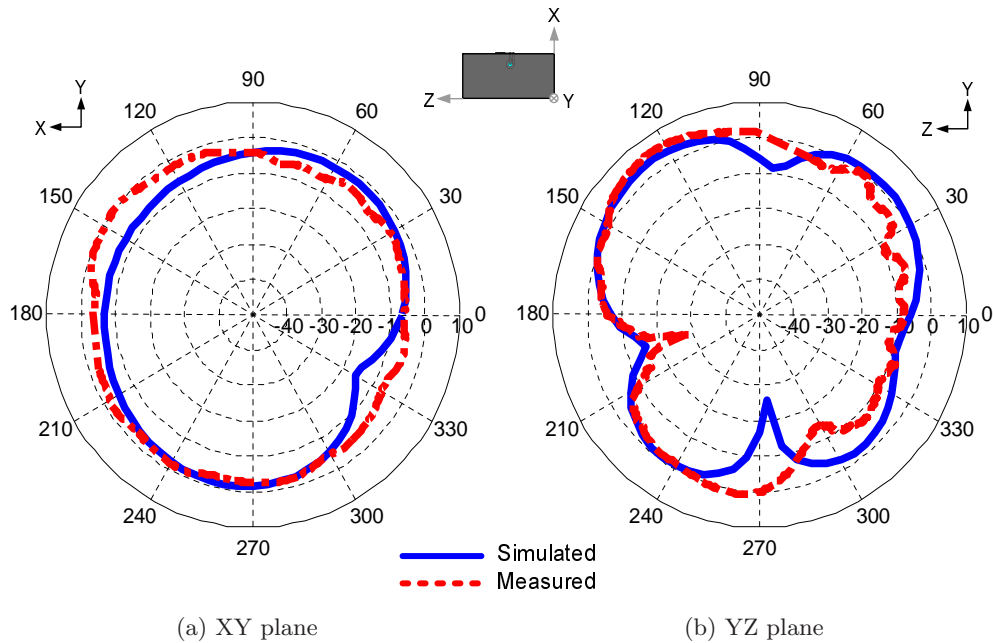
Figure 3.7: Simulated (blue) and measured (red) 2-D radiation patterns of handset PIFA antenna at 2440 MHz
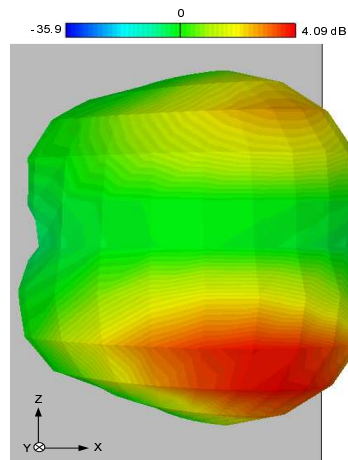
Figure 3.8: Simulated 3-D radiation pattern for handset PIFA antenna at 2440 MHz

The comparison of simulated and measured 2-D radiation patterns on the XY and YZ planes is illustrated in Figure 3.7 where an acceptable agreement between the two results can be observed.

The presented comparison of the simulated and measured results for the headset and handset antennas also indicate that although, a worst case scenario in terms of PCB components can be realised by replacing them with a perfect electric conductor (PEC)

in the numerical model, the protective casing of the two devices affects the performance quite significantly. This effect is more visible in case of handset antenna as a difference of 3 dB in S11 (Figure 3.6) and 5 dBi in the radiation patterns at 2440 MHz in certain directions (Figure 3.7) can be noted. Therefore, besides increasing the complexity, inclusion of the casing in the modelled structure would have given a more realistic operating scenario for the two antennas.

3.3   Numerical Modelling of Human Body

The human body is primarily made of four types of tissues: skin, fat, muscles and bones. Muscle is the most abundant tissue in the human body while skin is the largest organ of the human body with a thickness of 0.07-2 mm depending on the part of the body. The human skeleton has 206 bones of different sizes and shapes while the fatty tissues are found in almost all parts of the body. In a healthy person of average weight, the muscle tissues contribute about 40%, fat is nearly 30% while bones make up 20% of total body weight. The remaining body weight is composed of the skin and other organs including connective tissues, blood, etc.

In this study, a single layer human body model has been developed using the CST Microwave Studio®. Owing to the complexity of the human body composition, the tissue properties have been averaged out by estimating weight of the main tissue contents.

Table 3-1: Electric properties of specific human tissues at 2440 MHz used within the constructed homogeneous body model

Tissue	Electric Properties	
	Dielectric Constant (ε_r)	Tissue Conductivity (σ) (S/m)
Bone	18.24	0.81
Fat	5.28	0.11
Muscle	52.34	1.73
Skin	38.02	1.46
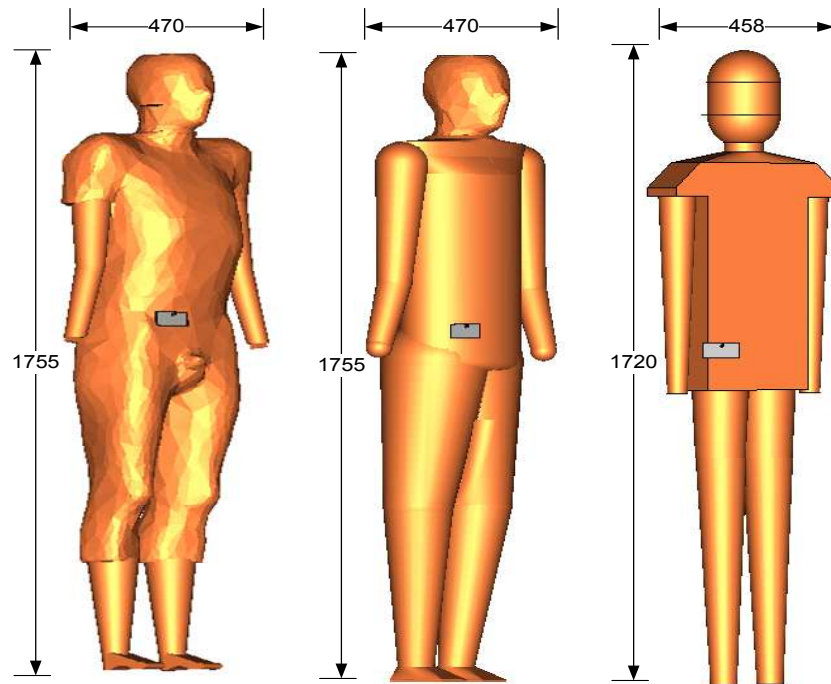
(a) High-resolution model   (b) Medium-resolution model   (c) Low-resolution model

Figure 3.9: Structure of high-resolution, medium-resolution and low-resolution numerical models of the human body with on-body positioned headset and handset antennas (all lengths are in mm)

Hence, the homogeneous human body model is approximated to include 10% skin, 30% fat, 40% muscle and 20% bone, which leads to an averaged relative permittivity of 28.16 and conductivity of 1.14 S/m at 2440 MHz. The dielectric properties of the human body tissue are taken as described in [11–13]. The values for the four types of tissues at 2440 MHz used in this study are summarised in Table 3-1.

The high level discretisation of the whole-body model represents an average built human with a height of 1755 mm, as shown in Figure 3.9(a). An adaptive meshing scheme has been implemented where finer cell sizes have been used around the vital parts of the body. This scheme reduces the required number of cell volumes (voxels) in the computational domain significantly, hence the computation and time requirements. The Perfectly Matched Layer (PML) absorbing boundary conditions are used [14], with a maximum mesh cell size of 10 mm near the boundaries of the computational domain and a minimum mesh cell size of 0.08 mm at the edges of the solids in the computational

domain. The headset antenna was placed 10 mm away from the head at the approximate location of the ear in order to incorporate the clearance for the cover assembly. The handset antenna was placed on the right side of the body model at the waist realising a typical body worn position, with the same separation of 10 mm from the body to add the cover assembly clearance.

The choice of the right model for the study is very critical as computational efficiency decreases with increase of model resolution and its size. In this study, the main interest lies in the investigation of the surface wave behaviour in on-body communication links. Earlier publications have reported that in such studies, simple human body models could also deliver accurate results [5]. To confirm this, two simplified models have also been designed. First, the high-resolution human body model is modified keeping the head as a high-resolution object while the remaining organs are simplified. This medium-resolution model represents a nearly realistic shape of an average built human with a height of 1755 mm and thickness of 220 mm, as illustrated in Figure 3.9(b). This model has benefits of reduced complexity and flexibility in terms of re-positioning body parts (e.g., sitting, standing, talking and holding phone positions). Finally, a low-resolution simpler homogeneous model following the average physical size of a volunteer is developed. The complete height of this low-resolution body model is 1720 mm. The thickness of the torso for this low-resolution model is 120 mm while radius of the head is 86 mm. The location of the headset and the handset antennas were kept the same as above with 10 mm separation from the body surface.

The electric field distributions on the body surface are investigated on the cross-section plane through the headset as shown in Figure 3.12 and are then compared for the three models. The fields are normalised to the value at the feeding point of the horizontally placed handset antenna as presented in Figure 3.10. From these results, it is obvious that the three models support a similar field pattern. In the three cases, the field strength at the headset antenna is in the order of -18 dB. It is also evident from Figure 3.10 that the lower part of the body (knees to feet) is not a contributor to

(a) High-resolution model   (b) Medium-resolution model   (c) Low-resolution model
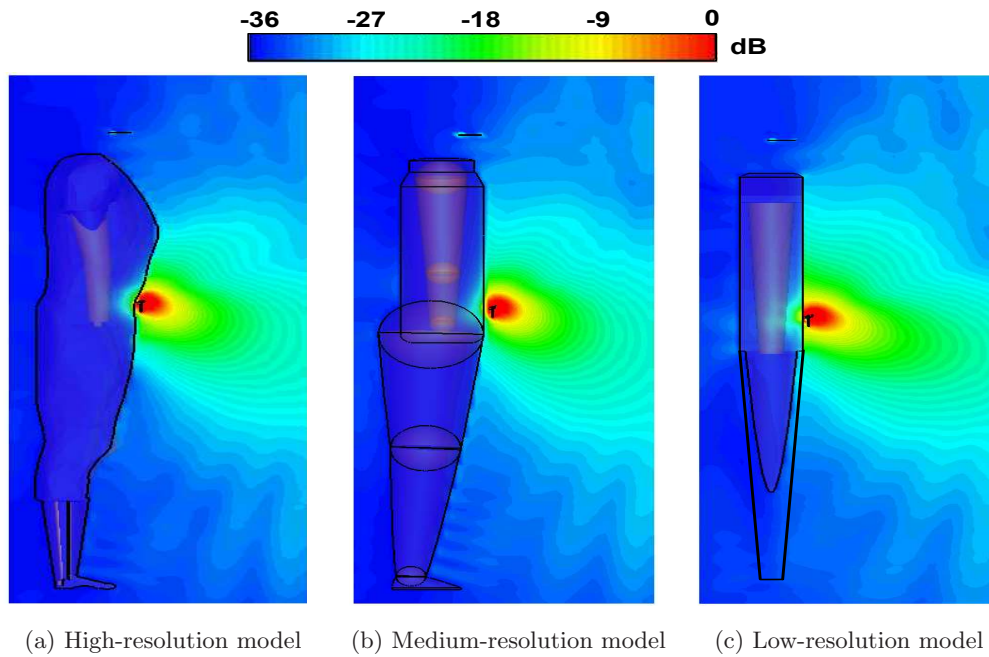
Figure 3.10: Comparison of normalised electric field distributions and on-body surface waves on realistic high-resolution and medium-resolution whole body models and simple thigh-to-head body model for horizontally oriented handset antenna on the cross section plane through headset
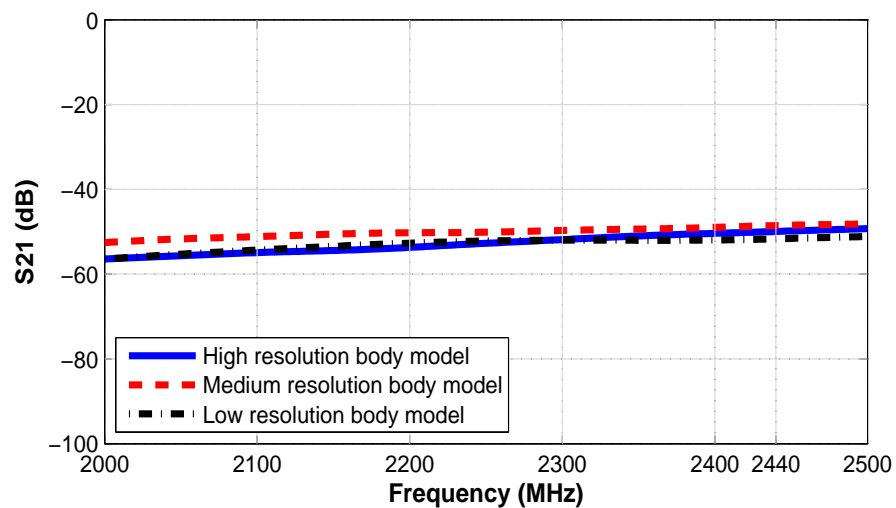
Figure 3.11: Comparison of simulated path gain curves for horizontal handset PIFA antenna using three types of human body models

the Bluetooth on-body link between the handset and the headset antennas and only the upper part of the body (from thighs to head) is the major area of concern in this study.

The simulated path gains obtained using the three models of the human body are also compared in Figure 3.11. It also shows that the three models produce very similar results. The difference between the path gains for the detailed high-resolution model and simpler low-resolution model is only 1.7 dB at 2440 MHz. These factors lead to the choice of a simpler low-resolution model for further investigations. Also, based on the electric field distribution results, the human body model is modified to exclude the lower part of the body (knees to feet) from the simulation setup for the sake of computational efficiency. This approach reduces the effective length of the body model to 1100 mm (Figure 3.12). The close agreement between the simulated and measured values of path gain observed in the next section further increases the level of confidence in the use of this simple model whose benefits in terms of computational efficiency are clear.

3.4   Simulation and Measurement Set-Up

Two orientations of the handset antenna, horizontal and vertical, have been considered. In the horizontal arrangement, the antenna ground plane is parallel to the body, longitudinal in x-axis with the PIFA at the top of the ground plane. In the vertical arrangement, the antenna is rotated 90°, now having the ground plane longitudinal in z-axis with the PIFA on the left as described in Figure 3.12. The vertical distance between the headset and the handset antennas is 620 mm.

The Bluetooth link is characterised in terms of average path gain ($S21$). The simulated results are confirmed through the measurements using Agilent HP8720ES Vector Network Analyser. The headset and handset antennas have been worn by the volunteer arranged in the same configurations as were modelled. The two antennas are fed by low-loss coaxial cables of 5 m length. The coupling between two feed cables is measured separately and a loss variation of 0.5 dB (maximum) is found on-body. The measurement set-up in an anechoic chamber is illustrated in Figure 3.13(a).
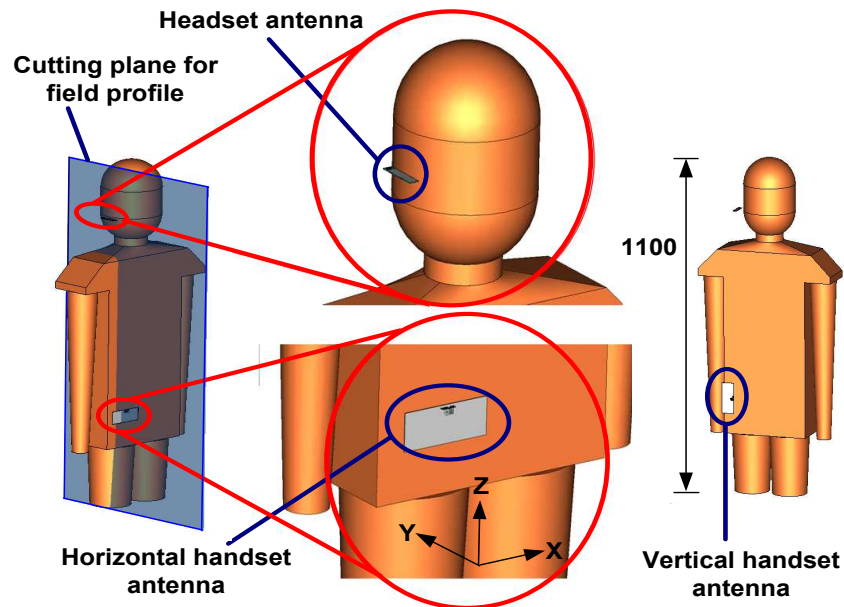
Figure 3.12: Simulation set-up with low-resolution thigh-to-head numerical model of the human body and on-body test configurations with headset and handset antenna positions and location of cross-section plane for observation of electric field distribution (all lengths are in mm)

3.5 On-Body Bluetooth Transmission

3.5.1 Transmission in Absence of Human Body

Initially, the Bluetooth link is studied in the absence of the human body. In this scenario, the handset PIFA antenna and the headset meander line monopole antenna are placed exactly at the same locations where they would be in the presence of the human body. Therefore, the test set-up is essentially the same as described in Figure 3.12, but without the presence of the human body model. To locate these exact positions, a cube of polystyrene replicating the on-body gap between the two antennas was used.

It is observed that the direct link between the handset and the headset antenna is -36.8 dB in simulation and -36.5 dB in measurement at 2440 MHz when the handset antenna is placed horizontally, as illustrated in Figure 3.14. Placing the handset antenna in vertical orientation causes some drop in path gain and the simulated and measured values of the
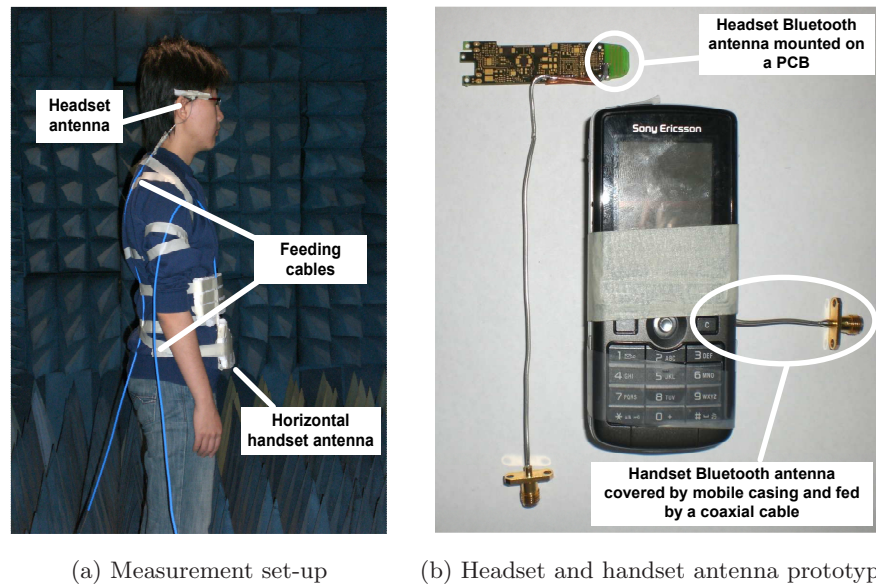
(a) Measurement set-up   (b) Headset and handset antenna prototypes

Figure 3.13: Measurement set-up with headset and handset antenna prototypes for the study of on-body Bluetooth transmission mechanism in an anechoic chamber

path gain appears to be -38.3 dB and -37.2 dB respectively, as shown in Figure 3.15. This decrease in the path gain can be easily understood as the changing orientation of the antenna varies its polarisation. The directivity of the vertically oriented handset antenna is also dropped in the upward direction (z-axis) as shown in the radiation pattern in Figure 3.8. In general, the simulated and measured results represent a close agreement to each other.

3.5.2 Transmission in Presence of Human Body

The Bluetooth link is then investigated for the on-body transmission with body-worn handset and headset antennas. Both horizontal and vertical placements of the handset antenna are taken into account. The simulated and measured average path gain between the body-worn, horizontally placed handset and the headset antennas is found to be -51.6 dB and -52.0 dB respectively at 2440 MHz, as indicated in Figure 3.14. On the other hand, the path gain for the body-worn vertically placed handset antenna configuration is found to be -49.1 dB in simulation whereas -47.6 dB in measurement as shown in Figure 3.15. Table 3-2 summarises the simulated and measured results of the average path gains
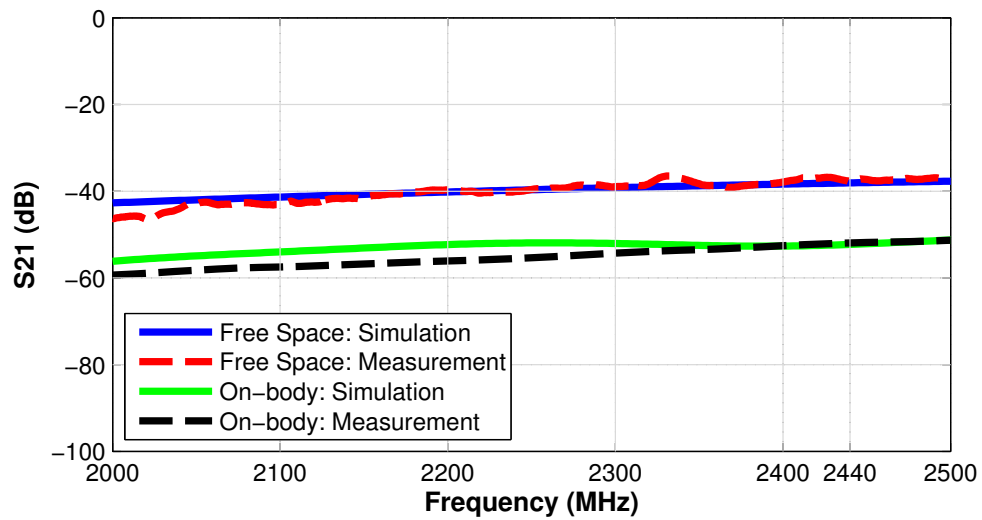
Figure 3.14: Comparison of simulated and measured path gains for horizontally placed handset antenna with and without presence of the human body

between the handset and the headset antennas in different test configurations.

It is not surprising that the path gain drops substantially in the presence of the human body, which blocks the line-of-sight between the headset and handset antennas. However, the decrease in link differs with the change in handset antenna orientation: 14.8 dB (simulation) or 15.5 dB (measurement) in case of horizontally placed handset
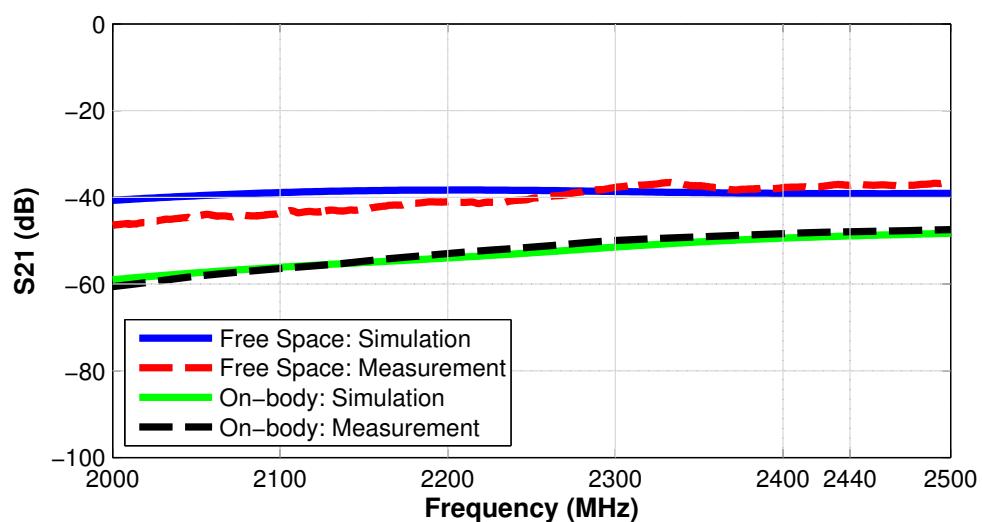
Figure 3.15: Comparison of simulated and measured path gains for vertically placed handset antenna with and without presence of the human body

antenna and 10.8 dB (simulation) or 10.4 dB (measurement) in case of vertically placed handset antenna. This apparent difference caused by the orientation of the handset antennas is associated with varying polarisation and will be explained when the role of the surface waves is addressed in the next section.

The simulated path gains have shown a good overall agreement to the measured values. A maximum difference of 1.5 dB occurred in the case of the vertically placed handset antenna on-body. The reasons for this error lie in small differences between the computer model and the experiment, such as the shape of the body, tissue properties, presence of clothes and feeding cables. However, this close agreement between the two values validates the computer models and serves as a benchmark for further study of the on-body communication link. It also justifies the choice of a simple homogeneous model to study the on-body Bluetooth transmission mechanism in the following section.

3.6 Role of Surface Waves in On-Body Bluetooth Transmission

The path gain values obtained in the previous section are useful in designing the Bluetooth enabled handsets and headsets. However, further insights into the electromagnetic wave propagation are required in order to devise means to improve this communication

Table 3-2: Simulated and measured values of the average path gain ($S21$) for different test configurations, with different handset antenna orientations and with and without human body at 2440 MHz

Test Set-up	Average Path Gain ($S21$) (dB)	
	Simulated	Measured
Horizontal handset antenna, without body	-36.8	-36.5
Horizontal handset antenna on-body	-51.6	-52.0
Vertical handset antenna , without body	-38.3	-37.2
Vertical handset antenna on-body	-49.1	-47.6
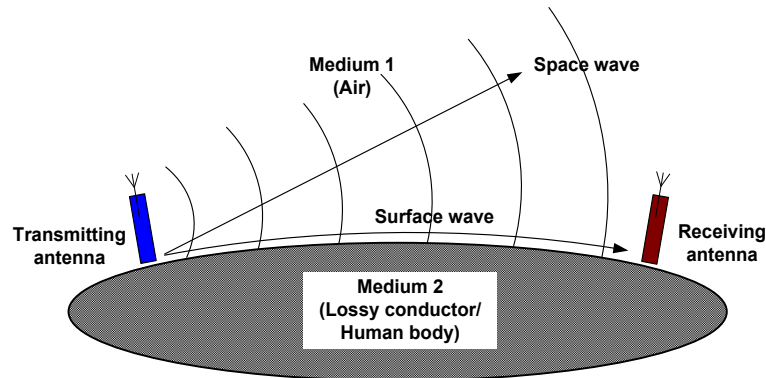
Figure 3.16: Illustration of radio wave propagation between two antennas positioned above a lossy conductor via space (air) wave and surface wave

link. The electromagnetic energy travels from a transmitting antenna to a receiving antenna placed at short distances above a lossy conductor such as the human body in two ways; air waves and the surface waves [15]. When a wave hits a thin layer of a lossy conductor (the human body tissue in current case as the penetration depth is very small) at an arbitrary incidence angle, reflection or refraction of the wave components occurs. However, the boundary conditions force some of the wave components to propagate along the curvature of the interface of the two mediums resulting in the formation of the surface waves [16, 17] as depicted in Figures 3.16 and 3.17. In the absence of a line-of-sight link, these surface waves play an important role to establish an efficient wireless communication link. Attenuation of these surface waves depends considerably on the electric properties of the surface [18, 19].

In this section, the distribution of electric field magnitude and electric field strength is employed to investigate the role of surface waves in the on-body Bluetooth link. The electric field strength is calculated on the human body surface along the path between the two antennas. The electric field distribution is plotted on the cross-section plane normal to the x-axis cutting through the headset antenna as illustrated in Figure 3.12 and on the front surface of the body, respectively. The electric field is normalised to the value at the feeding point of the handset PIFA antenna. Different scenarios including changing handset antenna orientation, varying handset-body separation and presence
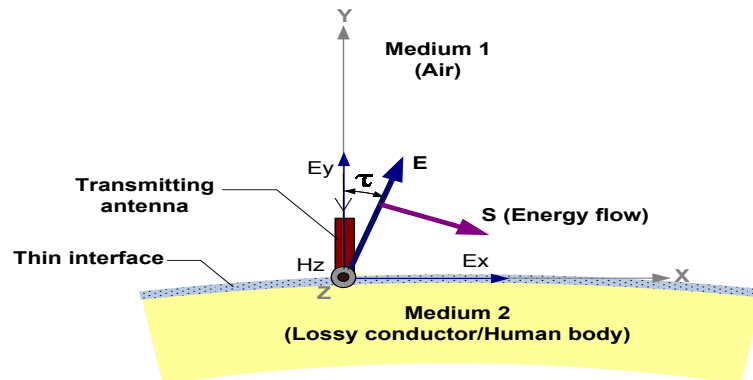
Figure 3.17: Generation of surface waves on the interface of air and lossy conductor

of blocking object in the transmission path at varying gaps from the human body are considered to study the importance of the surface waves.

3.6.1 Effects of Handset Antenna Orientation

The two orientations of the mobile handset PIFA antenna; horizontal and vertical are re-investigated to study the surface wave's behaviour. Figures 3.18 and 3.19 show distributions of normalised electric field magnitude, viewed on the cross-section plane through the headset and the front surface of the body for horizontal and vertical orientation, respectively. A zoomed-in view, highlighting the strength of on-body surface waves for the two orientations of the handset antenna, is depicted in Figures 3.20 and 3.21. It is evident from the electric field distributions in Figure 3.18 and Figure 3.19 that the surface waves are generated on the surface of the human body. These surface waves are guided by the air-body interface and creeps towards the headset antenna. These surface waves reach almost all parts of the body but their decay is rapid due to high losses of the human body tissues as illustrated in Figure 3.18(b). Also, the direction of propagation of stronger air waves is away from the body because of reflections and hence, little contribution can be noted at the headset antenna.

The electric field distribution for the vertical oriented handset antenna in Figure 3.21 depicts much stronger surface waves as compared to the horizontal oriented hand-

(a) Cross-section plane view · (b) Front view
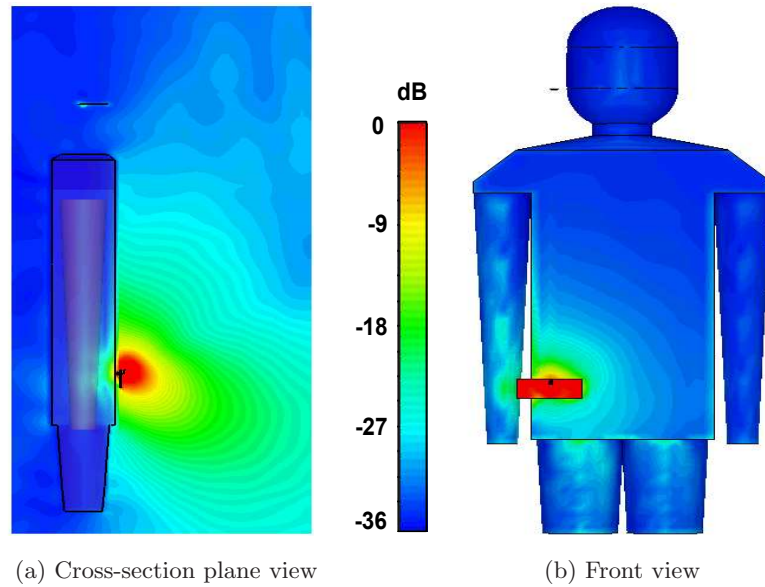
Figure 3.18: Normalised electric field distribution and on-body surface waves for horizontally oriented handset antenna

(a) Cross-section plane view · (b) Front view
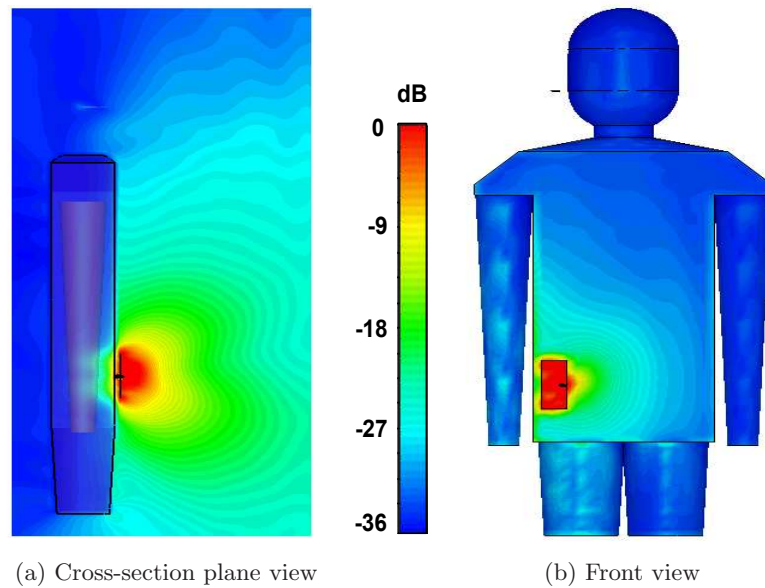
Figure 3.19: Normalised electric field distribution and on-body surface waves for vertically oriented handset antenna

set antenna (Figure 3.20). It is due to the fact that stronger vertical polarised signal generated by the vertical placement of the handset antenna results in the electric field perpendicular to the human body surface. It minimises the contact of the electric field with the human body reducing the energy absorption in the lossy tissues. On the other

hand, the electric field is parallel to the human body surface when the radio signal is in horizontal polarisation. A constant contact with the human body surface of such wave makes it to attenuate more rapidly as evident from Figure 3.18. Therefore, the vertical orientation of the handset antenna forms a stronger on-body link with the headset antenna than the one observed for the horizontal placement of the handset. The path gains for the two orientations given in Table 3-2 further confirm it with higher values for the vertically placed handset antenna than that with a horizontally placed handset antenna. Moreover, a weaker link for the vertically placed handset antenna in the absence of the human body, observed in the previous section, further supports the argument.

The electric field strength on the body surface in Figure 3.18(b) and 3.19(b) is used to get more insight of the surface wave behaviour in on-body transmission mechanism. The electric field strength for both the horizontal and vertical placed handset antennas is plotted as a function of distance towards the headset antenna. The origin of the three axes is located on the right side of the body, above the handset antenna. The starting point in vertical direction (the origin of z-axis) for all the plots are chosen 180 mm away from the handset antenna to avoid the antenna near field region as shown in Figure 3.22(a).

Figure 3.23 illustrates the electric field strength along the width of the body surface (from right to left: -80 to 280 mm) for horizontally placed handset antenna whereas Figure 3.24 describes the electric field strength for vertical orientation of the handset antenna in the same fashion. The curves on the two extremes are excluded to avoid the diffraction effects on the edges. Similarly, Figures 3.25 and 3.26 presents the electric field strength in front of the human body, starting from the body surface and extending to a separation of 280 mm, for both the horizontal and vertical oriented handset antennas respectively.

Figure 3.24 (vertically oriented handset antenna), shows that in the region of 300 mm to 500 mm (from chest to ear) along the body surface (in the z-axis direction), the
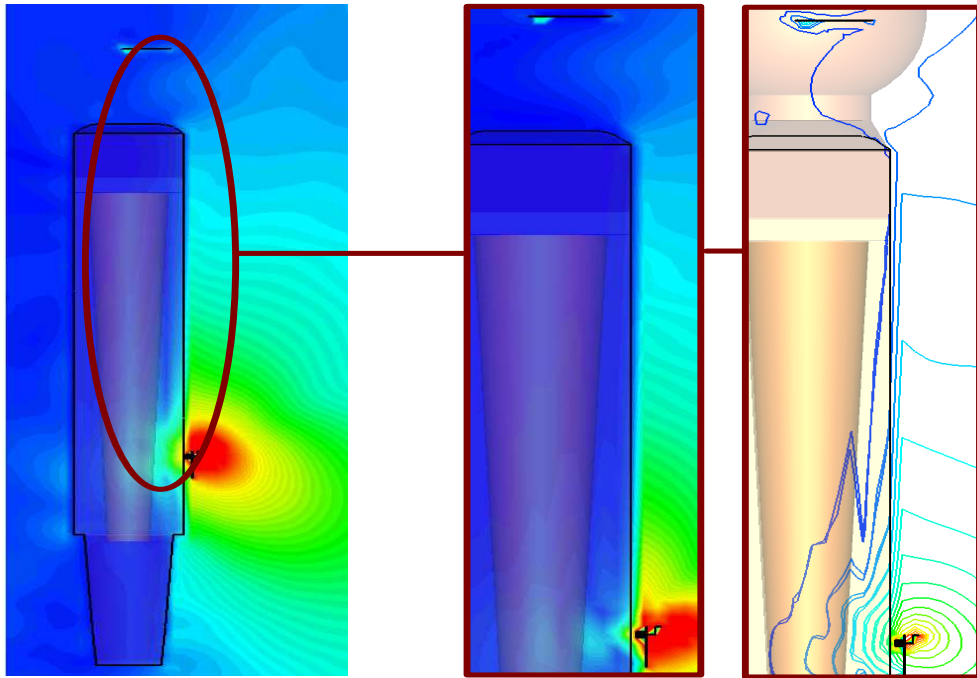
Figure 3.20: On-body surface waves for horizontal handset antenna
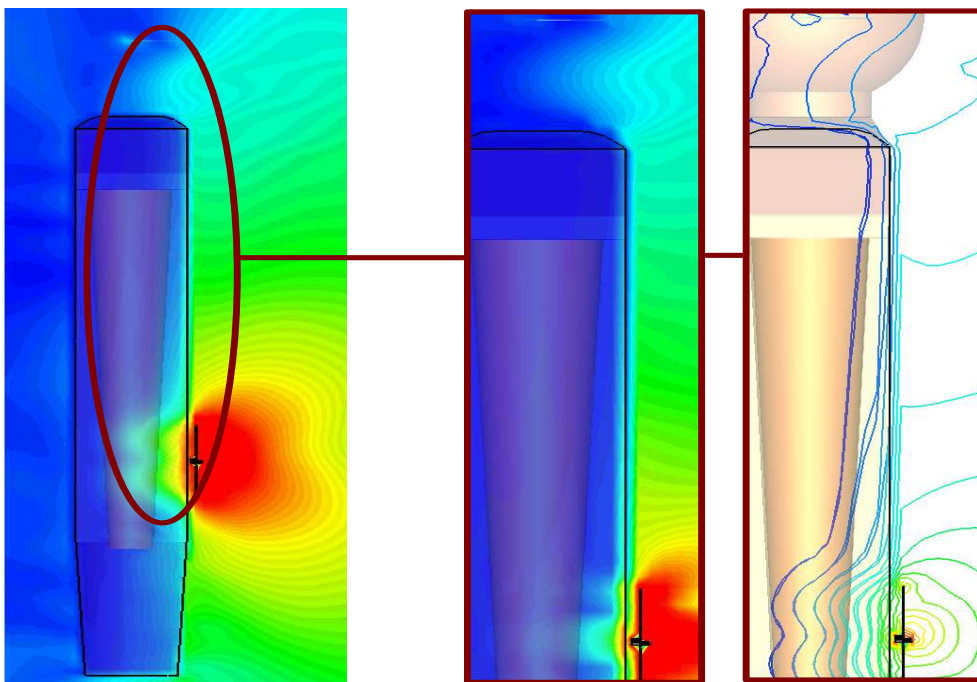
Figure 3.21: On-body surface waves for horizontal handset antenna

curves descent very gradually indicating a slower decrease in the electric field strength and hence the surface waves. On the other hand, the slope of the curves in this region

(a) Defined curves from right-to-left on body surface (x-axis)

(b) Defined curves away from body surface (y-axis)
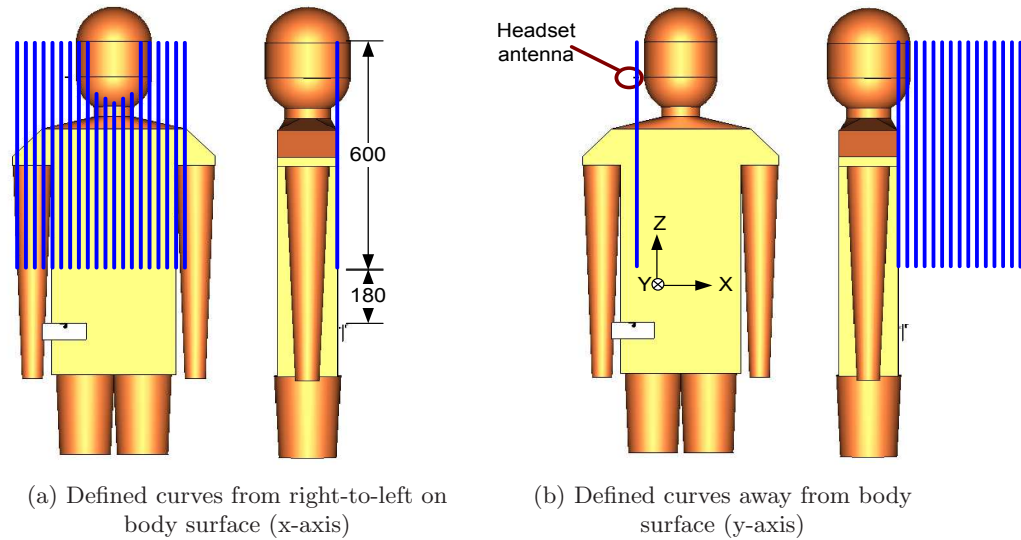
Figure 3.22: Definition of curves to observe the received electric field strength between the handset and headset antennas on the body surface (right-to-left) and away from the body surface (all lengths are in mm)

has comparatively sharper decline when the handset antenna is placed in horizontal orientation in Figure 3.23, which illustrates more rapid decay of the surface waves. Also, the strength of the electric field for vertical orientation of the antenna in front of the body is greater as compared to that observed along the body surface depicting less contact with the lossy body surface as shown in Figure 3.26, observed on the curves defined away from the body (Figure 3.22(b)). An opposite trend could be noted in Figure 3.25 showing greater contact of the electric field generated by the horizontal orientation of the handset antenna with the body surface. Hence, the surface wave component of the vertically polarised signal undergoes less attenuation and results in a much stronger communication link. This, along with the field distributions shown in Figure 3.18 and 3.19 confirms that the surface waves have a more dominant role than the air waves in the Bluetooth on-body link.
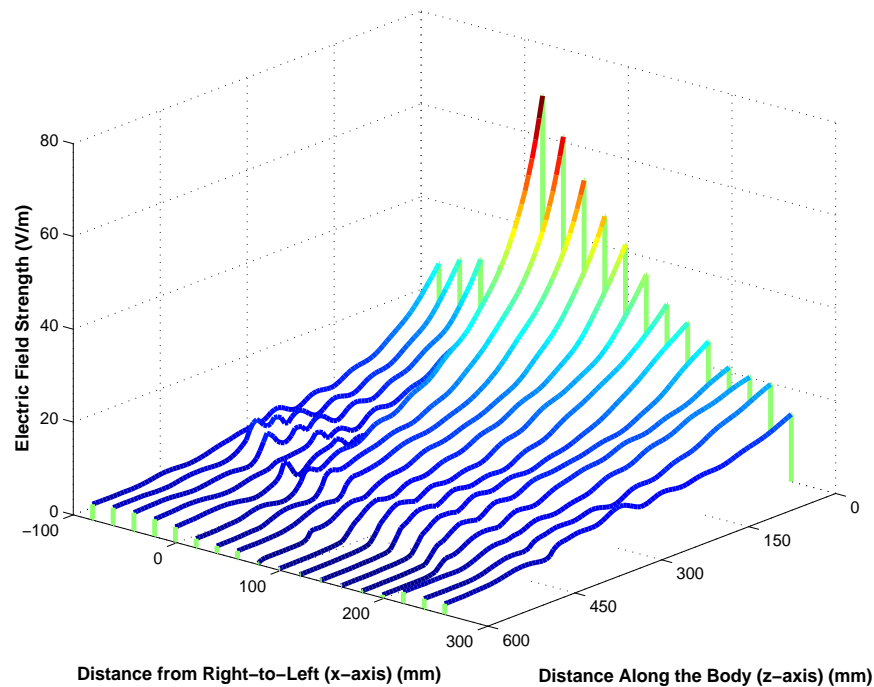
Figure 3.23: Electric field strength on the path along the body surface between the horizontal handset and the headset antennas, corresponding to Figure 3.22(a)

3.6.2 Dependency on Handset and Body Separation

The excitation condition of the on-body surface waves has been examined by analysing the effects of varying separations between the human body and the handset antenna on the Bluetooth link. The horizontally oriented handset antenna is used to investigate the worst-case scenarios. The path gain and electric field strength has been studied for handset-body separations (d_h) of 10 mm, 20 mm and 30 mm. Table 3-3 presents the path gain values obtained via simulations for the three set-ups. It is evident from these results that increasing the gap between the antenna and the human body deteriorates the on-body Bluetooth communication link.

The electric field strength on the path between the two antennas on the body surface is plotted in Figure 3.27 as a function of separations between the body and the handset antenna. The degradation of the Bluetooth link at 20 mm gap is apparent from the
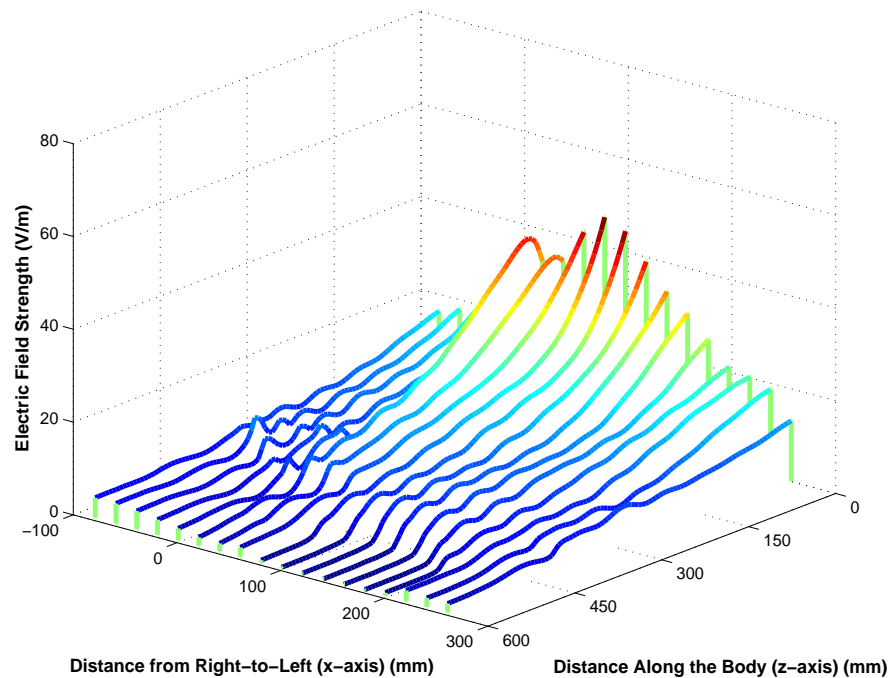
Figure 3.24: Electric field strength on the path along the body surface between the vertical handset and the headset antennas, corresponding to Figure 3.22(a)

signal strength values as the surface waves are weakened because of a reduced coupling to the surface of the human body. Increase in antenna-body separation to 30 mm further reduces the strength of the surface wave component that causes the path gain to drop to -53.3 dB. These results further confirm that the surface waves are a major factor in this communication link as compared to the air waves and the 10 mm separation is the optimal position for the horizontally placed handset antenna (of the three studied cases) to excite the surface waves.

Table 3-3: Simulate results for average path gains obtained with different handset-body (d_h) separations for horizontally placed handset antenna at 2440 MHz

Handset-Body Separation (d_h) (mm)	Average Path Gain ($S21$) (dB)
10	-51.6
20	-52.5
30	-53.3
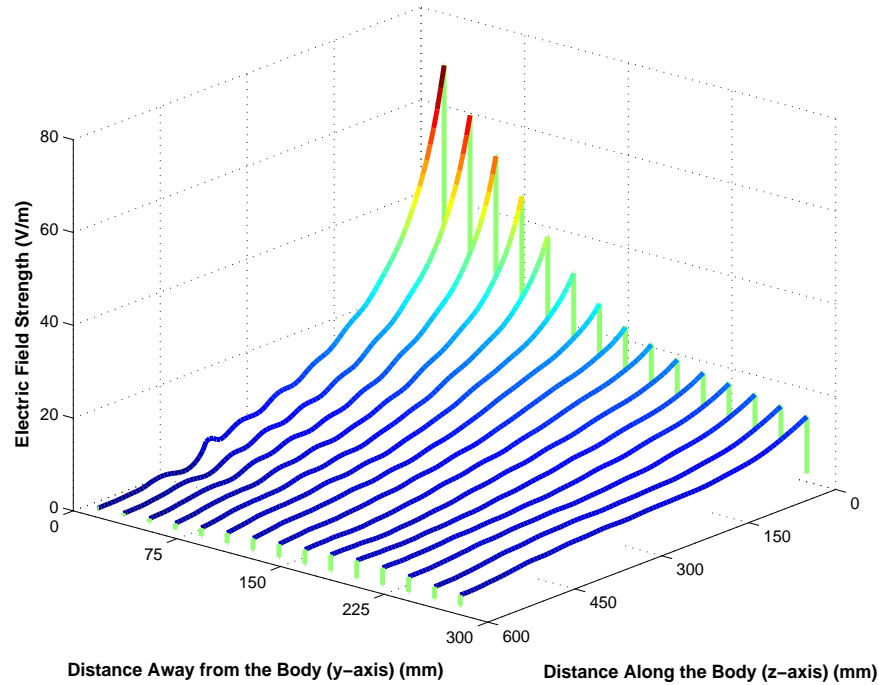
Figure 3.25: Electric field strength away from the body surface between the horizontal handset and the headset antennas, corresponding to Figure 3.22(b)

3.6.3 Effects of Blockade by Surrounding Objects

Identification of the dominant transmission channel in this on-body communication link is of particular interest. It is helpful to the antenna designers to come up with designs that support the dominant medium of transmission, increasing efficiency and reliability of the communication channel. The dominant transmission medium is further determined by blocking the direct path between the handset and the headset antennas and investigating the subsequent effects on the link budget. The direct path between the two antennas is blocked using a metal barrier. The barrier has dimensions of 458 mm×261 mm×20 mm and is located at a height of 140 mm from the horizontally placed handset antenna as shown in Figure 3.28. Variation in the path gain values and behaviour of the surface waves because of the presence of the barrier is studied for varying barrier-body gaps. Three separating distances (d_b) between the body and the barrier, i.e. 0 mm, 20 mm
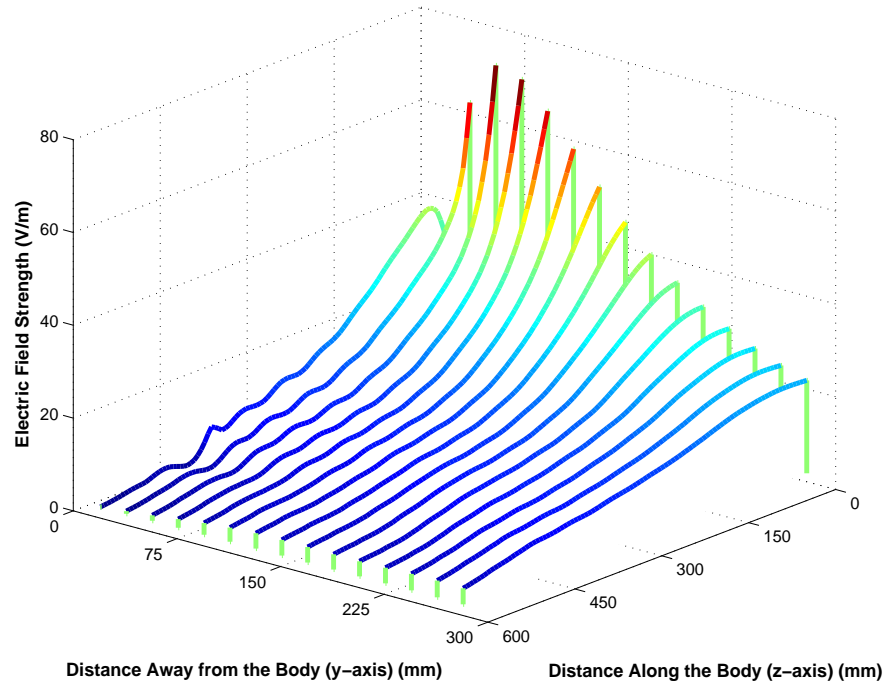
Figure 3.26: Electric field strength away from the body surface between the vertical handset and the headset antennas, corresponding to Figure 3.22(b)
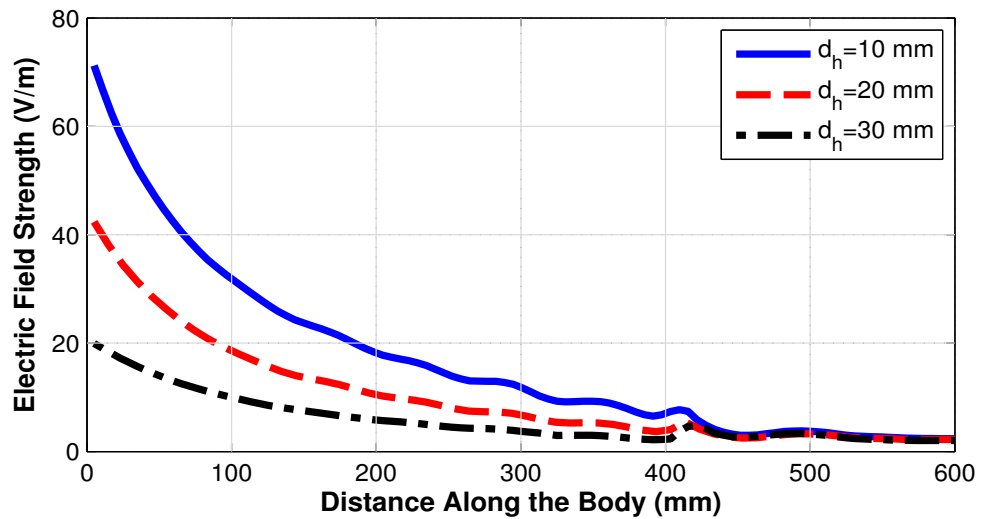
Figure 3.27: On-body surface waves for different separations of horizontal handset antenna and body (d_h)

and 60 mm have been considered. Table 3-4 gives an account of the path gain values obtained from the simulated configurations.
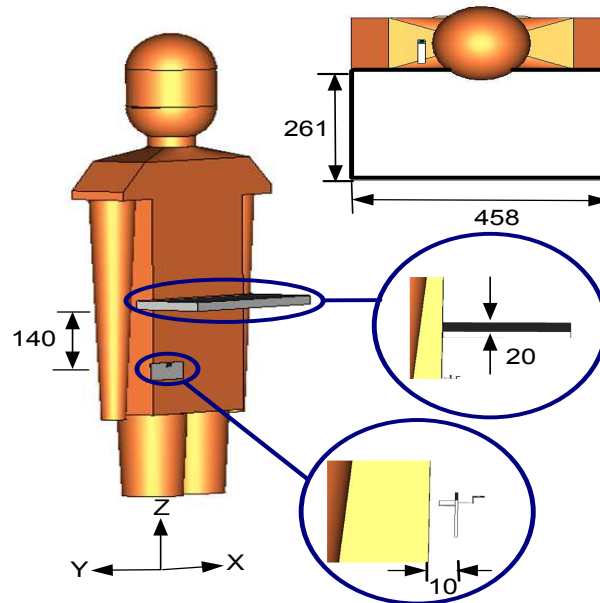
Figure 3.28: On-body test configuration for the study of transmission mechanism in the presence of a horizontal barrier (all lengths are in mm)

It can be seen that the path gain drops dramatically to -70.4 dB when the separation between the barrier and the body is set to 0 mm. Increasing the body-barrier separation shows a tendency to improve the on-body Bluetooth link. With 20 mm separation, path gain is enhanced to -58.2 dB while this value reaches to -50.2 dB with a separation of 60 mm between the body and the barrier.

Figure 3.29 illustrates the normalised electric field distributions in the presence of the barrier. The link is worst when there is no gap between the body and the barrier. Although, a few surface waves could creep through the gap at the arms, the barrier blocks most of the air waves and the surface waves as described in Figure 3.29(a). It also

Table 3-4: Simulated values of average path gain for on-body transmission with blocking effects due to a metal barrier placed at various separations from the body surface at 2440 MHz

Barrier-Body Separation (d_b) (mm)	Average Path Gain ($S21$) (dB)
0	-70.4
20	-58.2
60	-50.2

(a) d_b=0 mm   (b) d_b=20 mm   (c) d_b=60 mm
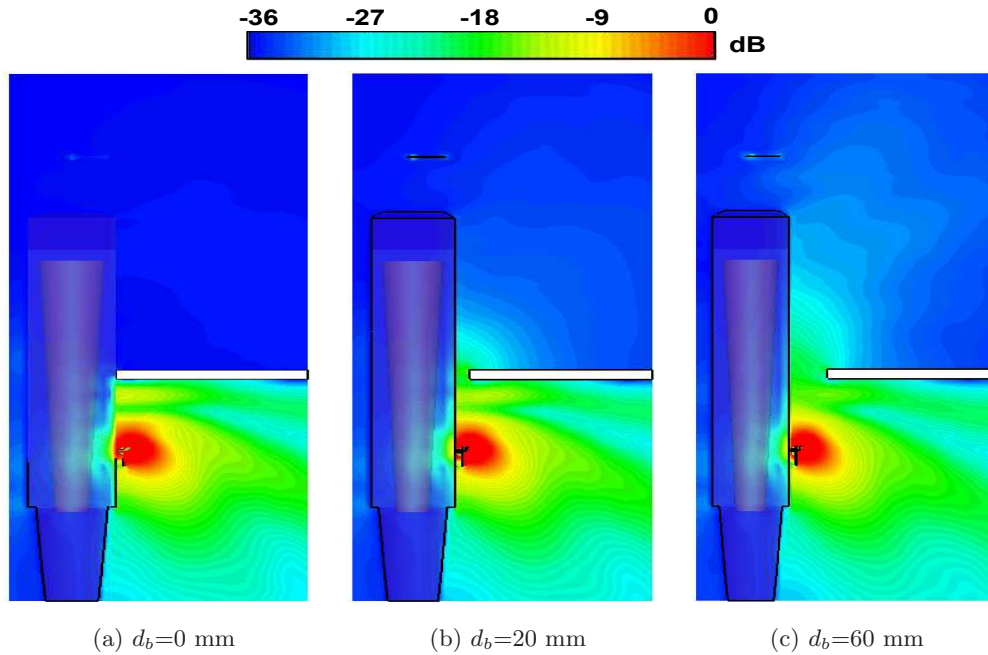
Figure 3.29: On-body surface waves observed on the cross-section plane with barrier at different separations (d_b) from the body surface

shows that the human body is not a good medium for communication link as little electromagnetic energy is passing through the body. Increasing the barrier-body separation to 20 mm, the path gain improves because of generation and propagation of the surface waves as shown in Figure 3.29(b). In this configuration, surface waves are the dominant medium as air waves are still blocked.

The electric field distribution for 60 mm separation is shown in Figure 3.29(c). The link shows greater enhancement for this separation as path gain becomes -50.2 dB, 1.4 dB more than that achieved with no blocking. It can be seen that much stronger surface waves can reach the top part of the body in this case as the barrier blocks the air waves. Reflections from the barrier and diffraction at the edge of the barrier also contributes to strengthen the surface waves. Moreover, a separation of 60 mm is almost equal to the half wavelength (wavelength is 122.95 mm at 2440 MHz) whereas 20 mm is less than the quarter wavelength. The surface wave needs at least half wavelength space to pass through efficiently. Therefore, the link is improved at 60 mm separation as compared to the configurations with narrower gaps. These results confirm that the surface waves

creeping on the air-body interface from the handset to the headset antenna are the dominant path in this on-body Bluetooth transmission channel.

3.7   Summary

The on-body Bluetooth link between a mobile handset and Bluetooth headset has been analysed using computer simulations and verified through the measurements in this chapter. The link characteristics have been investigated for its dependency on the handset antenna orientation, distance between the handset and the human body and presence of line-of-sight blocking objects in the transmission path.

It is shown that the human body causes a loss of 10-15 dB in the Bluetooth path gain due to blocking of line-of-sight between the handset and the headset antennas. The handset antenna in vertical orientation forms a stronger link due to less rapid decay of the surface waves as compared to the horizontal orientation. The surface wave excitation also depends on the distance between the handset antenna and the human body besides the handset antenna orientation. The increasing handset-body separation results in a weaker on-body Bluetooth link because of decrease in the strength of the on-body surface waves. It is deduced that surface waves extend to at least one half wavelength away from the human body and blocking objects located nearer than that can cause the on-body link to degrade due to blockage of the surface waves.

References

[1] M. A. Jensen and Y. Rahmat-Samii, "EM interaction of handset antennas and human in personal communications," *IEEE Transactions on Antennas and Propagation*, vol. 83, no. 1, pp. 7–17, January 1995.

[2] M. Okoniewski and M. A. Stuchly, "A study of the handset antenna and human body interaction," *IEEE Transactions on Microwave Theory and Techniques*, vol. 44, no. 10, pp. 1855–1864, October 1996.

[3] Z. Wang, X. Chen, and C. G. Parini, "Effects of the ground and the human body on

the performance of a handset antenna," *IEE Proceedings on Microwave and Antenna Propagation*, vol. 151, no. 2, pp. 131–134, April 2004.

[4] J. Ryckaert, P. De Doncker, R. Meys, A. de Le Hoye, and S. Donnay, "Channel model for wireless communication around human body," *IEE Electronics Letters*, vol. 40, no. 9, pp. 543–544, April 2004.

[5] P. S. Hall and Y. Hao, "Antennas and propagation for body-centric wireless networks," *Artech House Publishers, (UK)*, 2006.

[6] Z. N. Chen, A. Cai, T. S. P. See, X. Qing, and M. Y. W. Chia, "Small planar UWB antennas in proximity of the human head," *IEEE Transactions on Microwave Theory and Techniques*, vol. 54, no. 6, pp. 1846–1857, June 2006.

[7] M. Gallo, P. S. Hall, and M. Bozzetti, "Simulation and measurement of body dynamics for on-body channel characterization," *IET Seminar on Antennas and Propagation for Body-Centric Wireless Communications*, April 2007.

[8] G. A. Conway and W. G. Scanlon, "Low-profile patch antennas for over-body-surface communication at 2.45GHz," *IEEE International Workshop on Antenna Technology (iWAT)*, April 2007.

[9] P. S. Hall, Y. Hao, Y. I. Nechayev, A. Alomainy, C. G. Constantinou, C. Parini, M. R. Kamarudin, T. Z. Salim, D. T. M. Hee, R. Dubrovka, A. S. Owadally, W. Song, A. Serra, P. Nepa, M. Gallo, and M. Bozzetti, "Antennas and propagation for on-body communication systems," *IEEE Antennas and Propagation Megazine*, vol. 49, no. 3, pp. 41–58, June 2007.

[10] K. Fujii, M. Takahashi, K. Ito, K. Hachisuka, Y. Terauchi, K. Y., K. Sasaki, and K. Itao, "Study on the transmission mechanism for wearable device using the human body as a transmission channel," *IEICE Transactions on Communications*, vol. E88-B, pp. 2401–2410, 2005.

[11] C. Gabriel, "Compilation of the dielectric properties of body tissues at RF and microwave frequencies," *Brooks Air Force Technical Report, AL/OE-TR-1996-0037*, 1996.

[12] "Body tissue dielectric properties," *Federal Communication Commision (FCC), URL:http://www.fcc.gov/oet/rfsafety/dielectric.html*.

[13] "Caculation of the dielectric properties of body tissues," *Institute of Applied Physics, Italian National Research Council, URL:http://niremf.ifac.cnr.it/tissprop*.

[14] *CST Microwave Studio® 2010 User Manual*.

[15] K. A. Norton, "The physical reality of space and surface waves in the radiation field of radio antennas," *IRE Proceedings*, vol. 25, no. 9, pp. 1192–1202, September 1937.

[16] H. M. Barlow, "Surface waves," *IRE Proceedings*, vol. 46, no. 7, pp. 1413–1417, July 1958.

[17] H. M. Barlow and J. Brown, "Radio surface waves," *Oxford University Press, (UK)*, 1962.

[18] T. S. M. Maclean and Z. Wu, "Radio wave propagation over ground," *Springer*, 1993.

[19] R. Belmonte, S. Fast, and J. Schuster, "A comparison of near earth propagation over layered media," *IEEE Military Communications Conference (MILCOM)*, November 2008.

Chapter 4

Effects of Multipath Environment on GPS Antennas

The introduction of built-in GPS in portable Personal Navigation Devices (PNDs) especially the mobile phones has revolutionised the navigation industry. The ever growing demand of availability of the navigation facilities in these devices has made the GPS an essential part of the modern Wireless Personal Area Network (WPAN) and Wireless Body Area Network (WBAN) applications. The portable GPS mobile terminal antennas experience multipath fading due to reflections or diffractions of the incident radio waves from the surrounding environment. Therefore, the GPS antenna's performance in real working environment cannot be judged on the basis of traditional analysis of the free space antenna parameters.

This chapter details a novel technique to characterise these environmental effects on the GPS antennas using statistical models. The antenna performance is accounted in terms of GPS Mean Effective Gain (MEG_{GPS}), GPS Angle of Arrival (AoA_{GPS}) distribution and GPS Coverage Efficiency (η_c). This statistical approach provides an efficient alternative to the actual field test with added benefits of repeatability and accuracy. The validation of the model is carried out both through measurements and

performance analysis of various GPS antennas.

4.1 Antennas and Multipath Environment

The performance of the antennas in the WPAN/WBAN applications is usually tested by the antenna designers using traditional electromagnetic procedures considering free space input impedance, radiation efficiency and radiation patterns. However, the real working environment for these antennas is quite different from the conditions under which they are tested in an anechoic chamber. The free space antenna parameters are modified greatly due to reflections, diffractions and scattering of the incoming radio waves from the objects located in the vicinity, including buildings, trees, vehicles and ground as shown in Figure 4.1.

Theoretically, the GPS antennas should have good Right Hand Circular Polarisation (RHCP) with a uniform radiation pattern over entire upper hemisphere in order to receive the incoming GPS signal efficiently and provide better coverage. A good rejection of Left Hand Circular Polarisation (LHCP) is also required to avoid multipath fading [1–3]. However, these requirements are hard to fulfil in portable devices. The reasons involved are the limitations of size and space of the hand-held GPS receivers, especially the mobile phones, that have to provide a number of other services including Wi-Fi, FM radio, digital camera and mobile TV [4, 5]. Also, in the common working conditions of cluttered environments including indoors and city streets, a weak signal is available directly from the satellite while the reflected signals may have arbitrary polarisations. Moreover, the mobile phones are hardly used in a fixed position and the "up" direction of the antenna changes depending on the used orientation. Therefore, a wide-beam linearly polarised GPS antenna is a preferred choice as it gives better performance compared to the conventional RHCP antennas [6–8].

Since, the WPAN/WBAN applications are desired to allow maximum mobility of the user and flexibility of use in different situations with reliable data transmission,

the antennas in these devices should cope all these effects successfully. It makes the traditional electromagnetic techniques incapable to give a correct account of the antenna performance in the real working environment. Many efforts have been reported in the literature to study the performance of the mobile antennas in land mobile environment using the Mean Effective Gain (MEG) and statistical models for Angle of Arrival (AoA) of the incident waves [9, 10]. The increasing use of the GPS antennas in portable devices make it pertinent to study these effects thoroughly.

4.2 Statistical Environmental Model for GPS Operation

Performing field tests to analyse the performance of a GPS antenna has the drawback of longer procedures where weather, temperature and location hazards make it hard to control the test environment. It results in lack of accuracy due to poor repeatability and efficiency. The statistical models representing the real multipath scenarios provide an excellent alternative to the field tests, predicting the antenna performance while avoiding the short-comings of the field tests. Moreover, effects of antenna properties of gain and polarisation and directional response of the environment on the antenna performance could be characterised separately.

A novel stochastic method is developed to characterise the environmental factors on the performance of the GPS antennas, introducing the parameters of GPS Mean Effective Gain (MEG_{GPS}) and Coverage Efficiency (η_c). This method models the GPS multipath environment using statistical definitions of the antenna MEG and incident wave AoA distributions. The MEG equation derived by Taga [9] is re-formulated to suit the GPS environment with RHCP incoming waves and environmental reflections. An overview of the expected performance of the GPS antennas in the multipath environment can be achieved using this method having the knowledge of 3-D free space antenna radiation patterns and average angular distribution of incident power in the environment. The power distribution must be known in both azimuth and elevation, and separately
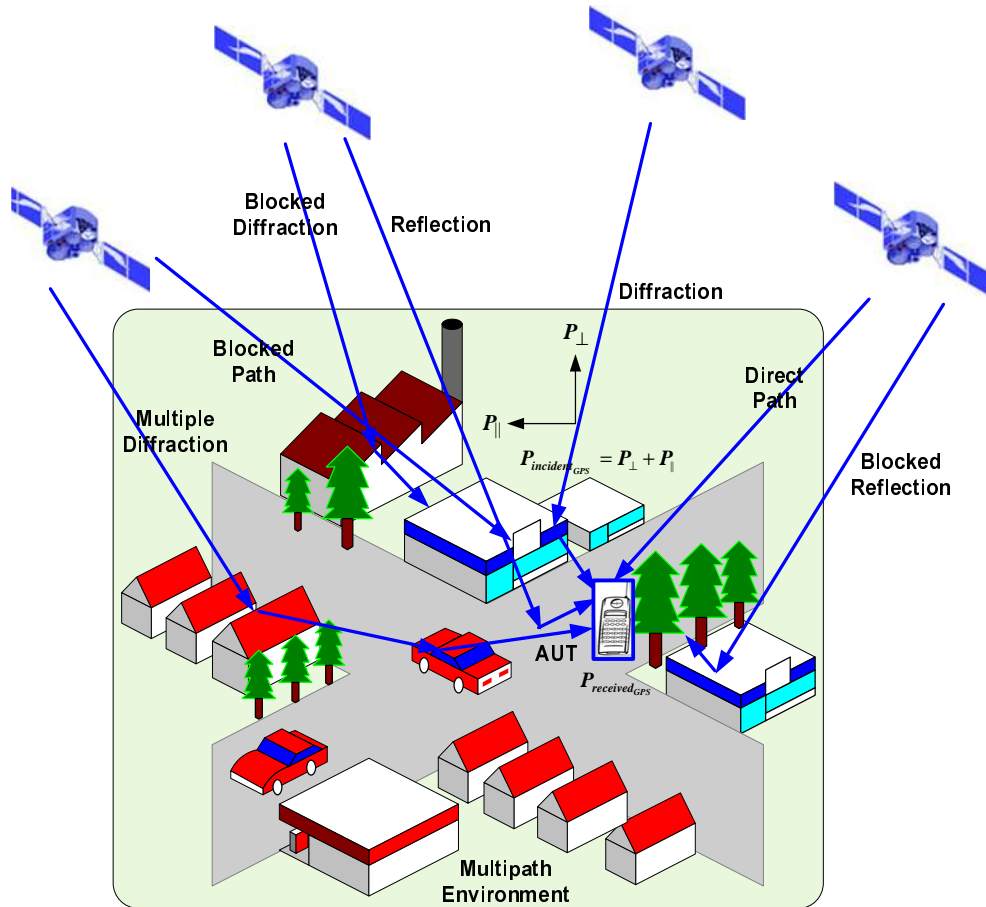
Figure 4.1: GPS environment and multipath signals

for perpendicular and parallel polarised field components. It effectively eliminates the need of an actual field test with clear benefits of repeatability, flexibility and efficient computation.

4.2.1 GPS Mean Effective Gain (MEG_{GPS})

The MEG is the average gain of the antenna performance in a multipath radio environment compared to the performance of a reference antenna in the same environment. It characterises average performance of an antenna by taking into account the polarisation and probability of the incident radio waves and the gain patterns of the antenna under test in the multipath environment. The MEG of an antenna in a mobile terminal is

defined as [9]:

$$MEG = \frac{Mean\ Received\ Power\ (P_{received})}{Total\ Mean\ Incident\ Power\ (P_{incident})} \tag{4.1}$$

For spherical coordinates, $P_{received}$ can be expressed as [11]:

$$P_{received} = \int_0^{2\pi} \int_0^{\pi} \left[P_1 G_\theta \left(\theta, \phi \right) p_\theta \left(\theta, \phi \right) + P_2 G_\phi \left(\theta, \phi \right) p_\phi \left(\theta, \phi \right) \right] \sin \theta d\theta d\phi \tag{4.2}$$

where $G_\theta \left(\theta, \phi \right)$ and $G_\phi \left(\theta, \phi \right)$ are θ and ϕ components of the antenna power gain pattern respectively, $p_\theta \left(\theta, \phi \right)$ and $p_\phi \left(\theta, \phi \right)$ indicate the θ and ϕ components of angular density functions of the incoming waves respectively. P_1 is the mean power that would be received by an isotropic antenna in θ polarisation while P_2 is the mean power received by an isotropic antenna in ϕ polarisation.

The total mean incident power $(P_{incident})$ arriving at the antenna would be the summation of the mean power in the two polarisations, given as:

$$P_{incident} = P_1 + P_2 \tag{4.3}$$

The incident wave in the GPS mobile environment can be split into two components, perpendicular polarised component and parallel polarised component. Therefore, θ and ϕ components respectively correspond to the perpendicular and parallel polarised components. Reformulating Equation 4.2 to suit the GPS environment results as follows:

$$P_{received_{GPS}} = \int_0^{2\pi} \int_0^{\pi} \left[P_\perp G_\perp \left(\theta, \phi \right) p_\perp \left(\theta, \phi \right) + P_{||} G_{||} \left(\theta, \phi \right) p_{||} \left(\theta, \phi \right) \right] \sin \theta d\theta d\phi \tag{4.4}$$

Now, $P_\perp$ and $P_{||}$ are the mean received power in the perpendicular and parallel polarisations with respect to the ground plane while $p_\perp \left(\theta, \phi \right)$ and $p_{||} \left(\theta, \phi \right)$ represent the perpendicular and parallel components of the angular density functions of the incoming waves respectively, as shown in Figure 4.1. $P_{incident}$ arriving at the mobile GPS terminal
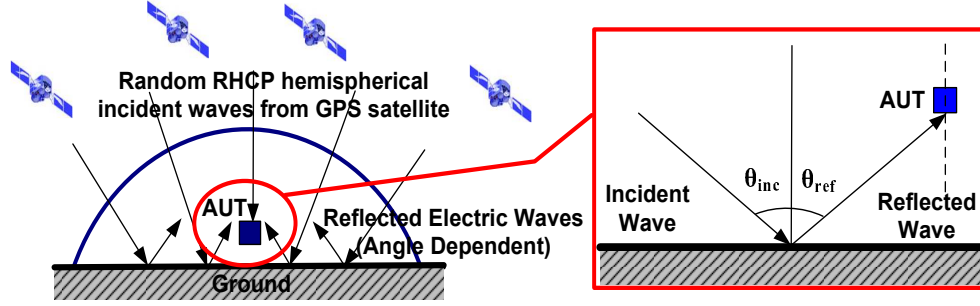
Figure 4.2: Multipath environment model around the GPS receiver antenna

is then:

$$P_{incident_{GPS}} = P_\perp + P_\parallel \tag{4.5}$$

The ratio of the mean powers received in perpendicular and parallel polarisations when the transmitted radio wave is perpendicular polarised is termed as XPR (Cross Polarisation Ratio) and described by:

$$XPR = \frac{P_\perp}{P_\parallel} \tag{4.6}$$

Using Equations 4.4-4.6, the MEG expression for the GPS antenna can be formulated as:

$$MEG_{GPS} = \int_0^{2\pi} \int_0^\pi \left[\frac{XPR}{1 + XPR} G_\perp(\theta, \phi) p_\perp(\theta, \phi) \right.$$
$$\left. + \frac{1}{1 + XPR} G_\parallel(\theta, \phi) p_\parallel(\theta, \phi) \right] \sin\theta d\theta d\phi \tag{4.7}$$

Since, XPR governs the polarisation of the incoming wave in this model; the circular polarised nature of the incoming GPS satellite signal is accumulated by making $XPR = 0\ dB$. It employs the fact that simultaneous transmission of two linearly polarised waves that have a phase difference of $\pi/2$ (radian) results in the generation of a circularly polarised wave.

4.2.2 GPS Angle of Arrival Distribution GPS (AoA_{GPS})

The AoA_{GPS} defines the direction of arrival of the incident waves at the GPS receiver from the satellite antenna. In order to evaluate the actual antenna performance in a multipath environment, it is necessary to apply a suitable statistical model similar to the real environment. Since, at least four GPS satellites are visible at a single point on earth at any time, it can be assumed that at least four incident waves arrive at the GPS receiving antenna placed in a wireless communication environment. Most of the incident waves are reflected, diffracted and scattered from the objects surrounding the receiving antenna including buildings and the ground plane. This provides a reasonable basis to the assumption that the angular density function in azimuth can be considered as uniform, similar to the case of land mobile environment [9, 12, 13]. However, in the elevation, situation becomes different as reflections take place from the ground plane, in the lower hemisphere as illustrated in Figure 4.2. Since, no measurements are reported in the literature for angle of arrivals for the GPS antenna, it is assumed as a starting point that angular density function is uniform in upper hemisphere while in lower hemisphere; it is uniform but reduced by a factor governed by the reflection coefficients for perpendicular and parallel polarised components.

In accordance with the preceding assumptions, a novel statistical model for the GPS antenna in a multi-path environment is proposed as follows:

$$p_\perp(\theta, \phi) = p_{inc_\perp}(\theta, \phi) + p_{ref_\perp}(\theta, \phi)$$

$$= \begin{cases} 1 & 0 \leq \theta \leq \pi/2 \\ 1 \cdot A(\theta)_\perp & \pi/2 \leq \theta \leq \pi \end{cases} \tag{4.8}$$

$$p_\parallel(\theta, \phi) = p_{inc_\parallel}(\theta, \phi) + p_{ref_\parallel}(\theta, \phi)$$

$$= \begin{cases} 1 & 0 \leq \theta \leq \pi/2 \\ 1 \cdot A(\theta)_\parallel & \pi/2 \leq \theta \leq \pi \end{cases} \tag{4.9}$$

Where $A\left(\theta\right)$ depends upon the reflection coefficients for the perpendicular and parallel components that varies with angle of incidence (θ). Hence:

$$A(\theta)_{\perp} = P_{\perp} \cdot \Gamma_{\perp} \tag{4.10}$$

$$A(\theta)_{||} = P_{||} \cdot \Gamma_{||} \tag{4.11}$$

The reflection coefficients for the two polarisations are defined as [14, 15]:

$$\Gamma_{\perp} = \frac{\cos\theta_i - \sqrt{(\varepsilon_2/\varepsilon_1) - \sin^2\theta_i}}{\cos\theta_i + \sqrt{(\varepsilon_2/\varepsilon_1) - \sin^2\theta_i}} \tag{4.12}$$

$$\Gamma_{||} = \frac{(\varepsilon_2/\varepsilon_1)\cos\theta_i - \sqrt{(\varepsilon_2/\varepsilon_1) - \sin^2\theta_i}}{(\varepsilon_2/\varepsilon_1)\cos\theta_i + \sqrt{(\varepsilon_2/\varepsilon_1) - \sin^2\theta_i}} \tag{4.13}$$

4.2.3 GPS Coverage Efficiency (η_c)

Coverage efficiency of the receiving GPS antenna is another important parameter. It is the capability of the antenna to receive the signals coming directly from the satellites. It defines the quality and number of the GPS satellites an antenna can track for efficient navigation and positioning services.

Currently, the GPS antenna performance is characterised by its ability to receive the signals at elevation angles higher and lower than 10° as antenna performance is hugely degraded by multipath fading at lower angles [16]. This merit requires separate analysis for both the elevation regions and hence, fails to describe the true coverage of the antenna. The concept of the antenna coverage efficiency overcomes this drawback by giving information about the antenna coverage in the whole upper hemisphere. The GPS antenna can receive signals from all directions that lie within its coverage area. The signals incident at angles beyond this limit are too weak to be used in the navigation solution, resulting in the rise of the wasted component of the incident waves.
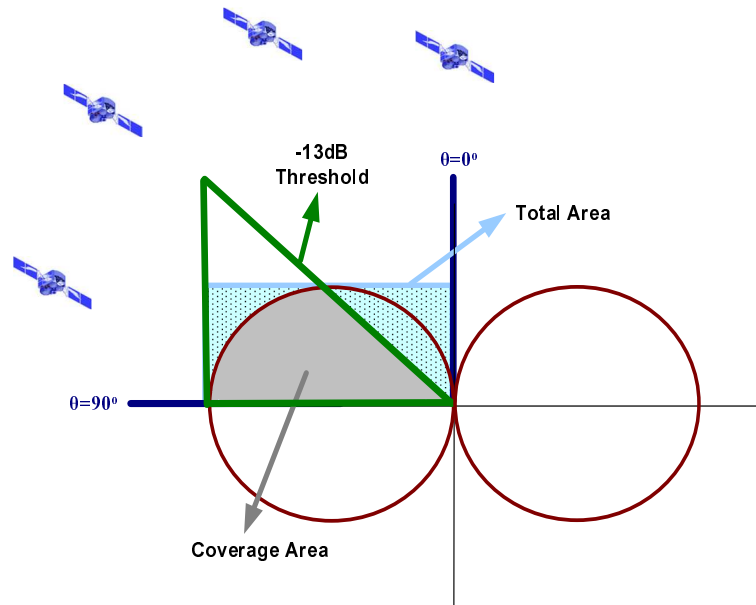
(a) Coverage efficiency calculation
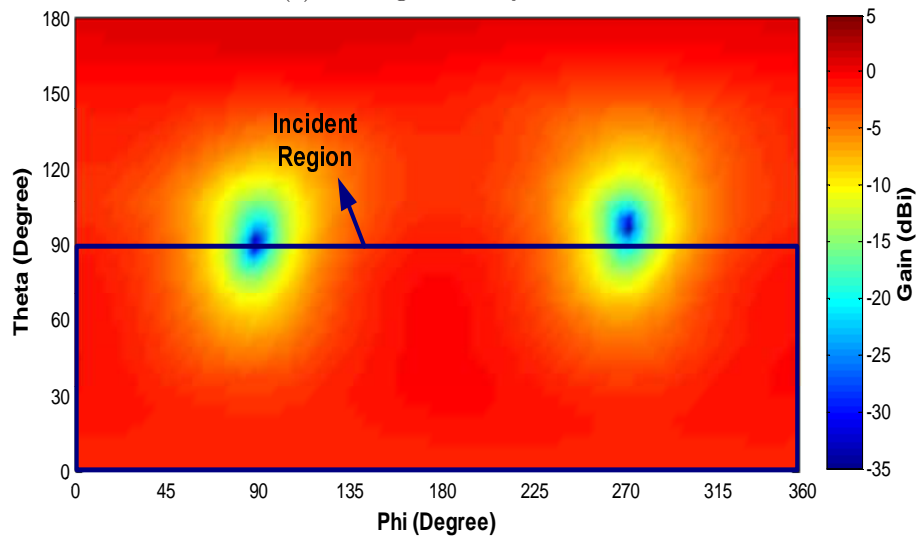
(b) 2-D RHCP radiation pattern showing gain levels in covered area

Figure 4.3: Illustration of Coverage Efficiency calculations and corresponding RHCP gain levels in the covered area of a GPS antenna with an arbitrary donut shaped gain pattern

The coverage efficiency of the GPS antenna can be calculated in terms of the solid angle by defining a threshold level. Signals below this level are considered too weak to make an impact and hence, they are wasted. Figure 4.3(a) illustrates the coverage efficiency calculations in the incident region ($0^o \leq \theta \leq 90^o$) with 0° representing the zenith and 90° the horizon. The coverage area of the antenna under test is made up

of those AoAs where received GPS signal is above the selected threshold level. The threshold line is shown in green while grey coloured area depicts the coverage area in Figure 4.3. The total area describes the maximum coverage that can be obtained by a reference GPS antenna. In case of a hypothetical isotropic antenna, the whole incident region is the total area, illustrated by shaded cyan colour in Figure 4.3.

The coverage efficiency of the antenna under test is then calculated as the ratio of the solid angles subtended by the coverage area and the total area, resulting in the following expression:

$$\eta_c = \frac{Coverage\ Area}{Total\ Area} \tag{4.14}$$

In this equation, the total area is the half hemispherical solid angle for an isotropic antenna, that is equal to 2π. To incorporate the Right Hand Circular Polarisation of the incoming wave, RHCP gain pattern is used in this calculation as described in Figure 4.3(b). The coverage area of this arbitrary antenna would be the solid angle subtended by the useful angles i.e. the parts where the RHCP gain is above the selected threshold in the incident region ($0^o \le \theta \le 90^o$).

Selection of an appropriate signal threshold level could be obtained from the GPS link budget calculations. The GPS link budget for L1 band is calculated using the following equation [17]:

$$P_r = P_t + G_t - L_p - L_m + G_r \tag{4.15}$$

Where, P_r is the receiver sensitivity in dBW while P_t is transmitted output power including the transmitter losses in dBW. G_t and G_r indicate gain of the transmitting and receiving antennas in dBi respectively, while L_p is the free space loss in dB and L_m indicates the miscellaneous losses including polarisation mismatch and atmospheric losses in dB. The link budget is calculated as follows:

Frequency of operation = f = 1575.42 MHz
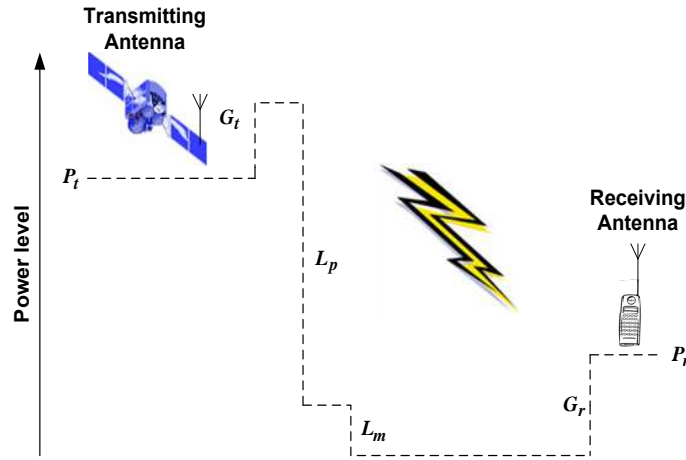
Figure 4.4: Power levels in a GPS L1 band link budget

Satellite altitude = R = 20,180 km

G_t = 13 dBi [17, 18]

P_t = 16.99 dBW (corresponds to 50 W typical) [17]

However, impedance mismatches and circuit losses reduce the transmitted power in practical scenarios and therefore,

$$P_t = 14.3 \text{ dBW [18]}$$

$$L_p = (4\pi R/\lambda)^2 = 182.5 \text{ dB}$$

$$L_m = 2 \text{ dB [17, 18]}$$

$$P_r = \text{-160 dBW (corresponds to -130 dBm typical)}$$

Vendor values for different GPS receivers show that the sensitivity of the GPS receiver could be as high as -145 dBm (corresponding to -175 dBW) [19]. Therefore,

$$P_r = \text{-175 dBW}$$

Rearranging Equation 4.15 and putting the values gives:

$$G_r = \text{-17.8 dBi}$$

The link budget calculations show that a minimum threshold level of -17.8 dBi is required to calculate the coverage efficiency of the GPS antenna. However, a threshold level of -13 dBi has been selected for the proposed model to investigate the worst case scenarios. This threshold level has been verified by a close agreement between the values obtained through calculations using the proposed model and the open field test results

observed in the following sections.

4.3   Open Field Test Procedure

A detailed open field test procedure is adopted to verify and validate the model's predictions. In these measurements DG-100 GPS receiver from GlobalSat Technology is used for the GPS signal reception. This receiver uses a SIRF Star III chipset module with 20 channels (can track up to 20 satellites) and has a built-in patch antenna. It also provides a micro-miniature coaxial connector (MMCX) port for external antennas. The sensitivity of the receiver is -145 dBm. The measurements has been performed independently at QMUL and Sony Ericsson Communications, Sweden.

4.3.1   Measurement of GPS Mean Effective Gain

For MEG_{GPS}, the received signal power (P_{signal}) should be known. The Signal-to-noise ratio (SNR) is a measure that is used to evaluate the performance of the designed GPS antennas. It indicates how strongly the satellite's radio signal is being received. It is computed as a ratio of the signal power to the noise power attenuating the signal:

$$SNR = \frac{Signal\ Power\ (P_{signal})}{Noise\ Power\ (P_{noise})} \tag{4.16}$$

And:

$$SNR\ (dB) = P_{signal}\ (dBm) - P_{noise}\ (dBm) \tag{4.17}$$

On re-arranging Equation 4.17:

$$P_{signal}\ (dBm) = SNR\ (dB) + P_{noise}\ (dBm) \tag{4.18}$$

Also [18]:

$$P_{noise}\ (dBm) = P_{sr}\ (dBm) + NF\ (dB) \tag{4.19}$$

Here, NF is the noise figure representing the noise generated within the GPS receiver while P_{sr} is the temperature dependent source resistance noise power. At a temperature of 25^oC and for a system bandwidth of 1 Hz, P_{sr} can be calculated as [20]:

$$P_{sr}\left(dBm\right) = kTB = 1.380 \times 10^{-23}\ J/K \times 298.15\ K \times 1\ Hz = -174\ dBm \quad (4.20)$$

Where, k is Boltzmann's constant and T is temperature in Kelvins. Now, putting these values in Equation 4.18, the following expression is being obtained:

$$P_{signal}\left(dBm\right) = SNR\left(dB\right) + NF\left(dB\right) - 174\ dBm \quad (4.21)$$

It implies that the signal strength delivered to the GPS receiver is linearly dependent on the SNR if the NF is constant and hence, Mean Received Power ($P_{received}$) in Equation 4.1 of a GPS antenna can be calculated using the mean SNR level for that antenna. Mean SNR level of the reference antenna (typically dipole antenna) gives the total Mean Incident Power ($P_{incident}$). Finally, MEG_{GPS} is calculated by taking the ratio of the SNR levels of the two antennas.

4.3.2 Measurement of GPS Coverage Efficiency

The coverage efficiency describes how well the antenna can view the sky and receive the satellite signal. In open field test, this quality corresponds to the number of satellites that the antenna can track. It is obtained by taking the ratio of the mean value of the useful tracked satellites (representing the coverage area of the antenna under test in Equation 4.14) and the maximum number of the tracked satellites observed during the whole measurement process (representing the total area in Equation 4.14).

$$\eta_c = \frac{N_{mean}}{N_{maximum}} \quad (4.22)$$
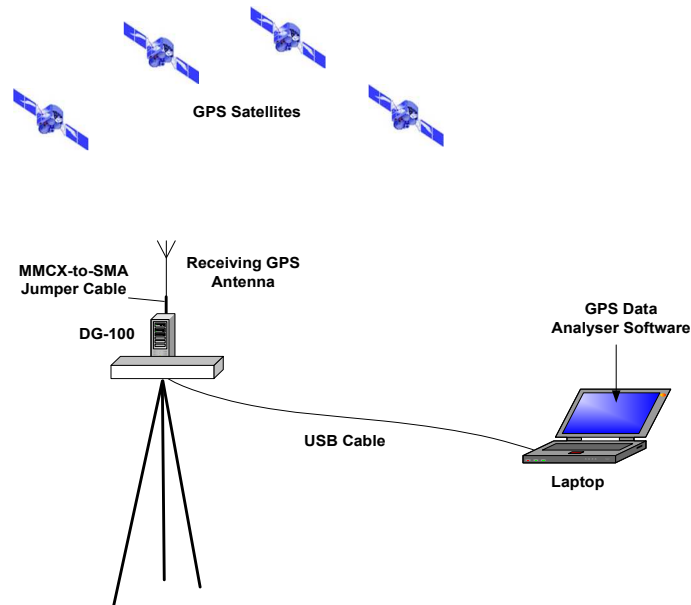
Figure 4.5: Illustration of the test set up used in the field measurements of Mean Effective Gain and Coverage Efficiency for the GPS antennas

4.3.3 Measurement Set-up

The performance of the GPS antenna is evaluated based on its capability to receive the GPS signal in outdoor environments using GlobalSat GPS receiver DG-100. The GPS antenna-under-test is used to observe the number of tracked GPS satellites and to collect the Signal-to-Noise ratio (SNR) data of the GPS signal. The field test set up is illustrated in Figure 4.5 and 4.6. The antennas are connected to the GPS receiver via a micro-miniature coaxial connector (MMCX) to sub-miniature version A connector (SMA) jumper cable.

The GPS receiver provides the following information on PC utility window shown in Figure 4.7.

- Date, time, direction and speed.

- Current location of the user in terms of latitude and longitude.

- A satellite distribution map as shown in the upper left of Figure 4.7. This map
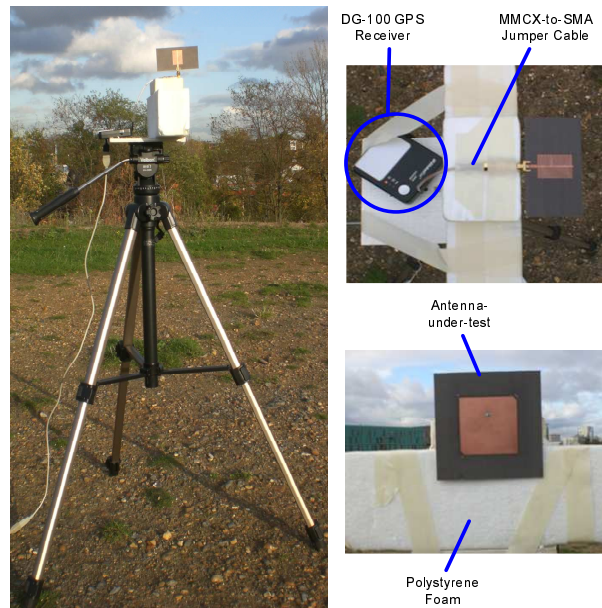
Figure 4.6: Field measurements of Mean Effective Gain and Coverage Efficiency for the GPS antennas

displays the position of all tracked satellites with North at top. Current location of the user is at the centre of the map. Outer circle represents the horizon while the inner circle is looking up at an angle of 45°.

- A satellite status chart shown in terms of vertical bars displays the SNR for the tracked GPS satellites. Each bar corresponds to a specific satellite. At the bottom of the each satellite bar are two numbers. The top number represents received SNR while the bottom number represents the satellite number. The bars in blue colour represent the satellites whose signal is good enough and are being used in position calculation. The red bars indicate the satellites that are tracked but signal is weaker, hence, not used in position calculation. Location of the corresponding satellites is indicated on the satellite distribution map in the same colours.

The designed antennas are tested for the GPS signal reception in outdoor open environment in both the horizontal and vertical orientations with respect to the ground. In this suburban environment, near by houses has been located at ~100 m distance from the test point. The GPS receiver and the antenna are placed at a height of 1 m from the
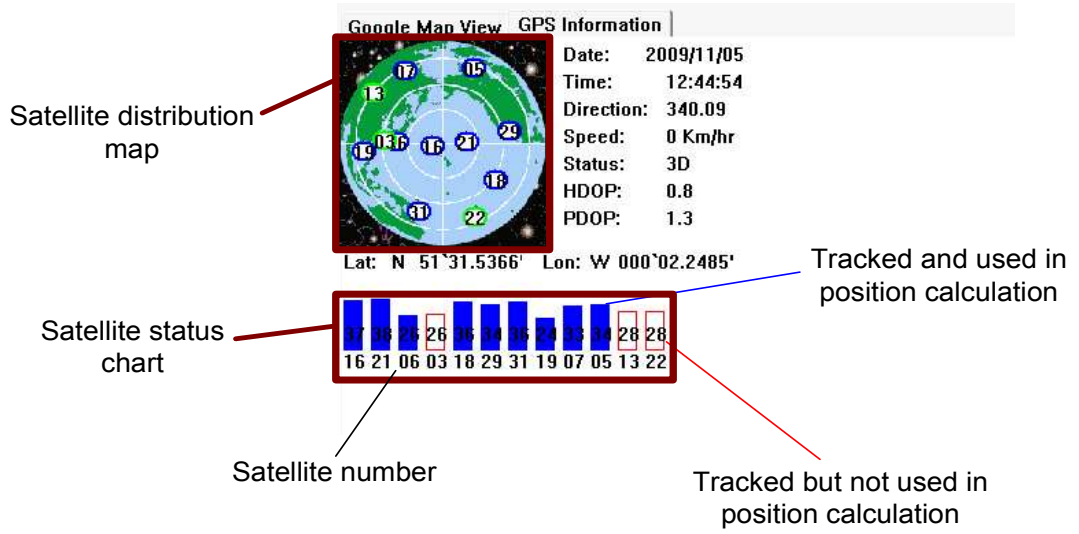
Figure 4.7: GPS status window shown by the GPS receiver on PC utility, observed to collect the SNR values and number of the tracked satellites

ground. The antennas were rotated horizontally and eight readings of the GPS signal reception information was recorded for the following angles:

$$\phi = n \times \frac{\pi}{4} \qquad n = 0, 1, 2, ..., 7 \qquad (4.23)$$

It effectively provides the average reception of the signal in the environment. MEG_{GPS} is calculated from the SNR values of the GPS signals. Both the red and blue bars are included in the calculations as they represent the tracked satellites. The information of the eight best values of the received SNR are used to calculate the mean SNR level for each antenna to represent the MEG_{GPS}. η_c is calculated using the mean number of the tracked satellites and dividing by 12, which appeared to be the maximum number of the tracked satellites during the measurements.

4.4 Validation of Proposed Statistical Model

Three approaches have been adopted to establish accuracy and efficiency of the proposed statistical model in the prediction of GPS antenna performance in the multipath

environment. The three methods are listed below:

- Comparison based on extreme environments

- Comparison based on simulated and measured 3-D gain patterns

- Comparison based on measured 3-D gain patterns and actual field measurements

4.4.1   Design of Generic GPS Antennas

Three types of generic GPS antennas; dipole, CP microstrip patch and PIFA; are analysed in the multipath environment for this study.

4.4.1.1   Dipole

The use of a standard simple antenna with known characteristics is inevitable to benchmark the model. Therefore, a half wavelength dipole antenna working at 1575.42 MHz is chosen for this purpose due to its simplicity and wide usage as a standard antenna.

The antenna is fed using a 50 Ω coaxial port and a quarter wavelength balun is used to balance the current distribution. The antenna dimensions and fabricated prototype are shown in Figure 4.8(a), while Figure 4.8(b) shows the measured S11 response for the antenna. The antenna performs well in the L1 frequency band with -10 dB bandwidth of 153 MHz covering all the frequencies from 1473 MHz to 1630 MHz. The highlighted region shows the frequency range for the desired ± 5 MHz bandwidth, based on the discussion in Chapter 2, Section 2.3.5.

The measured 3-D gain patterns for the perpendicular and parallel polarisations of the antenna in horizontal and vertical orientations are illustrated in Figures 4.9(a) and (b).
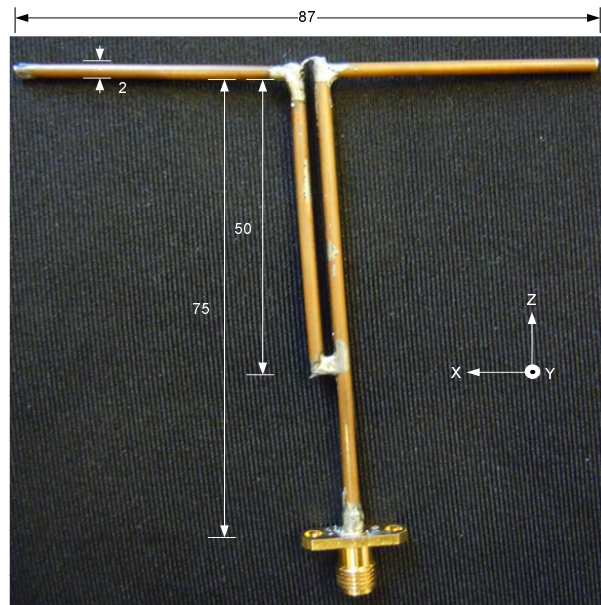
(a) Dipole prototype and geometry
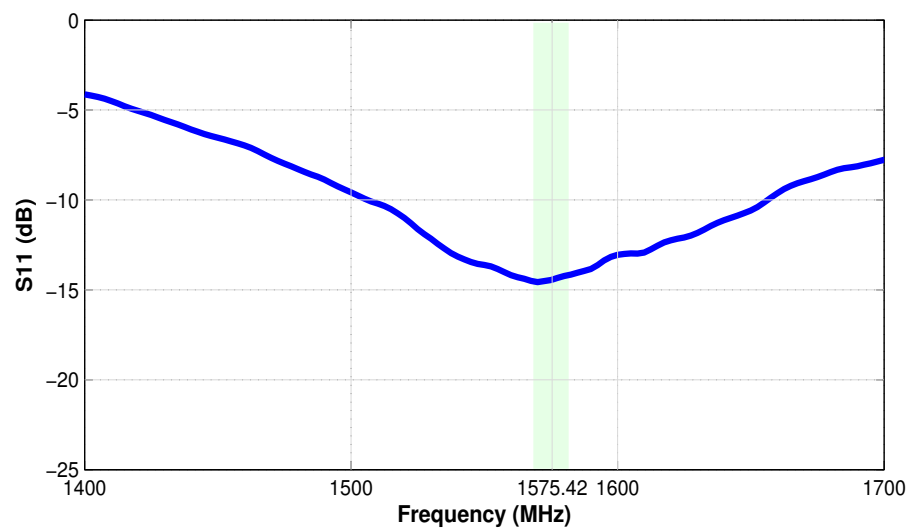
(b) Measured S11 curve

Figure 4.8: Geometrical structure of dipole GPS antenna with measured S11 curve (all lengths are in mm)

4.4.1.2 Microstrip Patch

The microstrip patch antennas are the most widely used designs in GPS applications [21]. The truncated corner microstrip patch antenna used in this study has a ground plane of 100 mm×100 mm. A printed square patch of 53.4 mm×53.4 mm, fed by a coaxial line,

(a) 3-D measured gain patterns for vertical orientation

(b) 3-D measured gain patterns for horizontal orientation
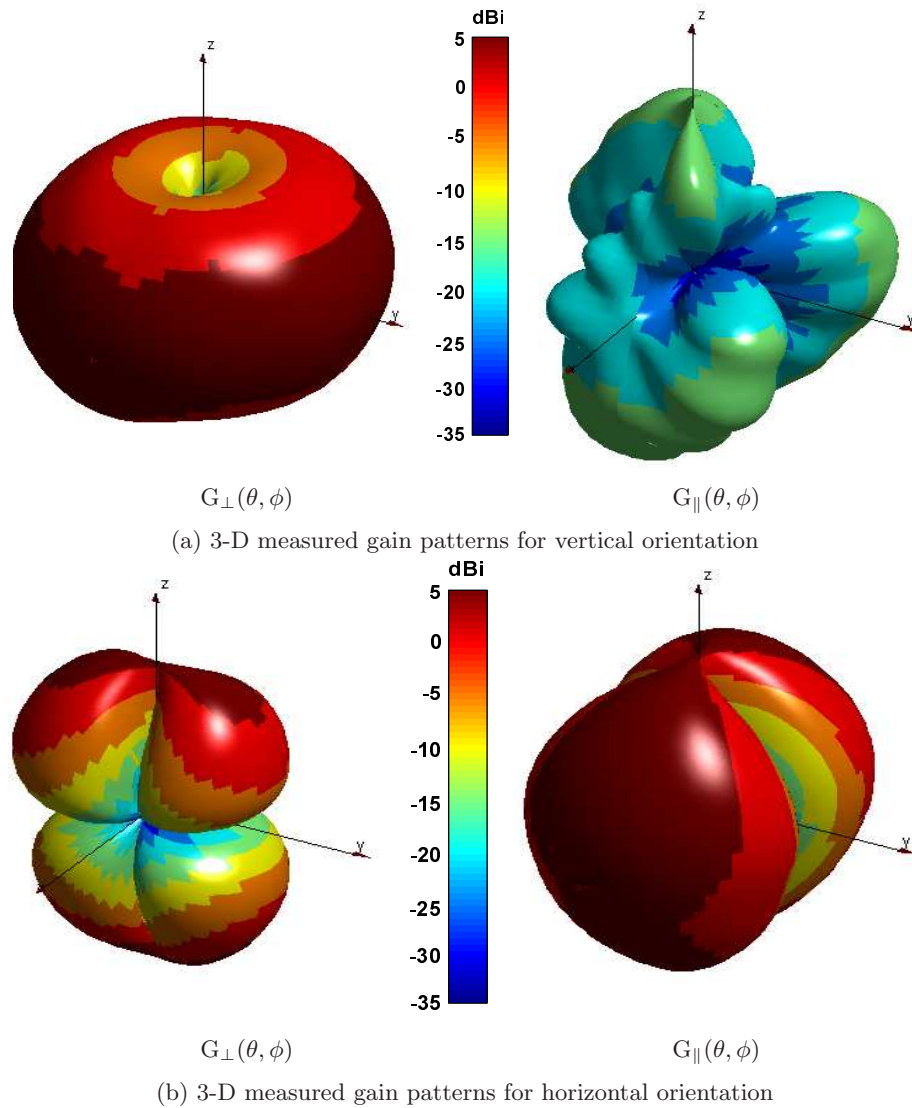
Figure 4.9: Measured 3-D gain patterns for perpendicular and parallel polarisations of dipole GPS antenna in vertical and horizontal orientations

is used as the radiating element. The substrate used is a FR4 with a thickness of 1.6 mm and ε_r=4.7. Figure 4.10(a) shows the geometry of the fabricated antenna. The free space S11 response of the antenna in Figure 4.10(b) shows excellent impedance matching in L1 band with centre frequency at 1578 MHz. The antenna has a -10 dB bandwidth of 25 MHz covering all the frequencies in the range of 1566 MHz to 1591 MHz. The measured 3-D gain patterns for perpendicular and parallel polarisation of the antenna for both the horizontal and vertical orientations are illustrated in Figures 4.11(a) and (b).
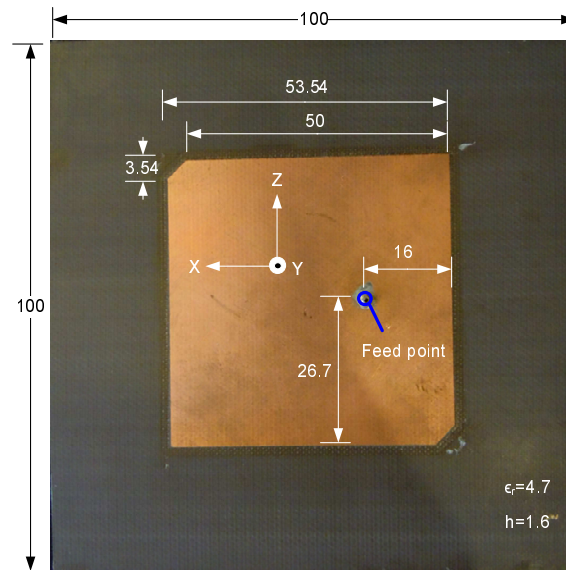
(a) CP patch prototype and geometry
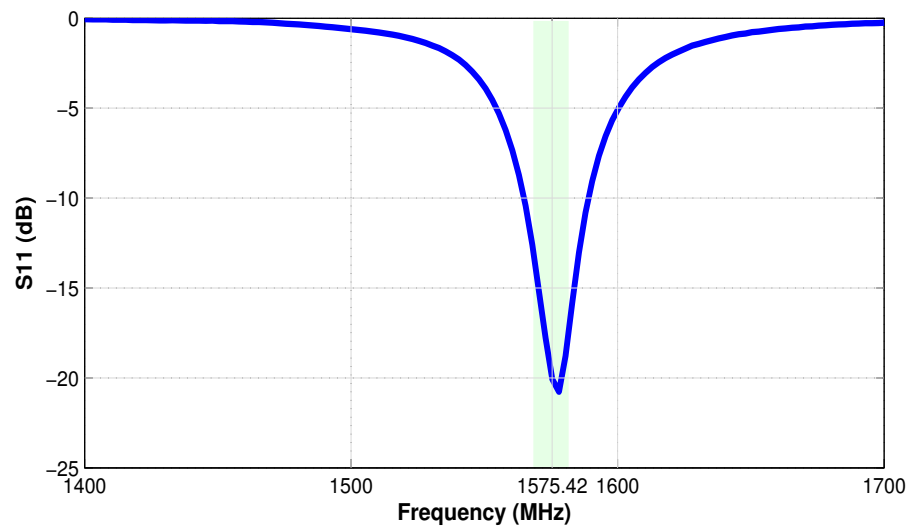
(b) Measured S11 curve

Figure 4.10: Geometrical structure of truncated corner microstrip patch GPS antenna with measured S11 curve (all lengths are in mm)

4.4.1.3 Generic PIFA

The planar inverted F antenna (PIFA) is a popular antenna choice when size is a matter of concern since it is compact and extends approximately 1/20 of a wavelength. The unobtrusive design makes it an often-used embedded type of antenna element in portable devices. Due to these characteristics, a PIFA antenna is designed and its performance is

$G_\perp(\theta, \phi)$ $G_\parallel(\theta, \phi)$

(a) 3-D measured gain patterns for vertical orientation

$G_\perp(\theta, \phi)$ $G_\parallel(\theta, \phi)$

(b) 3-D measured gain patterns for horizontal orientation
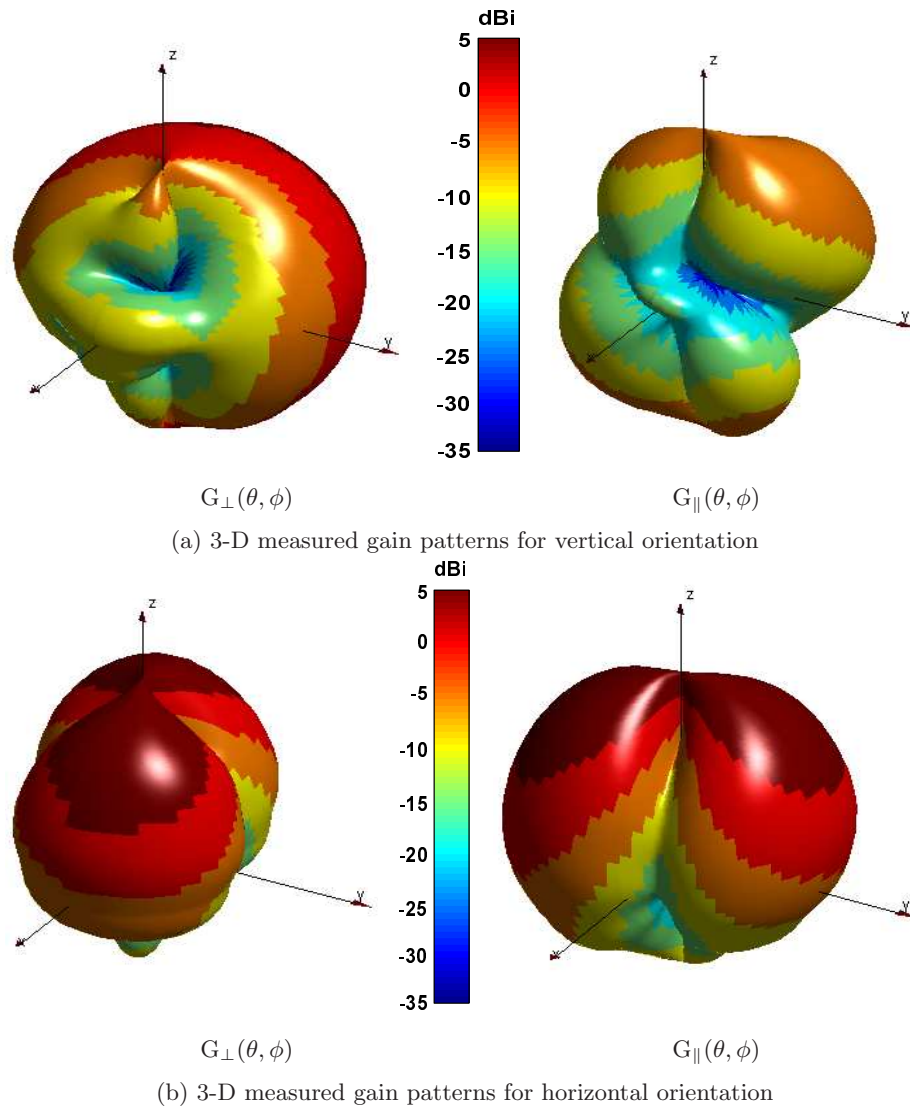
Figure 4.11: Measured 3-D gain patterns for perpendicular and parallel polarisations of truncated corner microstrip patch GPS antenna in vertical and horizontal orientations

studied for the GPS operation in the multipath environment. The antenna has a ground plane of 60 mm×31 mm with a shorting strap of 9 mm×7 mm. The planar radiator is of dimensions 38 mm×14 mm as shown in Figure 4.12(a). A polystyrene foam with ε_r=3.6 is used as the dielectric. The measured S11 curve of the antenna shown in Figure 4.12(b) indicates that the PIFA operates well in the L1 band having -10 dB bandwidth of 45 MHz and covers the frequencies ranging from 1545 MHz to 1590 MHz. Figures 4.13(a) and (b) give an account of the measured 3-D gain patterns for perpendicular and parallel polarisations of the antenna in both the horizontal and vertical orientations.
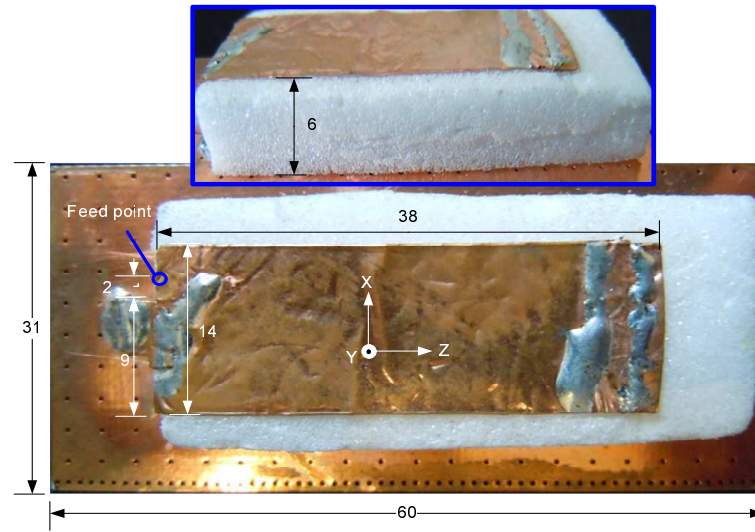
(a) Generic PIFA prototype and geometry
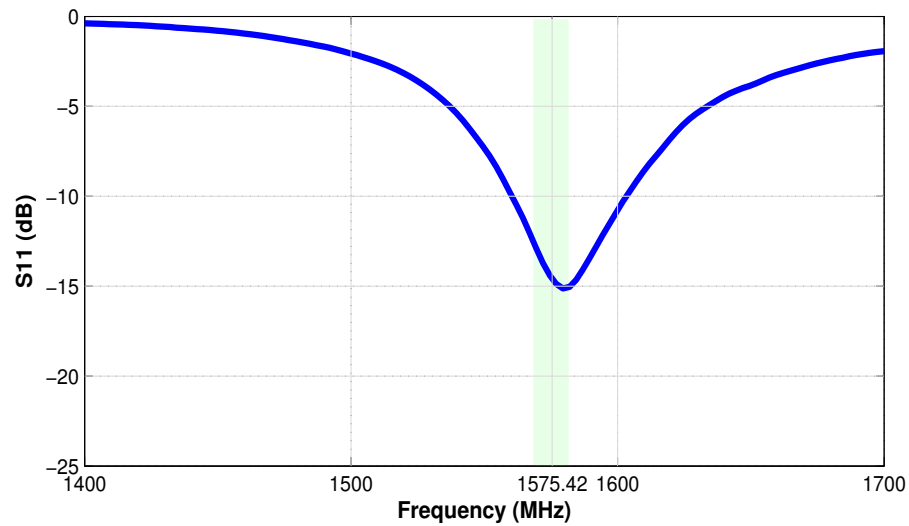
(b) Measured S11 curve

Figure 4.12: Geometrical structure of generic PIFA GPS antenna with measured S11 curve (all lengths are in mm)

4.4.2 Comparison Based on Extreme Ideal Environments

Theoretically, the performance of a GPS antenna in terms of its MEG_{GPS} in an actual reflection environment (AR) should lie between two extreme ideal environments i.e. total reflection environment (TR) and no reflection environment (NR). In the total reflection environment, all of the incident power is reflected with no loss of energy, while all of the incident power is absorbed with zero reflections in the no reflection environment. In the

$G_\perp(\theta,\phi)$ $G_\parallel(\theta,\phi)$

(a) 3-D measured gain patterns for vertical orientation

$G_\perp(\theta,\phi)$ $G_\parallel(\theta,\phi)$

(b) 3-D measured gain patterns for horizontal orientation
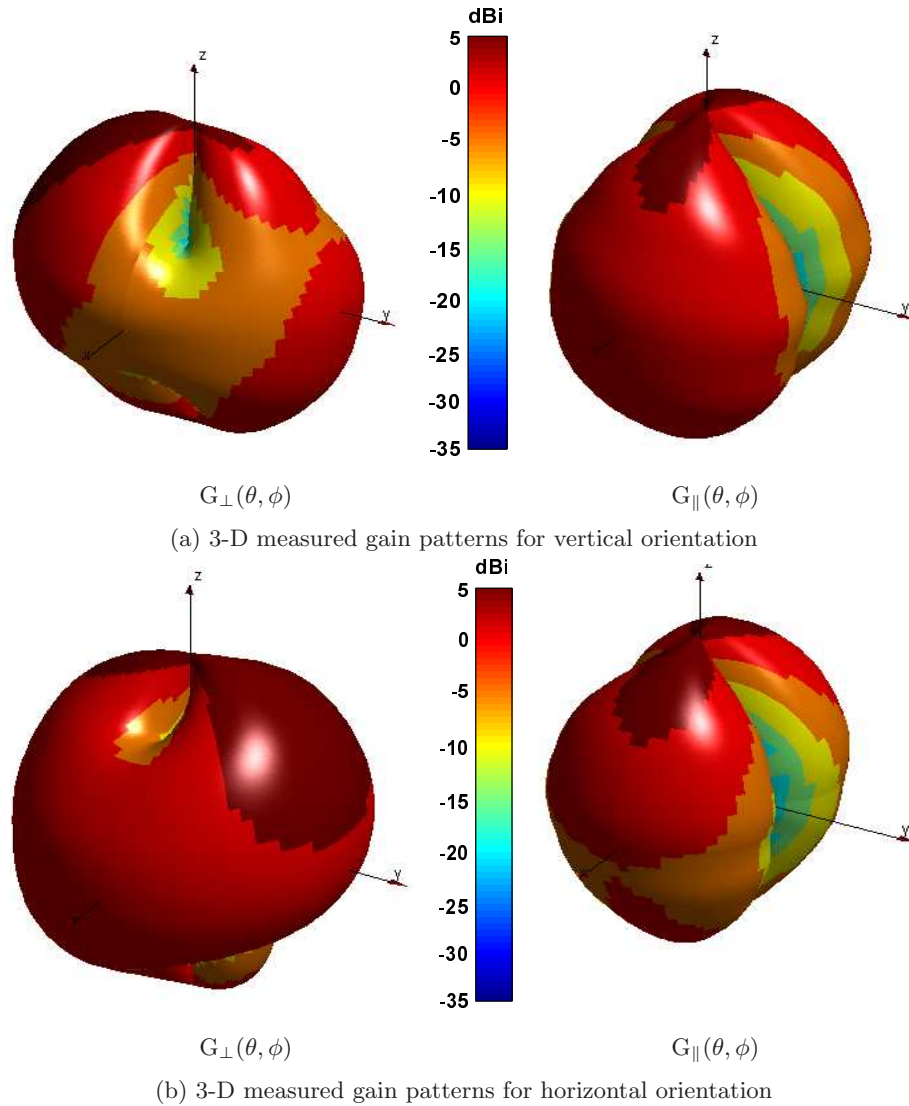
Figure 4.13: Measured 3-D gain patterns for perpendicular and parallel polarisations of generic PIFA GPS antenna in vertical and horizontal orientations

actual reflection environment, part of the incident wave is reflected, depending upon the corresponding reflection coefficients.

The three environments are incorporated in the model and the performance of the horizontal dipole antenna (with respect to the ground) is evaluated in terms of its η_c and MEG_{GPS} to test the accuracy of the model's predictions. The ground reflections in an actual environment are considered in the model from a dry concrete ground plane with a relative permittivity of 4.5 [22, 23]. The simulated 3-D gain patterns for perpendicular

Table 4-1: Comparison of calculated GPS Coverage Efficiency and GPS Mean Effective Gain of generic GPS antennas based on simulated 3-D gain patterns using three types of the multipath environment for validation of proposed GPS multipath model

Antenna	η_c (%)	MEG_{GPS} (dB)		
		Total Reflection (TR) $(A(\theta) = 1)$	No Reflection (NR) $(A(\theta) = 0)$	Actual Reflection (AR) $(A(\theta)$ corresponds to a ground permittivity of 4.5)
Isotropic	100	0	-3.0	-1.5
Horizontal Dipole	95	-3.2	-6.1	-5.2
Horizontal CP Patch	100	-5.2	-5.7	-5.4
Horizontal PIFA	98	-4.0	-5.8	-4.6

and parallel polarisations of the dipole antenna are used. To further establish the model's efficiency, comparison is also made to an idealised isotropic antenna that is often used as a figure of merit due to its known theoretical gain values.

The calculated values of η_c and MEG_{GPS} using the proposed model for the three antennas along with the hypothetical isotropic antenna are presented in Table 4-1. The results indicate that the proposed model works well exhibiting the expected behaviour since, the MEG_{GPS} values for the actual reflection environment lies in between the two ideal extreme environments for the tested antennas.

4.4.3 Comparison Based on Simulated and Measured 3-D Gain Patterns

In the second step of the validation process, the statistical calculation results of the model are compared for two different input methods. The 3-D gain patterns of the three antennas, obtained through the simulations and the anechoic chamber (Satimo Stargate 64) measurements, are used for the comparison. The results summarised in Table 4-2 show good agreement between the calculated results of η_c and MEG_{GPS} using the

simulated and the measured 3-D gain patterns. A maximum difference of 0.6 dB has been observed in MEG_{GPS} values in the actual reflection environment while 4% in η_c values. This difference is associated to antenna fabrication errors.

Table 4-2: Comparison of calculated GPS Coverage Efficiency and GPS Mean Effective Gain of the three generic GPS antennas in different reflection environments using simulated and measured 3-D gain patterns for validation of proposed GPS multipath model

Antenna	Model Calculations Using Simulated 3-D Patterns				Model Calculations Using Measured 3-D Patterns			
	η_c (%)	MEG_{GPS} (dB)			η_c (%)	MEG_{GPS} (dB)		
		TR	NR	AR		TR	NR	AR
Horizontal Dipole	95	-3.2	-6.1	-5.2	97	-3.7	-6.4	-5.4
Horizontal CP Patch	100	-5.2	-5.7	-5.4	99	-5.8	-6.2	-6.0
Horizontal PIFA	98	-4.0	-5.8	-4.6	94	-4.3	-6.3	-5.1

Since, the performance of the horizontal dipole antenna in the actual reflection environment is used as a standard of comparison for other tested GPS antennas, the MEG_{GPS} value for actual reflection environment (AR) of -5.4 would serve as a reference in the following sections.

4.4.4 Comparison Based on Measured 3-D Gain Patterns and Actual Field Tests

The final and most important step of the validation process is to verify the calculated results of η_c and MEG_{GPS} of the GPS antennas using the proposed stochastic model by comparing them to the results obtained in an actual open field test. The open field tests are performed both at the Sony Ericsson Communications, Sweden and QMUL, London.

Since, the field test results are described in reference to an antenna measured in the same test, the horizontal dipole is chosen as the reference antenna. For the calculated

values of MEG_{GPS} using the proposed model and 3-D measured gain patterns, the MEG_{GPS} value of -5.4 (for actual reflection environment given in Table 4-2) is used to get the normalised MEG_{GPS} for the antenna under test. Therefore, MEG_{GPS} is represented as dBd. The results obtained through the field tests are also normalised to the noted mean SNR level of horizontal dipole i.e. 40.2 dB. The field test performance of the dipole, CP patch and Generic PIFA are compared with the calculated results using the measured 3-D gain patterns. The antennas are placed horizontally with respect to the ground.

In these assessments, the repeatability of the measurement procedure must also be known. Therefore, in these as well as the following investigations, MEG_{GPS} and η_c are calculated performing three sets of measurements and mean values are reported. It has been noted that the two results are repeatable with a mean standard deviation of 0.6 dB.

Table 4-3: Comparison of calculated GPS Coverage Efficiency and GPS Mean Effective Gain of the three generic GPS antennas using measured 3-D gain patterns to the actual field test measurements for validation of proposed GPS multipath model

Antenna	Model Calculations Using Measured 3-D Patterns		Open Field Test Measurements	
	η_c (%)	MEG_{GPS} (dBd)	η_c (%)	MEG_{GPS} (dBd)
Horizontal Dipole (reference)	97	0 (corresponding to calculated value of -5.4 dB in AR)	96	0 (corresponding to measured average SNR of 40.2 dB)
Horizontal CP Patch	99	-0.6	97	-0.4
Horizontal Generic PIFA	94	0.3	94	0.2

Table 4-3 summarises the calculated and the measured results. The field test results show a good agreement with the model's predictions for the MEG_{GPS} and η_c values for the GPS antennas. Figures 4.14 and 4.15 present the comparison of the two results showing the ranking of the antennas achieved by two methods. It is evident from these results that the model has successfully translated and predicted the GPS antenna per-
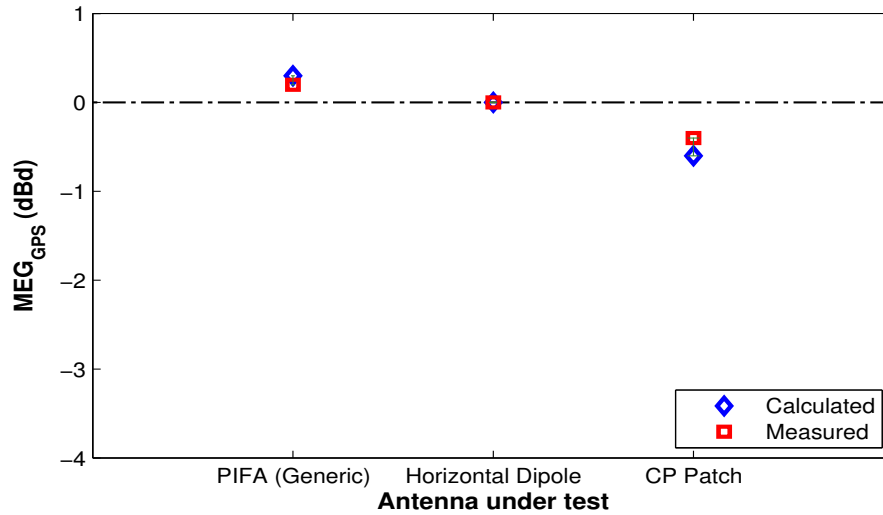
Figure 4.14: Comparison of calculated and measured values of MEG_{GPS} and performance ranking of the GPS dipole, CP patch and generic PIFA antennas in horizontal orientation taking horizontal dipole as reference (0 dBd)

formance and rated the antennas in the similar fashion as observed in the open field test. A maximum relative difference of 0.2 dB is noted for MEG_{GPS} values and 2% for η_c values. These differences are well below the accepted levels reported in literature [9, 12, 24]. These differences are mainly attributed to random errors caused by uncontrolled environment factors including height, temperature and wind in open field tests.

The results describe that MEG_{GPS} is an attractive measure to characterise the antenna performance. It simplifies the practical evaluation of the antenna performance as it is based on the antenna gain pattern measurements in anechoic chamber. It describes the antenna performance incorporating both the polarisation properties of the antenna under test and the directional properties of the radio environment. For example, from the prospects of antenna efficiency and maximum gain, the CP patch should out-perform the dipole and generic PIFA for the GPS operation. However, MEG_{GPS} results show that these methods are not enough to depict the real performance of the antennas in practical scenarios. A combined consideration of antenna gain, polarisation and the radio environment (i.e. the AoA_{GPS} distributions) in terms of MEG_{GPS} makes the generic
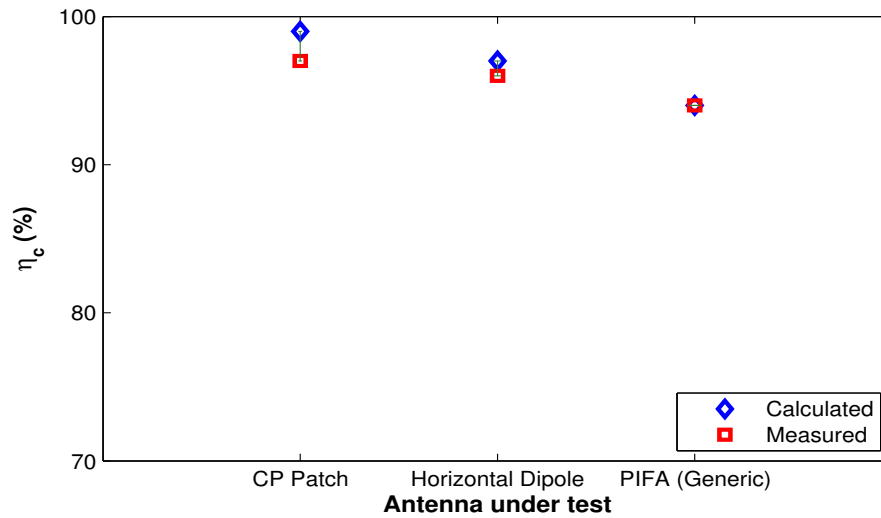
Figure 4.15: Comparison of calculated and measured values of η_c and performance ranking of the GPS dipole, CP patch and generic PIFA antennas in horizontal orientation

PIFA a better performing antenna in multipath.

The three validation steps confirm that the proposed statistical model successfully describes the multipath environment factors and their effects on the operation of the GPS antennas. It is therefore, an efficient tool to analyse the GPS antenna performance in the multipath environment. The calculated results using this model are further verified through the field tests to establish its accuracy using various GPS antennas in the following sections.

4.5 Performance Evaluation of GPS Mobile Terminal Antennas in Multipath Environment

The proposed model is used to evaluate the GPS antennas' performance in the multipath environment to get an insight of the environment effects. It also serves to further establish accuracy of the model. Five types of the GPS mobile terminal antennas; PIFA, IFA, DRA, helix and mono-loop antenna operating at 1575.42 MHz, in horizontal orientation are used in this study. The antennas are designed in CST Microwave Studio® package

and prototypes are fabricated and tested in the Antenna Measurement Lab at QMUL. The 3-D gain patterns are measured at Antenova Ltd., Cambridge. The measured 3-D gain patterns of the antenna configurations are then used to calculate MEG_{GPS} and η_c statistically. The calculated values are compared to the field test measurements by taking the horizontal dipole antenna as the reference.

4.5.1 Design of Mobile Terminal GPS Antennas

4.5.1.1 Mobile Terminal PIFA

A mobile terminal PIFA is also designed due to vast usage of this type of antennas in mobile applications. It is termed as "mobile terminal PIFA" due to its mobile phone standard ground plane size. The PIFA is designed using FR4 substrate of 1.6 mm thickness. The PCB size is 100 mm×40 mm. The antenna is fed using a 50 Ω coaxial port. Figure 4.16(a) shows the geometrical structure of the prototype while Figure 4.16(b) presents the measured S11 curve for the antenna. The antenna has 4.1% of -10 dB impedance bandwidth for a frequency range of 1560 MHz to 1625 MHz, adequate for the GPS operation. The measured 3-D gain patterns for the antenna at 1575.42 MHz for vertical and horizontal orientations are depicted in Figures 4.16(b) and (c).

4.5.1.2 IFA

The inverted F antenna (IFA) is designed on a metal plate of 0.45 mm thickness, 100 mm length and 40 mm width. The radiating element is mounted on the left side of the metal plate and has similar thickness (Figure 4.18(a)). The antenna is fed using a standard 50 Ω coaxial port. The antenna is fabricated and tested showing good performance for the GPS operation with excellent matching and exhibiting -10 dB bandwidth of 11.9% covering all the frequencies from 1480 MHz to 1668 MHz. Figure 4.18(b) shows the measured S11 response for the antenna while Figures 4.19(a) and (b) illustrate the mea-
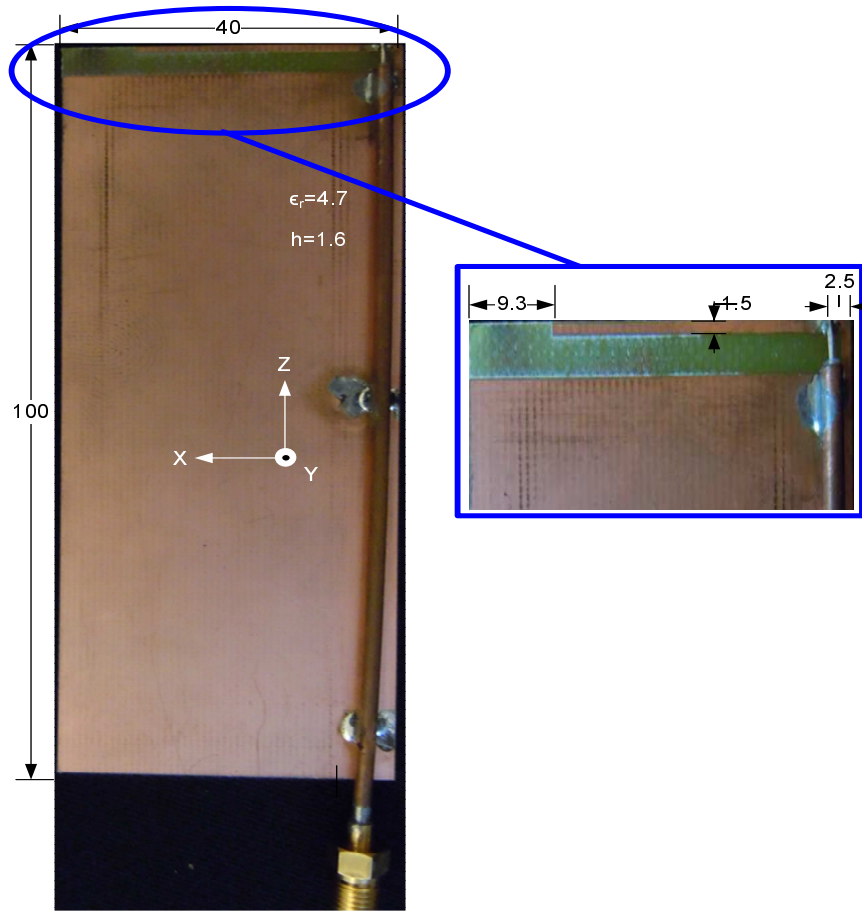
(a) Terminal PIFA prototype and geometry
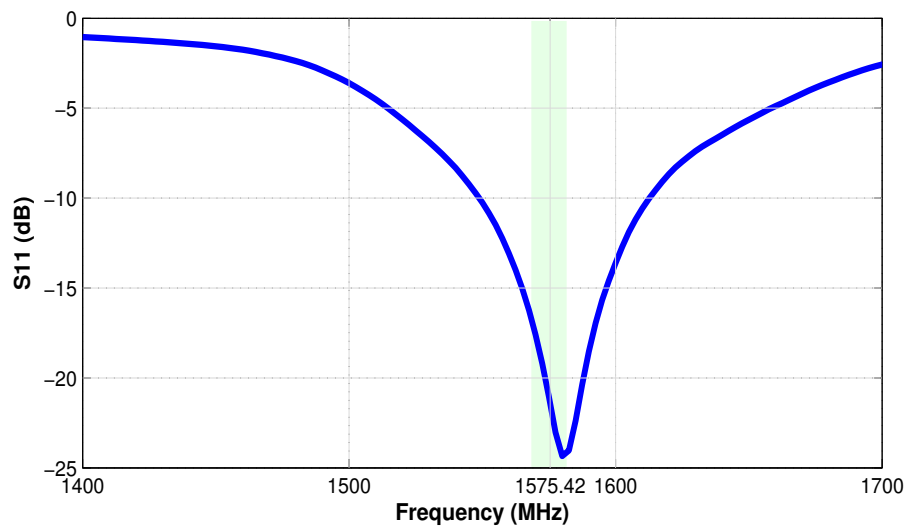
(b) Measured S11 curve

Figure 4.16: Geometrical structure of mobile terminal PIFA antenna for GPS operation with measured S11 response (all lengths are in mm)

$G_\perp(\theta,\phi)$ $G_\parallel(\theta,\phi)$

(a) 3-D measured gain patterns for vertical orientation

$G_\perp(\theta,\phi)$ $G_\parallel(\theta,\phi)$

(b) 3-D measured gain patterns for horizontal orientation

Figure 4.17: Measured 3-D gain patterns for perpendicular and parallel polarisations of mobile terminal PIFA antenna for GPS operation in vertical and horizontal orientations

sured 3-D radiation patterns for the antenna at 1575.42 MHz for vertical and horizontal orientations.

4.5.1.3 DRA

Ceramic antennas are another popular choice for embedded antennas due to their small size. Therefore, a dielectric resonant antenna (DRA) is designed for this study. The antenna is loaded with a dielectric of $\varepsilon_r = 21$. The ground plane is 100 mm$\times$40 mm$\times$1

(a) IFA prototype and geometry
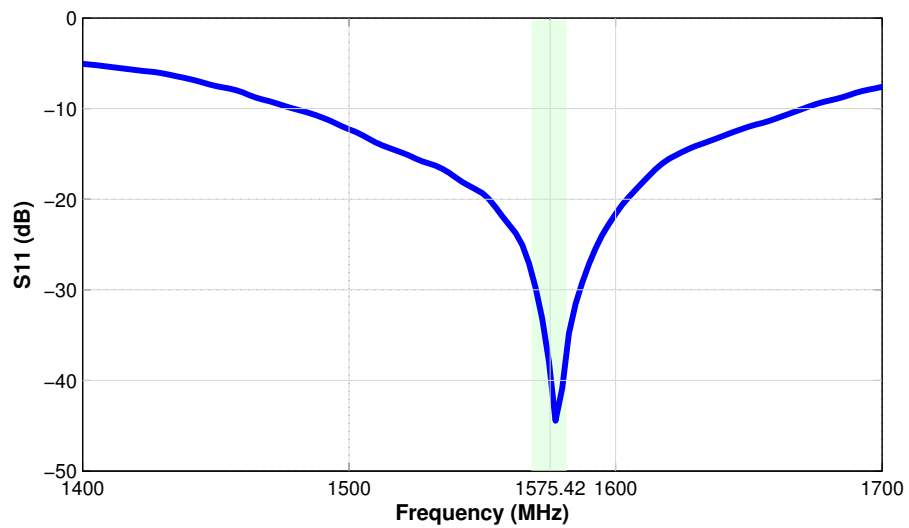
(b) Measured S11 curve

Figure 4.18: Geometrical structure of mobile terminal IFA antenna for GPS operation with measured S11 response (all lengths are in mm)

$G_\perp(\theta,\phi)$ $G_\parallel(\theta,\phi)$

(a) 3-D measured gain patterns for vertical orientation

$G_\perp(\theta,\phi)$ $G_\parallel(\theta,\phi)$

(b) 3-D measured gain patterns for horizontal orientation
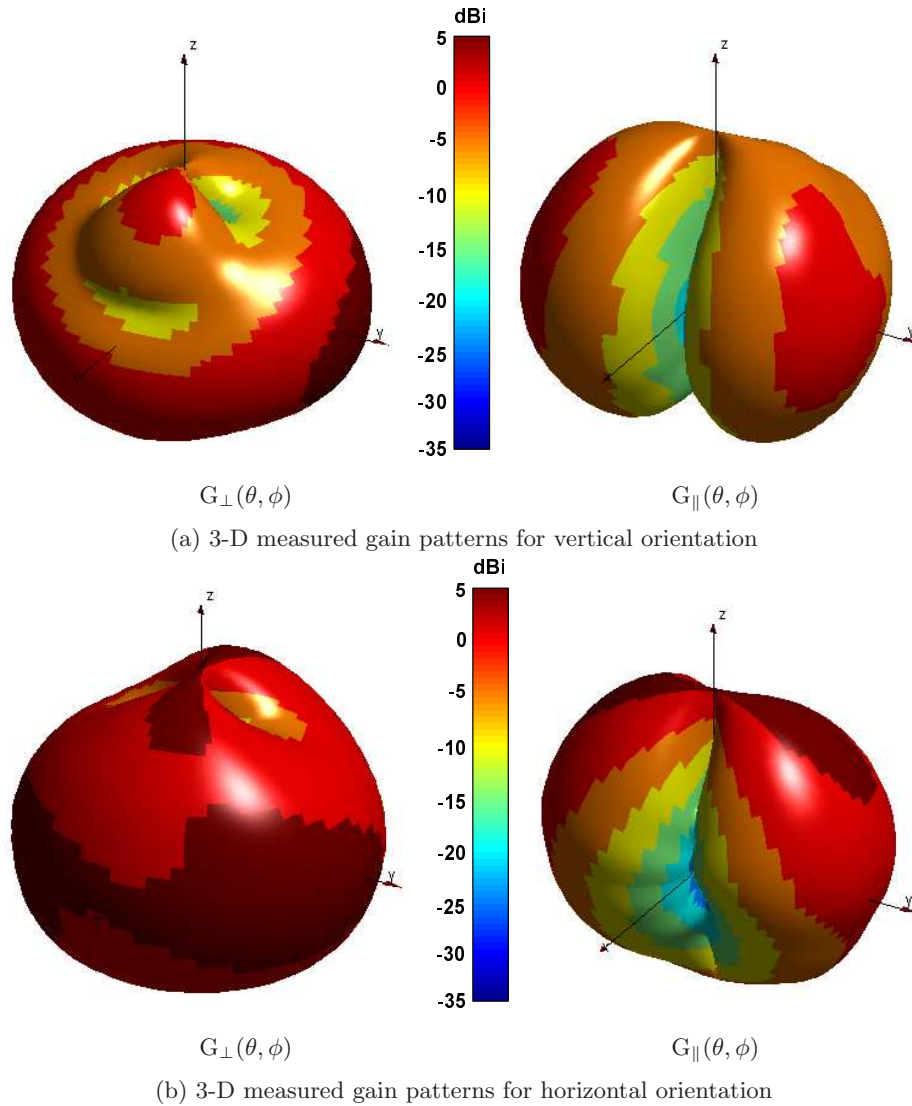
Figure 4.19: Measured 3-D gain patterns for perpendicular and parallel polarisations of mobile terminal IFA antenna for GPS operation in vertical and horizontal orientations

mm of lossy copper type with σ=5.8$\times10^7$S/m. The loaded dielectric is covered with lossy silver having σ=6.17$\times10^7$S/m. The antenna is fed using a 50 Ω coaxial port. The prototype is fabricated at Sony Ericsson Communications, AB, Sweden. Figure 4.20(a) describes the geometrical structure of the fabricated antenna. The measured S11 shown in Figure 4.20(b) indicates that the antenna works well in L1 band with 2.8% of -10 dB bandwidth that covers frequencies from 1553 MHz to 1597 MHz with centre frequency at 1574 MHz. The measured 3-D gain patterns for the antenna at 1575.42 MHz for vertical and horizontal orientations are described in Figures 4.21(a) and (b).
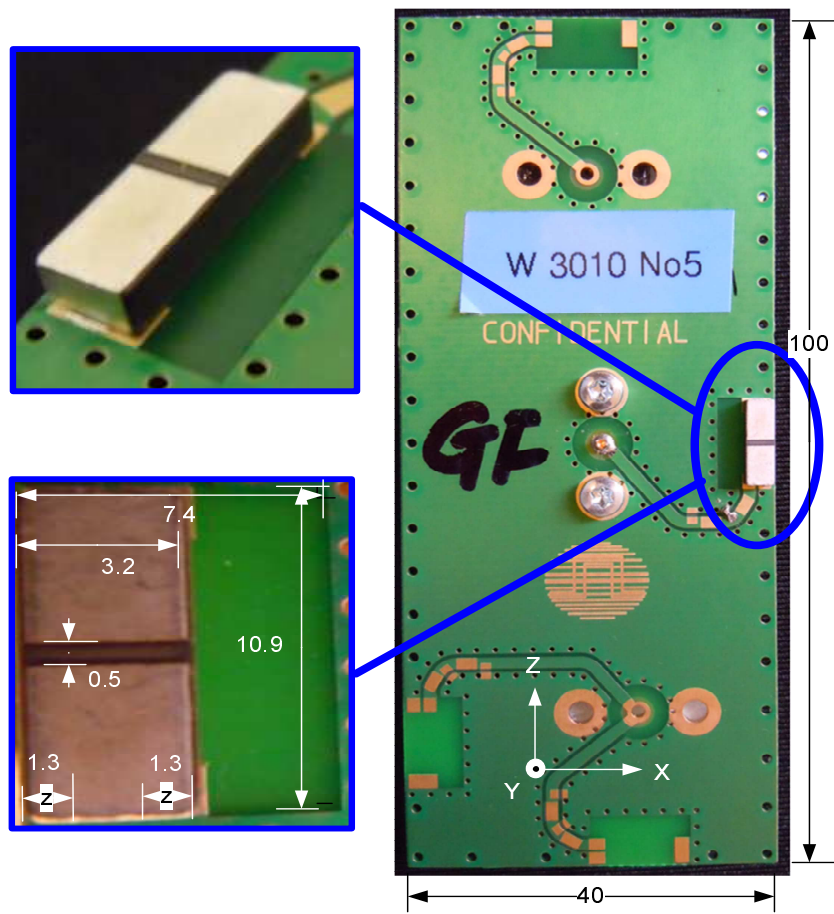
(a) DRA prototype and geometry
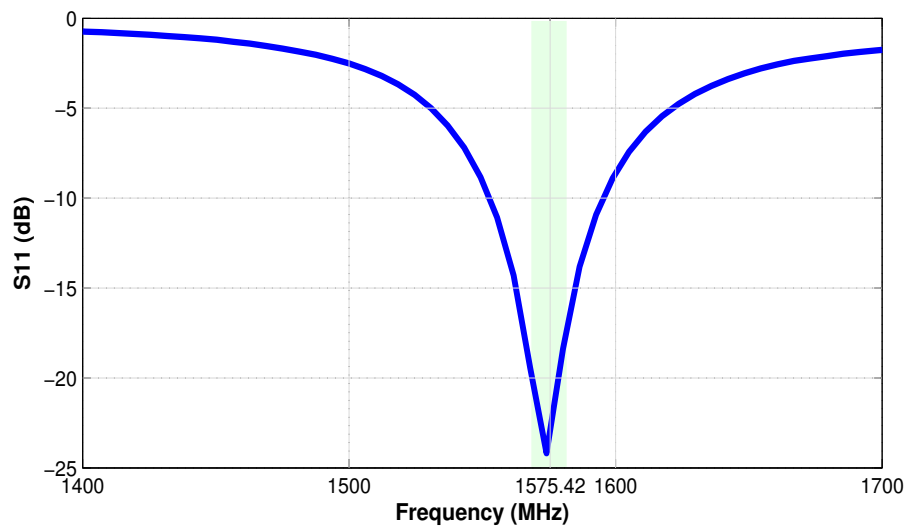
(b) Measured S11 curve

Figure 4.20: Geometrical structure of mobile terminal DRA antenna for GPS operation with measured S11 response (all lengths are in mm)

$G_\perp(\theta, \phi)$ $\qquad\qquad\qquad\qquad\qquad\qquad$ $G_\parallel(\theta, \phi)$

(a) 3-D measured gain patterns for vertical orientation

$G_\perp(\theta, \phi)$ $\qquad\qquad\qquad\qquad\qquad\qquad$ $G_\parallel(\theta, \phi)$

(b) 3-D measured gain patterns for horizontal orientation
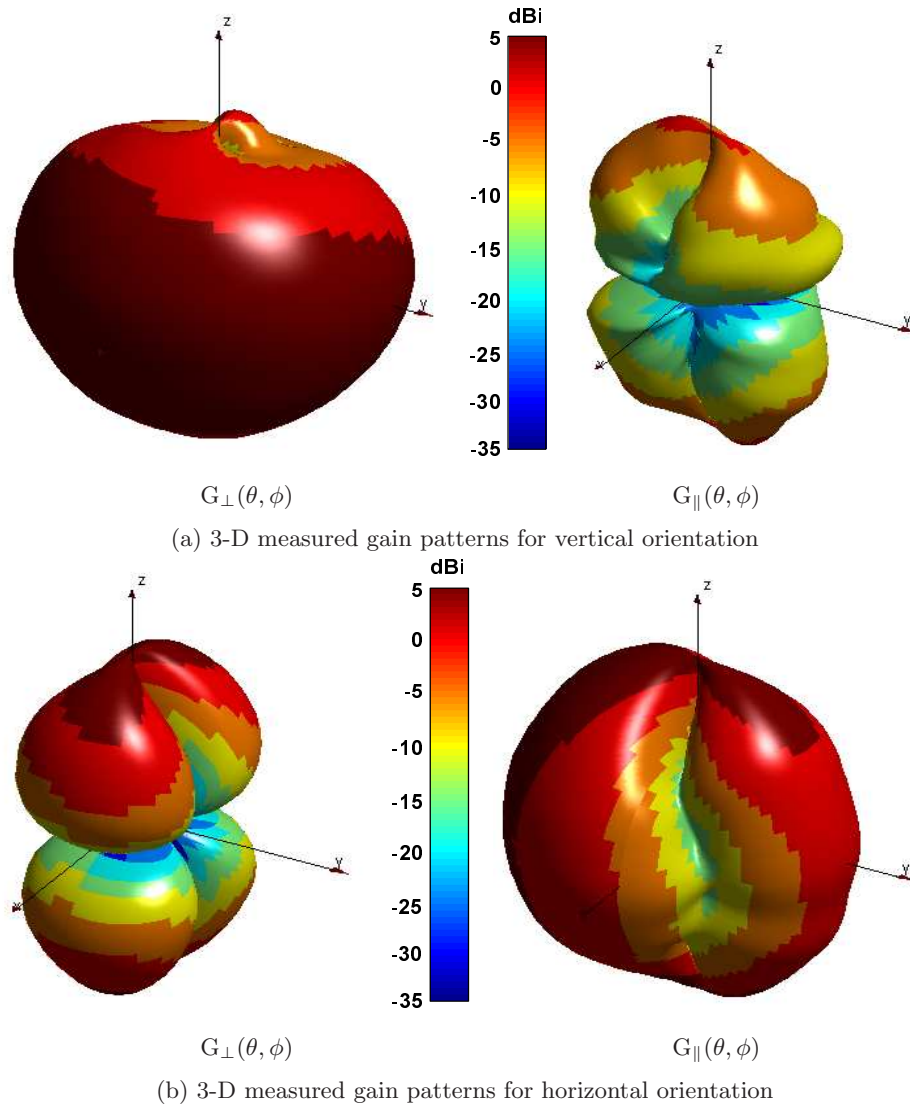
Figure 4.21: Measured 3-D gain patterns for perpendicular and parallel polarisations of mobile terminal DRA antenna for GPS operation in vertical and horizontal orientations

4.5.1.4 Helix

The external antennas, like the helix, are not used widely in the portable applications nowadays. However, a performance comparison needs such a type of antenna to understand the nature of the degradation caused by the multipath environment. Therefore, a helix antenna has also been designed for this study. The designed helix antenna has no substrate and is mounted on the left top of the metallic ground plane having dimensions of 100 mm×40 mm×0.45 mm, shown in Figure 4.22(a). The radius of the helix wire is

0.45 mm with a length of 26 mm. The antenna is fed through a 50 Ω coaxial port. The measurement result for S11 response plotted in Figure 4.22(b) describes that antenna works well in the L1 band having a -10 dB bandwidth of 9% ranging from 1495 MHz to 1638 MHz frequencies. The measured 3-D radiation patterns of the antenna in vertical and horizontal orientations are shown in Figures 4.23(a) and (b).

4.5.1.5 Mono-loop

The single-element mono-loop antenna is designed and fed by a microstrip line with a substrate of 100 mm×40 mm, having a dielectric permittivity of 4.7. The radiating element is a combination of monopole and loop structure. The ground plane size is only 18 mm×80 mm. The radiating element consists of 11 loops of 23.2 mm×2 mm. The antenna exhibits a -10 dB impedance bandwidth of 107 MHz covering the frequencies from 1520 MHz to 1627 MHz. Figure 4.24(a) illustrates the geometrical structure and Figure 4.24(b) shows the measured S11 curve for the antenna. Figures 4.25(a) and (b) depict the measured 3-D patterns for the antenna.

Table 4-4 gives the account of MEG_{GPS} and η_c results for different mobile terminal GPS antennas in the multipath environment in the horizontal orientation (with respect to the ground). The calculated MEG_{GPS} (in AR) and measured SNR values of horizontal dipole antenna i.e. -5.4 dB and 40.2 dB are used as the reference. The calculated results are compared and verified through the field test measurements and a good agreement between the two has been achieved. Figures 4.26 and 4.27 show the comparison of the antenna rankings achieved by the two methods. These results further validate the working of the model since, the antennas are ranked in the similar fashion as observed in the open field test. The model has given very precise results with a maximum relative difference of 0.4 dB for MEG_{GPS} values while 3% for η_c values due to random errors.

The results also indicate that the two parameters of MEG_{GPS} and η_c do no rely tightly on each other. An antenna with good η_c may exhibit poor MEG_{GPS} and vice
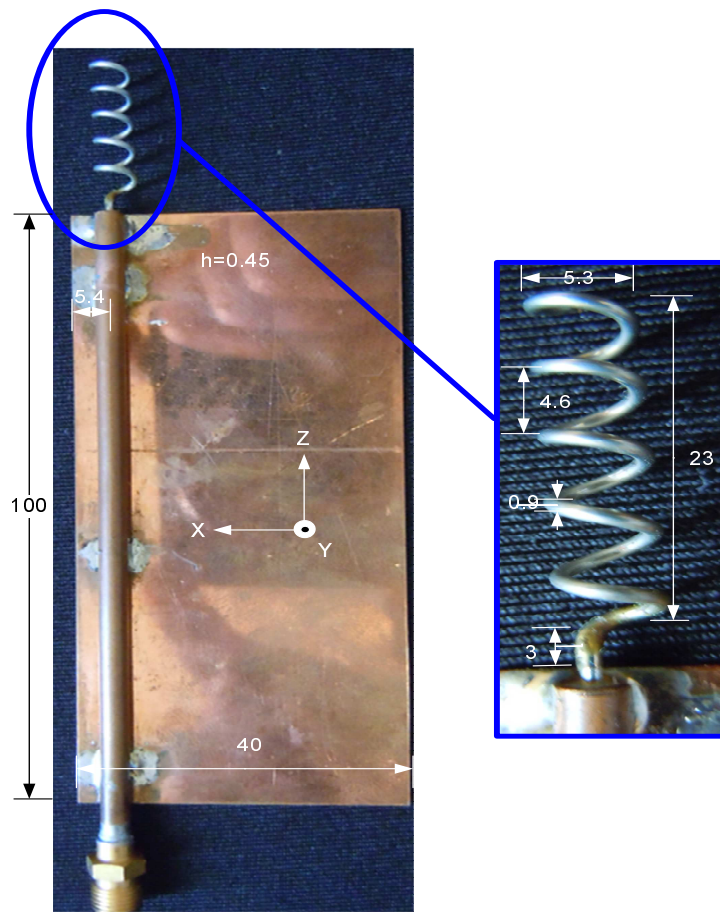
(a) Helix prototype and geometry
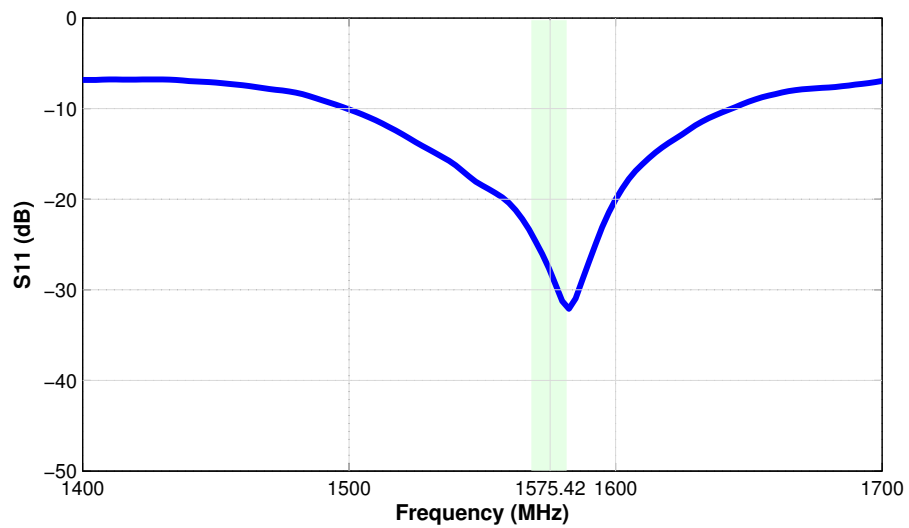
(b) Measured S11 curve

Figure 4.22: Geometrical structure of mobile terminal helix antenna for GPS operation with measured S11 response (all lengths are in mm)

$G_\perp(\theta,\phi)$ $G_\parallel(\theta,\phi)$

(a) 3-D measured gain patterns for vertical orientation

$G_\perp(\theta,\phi)$ $G_\parallel(\theta,\phi)$

(b) 3-D measured gain patterns for horizontal orientation
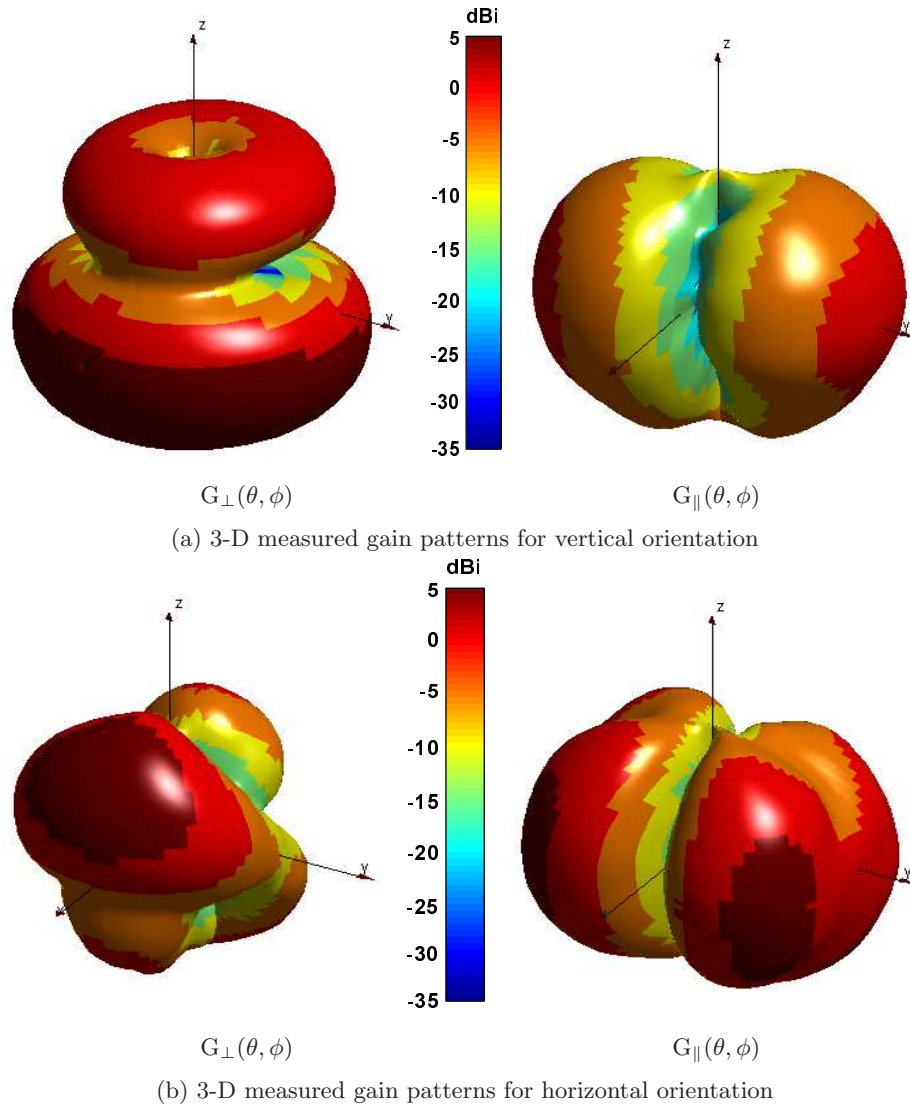
Figure 4.23: Measured 3-D gain patterns for perpendicular and parallel polarisations of mobile terminal helix antenna for GPS operation in vertical and horizontal orientations

versa, for example the case of the helix and DRA antennas. It is due to the fact that MEG_{GPS} incorporates the whole environment, especially the ground reflections, whereas η_c only describes the satellite tracking capability of the antenna. Therefore, it is observed during the measurements that even the antennas with poor MEG_{GPS} could efficiently get a number of GPS satellites locked. However, an optimal performance could only be achieved with an antenna exhibiting good MEG_{GPS} and η_c. It is further investigated in the following section when effects of the change in antenna orientation has been studied.
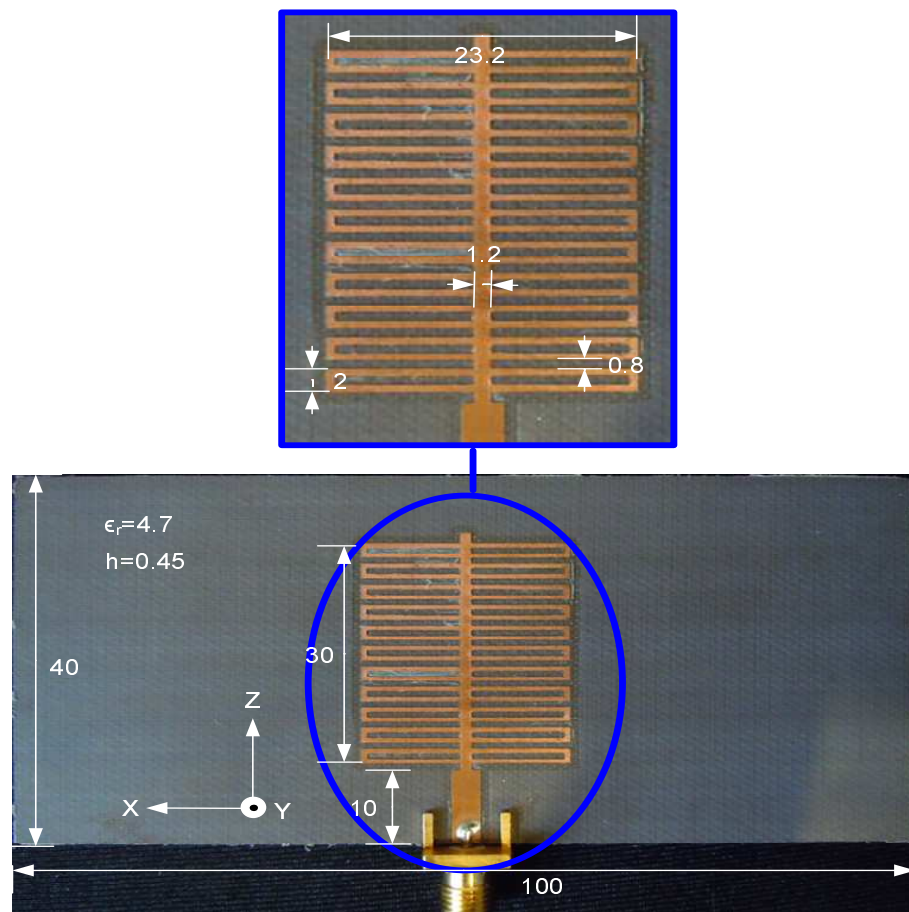
(a) Mono-loop prototype and geometry
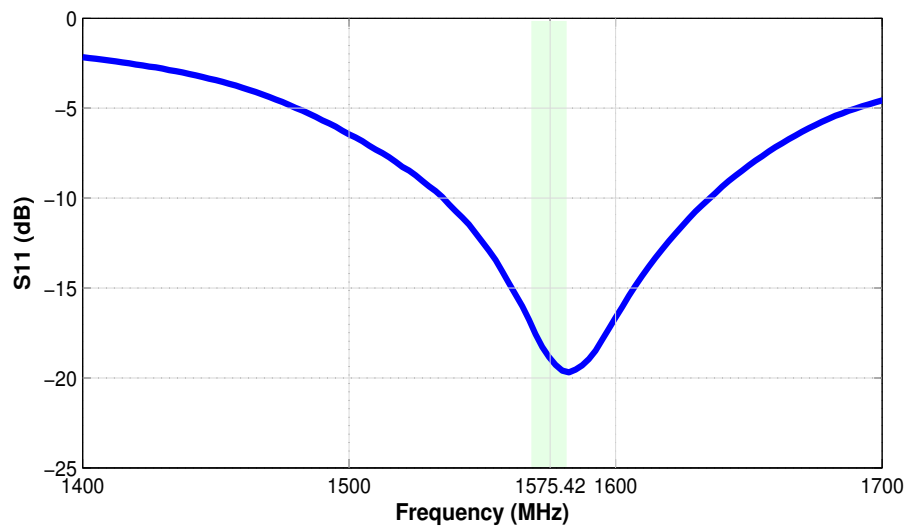
(b) Measured S11 curve

Figure 4.24: Geometrical structure of mobile terminal mono-loop antenna for GPS operation with measured S11 response (all lengths are in mm)

$G_\perp(\theta, \phi)$ $G_\parallel(\theta, \phi)$

(a) 3-D measured gain patterns for vertical orientation

$G_\perp(\theta, \phi)$ $G_\parallel(\theta, \phi)$

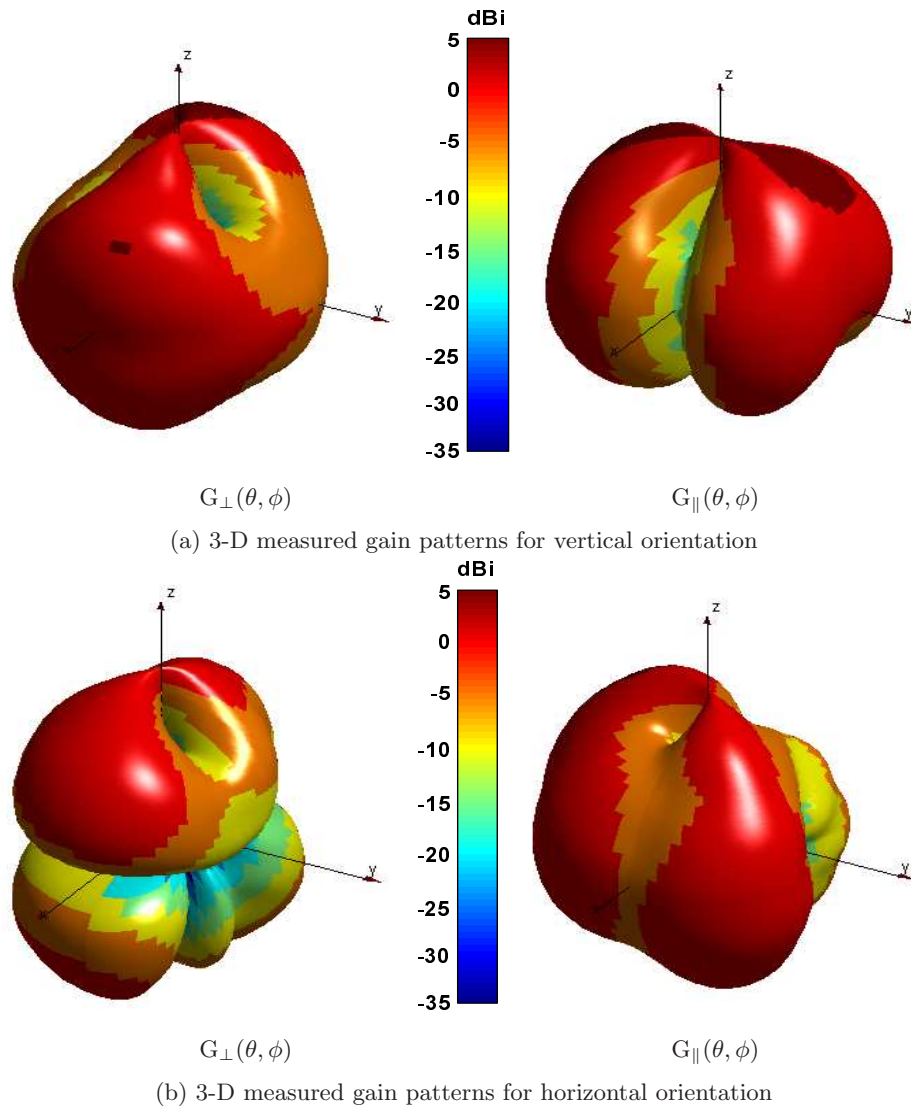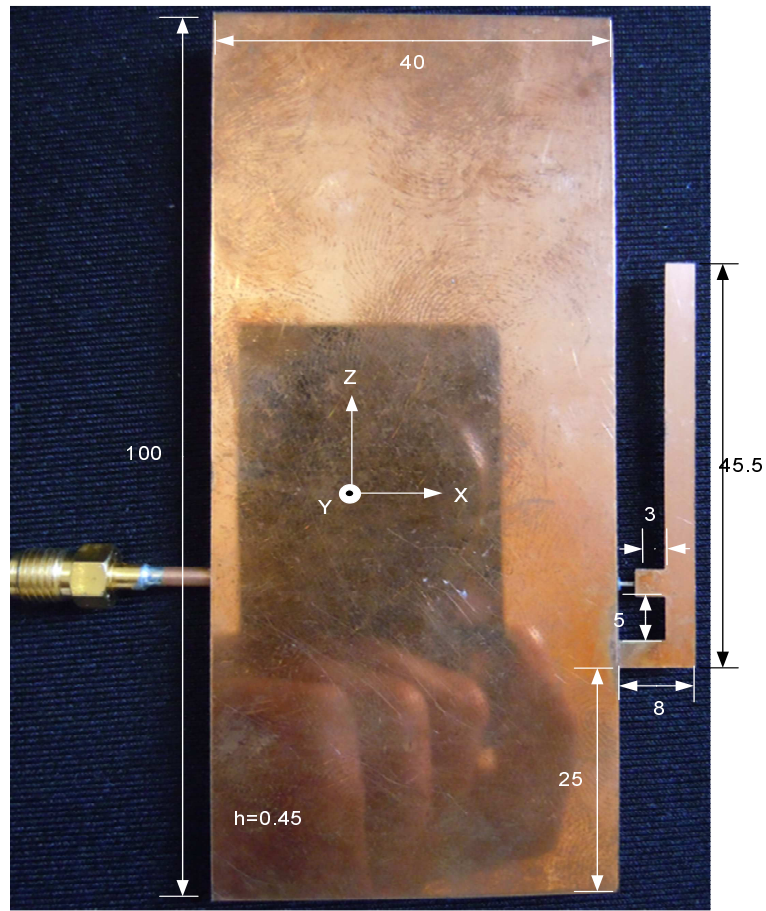(b) 3-D measured gain patterns for horizontal orientation
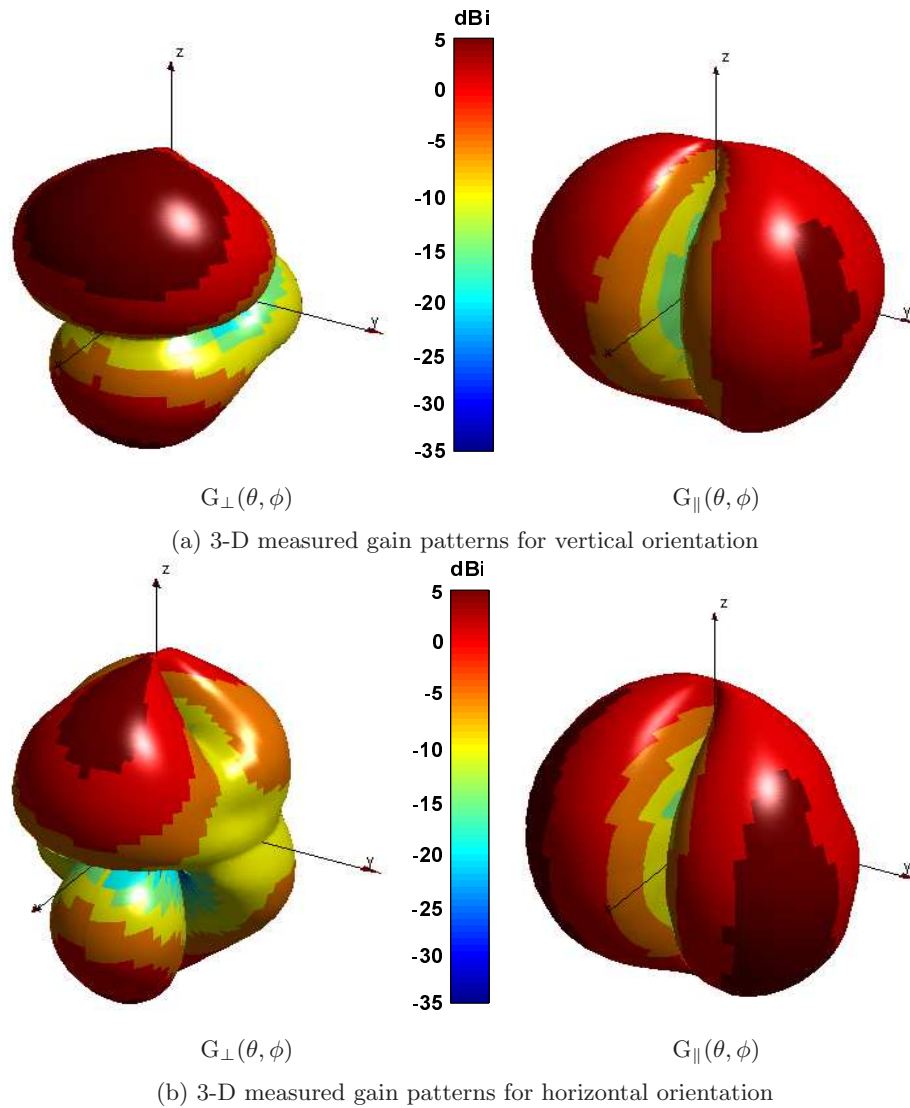
Figure 4.25: Measured 3-D gain patterns for perpendicular and parallel polarisations of mobile terminal mono-loop antenna for GPS operation in vertical and horizontal orientations

4.5.2 Dependance on Antenna Orientation

The antenna orientation plays vital role in the communication links as changing the orientation causes change in the antenna main lobe direction inflicting link losses. Since, the mobile terminal antennas are not fixed and operate in ever-changing orientations depending on the user's holding position, effects of change of orientation need to be considered for a reliable GPS link. Therefore, the performance of various GPS antennas,
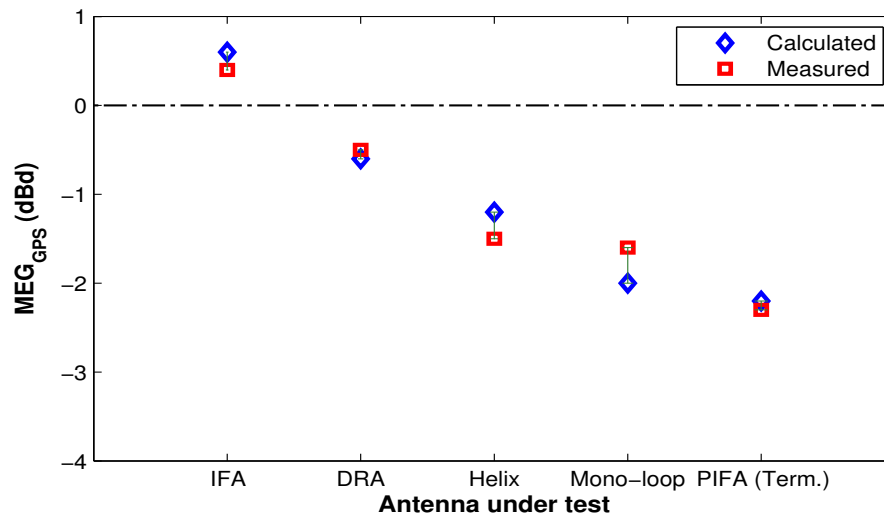
Figure 4.26: Comparison of calculated and measured values of MEG_{GPS} and performance ranking of the GPS mobile terminal antennas in horizontal orientation taking horizontal dipole as reference (0 dBd)
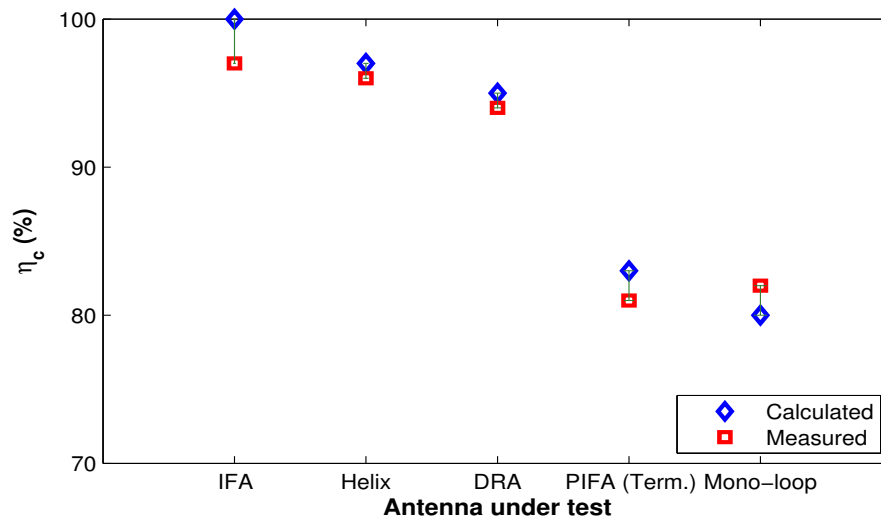
Figure 4.27: Comparison of calculated and measured values of η_c and performance ranking of the GPS mobile terminal antennas in horizontal orientation

discussed in the previous sections, is evaluated in vertical orientation using the proposed statistical model and verified through open field measurements.

The results are summarised in Table 4-4 while comparison of the antenna rankings in terms of their MEG_{GPS} and η_c based on the model's calculations and open field test measurements is presented in Figures 4.28 and 4.29. It is evident from the presented

results that the model delivers precise results with a close agreement to the field test observations. A maximum relative difference of 0.4 dB in MEG_{GPS} and 4% in η_c has been noted.

Table 4-4: Comparison of calculated GPS Coverage Efficiency and GPS Mean Effective Gain of various GPS antennas in vertical orientation using measured 3-D gain patterns to the actual field test measurements

Antenna	Orientation	Model Calculations Using Measured 3-D Patterns		Open Field Test Measurements	
		η_c (%)	MEG_{GPS} (dBd)	η_c (%)	MEG_{GPS} (dBd)
Dipole	Horizontal	97	0 (corresponding to calculated value of -5.4 dB in AR)	96	0 (corresponding to measured average SNR of 40.2 dB)
	Vertical	94	-0.2	92	-0.2
CP Patch	Horizontal	99	-0.6	97	-0.4
	Vertical	72	-2.1	72	-2.2
Generic PIFA	Horizontal	94	0.3	94	0.2
	Vertical	97	-0.5	97	-0.8
Terminal PIFA	Horizontal	83	-2.2	81	-2.3
	Vertical	95	-3.3	92	-3.1
IFA	Horizontal	100	0.6	97	0.4
	Vertical	79	-0.4	81	-0.3
DRA	Horizontal	95	-0.6	94	-0.5
	Vertical	94	-0.5	90	-0.5
Helix	Horizontal	97	-1.2	96	-1.5
	Vertical	87	-0.6	87	-1.0
Mono-loop	Horizontal	80	-2.0	82	-1.6
	Vertical	78	-1.6	80	-1.8

The results indicate that change in the antenna orientation plays an important role. Although, no set pattern could be described for the tested GPS antennas, comparing the vertically oriented antennas to those in horizontal orientation (Figures 4.30 and 4.31),
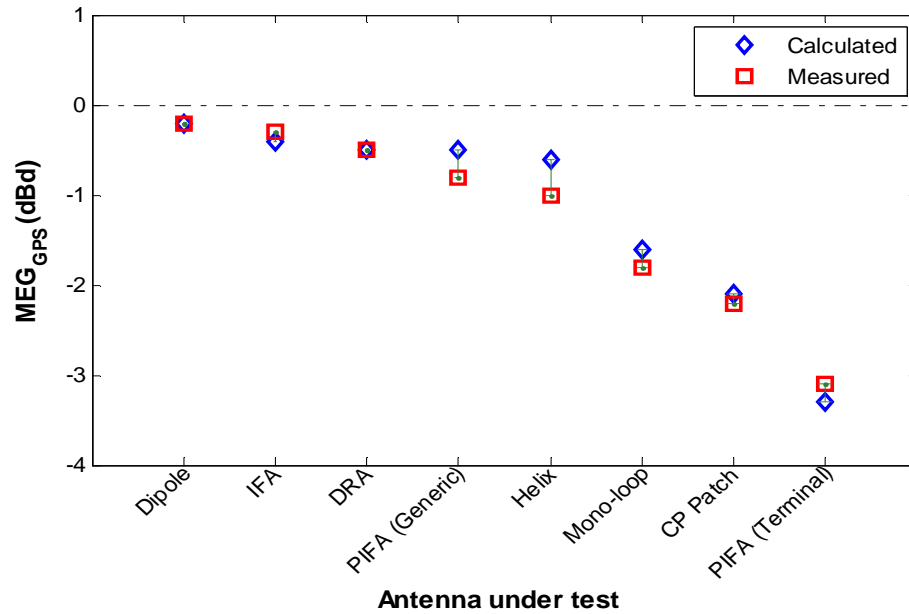
Figure 4.28: Comparison of calculated and measured values of MEG_{GPS} and performance ranking of various GPS antennas in vertical orientation taking horizontal dipole as reference
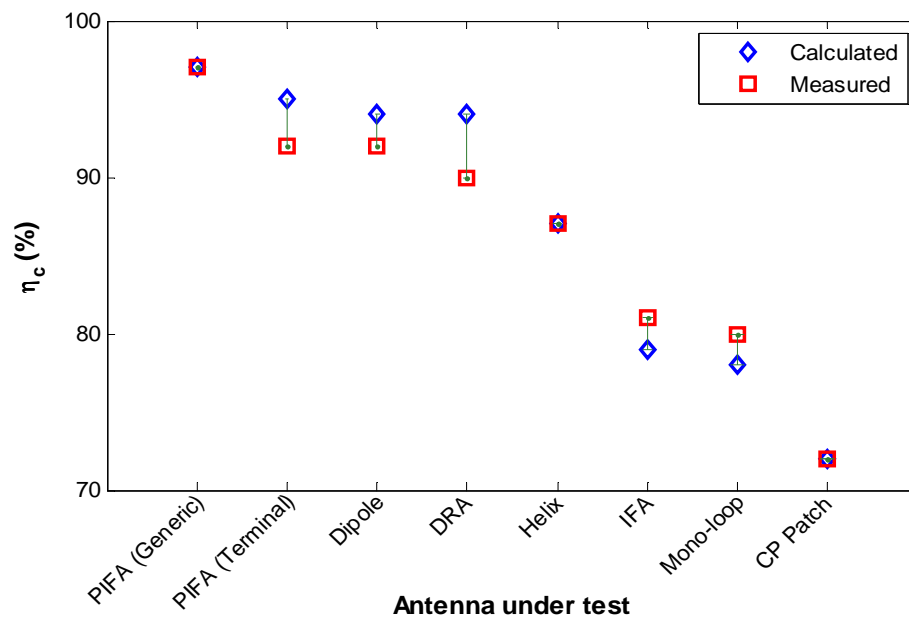
Figure 4.29: Comparison of calculated and measured values of η_c and performance ranking of various GPS antennas in vertical orientation

the horizontal configurations show an overall better performance in terms of MEG_{GPS}. It describes that the antenna gain and polarisation responds better to the nature of the incident plane waves when placed horizontally. The higher values of the antenna gain
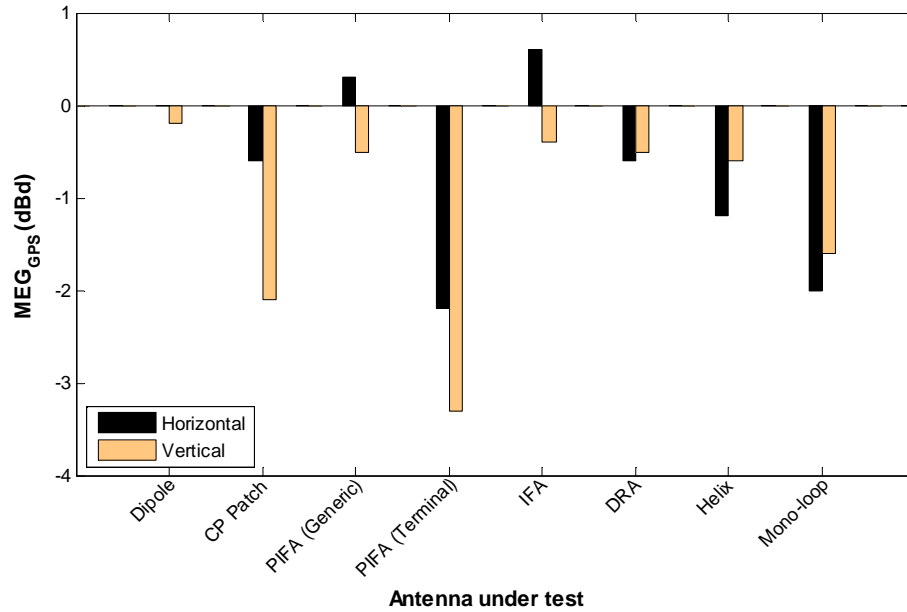
Figure 4.30: Performance comparison of various GPS antennas with effects of change in orientation in terms of calculated MEG_{GPS} taking horizontal dipole as reference

especially in the upper hemispherical space, in both the perpendicular and parallel polarisations (as presented in the gain pattern figures) is a key contributor. The horizontally oriented antennas also exhibit better η_c as more open sky view is available increasing the number of the tracked satellites. An increased level of received signal in the incident region ($0^o \leq \theta \leq 90^o$) lessens the wasted component and hence, increasing the overall η_c.

The DRA has been proved to be the most stable antenna to the changing orientation effects with similar values of MEG_{GPS} and η_c. It has been observed that the IFA, helix, CP patch and terminal PIFA are more vulnerable to change in orientation as MEG_{GPS} and η_c changes significantly. The vertical CP patch has lost 27% of its coverage as compared to the horizontal orientation while η_c of the vertical IFA is decreased by 20%. The performance of the horizontal CP patch is affected the most as its MEG_{GPS} is also reduced by 1.6 dB. It also shows that linear polarised mobile terminal antennas could deliver good performance as compared to the circular polarised antennas in real working scenarios.

The change in antenna η_c with changing orientation (with respect to the ground) is
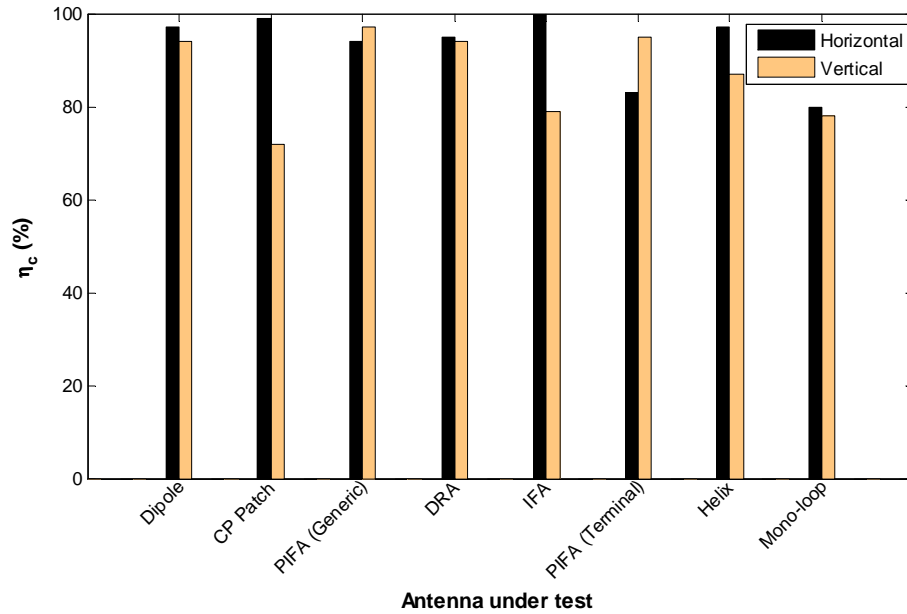
Figure 4.31: Performance comparison of various GPS antennas with effects of change in orientation in terms of calculated η_c

attributed to the sensitivity of the antenna to receive the incoming GPS signal. Since, the incoming GPS signal is RHCP, antenna RHCP gain patterns are evaluated in order to study the relation between η_c and RHCP gain with change in antenna orientation. Figures 4.32-4.39 present the comparison of measured RHCP gains in the incident region $(0^o \leq \theta \leq 90^o)$ for the tested antennas in both the horizontal and vertical orientations.

The comparison of the presented plots clearly indicates that η_c of the antenna depends upon the strength of the RHCP gain in the incident region. For example, in the case of the CP patch antenna, the vertical orientation exhibits much lower η_c of 72% as compared to 99% for the horizontal orientation. The comparison of the RHCP gain patterns clearly indicates that almost all of the incident region is above the required threshold level of -13 dB when the antenna is working in the horizontal orientation (Figure 4.33(a)). However, presence of the RHCP gain levels lower than -13 dB when the antenna operates in the vertical orientation, particularly in the angles $30^o \leq \theta \leq 90^o$, $0^o \leq \phi \leq 60^o$ and $40^o \leq \theta \leq 90^o$, $330^o \leq \phi \leq 360^o$, gives rise to the wasted signal resulting in a lower η_c.

Similarly, the IFA has also been observed to be an orientation sensitive antenna

(a) Horizontal orientation

(b) Vertical orientation
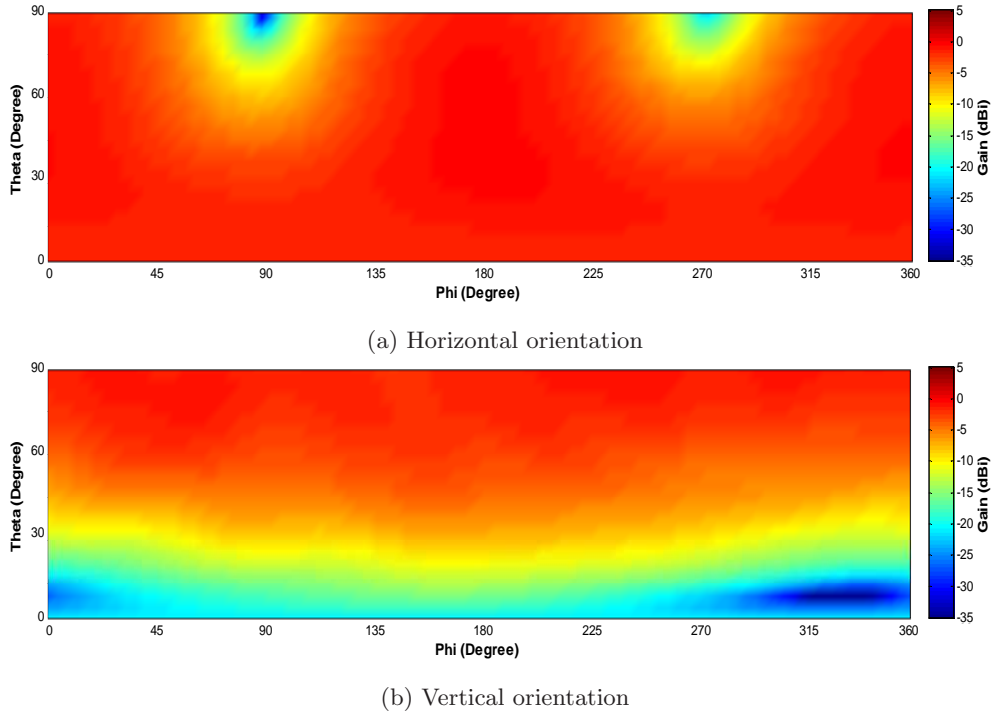
Figure 4.32: Measured RHCP gain patterns in the incident region for dipole GPS antenna in horizontal and vertical orientations

exhibiting 100% η_c in horizontal orientation but only 79% in vertical orientation. The difference in the RHCP gain patterns again explains the reason for this decrease in the antenna coverage. Figure 4.36(a) shows that the antenna covers whole of the incident region with the RHCP gain above -13 dB while operating in the horizontal orientation. However, the vertical configuration of the antenna loses coverage in most of the incident angles in the range of $30^o \leq \theta \leq 90^o$, $10^o \leq \phi \leq 165^o$ with lower than -13 dB RHCP gain as illustrated in Figure 4.36(b). The difference in η_c of the terminal PIFA and helix antennas with varying orientation is also because of the variation in the RHCP gain of the antenna in the incident region, depicted in Figures 4.35 and 4.38, respectively.

4.5.3 Effects of Antenna Position on PCB/Ground Plane

The position of the radiating element on the antenna ground plane could also play a role in its performance in the multipath environment by changing the radiation pat-
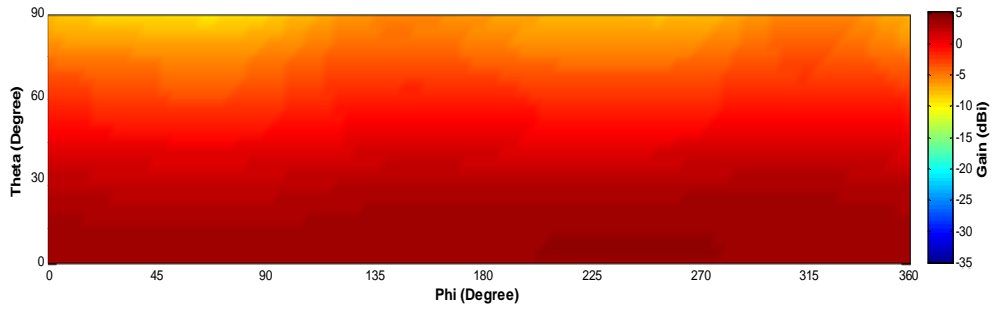
(a) Horizontal orientation
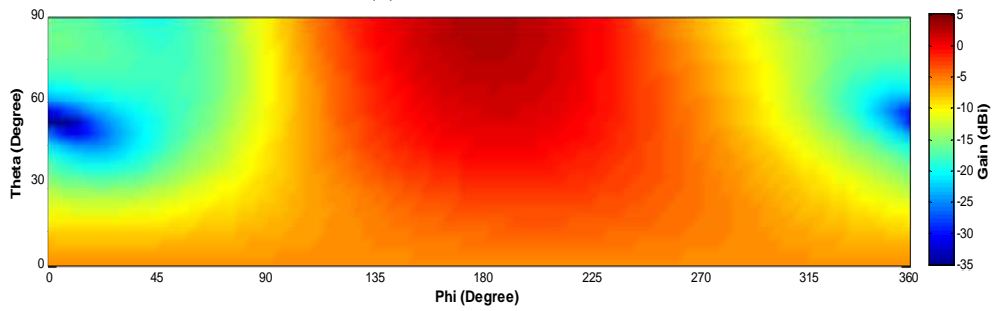
(b) Vertical orientation

Figure 4.33:   Measured RHCP gain patterns in the incident region for CP patch GPS antenna in horizontal and vertical orientations
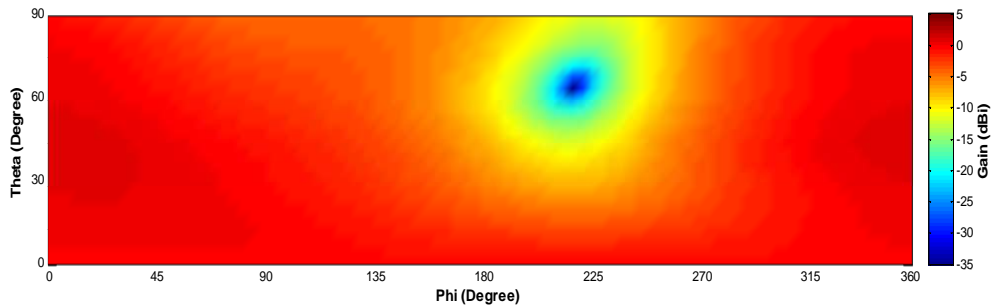
(a) Horizontal orientation
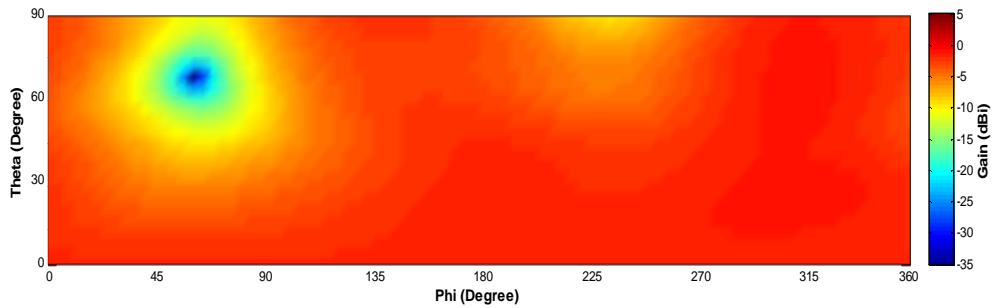
(b) Vertical orientation

Figure 4.34:   Measured RHCP gain patterns in the incident region for generic PIFA GPS antenna in horizontal and vertical orientations
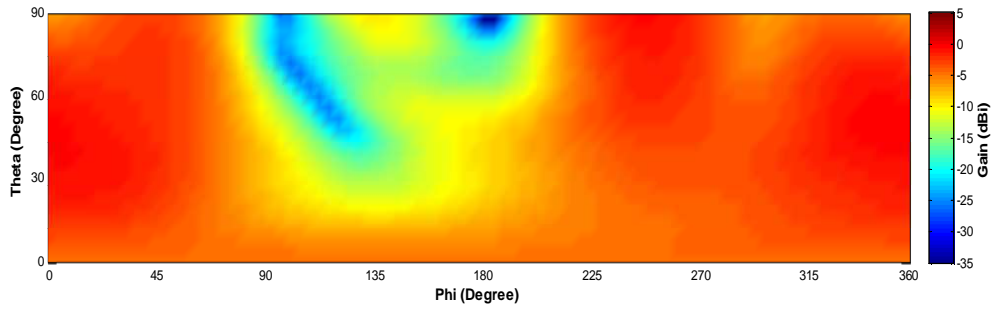
(a) Horizontal orientation
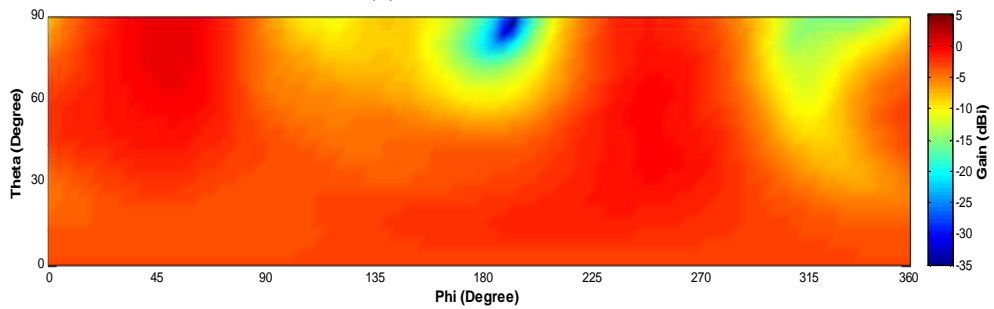
(b) Vertical orientation

Figure 4.35: Measured RHCP gain patterns in the incident region for mobile terminal PIFA GPS antenna in horizontal and vertical orientations
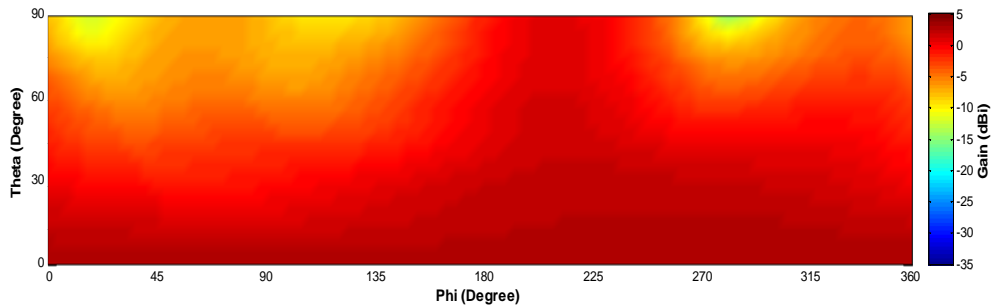
(a) Horizontal orientation
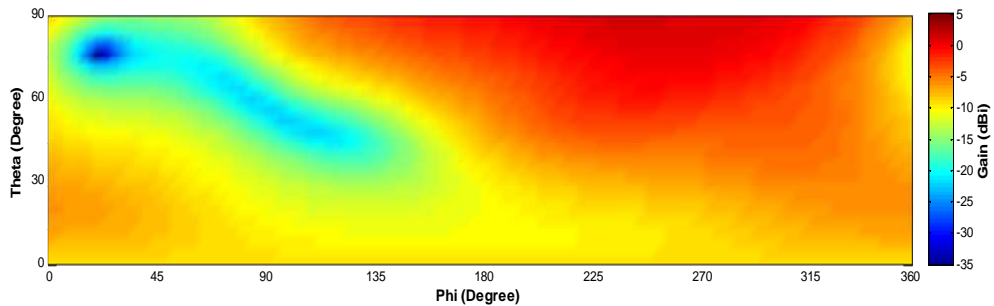
(b) Vertical orientation

Figure 4.36: Measured RHCP gain patterns in the incident region for IFA GPS antenna in horizontal and vertical orientations
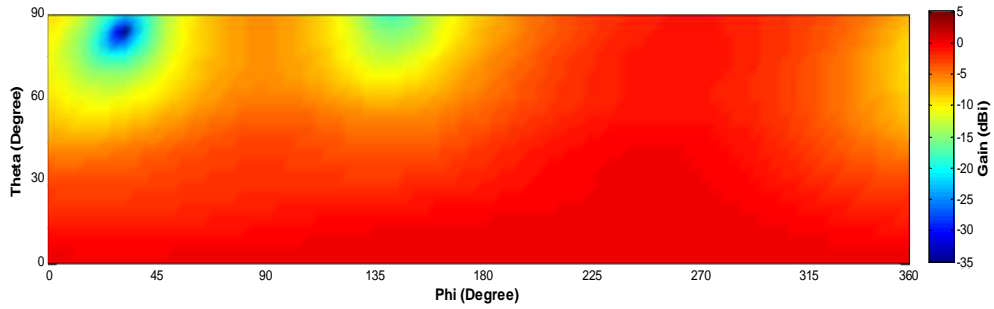
(a) Horizontal orientation
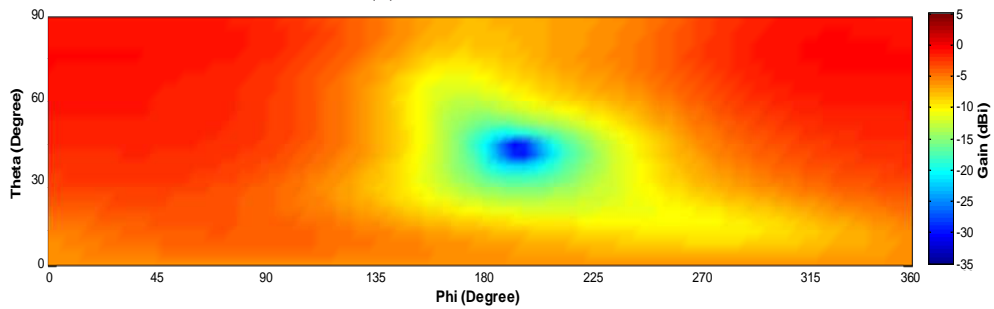
(b) Vertical orientation

Figure 4.37: Measured RHCP gain patterns in the incident region for DRA GPS antenna in horizontal and vertical orientations
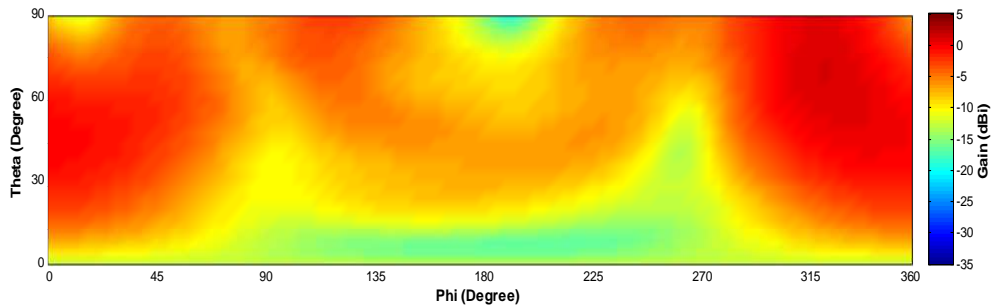
(a) Horizontal orientation
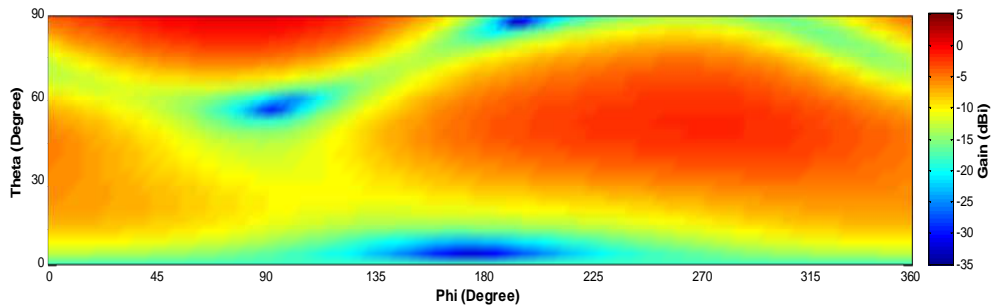
(b) Vertical orientation

Figure 4.38: Measured RHCP gain patterns in the incident region for helix GPS antenna in horizontal and vertical orientations

(a) Horizontal orientation

(b) Vertical orientation
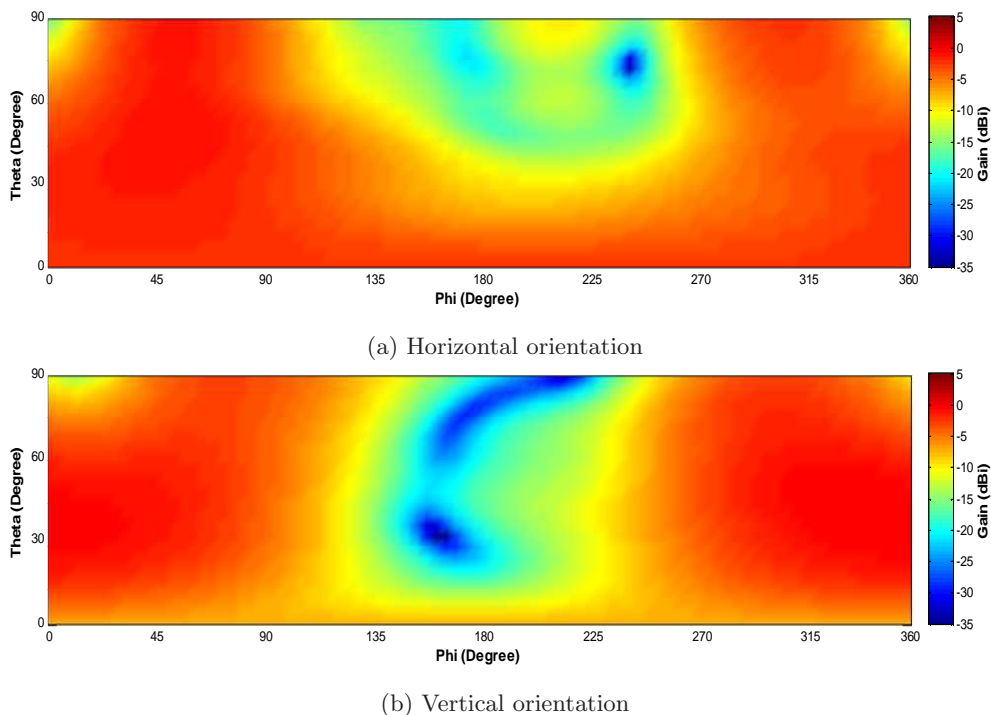
Figure 4.39: Measured RHCP gain patterns in the incident region for mono-loop GPS antenna in horizontal and vertical orientations

tern. Therefore, the performance of two mobile terminal GPS antennas; IFA and DRA is investigated by varying the position of the radiating element on the ground plane. The vertically oriented antennas are considered with different locations of the radiating element on the PCB/ground plane including left (i.e. original position), right, top and bottom edges.

Figures 4.40 and 4.43 illustrate the tested antenna configurations. The dimensions of the two antennas are similar as described in Figures 4.18 and 4.20. Figures 4.41 and 4.42 show the simulated 3-D gain patterns for perpendicular and parallel polarisations of the IFA with the radiating element positioned on the left, right, top and bottom edges of the ground plane respectively. Similarly, Figures 4.44 and 4.45 show the simulated 3-D gain patterns for perpendicular and parallel polarisations of the DRA for the left, right, top and bottom positioned radiating element on the PCB respectively. MEG_{GPS} and η_c are calculated using the proposed model and compared in Figures 4.46 and 4.47 for the two antennas.
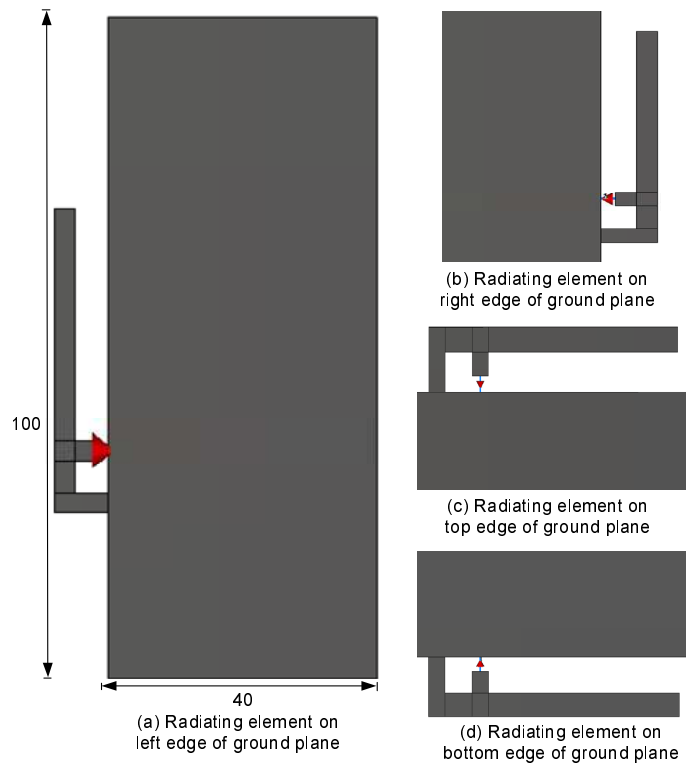
Figure 4.40: Schematic of re-positioned radiating element on the ground plane for IFA with respect to the original design (all lengths are in mm)

The results for the vertical IFA antenna in Figures 4.46 and 4.47 show that the bottom edge of the PCB is the most optimum location for the radiating element with a 8% increase in coverage efficiency, compared to the original position of the left edge placement reducing the wasted component significantly. The MEG_{GPS} value also increases by 0.3 dB. However, the draw back of this structure is that the size of the radiating element increases by 15% in the top and the bottom placements to get the right resonance. The worst performance is observed in the top placement that has reduced η_c by 5% and MEG_{GPS} by 0.4 dB. There is no significant change in antenna performance with left and right placements of the radiating element.

The comparison of the performance of the re-located vertical DRA antenna shown in Figures 4.46 and 4.47 indicates that shifting the radiating element from the original position i.e. on the left edge of the PCB to the right and bottom edges causes no significant change in the antenna operation with similar values of MEG_{GPS} and η_c.

$G_\perp(\theta, \phi)$ $G_\parallel(\theta, \phi)$

(a) 3-D simulated gain patterns for vertical IFA with radiating element on left

$G_\perp(\theta, \phi)$ $G_\parallel(\theta, \phi)$

(b) 3-D simulated gain patterns for vertical IFA with radiating element on right
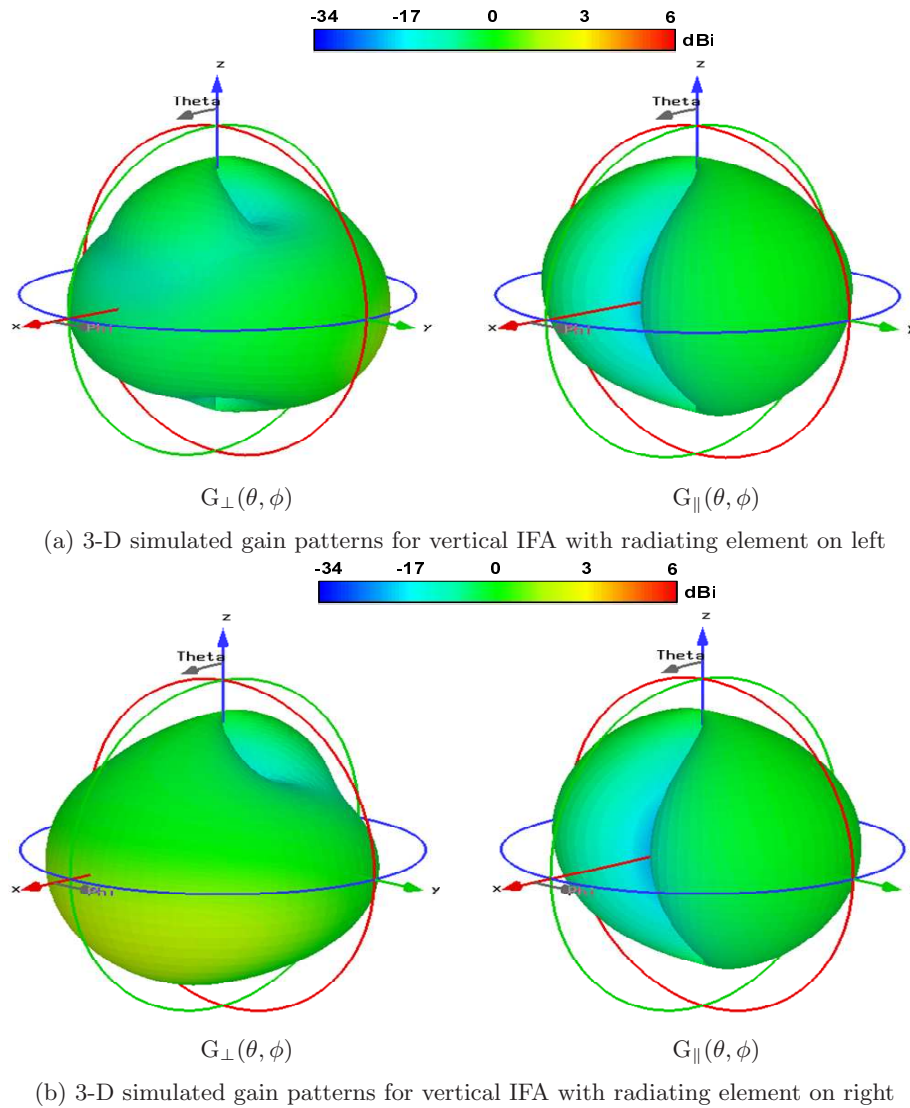
Figure 4.41: Simulated 3-D gain patterns for IFA GPS mobile terminal antenna in vertical orientation with antenna positioned at left and right edges of the ground plane

However, the placement of the radiating element on the top edge of the PCB increases η_c by 5% at the expense of a 0.3 dB reduction in MEG_{GPS}. It makes the enhanced η_c trivial by keeping the overall antenna performance in the same range.

The difference in the performance of the IFA and DRA has not changed hugely when the radiating element is re-located from its original position on the left edge. The small changes noted in MEG_{GPS} and η_c values with the top and bottom placements of the radiating element are associated to the variations in the antenna gain patterns. An

$G_\perp(\theta, \phi)$ $\quad\quad\quad\quad\quad\quad$ $G_\parallel(\theta, \phi)$

(a) 3-D simulated gain patterns for vertical IFA with radiating element on top

$G_\perp(\theta, \phi)$ $\quad\quad\quad\quad\quad\quad$ $G_\parallel(\theta, \phi)$

(b) 3-D simulated gain patterns for vertical IFA with radiating element on bottom
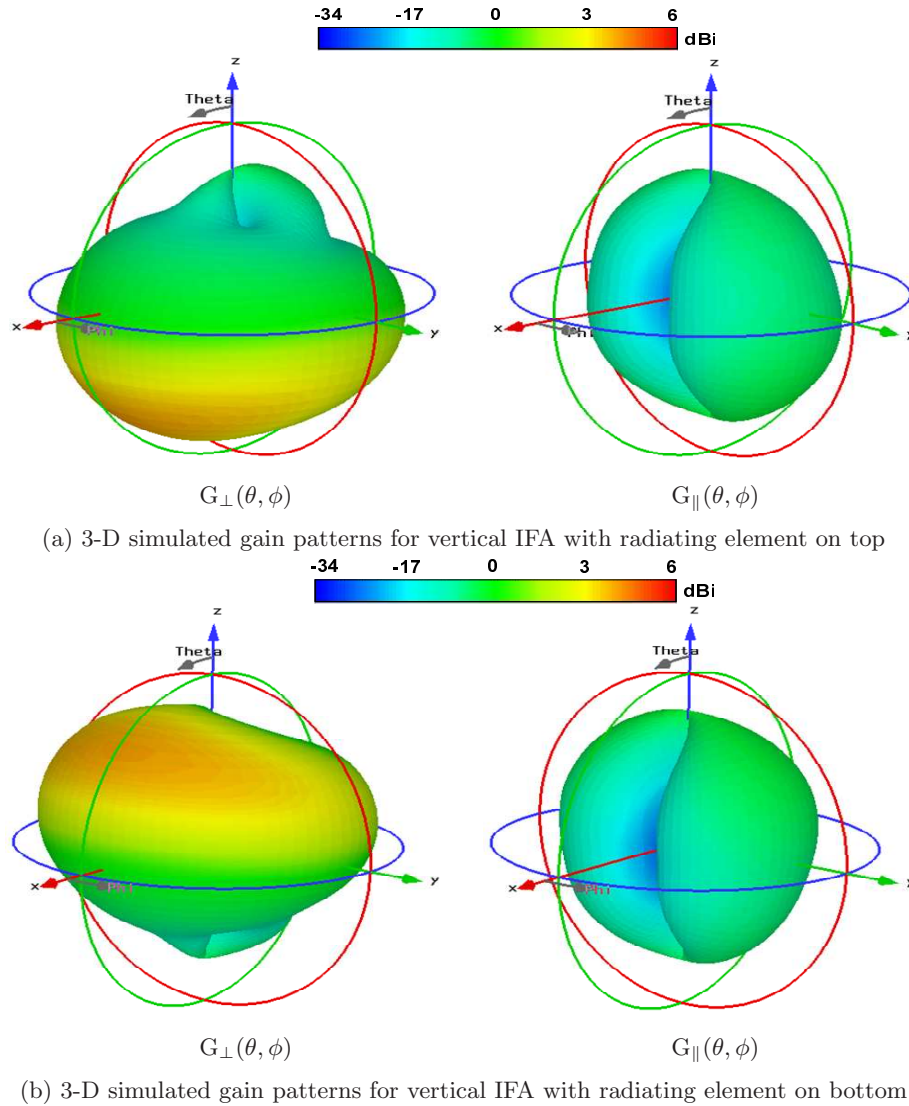
Figure 4.42: Simulated 3-D gain patterns for IFA GPS mobile terminal antenna in vertical orientation with antenna positioned at top and bottom edges of the ground plane

incense in η_c for the DRA in the top placement indicates that the antenna has more clear sky view and a larger area is above the threshold level of -13 dBi in the incident region. A decrease in η_c when the antenna is placed at the bottom edge, is caused by comparatively less area meeting this threshold. On the other hand, MEG_{GPS} incorporates the overall changes in the antenna gain pattern for both the polarisations and its response to the multipath environment in terms of AoA_{GPS} that also include ground reflections. Hence, MEG_{GPS} values decrease in both the top and bottom placements of
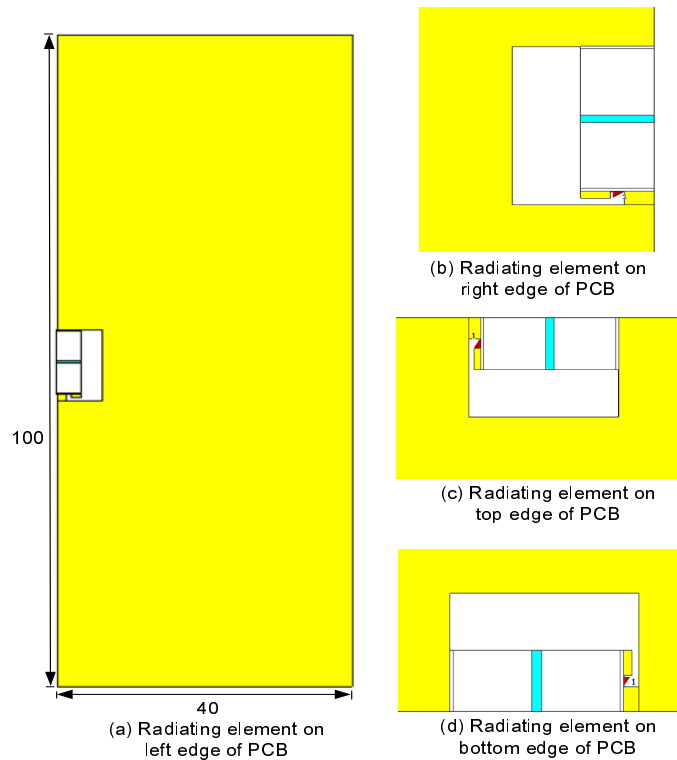
Figure 4.43: Schematic of re-positioned radiating element on the ground plane for DRA with respect to the original design (all lengths are in mm)

the radiating element due to reduction in overall gain levels, as illustrated by the gain patterns in Figure 4.45. The discussed factors also govern the performance of the IFA in the top and bottom placements in a similar fashion.

Based on the presented results, it can be deduced that a change in the location of the antenna radiating element on the PCB/ground plane offers no significant enhancement for the GPS antenna operation working in the multipath environment.

4.6 GPS Antenna Performance Enhancement Through Diversity

It is apparent from the discussion in the previous section that the multipath environment severely degrades the performance of the GPS mobile terminal antennas. Provision of a

$G_\perp(\theta,\phi)$ $G_\parallel(\theta,\phi)$

(a) 3-D simulated gain patterns for vertical DRA with radiating element on left

$G_\perp(\theta,\phi)$ $G_\parallel(\theta,\phi)$

(b) 3-D simulated gain patterns for vertical DRA with radiating element on right
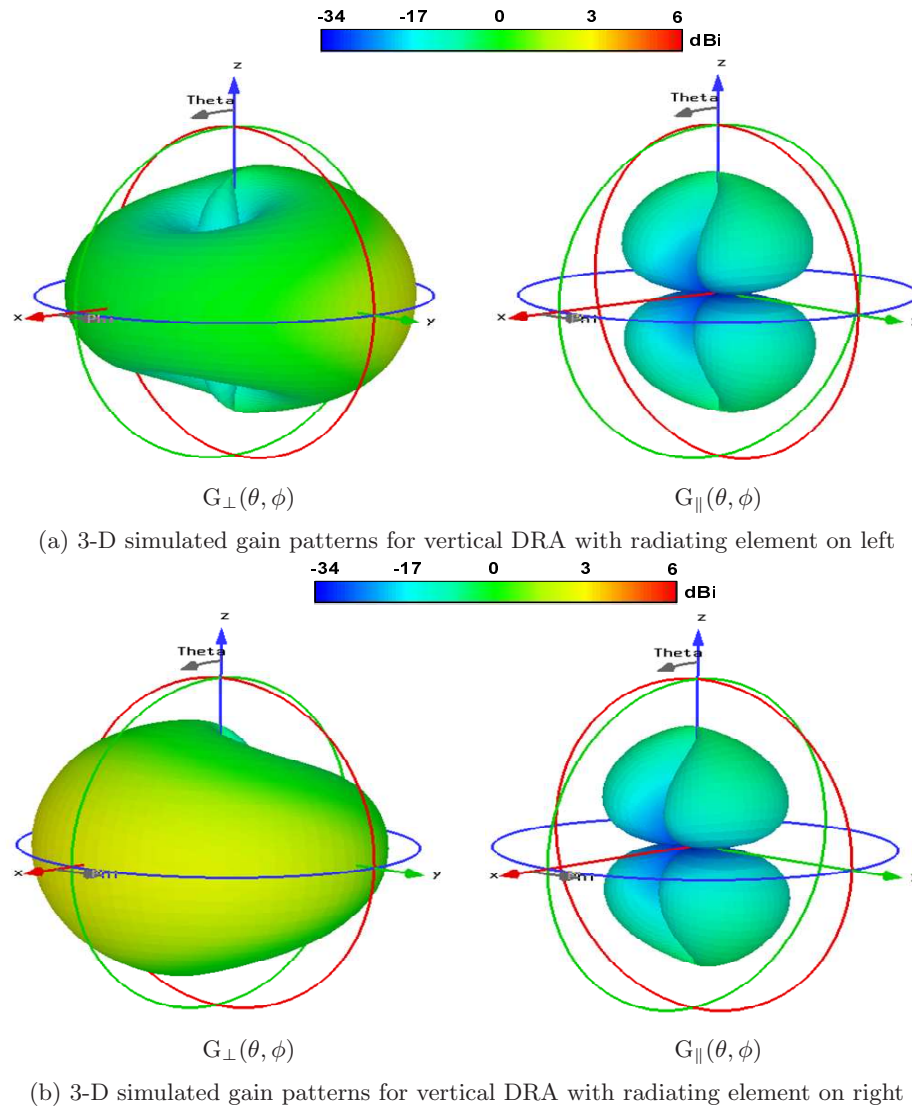
Figure 4.44: Simulated 3-D gain patterns for DRA GPS mobile terminal antenna in vertical orientation with antenna positioned at left and right edges of the ground plane

reliable navigation service demands mitigation of these degrading effects. A number of solutions are being proposed to improve the GPS antenna performance including dielectric loading, high value substrates, active circuits and diversity antennas. It is reported that diversity antennas have a potential to enhance the performance while maintaining relatively low profile, small size and low cost [25, 26]. Therefore, dual-element designs are considered and performance in the multipath environment is analysed for the mobile terminal PIFA and mono-loop antennas. It describes the benefit of using the diversity antennas in modern day navigation devices to counter the multipath degradations.

$G_\perp(\theta,\phi)$ $G_\parallel(\theta,\phi)$

(a) 3-D simulated gain patterns for vertical DRA with radiating element on top

$G_\perp(\theta,\phi)$ $G_\parallel(\theta,\phi)$

(b) 3-D simulated gain patterns for vertical DRA with radiating element on bottom
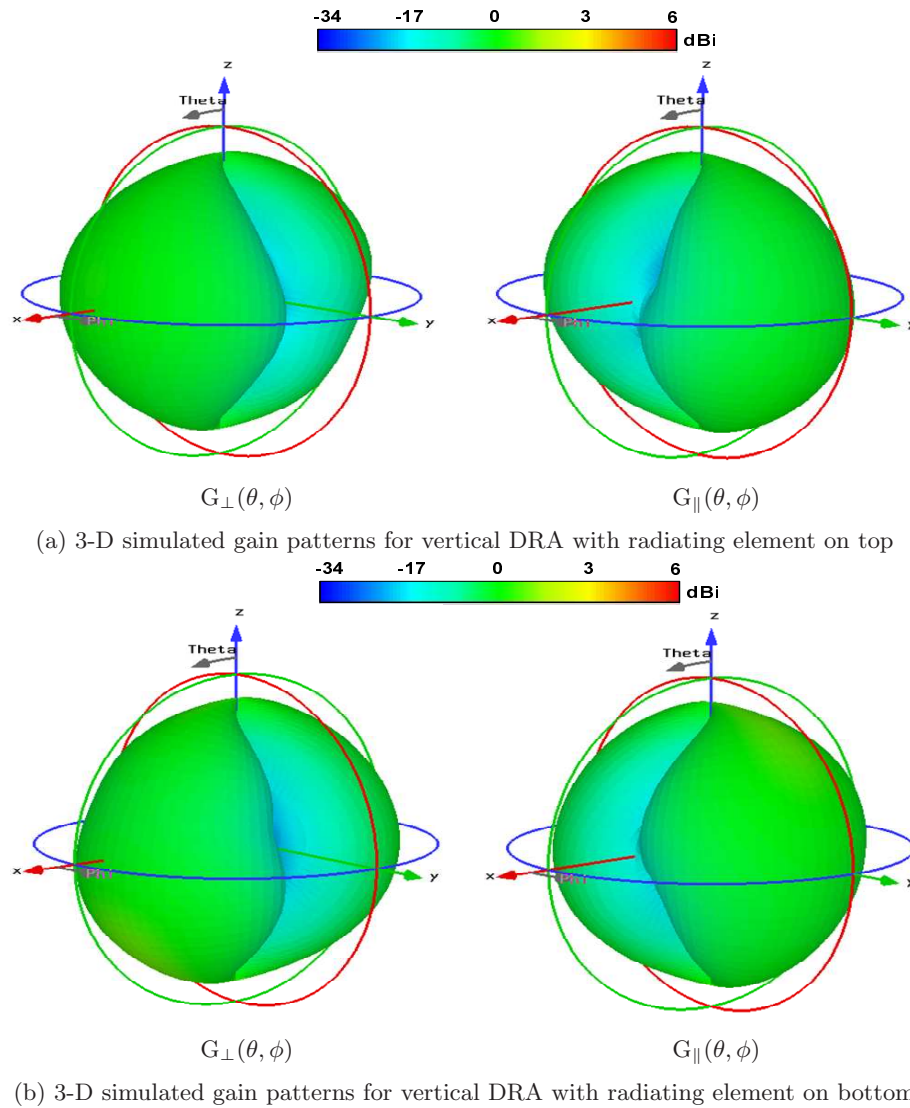
Figure 4.45: Simulated 3-D gain patterns for DRA GPS mobile terminal antenna in vertical orientation with antenna positioned at top and bottom edges of the ground plane

4.6.1   Mobile Terminal PIFA GPS Diversity Antenna

The PIFA antenna described in Section 4.5.1.1 is used to design a dual-element diversity PIFA antenna due to its vast usage in commercial applications. The fabricated prototype of the two element design is shown in Figure 4.48(a). The elemental dimensions are the same as described in Figure 4.16(a). The measured S11 and S21 curves are shown in Figures 4.48(b) and (c), respectively. The antenna exhibits -10 dB impedance bandwidth
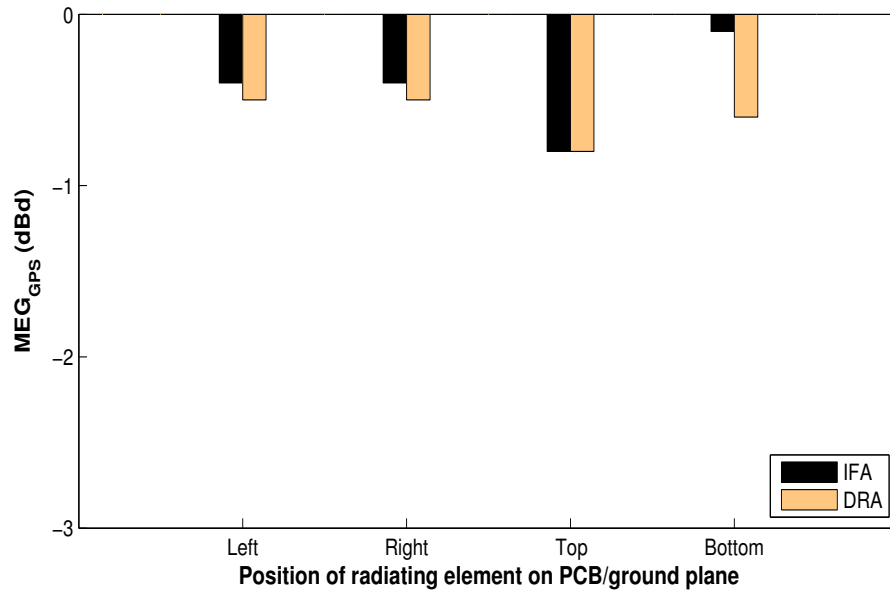
Figure 4.46: Comparison of calculated MEG_{GPS} values for varying positions of the radiating element of IFA and DRA GPS antennas taking horizontal dipole as reference
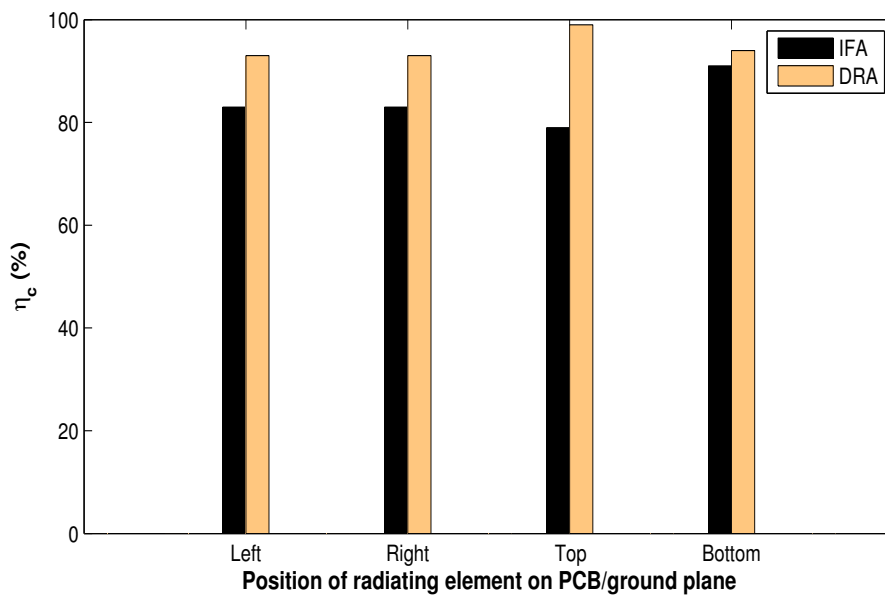
Figure 4.47: Comparison of calculated η_c values for varying positions of the radiating element of IFA and DRA GPS antennas

of 55 MHz covering the frequency range from 1552 MHz to 1607 MHz. The mutual coupling of the antenna is not very great as S21 value at 1575.42 MHz appeared to be -11.4 dB. Figure 4.49 illustrates the measured 3-D gainpatterns for the perpendicular
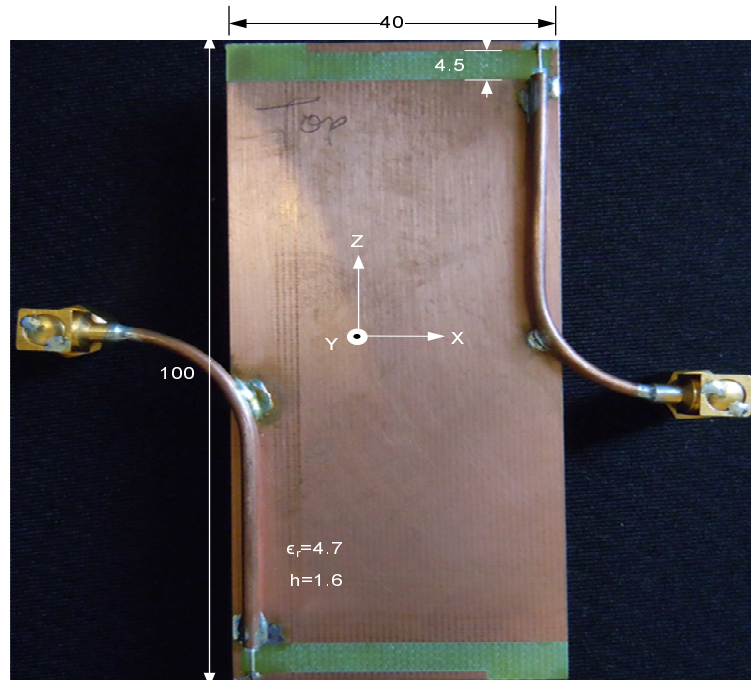
(a) Antenna prototype and geometry (in mm)
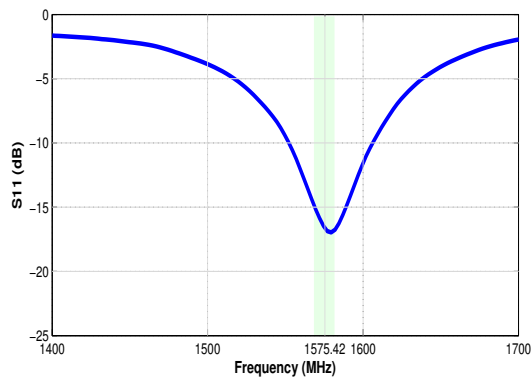
(b) Measured S11 curve
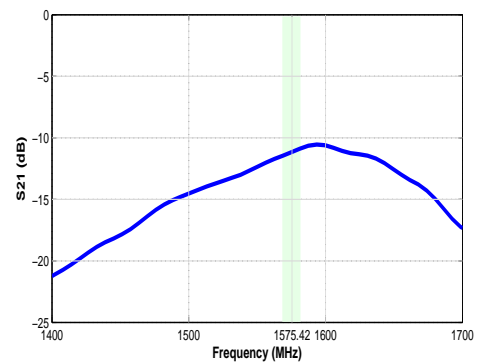
(c) Measured S21 curve

Figure 4.48: Geometrical structure of GPS mobile terminal dual-element PIFA diversity antenna with measured S11 and S21 curves

and parallel polarisations of the dual-element PIFA antenna.

4.6.2 Mono-loop GPS Diversity Antenna

A dual-element mono-loop antenna based on the mono-loop antenna design described in Section 4.5.1.5 is also designed to study the enhancement of the GPS antenna per-

$G_\perp(\theta,\phi)$ $G_\parallel(\theta,\phi)$

(a) 3-D measured gain patterns for vertical orientation

$G_\perp(\theta,\phi)$ $G_\parallel(\theta,\phi)$

(b) 3-D measured gain patterns for horizontal orientation
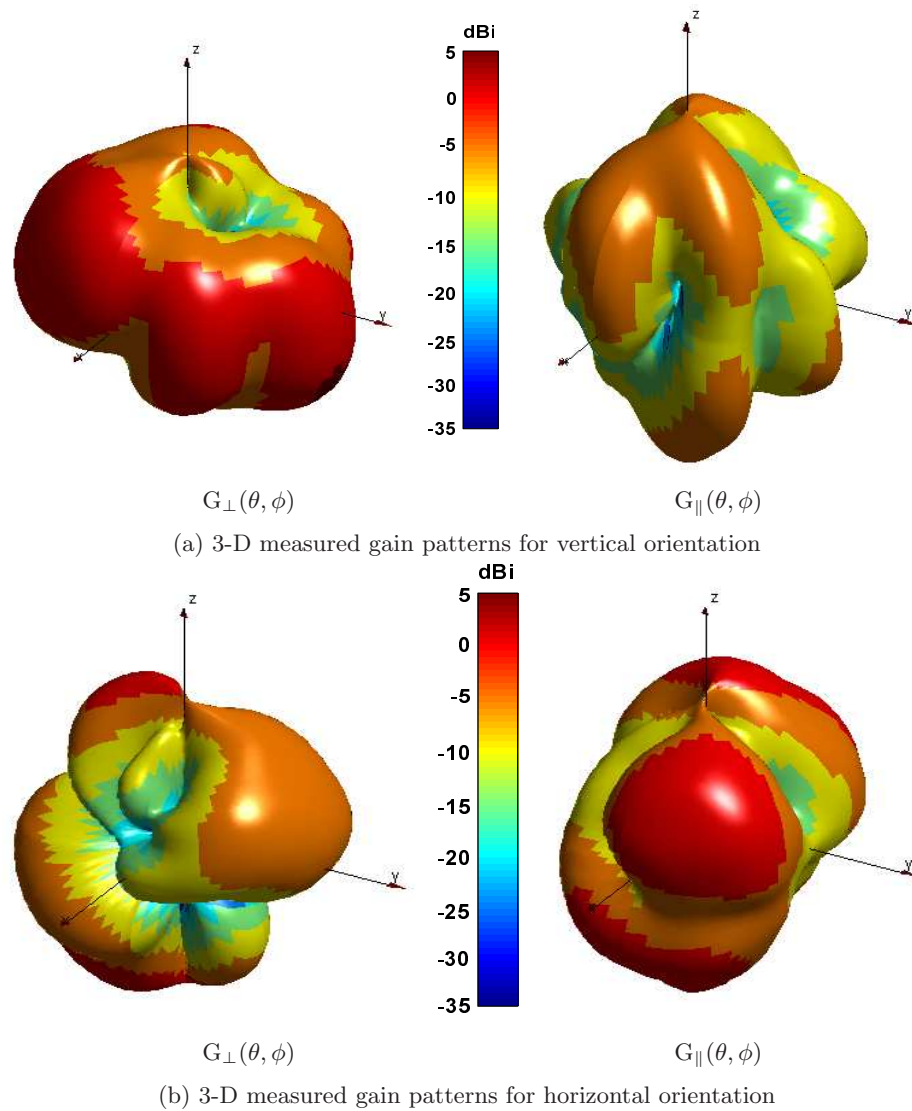
Figure 4.49: Measured 3-D gain patterns for perpendicular and parallel polarisations of GPS mobile terminal dual-element PIFA diversity antenna in vertical and horizontal orientations

formance in the multipath environment using diversity. The elemental dimensions are similar as illustrated in Figure 4.24(a) with a distance of 41.8 mm between the two elements. Figure 4.50(a) shows the fabricated prototype of the designed antenna while Figures 4.50(b) and (c) describe the measured S11 and S21 curves respectively for the antenna. The antenna has a -10 dB impedance bandwidth of 250 MHz covering all the frequencies ranging from 1385 MHz to 1635 MHz. An acceptable level of coupling between the two elements is observed with the measured S21 of -14.1 dB at 1575.42
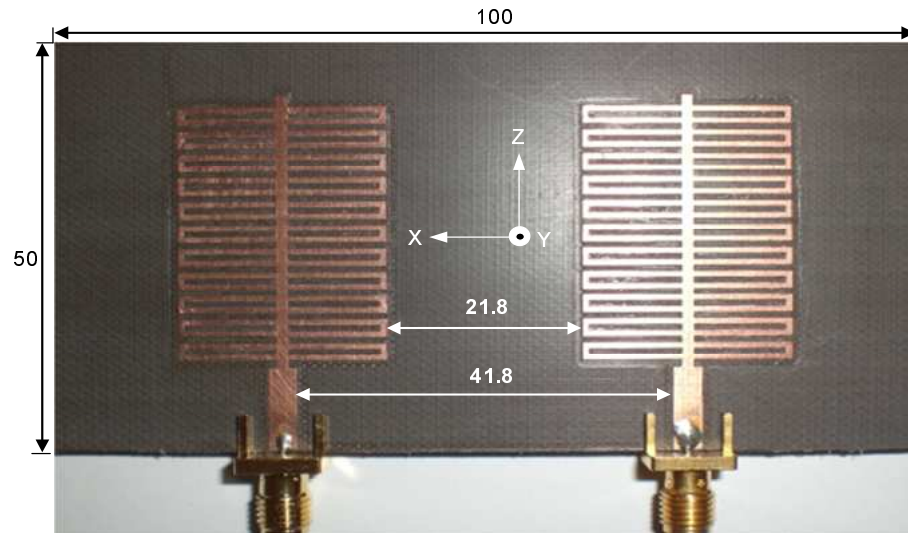
(a) Antenna prototype and geometry (in mm)
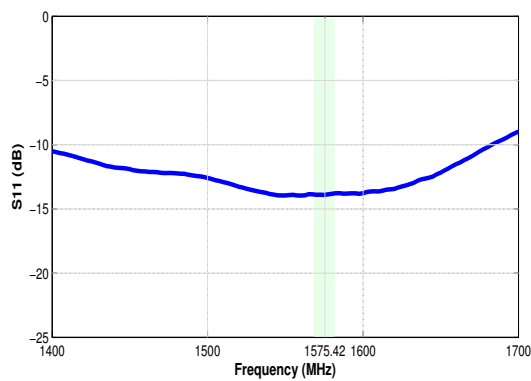
(b) Measured S11 curve
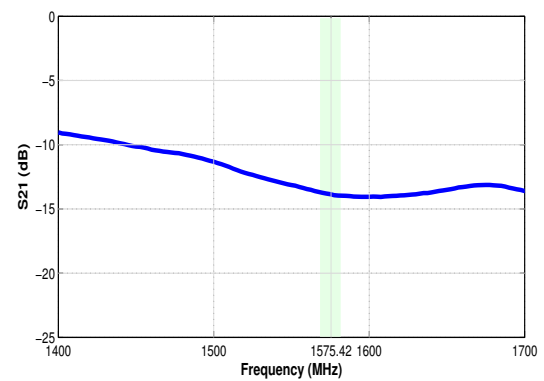
(c) Measured S21 curve

Figure 4.50: Geometrical structure of GPS mobile terminal dual-element mono-loop diversity antenna with measured S11 and S21 curves

MHz. The measured 3-D gain patterns for the perpendicular and parallel polarisations of the dual-element mono-loop antenna are illustrated in Figure 4.51.

4.6.3 Performance of GPS Diversity Antennas in Multipath Environment

The performance of the two diversity antennas in the multipath GPS environment is evaluated using the proposed statistical model and verified through open field test measurements. A power combiner is used to combine the signal from the two elements with

$$G_\perp(\theta, \phi) \qquad\qquad G_\parallel(\theta, \phi)$$

(a) 3-D measured gain patterns for vertical orientation

$$G_\perp(\theta, \phi) \qquad\qquad G_\parallel(\theta, \phi)$$

(b) 3-D measured gain patterns for horizontal orientation
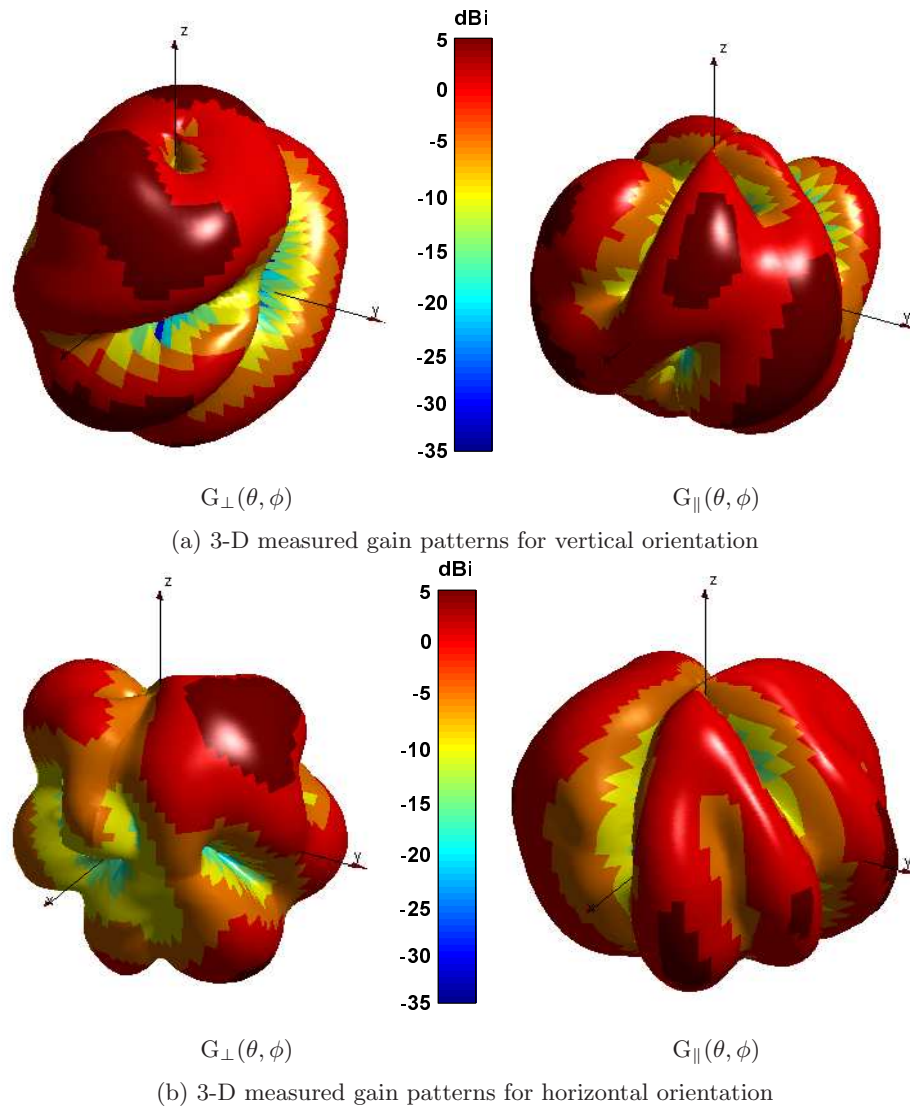
Figure 4.51: Measured 3-D gain patterns for perpendicular and parallel polarisations of GPS mobile terminal dual-element mono-loop diversity antenna in vertical and horizontal orientations

an insertion loss of 0.5 dB. The vertical orientation of the two antennas is taken into account. 3-D gain patterns of the antenna configurations are input to the model. The effectiveness of the diversity is analysed in terms of η_c and MEG_{GPS} with the horizontal dipole antenna taken as the reference.

Table 4-5 summarises the MEG_{GPS} and η_c results for the two antennas while a comparison with the performance of respective single element (non-diversity) antennas is presented in Figures 4.52 and 4.53.

Table 4-5: Performance evaluation of mobile terminal GPS Diversity antennas in horizontal and vertical orientations using the multipath environment model in comparison with the measured results

Antenna	Model Calculations Using Measured 3-D Patterns		Open Field Test Measurements	
	η_c (%)	MEG_{GPS} (dBd)	η_c (%)	MEG_{GPS} (dBd)
Horizontal Dipole (reference)	97	0 (corresponding to calculated value of -5.4 dB in AR)	96	0 (corresponding to measured average SNR of 40.2 dB)
Vertical Terminal PIFA	95	-3.3	92	-3.1
Vertical Dual Terminal PIFA	97	-2.7	97	-2.6
Vertical Mono-loop	78	-1.6	80	-1.8
Vertical Dual Mono-loop	95	-0.2	96	-0.3
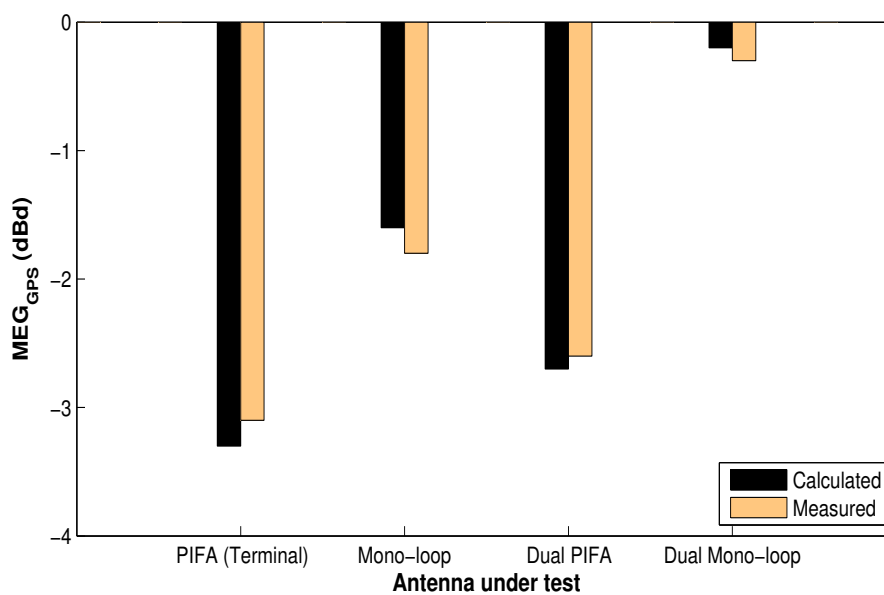
Figure 4.52: Performance enhancement of GPS diversity antennas in multipath environment in comparison of single element designs in terms of calculated MEG_{GPS} taking horizontal dipole as reference

Figure 4.52 shows that the use of the diversity antennas increases MEG_{GPS} for the GPS multipath operation significantly. The extent of this enhancement is different for the two antennas with 0.6 dB increase achieved by the dual-element PIFA while 1.4 dB
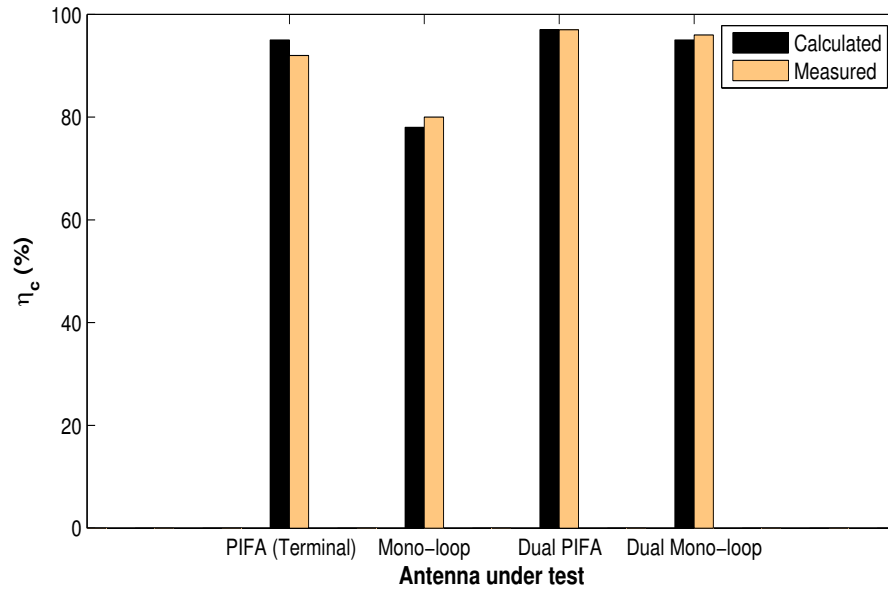
Figure 4.53: Performance enhancement of GPS diversity antennas in multipath environment in comparison of single element designs in terms of calculated η_c

increase is offered by the dual-element mono-loop.

Similarly, a significant improvement in the coverage of the incoming GPS signal has been exhibited by the dual-element mono-loop with a η_c increment of 17%. The η_c of the dual-element PIFA has also increased by 2% that is not very significant but shows a tendency of improvement.

The higher values of MEG_{GPS} and η_c achieved for the two diversity antennas are a result of enhanced gain patterns. The use of spatial diversity has broaden the antennas clear sky view, modified the gain patterns and increased the gain levels as illustrated in Figures 4.49 and 4.51. The modified gain patterns has enabled the antennas to cover a wider range of AoA_{GPS}. This, combined with an overall increased gain levels has resulted in comparatively larger values of MEG_{GPS} for the diversity antennas. The enhanced gain values have also increased the coverage of the antennas and hence their η_c as it depends on the solid angle subtended by the area where gain levels are higher than -13 dBi in the upper hemisphere. The results show that the diversity is good for the monoloop antenna but its benefit is marginal for the PIFA. The less resounding

performance of the dual-element PIFA is related to fabrication errors that lead to higher mutual coupling between the two elements. The S21 measurements, presented in Figures 4.48(c) and 4.50(c), show that the dual-element PIFA has a mutual coupling of -11.4 dB as compared to -14.1 dB for the dual-element monoloop at 1575.42 MHz. It reduces the performance of the dual-element PIFA to a greater extent resulting in less significant improvement in MEG_{GPS} and η_c values as compared to the dual-element monoloop antenna.

Overall, the dual-element diversity antennas have shown better performance in the multipath environment as compared to their single-element counterparts. It is therefore, deduced that diversity is a viable solution in terms of effective GPS reception. Further optimisation of the antenna designs and minimisation of the fabrication errors would result in more enhanced GPS multipath operation of the mobile terminal.

4.7 Model Limitations

Besides its precise predictive capabilities, the proposed statistical model for the GPS environment is currently only suitable for uniform AoA_{GPS} distributions in azimuth and elevation planes. This assumption is not very realistic in case of the elevation plane. Therefore, accuracy of the model could be further increased by looking into more practical AoA_{GPS} distributions, for example Gaussian and elliptical, that represent greater probability of the arrival of the GPS signal near the zenith as compared to the horizon angles.

4.8 Summary

A statistical model to evaluate the GPS antenna performance in a multipath environment is presented with a novel GPS Angle of Arrival (AoA_{GPS}) distribution and a new concept of the GPS Mean Effective Gain (MEG_{GPS}) and Coverage Efficiency (η_c). The

model is implemented and verified through extensive numerical studies and its precision is established through experimental procedures. The model efficiently predicts the GPS antenna performance showing close agreement to the open field measurements. Therefore, it provides a means to analyse antenna operation in actual working scenarios without doing open field measurements.

The performance of a number of GPS antennas, both generic and mobile terminal antennas is evaluated. Effects of the change in the antenna orientation with respect to the ground (earth) and effects of the varying radiating element position on the PCB/antenna ground plane on the performance of these GPS antennas in the multipath environment are also investigated. The use of diversity antennas to enhance the GPS operation in the multipath environment has also been studied using two different types of mobile terminal antennas.

It has been shown that the performance of the GPS antennas in the multipath environment could be characterised by its MEG_{GPS} and η_c. These factors are controlled by the AoA_{GPS} distribution of the incident radio wave and gain patterns of the GPS receiving antenna. It is also noted that change in the antenna orientation plays a vital role as it varies antenna gain patterns resulting in η_c deviations. However, it is hard to determine a fixed and generalised pattern caused by the variation in antenna orientation as it differs from antenna to antenna. Generally, the horizontal orientation of the antenna appears to be more efficient in terms of η_c due to wider clear sky view, for example the IFA and helix has η_c of 100% and 97% in horizontal orientation as compared to 79% and 87% in vertical orientation. The general trend is similar in case of MEG_{GPS} as most of the tested GPS antennas showed improved MEG_{GPS} for horizontal orientation as compared to the vertical one. It is due to an overall high level of gain values particularly in the upper hemisphere increasing the reception of the GPS signal.

The study of the varying position of the antenna radiating element on the PCB/ground plane for the IFA and DRA antennas has shown that no significant improvement could be achieved by employing this technique with little variation in MEG_{GPS} and η_c values.

The study of the performance of the dual-element diversity antennas in the GPS multipath environment has depicted performance enhancement both in terms of increased MEG_{GPS} and η_c. The dual-element mono-loop antenna has enhanced the MEG_{GPS} by 1.4 dB and η_c by 23% as compared the single-element mono-loop antenna. Therefore, the diversity antennas could be used effectively to reduce the degrading effects of the multipath environment making it a viable solution for the GPS multipath operation.

References

[1] R. Bancroft, "Microstrip and printed antenna design (2nd edition)," *SciTech Publishing, Inc., (USA)*, 2009.

[2] G. J. K. Moernaut and D. Orban, "GNSS antennas," *GPS World*, February 2009, URL: http://www.gpsworld.com/gnss-system/receiver-design/innovation-gnss-antennas.

[3] L. Boccia, G. Amendola, and G. Di Massa, "A shorted elliptical patch antenna for GPS applications," *IEEE Antennas and Wireless Propagation Letters*, vol. 2, pp. 6–8, 2003.

[4] G. Miller, "Adding GPS applications to an existing design," *RF Design*, pp. 50–57, March 1998.

[5] R. B. Langley, "A primer on GPS antennas," *GPS World*, pp. 50–55, July 1998.

[6] V. Pathak, S. Thornwall, M. Krier, S. Rowson, and L. Poilasne, G.and Desclos, "Mobile handset system performance comparison of a linearly polarized GPS internal antenna with a circularly polarized antenna," *IEEE Antennas and Propagation Society International Symposium (AP-S)*, vol. 3, June 2003.

[7] S. Kingsley, "GPS antenna design for mobile phones," *URL:http://www. electronicsweekly.com/Articles/2007/04/11/41146/GPS-antenna-design-for-mobile-phones.htm.*

[8] T. Haddrell, N. Ricquier, and M. Phocas, "Innovation: Mobile-phone GPS antennas: Can they be better?" *GPS World, URL:http://www.gpsworld.com/professional-oem/component-technologies/innovation-mobile-phone-gps-antennas-9457.*

[9] T. Taga, "Analysis for mean effective gain of mobile antennas in land mobile radio environments," *IEEE Transactions on Vehicular Technology*, vol. 39, no. 2, pp. 117 – 131, May 1990.

[10] A. Ando, T. Taga, A. Kondo, K. Kagoshima, and S. Kubota, "Mean effective gain of mobile antennas in line-of-sight street microcells with low base station antennas,"

IEEE Transactions on Antennas and Propagation, vol. 56, no. 11, pp. 3552–3565, November 2008.

[11] W. C. Jakes, "Microwave mobile communications," *John Wiley and Sons Inc., (USA)*, 1974.

[12] K. Kalliola, K. Sulonen, H. Laitinen, O. Kivekas, J. Krogerus, and P. Vainikainen, "Angular power distribution and mean effective gain of mobile antenna in different propagation environments," *IEEE Transactions on Vehicular Technology*, vol. 51, no. 5, pp. 823–838, September 2002.

[13] P. Carro and J. de Mingo, "Mean effective gain of compact WLAN genetic printed dipole antennas in indoor-outdoor scenarios," *International Conference on Personal Wireless Communications (PWC)*, pp. 275–283, September 2006.

[14] D. K. Cheng, "Field and wave electromagnetics (2nd edition)," *Addison Wesley, Inc., (USA)*, 1989.

[15] U. S. Inan and A. S. Inan, "Electromagnetic waves," *Prentice-Hall, Inc., (USA)*, 1999.

[16] G. Moernaut and O. D., "GNSS antennas," *URL:http://www.gpsworld.com/gnss-system/receiver-design/innovation-gnss-antennas*.

[17] J. H. Reed, "Software radio: A modern approach to radio engineering," *Prentice-Hall Inc., (UK)*, 2002.

[18] J. B. Tsui, "Fundamentals of Global Positioning System receivers: A software approach (2nd edition)," *John Wiley and Sons, Inc., (USA)*, 2000.

[19] "Ultra low power superior sensitivity GPS modules," *URL:http://www.starsnav.com/MTI-8T.htm*.

[20] D. M. Pozar, "Microwave engineering (3rd edition)," *John Wiley and Sons Inc., (USA)*, 2005.

[21] R. Waterhouse, "Printed antennas for wireless communications," *John Wiley and Sons, Inc., (UK)*, 2007.

[22] J. Jemai, T. Kurner, A. Varone, and J. Wagen, "Determination of the permittivity of building materials through wlan measurements at 2.4GHz," *IEEE International Symposium on Personal, Indoor and Mobile Radio Communications*, September 2005.

[23] G. Klysza, J. P. Balayssaca, and X. Ferriresb, "Evaluation of dielectric properties of concrete by a numerical FDTD model of a GPR coupled antennaparametric study," *NDT & E International*, vol. 41, no. 8, pp. 621–631, December 2008.

[24] J. O. Nielsen and G. F. Pedersen, "Mobile handset performance evaluation using radiation pattern measurements," *IEEE Transactions on Antennas and Propaga-*

tion, vol. 54, no. 7, pp. 2154–2165, July 2006.

[25] Y. Gao, X. Chen, and C. G. Parini, "Study of diversity antennas for Galileo/GPS receivers," *European Navigation Conference (ENC-GNSS)*, April 2008.

[26] M. G. Douglas, M. Okoniewski, and M. A. Stuchly, "A planar diversity antenna for handheld PCS devices," *IEEE Transactions on Vehicular Technology*, vol. 47, no. 3, pp. 747–754, August 1998.

Chapter 5

Human Body and GPS Antennas in Multipath Environments

The GPS devices in Wireless Personal Area Networks (WPAN) and Wireless Body Area Networks (WBAN) typically operate either in on-body positions (held by the user) or in near-body positions (working in the proximity of the human body). In either case, the presence of the human body in the vicinity, affects the performance of the embedded GPS antennas of such devices. To gain a complete picture of the working of the GPS mobile terminal antennas, the effects of the presence of the human body needs to be considered along with the multipath environment.

This chapter provides an understanding of the effects caused by the presence of the human body on the operation of a standard GPS antenna. Numerical investigation shows the behaviour of the antenna in the proximity of the human body. The effects of the body on the antenna parameters are studied, considering varying antenna-body separations, different on-body antenna positions and various antenna held-in-hand conditions. The performance study of the GPS mobile terminal antennas in the multipath environment is also extended by including the effects of the human body presence considering various on-body scenarios. The statistical model for the multipath environment, proposed in

143

Chapter 4, is used to analyse the working of the body-worn GPS antennas.

5.1 Interaction of Human Body and GPS Antennas

The human body is a principle element of the WPAN/WBAN devices. It is now a well established phenomenon that the human body is a very lossy medium that affects the performance of the antenna in these applications in three ways; reduction in efficiency due to electromagnetic absorption in the tissues, degradation of the radiation pattern and variation in the feed point impedance [1–7].

Characterisation of these effects is a challenging but necessary task to provide guidelines for the design of an optimal performance antenna resilient to these degrading factors [8–11].

A detailed investigation is carried out to study the effects of the presence of the human body in the vicinity of a GPS antenna. Different practical scenarios for the use of portable GPS receivers are considered.

5.1.1 Design of Truncated Corner Microstrip Patch GPS Antenna

The object of this study is to analyse the effects of the human body presence on the performance of a GPS antenna. Therefore, a simple truncated corner microstrip patch antenna is chosen [12]. The antenna design is similar to that described in Chapter 4 having a ground plane of 100 mm×100 mm with a printed square radiating patch of 53.4 mm×53.4 mm and fed by a coaxial port. A FR4 substrate of 1.6 mm thickness and ε_r=4.7 is used. Figure 5.1 shows the geometry of the antenna.

Antenna performance is analysed via simulations and validated through measurements. The comparison of the simulated and measured S11 curves of the antenna are shown in Figure 5.2. A good agreement between the two has been observed. The high-
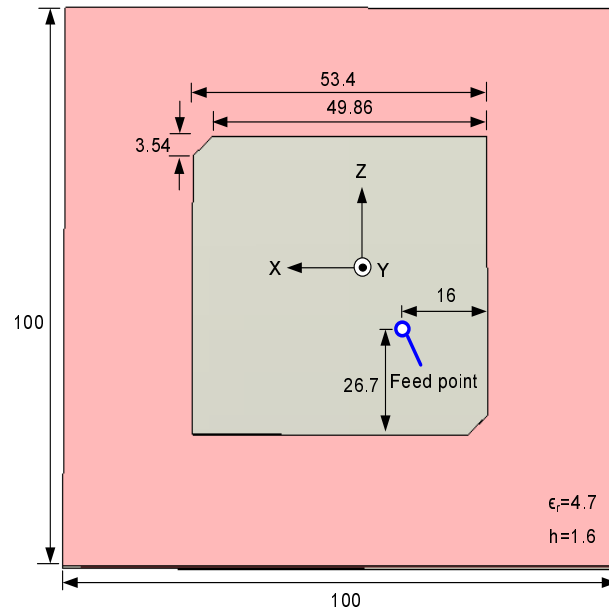
Figure 5.1: Schematic layout of the truncated corner microstrip patch antenna for GPS operation at 1575.42 MHz fed by a coaxial port
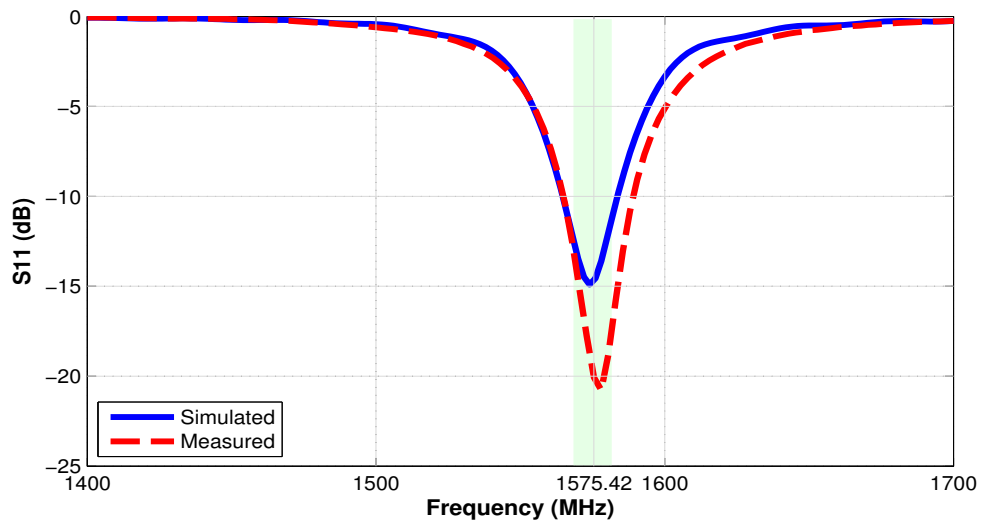
Figure 5.2: Simulated (blue) and measured (red) S11 curves for the truncated corner microstrip patch GPS antenna in free space

lighted area shows ±5 MHz impedance bandwidth region typically desired for a good performing GPS antenna [13, 14]. The antenna performs well in L1 band with centre frequency at 1578 MHz. The antenna has a -10 dB bandwidth of 25 MHz covering frequencies in the range of 1566 MHz to 1591 MHz.

(a) XY plane   (b) YZ plane
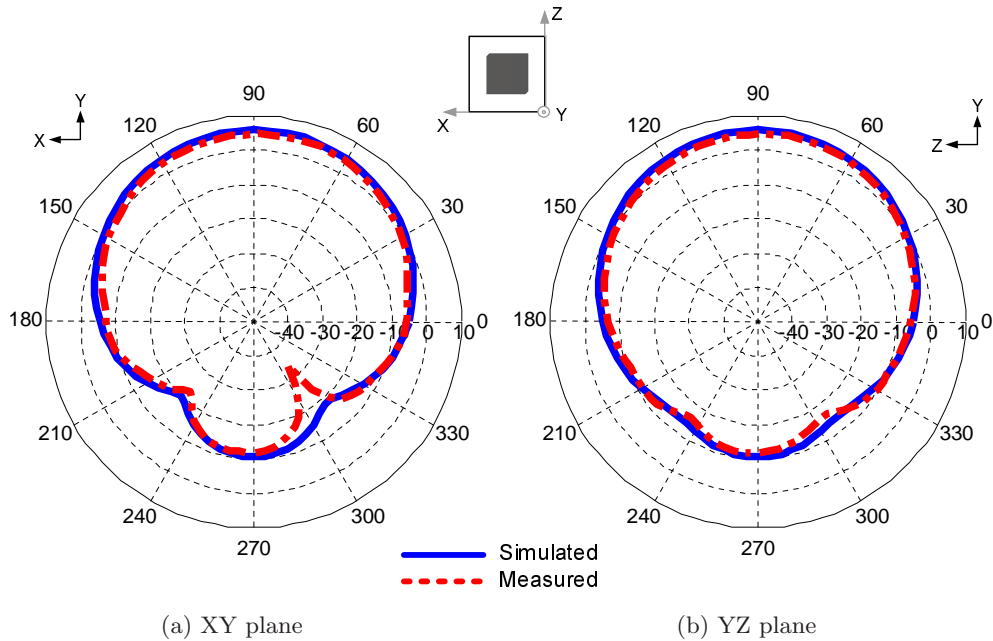
Figure 5.3: Simulated (blue) and measured (red) 2-D gain patterns in XY and YZ planes of the truncated corner microstrip patch GPS antenna in free space at 1575.42 MHz

(a) RHCP   (b) LHCP
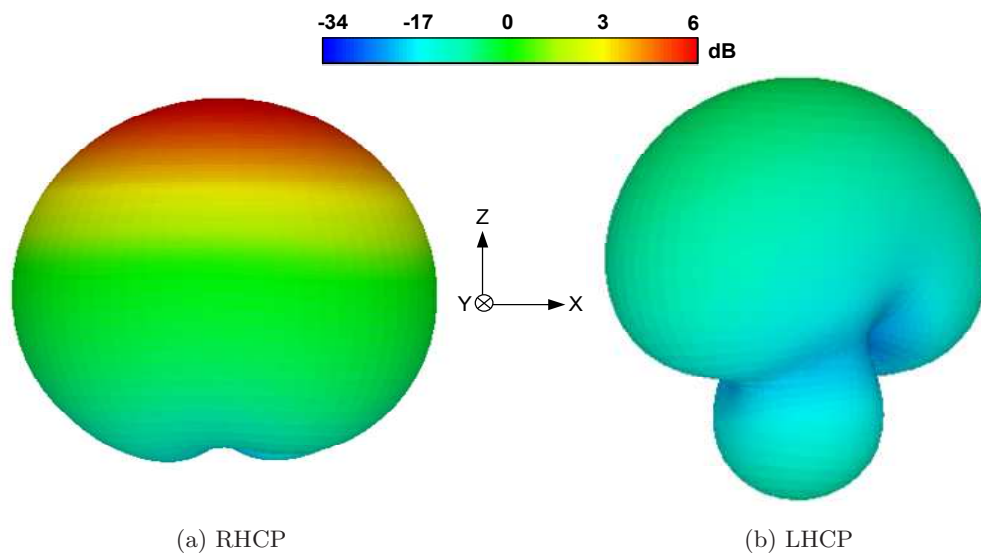
Figure 5.4: Simulated 3-D RHCP and LHCP gain patterns of the truncated corner microstrip patch GPS antenna in free space at 1575.42 MHz

Since, the microstrip patch antenna radiates normal to its patch surface, the gain patterns for both XY plane and YZ plane are of importance. The simulated and measured 2-D gain patterns in XY plane and YZ plane are shown in Figure 5.3. A good agreement can be found between the simulated and measured patterns. The small differences are

Table 5-1: Electric properties of specific human body tissues used within the constructed homogeneous body model at 1575.42 MHz

Tissue	Electric Properties	
	Dielectric Constant (ε_r)	Tissue Conductivity (σ) (S/m)
Bone	19.65	0.52
Fat	5.37	0.07
Muscle	53.83	1.22
Skin	39.28	1.09

due to the fabrication imperfections. Figure 5.4 illustrates the simulated 3-D RHCP and LHCP gain patterns of the antenna. These results confirm that the antenna performance is excellent for the GPS operation with good RHCP and a small back side radiation of order -20 dB, in accordance to the specified requirements in classic literature summarised in Chapter 2.

5.1.2   On-Body Test Set-up

The single layer human body model, constructed and described in Chapter 3, is used in this study. Simulations were carried out in CST Microwave Studio$^{\circledR}$. The body model is kept homogeneous for simplicity and to get a starting point of the electromagnetic interaction between the human body and the GPS antennas. The weighted average tissue properties have been adopted in continuity of the previous study. The homogeneous human model is therefore, considered as a compound with 10% skin, 30% fat, 40% muscle and 20% bone, which resulted in an averaged relative permittivity of 30.98 and conductivity of 0.73 S/m at 1575.42 MHz. The dielectric properties of the human body tissue are taken as described in [15–17]. The values for the four types of tissues at 1575.42 MHz used in this study are given in Table 5-1.

A complete body model with a height of 1720 mm is used in this study. Effects of the presence of the human body on the GPS receiver antenna are studied for different configurations considering varying separations of the body and the antenna, different
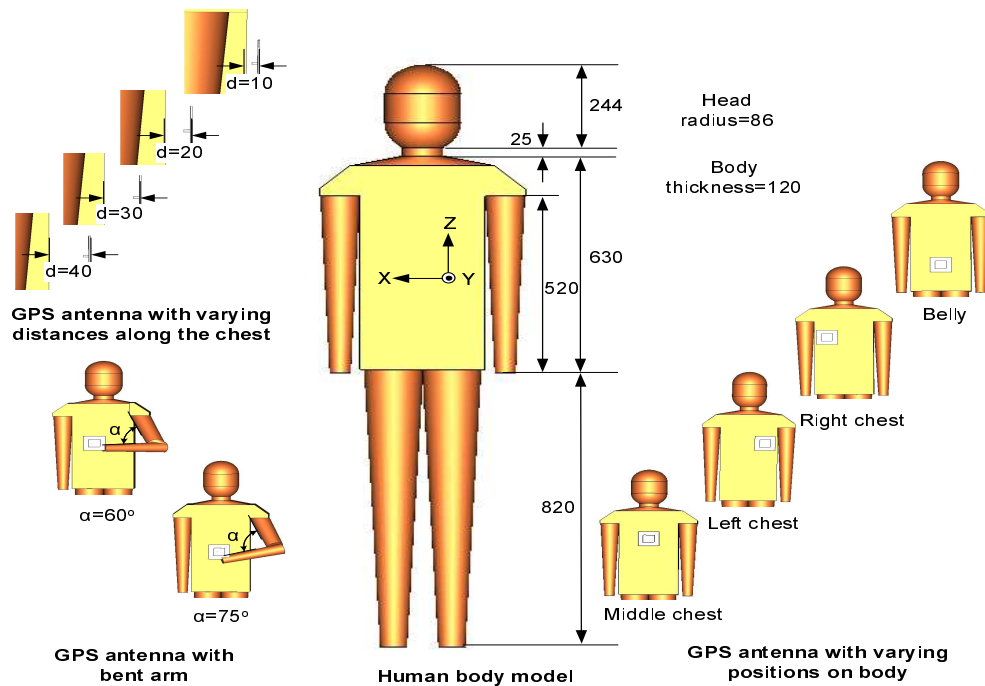
Figure 5.5: Human body model and different on-body configurations of the truncated corner microstrip patch antenna used to study the effects of the human body presence on the GPS antenna (all lengths are in mm)

positions of the antenna on the body and different body postures shown in Figure 5.5.

5.1.3   Effects of Varying Antenna-Body Separation

The GPS antennas in portable devices, especially the mobile phones, are often integrated with other radio communication systems. For the navigation use, the separation between the portable device and the human body can change which results in varying the antenna performance.

The effects of the human body on the performance of the microstrip patch GPS antenna are studied by varying the separation (d) along the chest, illustrated in Figure 5.5. Different gaps between the antenna and the body are considered ranging from d=10 mm to d=120 mm. Figures 5.6-5.7 provide a comparison of the antenna performance in free space and in the presence of the human body at these separations. A summary of various antenna parameters for different simulated configurations including
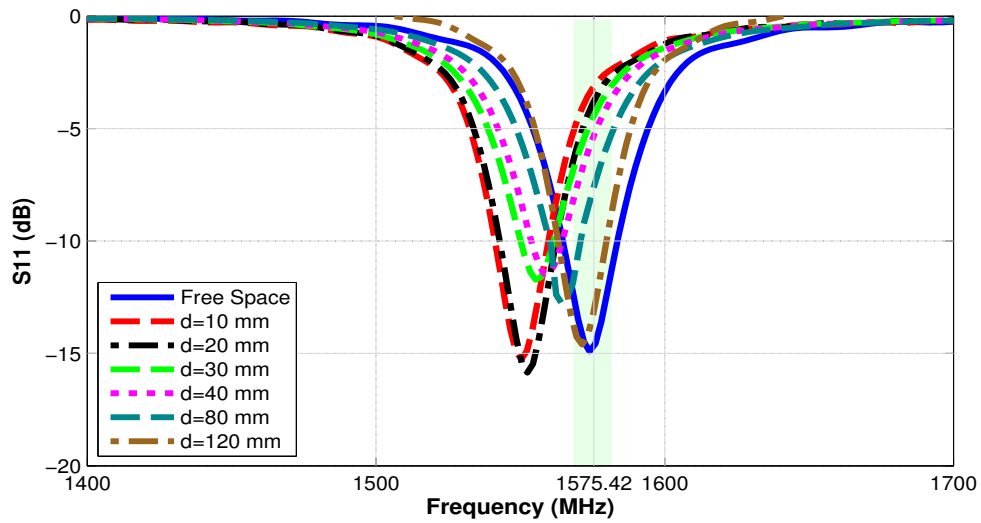
Figure 5.6: Comparison of the simulated S11 responses of the truncated corner microstrip patch GPS antenna for various antenna-body separations (d) along the chest

(a) XY plane   (b) YZ plane
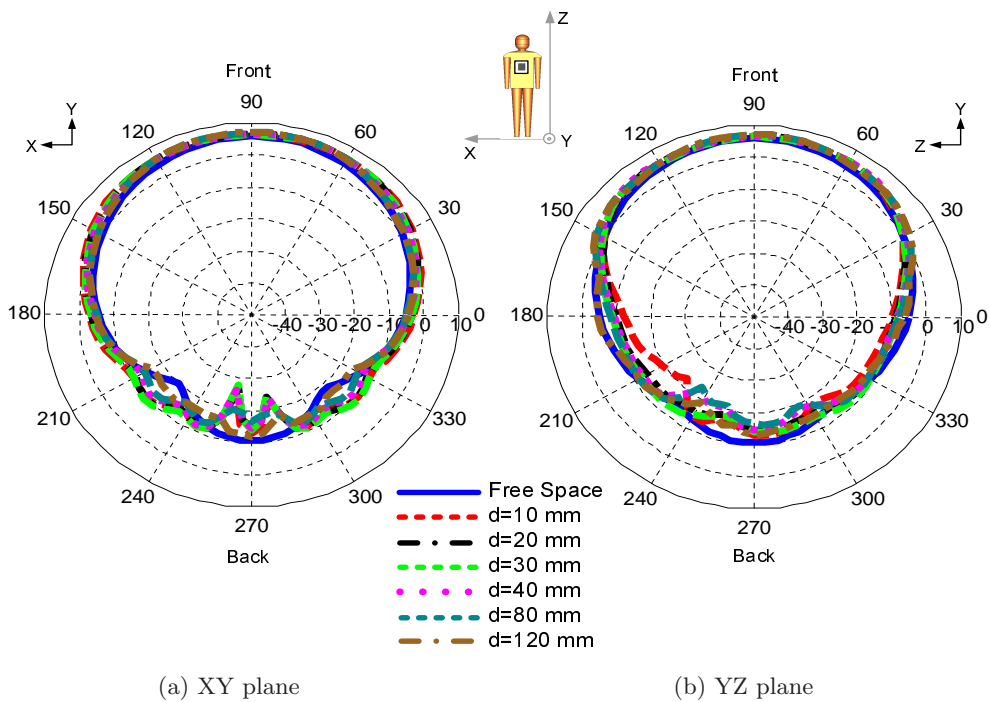
Figure 5.7: Comparison of simulated 2-D gain patterns in XY and YZ planes of the truncated corner microstrip patch GPS antenna as a function of the antenna distance (d) from the body along the chest at 1575.42 MHz

f_c, bandwidth, total efficiency and maximum gain (in XY plane) is presented in Table 5-2.

The S11 curves in Figure 5.6 show a shift in the resonance frequency from 1575.42 MHz to lower frequencies depending upon the separation. The detuning of the antenna is caused due to the fact that while the antenna is placed on-body, the electromagnetic field produced in the space near human body contains both the fields induced by the antenna itself and the fields reflected from the body surface. These reflected fields induce currents on the antenna surface disturbing the free space distribution. It changes the antenna impedance and hence, detunes the resonance frequency. A maximum drop of 49% in the antenna efficiency (simulated), compared to that in free space (93%), has been observed when the antenna is placed at d=10 mm from the human body.

Table 5-2: Comparison of different simulated parameters of CP patch antenna analysed for various body-worn configurations working at the GPS frequency of 1575.42 MHz

Antenna Body-worn Configuration		f_c (MHz)	BW (MHz)	η_t (%)	Gain (dBi)
Antenna with no body presence (free space)		1575	19	93	5.8
Varying separation of antenna and body	d=10 mm	1550	19	44	6.3
	d=20 mm	1552	20	48	6.6
	d=30 mm	1555	12	53	6.5
	d=40 mm	1560	11	55	6.7
	d=80 mm	1564	13	68	7.1
	d=120 mm	1571	17	79	6.2
Varying antenna position on-body	Middle chest	1550	19	44	6.3
	Right chest	1549	17	45	6.9
	Left chest	1549	17	46	7.1
	Near belly	1537	13	16	3.7
Varying hand-held antenna position	α=60°	1554	8	51	7.0
	α=75°	1557	9	53	6.4

It appears that greater separations between the antenna and the human body tend to improve the antenna performance. At d=40 mm, the antenna resonates at 1560 MHz as compared to 1550 MHz when d=10 mm. It could be observed from the presented results that further the antenna from the body, the closer is its resonance to that in free

space. The antenna efficiency also show improvement. With d=120 mm, the antenna exhibits very close performance to the free space operation with resonating at 1571 MHz having an efficiency of 79%. This enhanced performance is caused by change in the amount of the reflected fields by changing the antenna-body gap. At larger separations, the effective permittivity of the medium becomes closer to the value for the free space that reduces the extent of frequency detuning and the radiation deformation.

Figure 5.7 demonstrates the antenna performance from radiation perspective in both XY and YZ planes. The antenna radiation is compared for the absence of the human body to that in its presence, as a function of the antenna and the human body separation, along the chest. These results show that the human body presence deforms the antenna radiation patterns substantially in both planes due to power absorption in the lossy tissues. It also causes increased gain levels and reduced antenna efficiency. The antenna pattern shape keeps constant with increasing separations from the body. However, radiated power increases in front direction, away from the body because of greater reflected waves. An increase of 0.5-1.3 dB is noted in the antenna gain in front direction while it reduces by up to 5 dB in backward direction. It is also observed that the antenna radiation patterns have a tendency of improvement by getting closer to free space performance as value of d increases from 10 mm to 120 mm due to reduced losses in the human body tissues. Also, large ground plane used for the matching and opti-mised performance of the antenna has played a part to reduce the pattern deformations by shielding the antenna from some of the reacting field reflected by the body at closer gaps. These effects would have a greater impact on antennas with smaller or no ground plane.

It could also be noted from Figure 5.7 that antenna radiation characteristics are affected more in YZ plane as compared to XY plane. It is a result of the presence of greater body mass with increased losses in the tissues since, the height of the torso is larger than the width as shown in Figure 5.5.
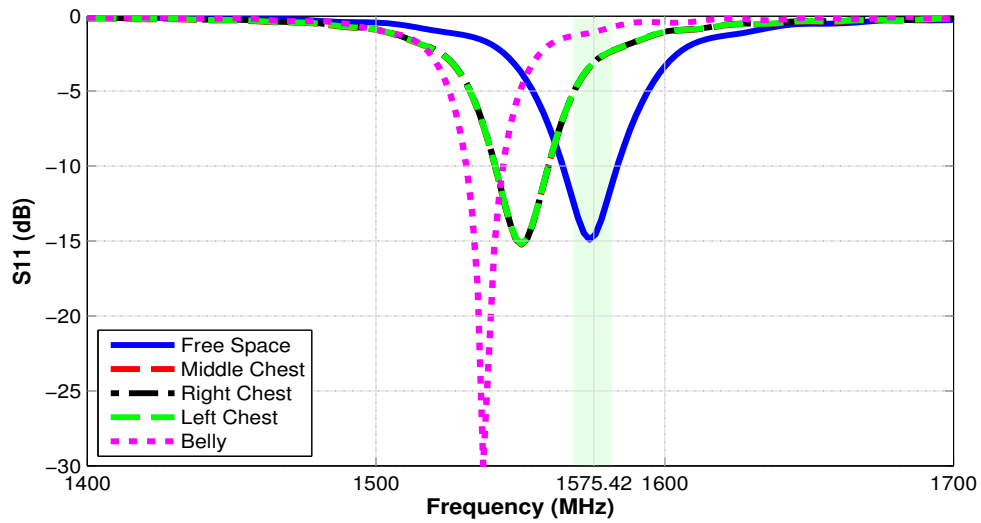
Figure 5.8: Comparison of simulated S11 of the truncated corner microstrip patch GPS antenna for different antenna positions on-body

5.1.4 Dependency on On-body GPS Antenna Position

The portable devices are commonly placed at different positions near the human body, for example in the pocket of a shirt (near chest) or in the pocket of a jacket (near belly). Difference in the shape of the body parts at different locations could influence the GPS antenna to perform with varying radiation characteristics. The effects of varying on-body placements of the antenna are also analysed to study the change in the antenna performance.

The microstrip patch GPS antenna is placed at different positions on-body while maintaining a gap of 10 mm between the antenna and the body to allow the covering assembly clearance. The considered on-body positions include the antenna placed at the middle chest, the right chest, the left chest and right waist near the belly. The results are compared to the antenna performance in the absence of the human body.

The S11 curves in Figure 5.8 depict that resonance shifts from 1575.42 MHz to lower frequencies depending upon the placement of the antenna on the body. The effect on the antenna impedance is nearly equal for the three positions along the chest. An average

(a) XY plane (b) YZ plane
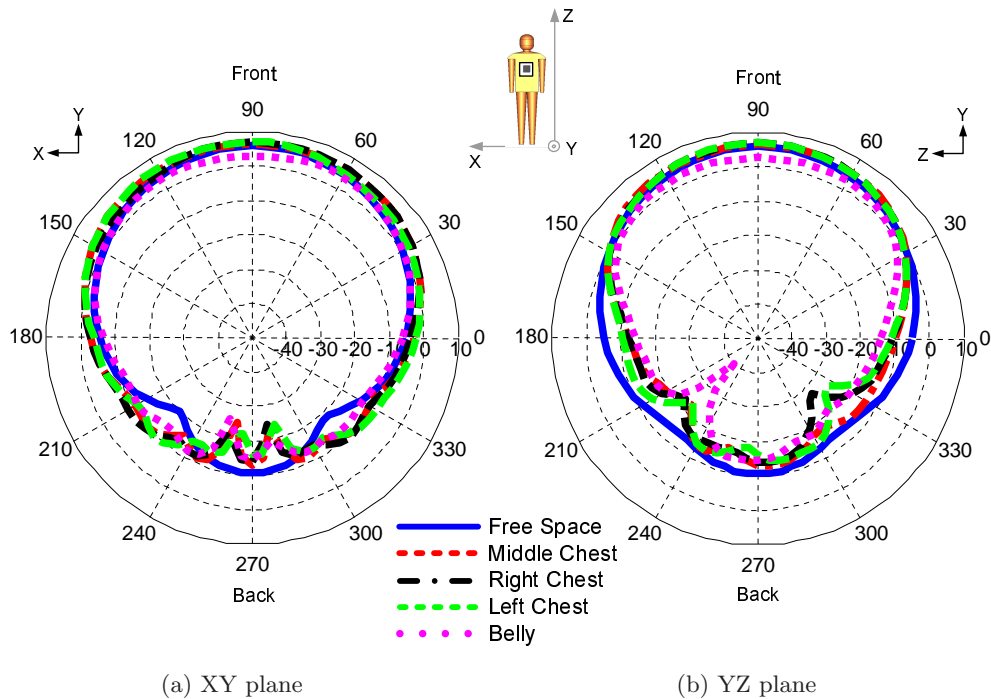
Figure 5.9: Simulated 2-D gain patterns in XY and YZ planes for the truncated corner microstrip patch GPS antenna with effects of variation in on-body antenna position at 1575.42 MHz

drop of 48% in the antenna total efficiency, compared to the free space efficiency, is observed. However, the antenna is detuned to a larger extent and centre frequency comes down to 1537 MHz when placed near the belly. The antenna efficiency also experiences a huge drop reaching to 16%. It is because the presence of discontinuities towards legs and arms near the belly changes size and shape of the lossy tissue more as compared to the three chest positions. Hence, the resulting modification of the effective medium causes larger variation in the antenna input impedance.

The gain patterns shown in Figure 5.9 confirm that the radiation characteristics of the antenna are also affected but the shielding provided through the ground plane minimises this effect. The pattern shapes are again similar for the three chest positions with reduced back lobes. The discontinuities towards legs and arms near the belly have also caused scattered fields with greater pattern deformations.
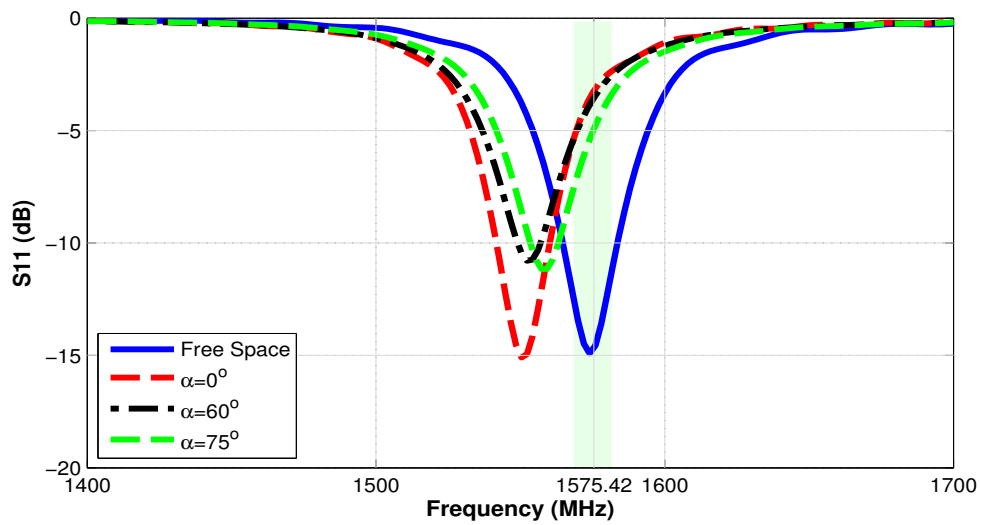
Figure 5.10: Simulated S11 responses of the truncated corner microstrip patch GPS antenna for hand-held configurations with arm bent at three different angles (α)

5.1.5 Performance of GPS Antenna Held in User's Hand

The portable devices, especially the GPS navigators, are usually used in held-in-hand scenarios with the user watching the screen. The direct contact of the human hand with the GPS antenna affects the radiation properties of the antenna resulting in a reduced performance. The presented microstrip patch GPS antenna is tested to demonstrate the human body effects on its performance for held-in-hand scenarios. Although, a realistic hand model (constructed in later studies) could not be added to the designed structure due to the model limitations, the human body model is modified to represent the user's watching position with the antenna held in the left hand. The bending angle of the arm is represented by α. Two held-in-hand configurations with the arm bent at an angle of $\alpha=60^o$ and $\alpha=75^o$ are considered and results are compared with the antenna in the absence of the human body and antenna placed on-body at the middle chest ($\alpha=0^o$). The three configurations have the separation between the body and the antenna equal to 10 mm, 190 mm and 350 mm, respectively, as illustrated in Figure 5.5.

The antenna impedance performance is compared in Figure 5.10. The presence of the human body has detuned the antenna causing the resonance frequency to shift from 1575

(a) XY plane (b) YZ plane
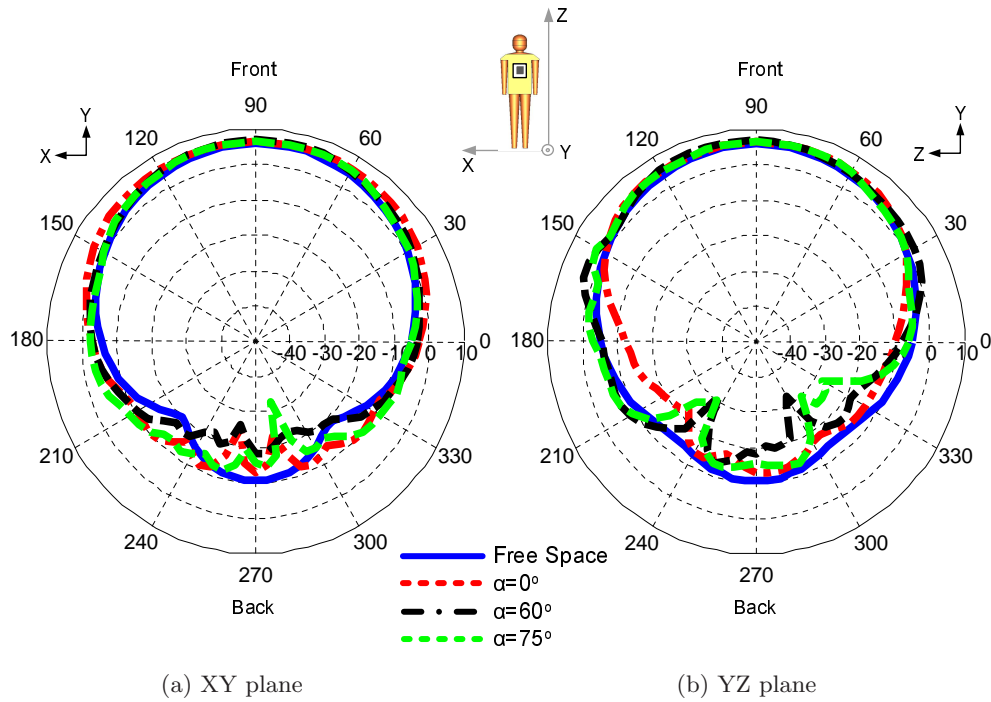
Figure 5.11: Comparison of 2-D gain patterns in XY and YZ planes of the truncated corner microstrip patch GPS antenna for hand-held configurations with arm bent at three different angles (α) at 1575.42 MHz

MHz to lower values. The detuning of the antenna again depends upon the separation of the antenna and the human body. The resonance gets closer to the one observed for the antenna in free space scenario with wider bending angles as antenna becomes less affected by the torso. It also improves the antenna efficiency to 51% in comparison to the free space value with $\alpha = 75^o$ while it is 53% when $\alpha = 60^o$ as drop is minimised. However, the antenna impedance undergoes detuning in the two cases due to the currents induced in hand tissues causing the drop in the efficiency.

The antenna radiation performance is compared in Figure 5.11. The reflected fields again have caused changes in the gain and introduced deformations in the polar patterns. Increasing distance between the body and the antenna due to increased bending angle has modified the patterns with high backward radiations. It is because of the fact that the antenna is less affected by the greater body mass of torso and legs at these separations. The major part of the degradation in these configurations, comes from the bent arm.

The presented results confirm that the GPS antenna undergoes frequency detuning while operating in the vicinity of the human body depending upon the on-body antenna placement, present body mass and physiological parameters of the body. This tends to decrease the resonant frequency of the antenna, causing it to be mismatched at its intended operating frequency of 1575.42 MHz. The antenna loses the desired ± 5 MHz bandwidth in most of the cases whereas its radiation pattern also deforms. It is, therefore, evident that the human body presence affects the GPS antenna performance to a visible extent and should be taken into account to design an efficient navigation system.

5.2 Human Body Effects on GPS Mobile Terminal Antennas in Multipath Environment

The discussion in the above sections has established that the performance of the GPS antennas tends to deteriorate while placed near the human body. It increases the magnitude of degradations in mobile terminal GPS antennas operating in the multipath environment, that already have been suffering from reflections, diffractions and scattering of the incoming radio waves from the surrounding objects, as illustrated in Figure 5.12. It results in attenuation, delay and distortion of the communication link. To guarantee a reliable navigation system, the GPS mobile terminal antennas should cope these deteriorations. Therefore, these antennas must be tested not only for the effects of the multipath environment but also for the presence of the human body in this environment.

The study of the human head presence in the multipath environment and its effects on the land mobile antennas has been reported [18–20]. The Mean Effective Gain of the antenna is taken as a figure of merit for the antenna performance in these studies. Since, the calculations of antenna Mean Effective Gain are based on the antenna power gain patterns, it simplifies antenna performance evaluation in practical scenarios including antenna on-body placements as follows [19, 21–23]:
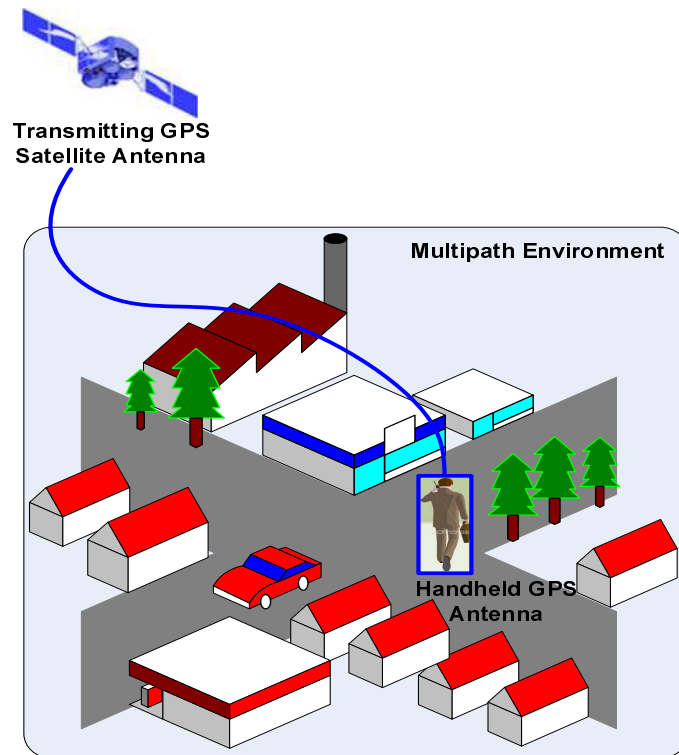
Figure 5.12: GPS environment and reception of multipath signal by GPS mobile terminal antenna operating near human user

- The gain degradations due to radiation pattern deformations can be easily accommodated.

- The degradations of the antenna efficiency as a result of variations in the input impedance can also be accounted for, irrespective of whether it is caused by the human body proximity or absorptions by the human body.

The fast growing demand of the portable navigation devices necessitate the extension of this investigation to the GPS mobile terminal antennas. The effects of the presence of the human body on the performance of the GPS mobile terminal antennas is studied and characterised using the statistical model for the GPS multipath environment discussed in Chapter 4. The computer simulations with realistic numerical models of human head, hand and the whole body are used to analyse the performance of various GPS mobile terminal antennas.

The study is conducted in two parts; first, investigating the effects of the presence of the human head and hand, second, investigating the effects of the presence of the whole body in the vicinity of the antennas. Different possible on-body scenarios are investigated including antenna held in user's hand, antenna placed by the user's head, antenna held in user's hand near to the head in talking position and antenna placed at user's pocket position. Effects of a multi-layered human head are also taken into account. The performance of the GPS mobile terminal antennas is characterised in terms of MEG_{GPS} along with η_c. Since, these parameters are calculated using simulated 3-D power gain patterns that only considers the power absorptions in the human body tissues [24], it is essential to include the mismatch losses caused by the antenna detuning in these on-body configurations. These losses are accumulated in MEG_{GPS} and η_c employing the concept of 'Realised Gain', calculated using the following equation [25]:

$$Gain_{realised} = Gain \times \eta_m \tag{5.1}$$

Where, $Gain$ is the simulated gain that takes material losses into account. η_m represents the antenna mismatch efficiency that accounts for the antenna detuning losses and is calculated as follows:

$$\eta_m = 1 - |S11|^2 \tag{5.2}$$

The CST Microwave Studio$^{\circledR}$ provides an embedded option for the realised gain mode [24].

5.2.1 Design of GPS Mobile Terminal Antennas

Three types of the GPS mobile terminal antennas are considered in this study to investigate the human body effects. The three antennas include PIFA, DRA and helix antennas and are similar in design as described in Chapter 4. The antennas operate at the GPS frequency of 1575.42 MHz. The PIFA is designed using FR4 substrate of 1.6 mm thick-
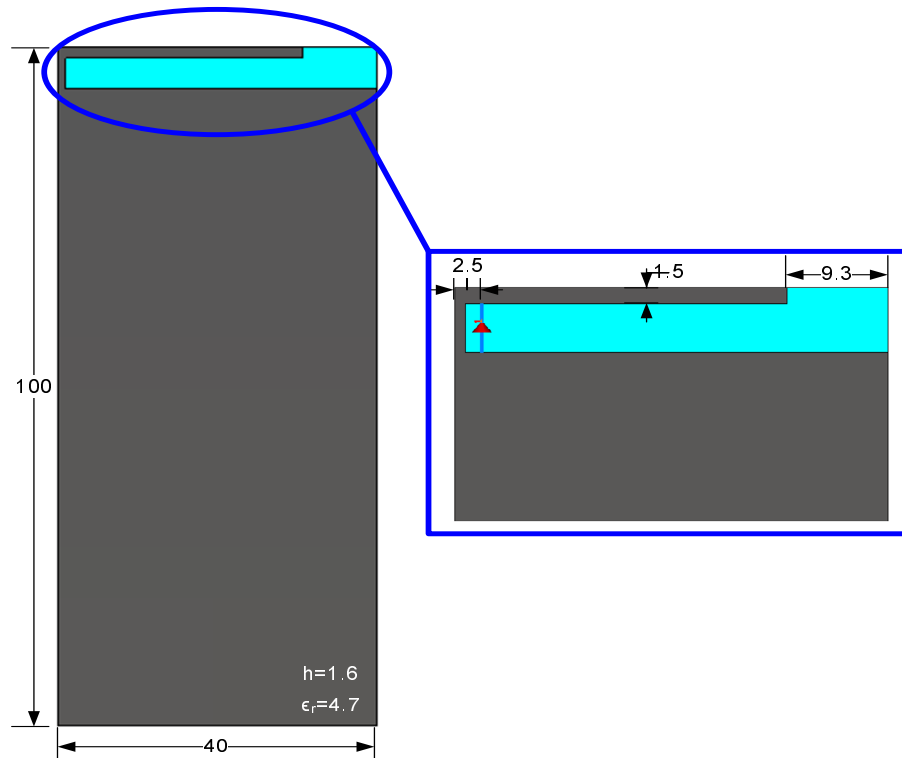
Figure 5.13: Geometrical structure of GPS mobile terminal PIFA antenna used to study the effects of human body presence on the antenna performance in multipath environment (all lengths are in mm)

ness. The PCB size is 100 mm×40 mm. The DRA antenna is loaded with a dielectric of $\varepsilon_r = 21$. The ground plane is 100 mm×40 mm of lossy copper type while the loaded dielectric is covered with lossy silver. The helix has no substrate and is mounted on the left side of the metallic ground plane of dimensions 100 mm×40 mm×0.45 mm. The PIFA and DRA antennas are fed using discrete ports with 50 Ω impedance to represent the commonly used 50 Ω coaxial port feed. Figures 5.13-5.15 show the schematic layout of the three antennas. The antenna prototypes are fabricated and tested in the Antenna Measurement Lab at QMUL and results have been reported in Chapter 4. In current study however, only the simulation results are of interest.
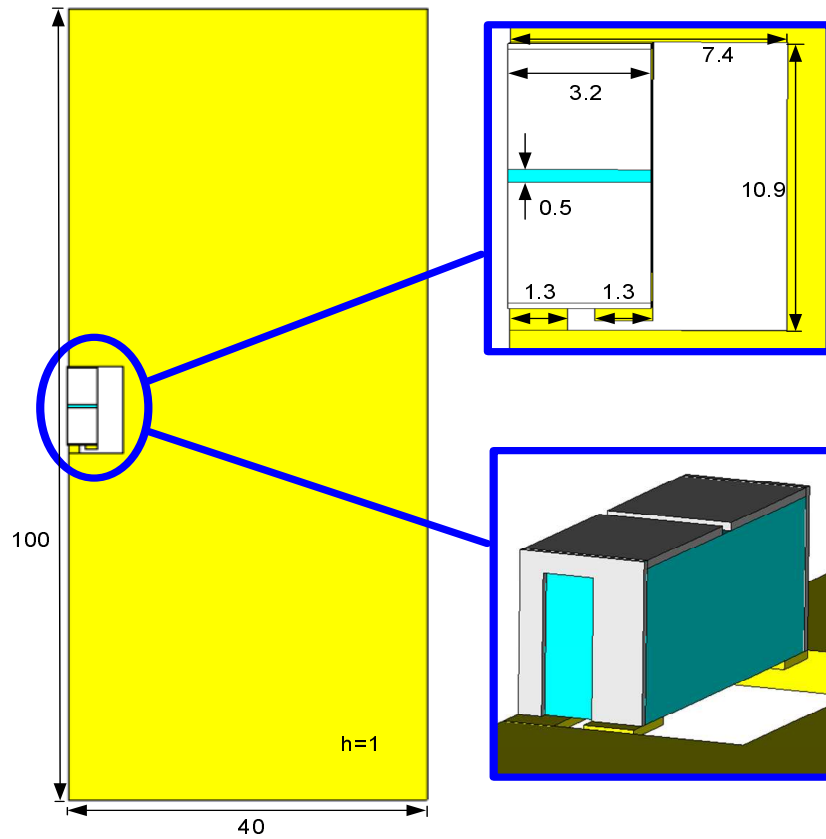
Figure 5.14: Schematic layout of GPS mobile terminal DRA antenna to study the effects of human body presence on the antenna performance in multipath environment (all lengths are in mm)

Table 5-3: Electric properties of specific human tissues at 1575.42 MHz used within the constructed inhomogeneous multi-layer head model

Tissue	Electric Properties	
	Dielectric Constant (ε_r)	Tissue Conductivity (σ)(S/m)
Skin (Dry)	39.28	1.10
Muscle	53.86	1.22
Skull (Average Bone)	12.33	0.27
Brain (Average Grey and White)	43.96	1.04
Spinal Chord	31.17	0.77
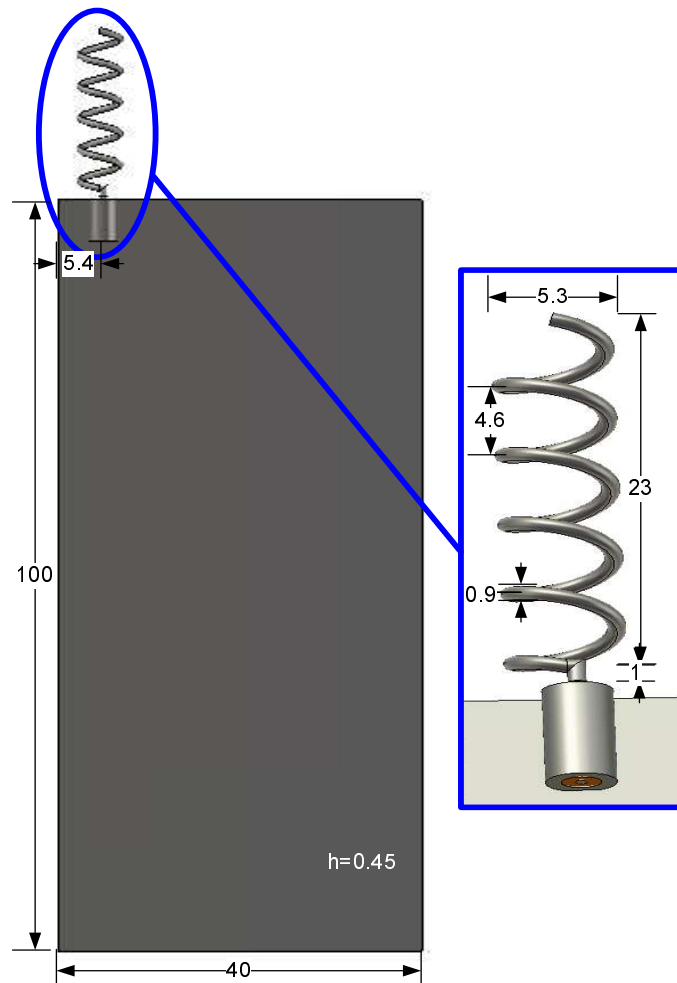
Figure 5.15: Geometry and dimensions of GPS mobile terminal helix antenna for the study of the presence of the human body effects on the antenna performance in multipath environment (all lengths are in mm)

5.2.2   Effects of Human Hand and Head Presence

In the first part of the study, only the effects of the presence of a realistic human head and hand model are investigated for the performance of the GPS mobile terminal antennas in the multipath environment.
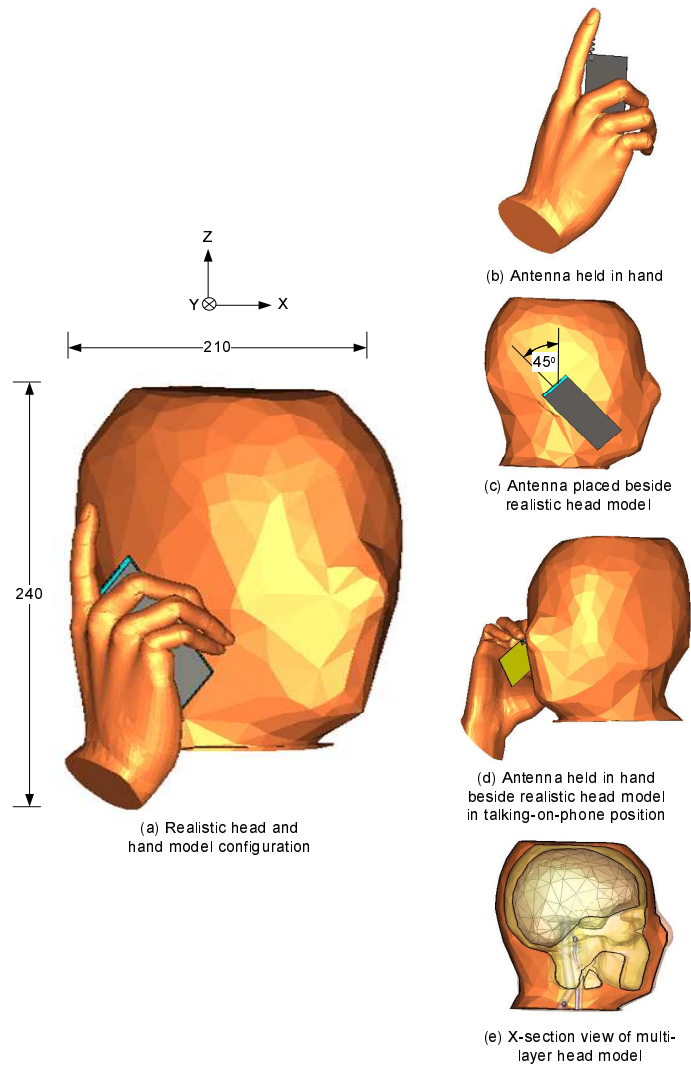
Figure 5.16: High resolution model for human head and hand with different test configurations for three GPS antennas-under-test (all lengths are in mm)

5.2.2.1 Test Set-up

A high resolution realistic model of the human head and hand with dimensions for an average built human is used as shown in Figure 5.16. The electric properties of the muscle tissues are considered for the homogeneous head and hand models at 1575.42 MHz with a permittivity of 53.86 and conductivity of 1.22 S/m [15–17]. An inhomogeneous multi-layer head model is also employed to characterise the effects of different head tissues on the antenna working. Five head tissues including skin, muscle, skull, brain and

spinal chord are incorporated in this inhomogeneous model. Table 5-3 summarises the electric properties of these tissues at 1575.42 MHz and Figure 5.16(e) depicts the x-section view of the multi-layer head model with anatomical details. An adaptive mesh is employed with different cell sizes that has reduced the number of volume cells (voxels) in the computational domain significantly. The Perfectly Matched Layer (PML) absorbing boundary conditions [24] are used with a maximum cell size of 10 mm near the boundaries and a minimum size of 0.08 mm at the edges of the solids in the computational region.

Various on-body scenarios including the antennas placed by the homogeneous head, held in hand and held in hand near to the head in talking position are taken into consideration to investigate the added effects of the human head and hand on the antenna performance in the GPS multipath environment. The effects of the multi-layer head model in all the above configurations are then analysed. The antennas are placed beside the head inclined at 45° for the talking positions. A separation of 10 mm between the antenna and the head is kept to allow clearance for mobile casing. The statistical analysis of the antenna performance in the multipath environment in these on-body configurations needs the information of the 3-D gain patterns in the perpendicular and the parallel polarisations. Therefore, the simulated 3-D gain patterns for all the test setups are recorded.

5.2.2.2 Performance of GPS Antennas

The S11 response of the three antennas is shown in Figures 5.17-5.19. These figures confirm the well known phenomenon of antenna detuning caused by the presence of the human body. The amount of this detuning varies from antenna to antenna. The most resilient antenna to this detuning effect has proved to be the helix, that offered the required -10 dB bandwidth of ± 5 MHz (desired for efficient GPS operation) in all the cases due to its wide bandwidth. The S11 responses for the DRA antenna (Figure 5.18) makes it the most sensitive, of the three tested antenna types, to the human body effects. It has shown greater detuning than the PIFA and helix antenna whereas loosing

-10 dB impedance bandwidth in the desired ±5 MHz L1 band for held in hand and the talking positions (held in hand placed beside head). The performance of the PIFA is also degraded greatly with the antenna held in talking position has suffered worse. These results also show that the S11 response is similar for the single layer and the multi-layer head models and the inner organs incorporated in the inhomogeneous multi-layer model have little impact. It is due to the fact that input impedance is a relatively local phenomenon. It is influenced more significantly by the objects located close to the antenna feed point while the inner organs of the multi-layer head are comparatively more displaced [1].

Figures 5.21-5.25 illustrate the simulated 3-D gain patterns for the perpendicular and parallel polarisations of the PIFA, DRA and helix, operating in different scenarios near the human hand and head. It is evident from these results that the antenna detuning effect is also replicated in the radiation pattern deformations depending on the posture of the human hand and head.

In the held-in-hand position (Figure 5.21), the radiating element of the PIFA is in the negative x-direction while the DRA is in the negative x-direction. Hence, the PIFA
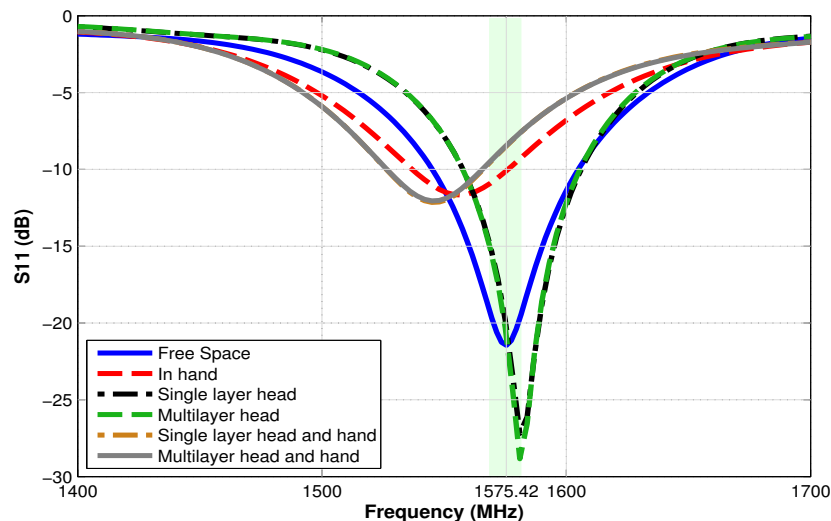
Figure 5.17: S11 curves for PIFA with effects of different placements near human hand and head
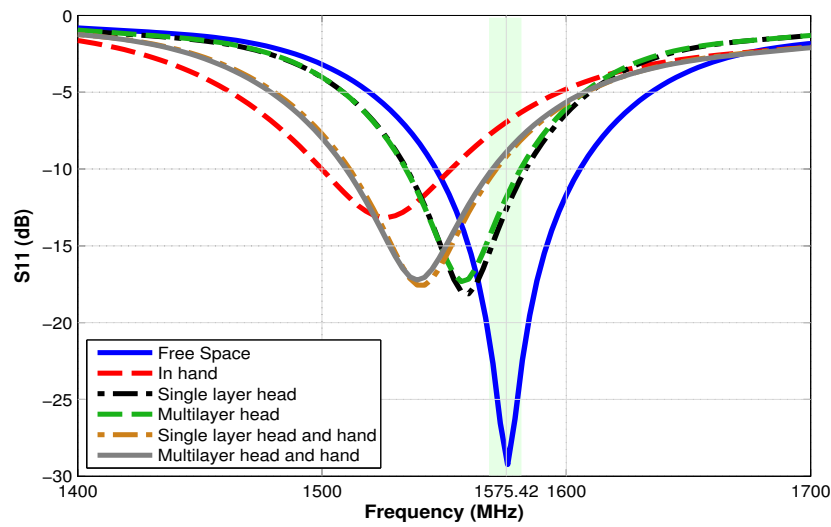
Figure 5.18: S11 curves for DRA with effects of different placements near human hand and head
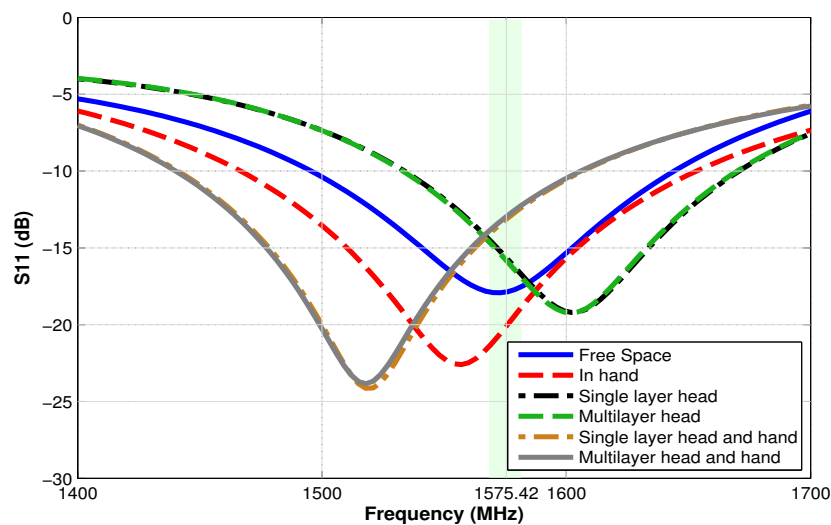
Figure 5.19: S11 curves for helix with effects of different placements near human hand and head

is affected more by the gripping fingers while the DRA suffers more by the absorptions in the palm. For the helix in free space, the ground plane is a major contributor in the radiation. Therefore, it is also affected by the gripping fingers. In the antenna placed near head position, a greater body mass reduces the radiation of the three antennas in positive x-direction making the gain patterns directive in negative x-direction as shown in Figures 5.22 and 5.23. It could also be observed from these results that gain levels are

(a) 3-D gain patterns of PIFA in free space

(b) 3-D gain patterns of DRA in free space

(c) 3-D gain patterns of helix in free space
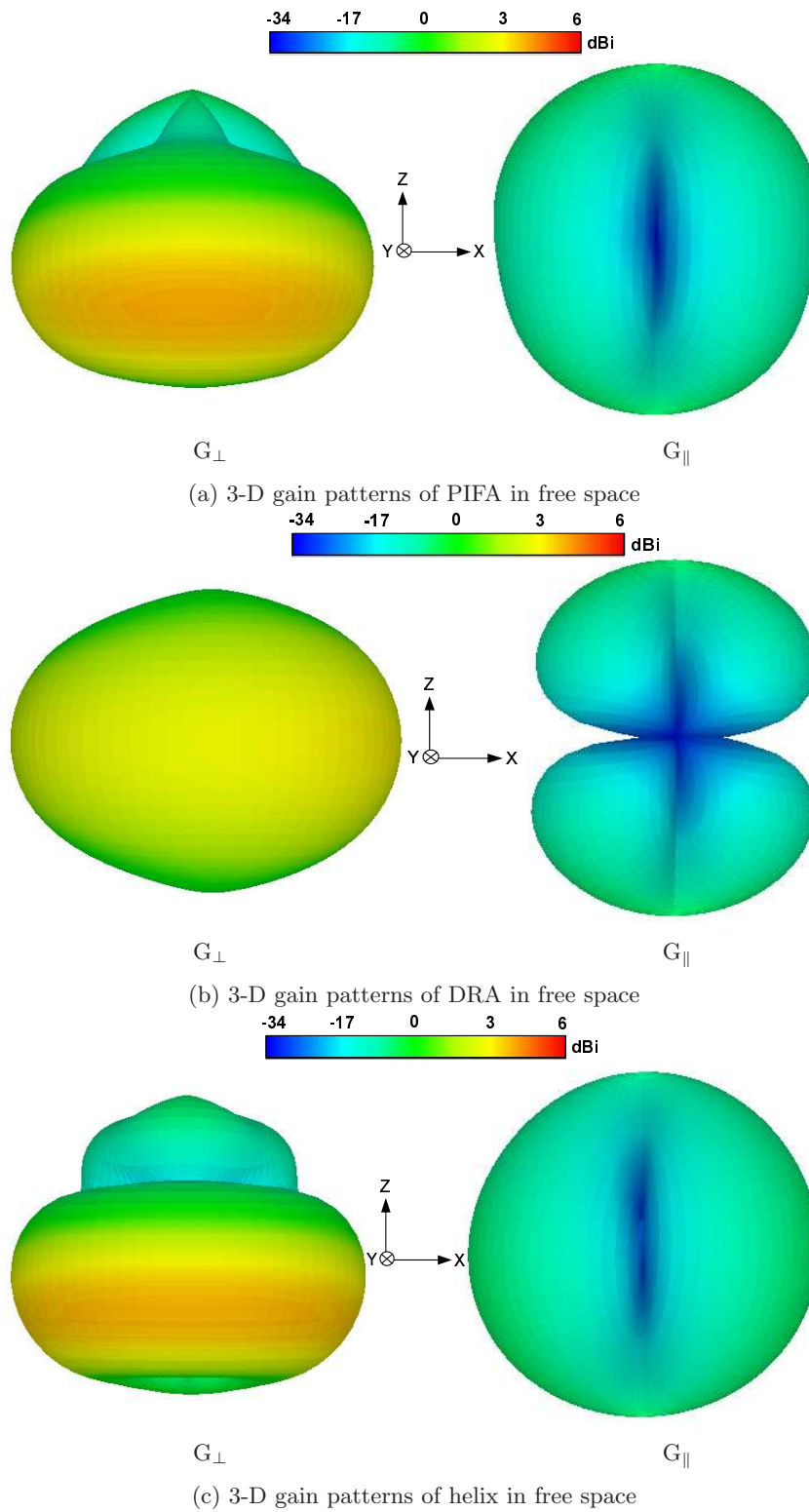
Figure 5.20: Simulated 3-D gain patterns for perpendicular and parallel polarisations of PIFA, DRA and helix GPS mobile terminal antennas in free space

(a) 3-D gain patterns of PIFA held in user's hand

(b) 3-D gain patterns of DRA held in user's hand

(c) 3-D gain patterns of helix held in user's hand
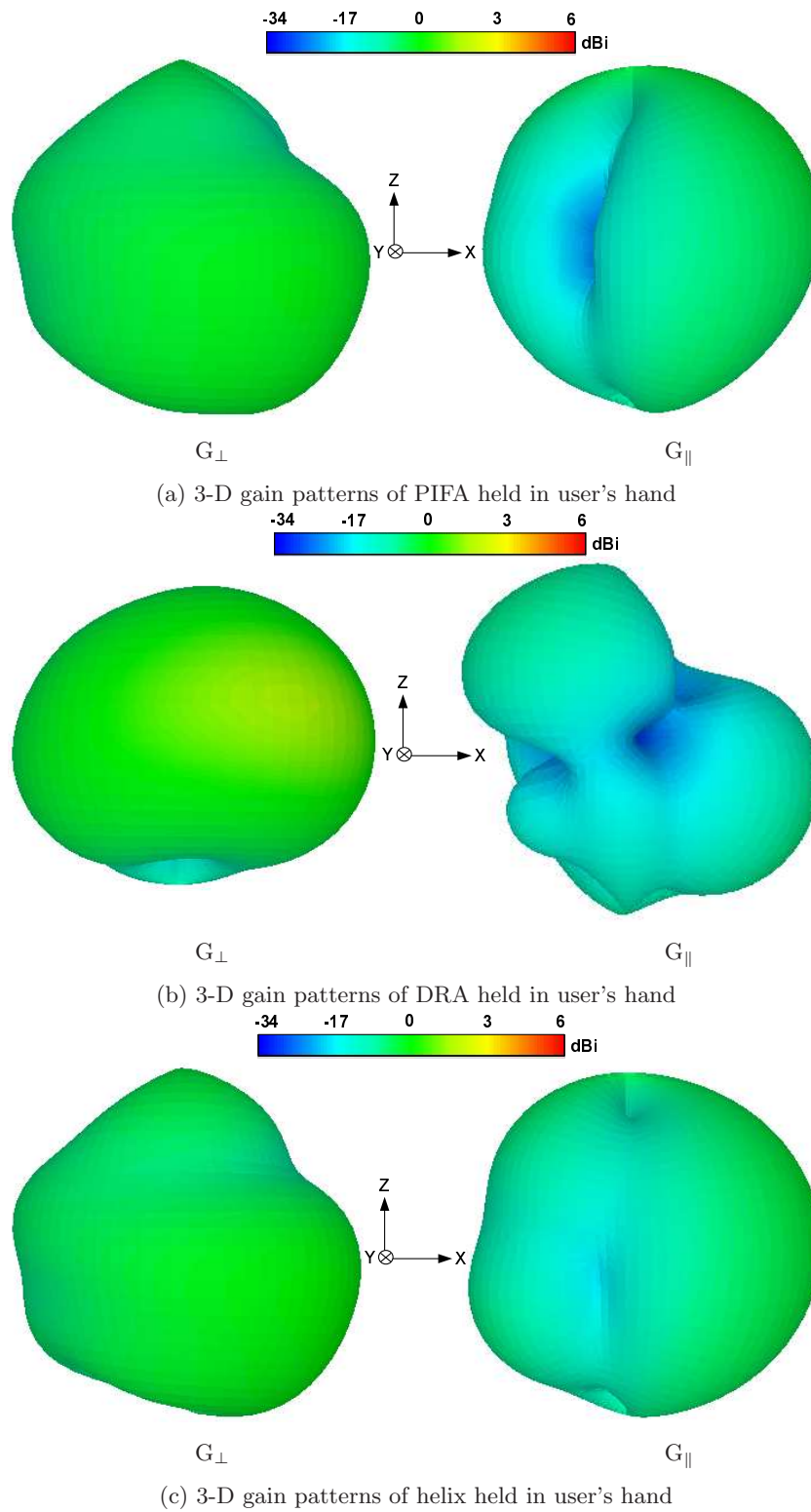
Figure 5.21: Simulated 3-D gain patterns for perpendicular and parallel polarisations of PIFA, DRA and helix GPS mobile terminal antennas held in user's hand
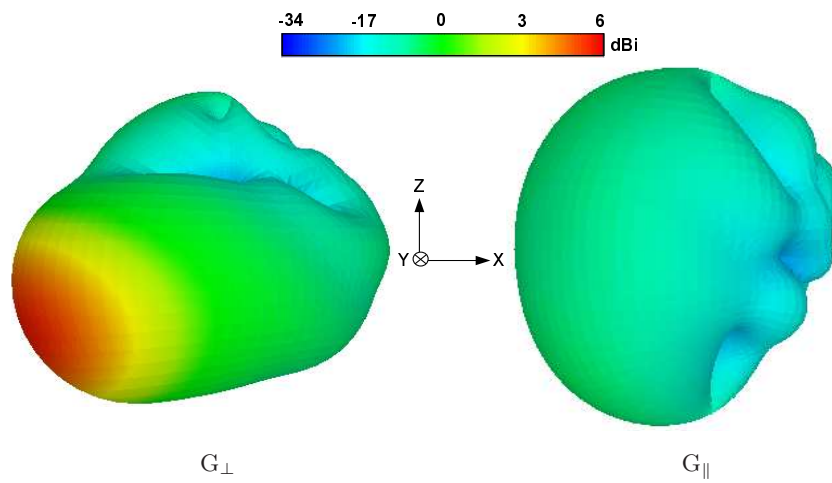
(a) 3-D gain patterns of PIFA placed beside user's single layer head
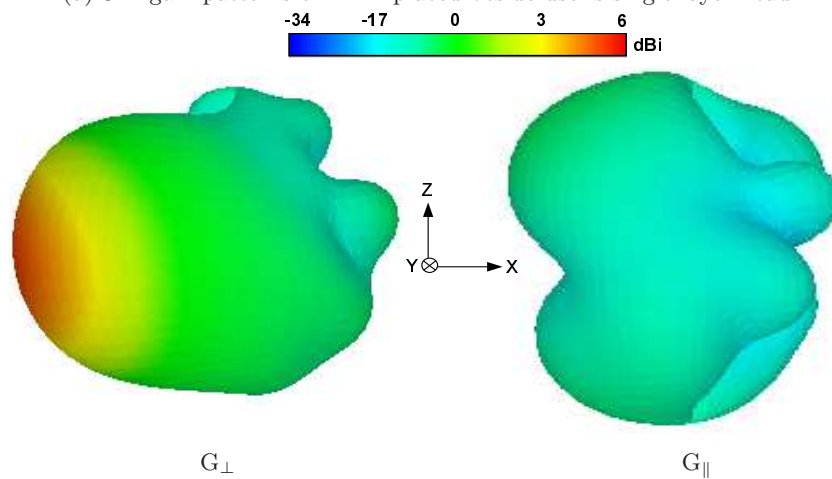
(b) 3-D gain patterns of DRA placed beside user's single layer head
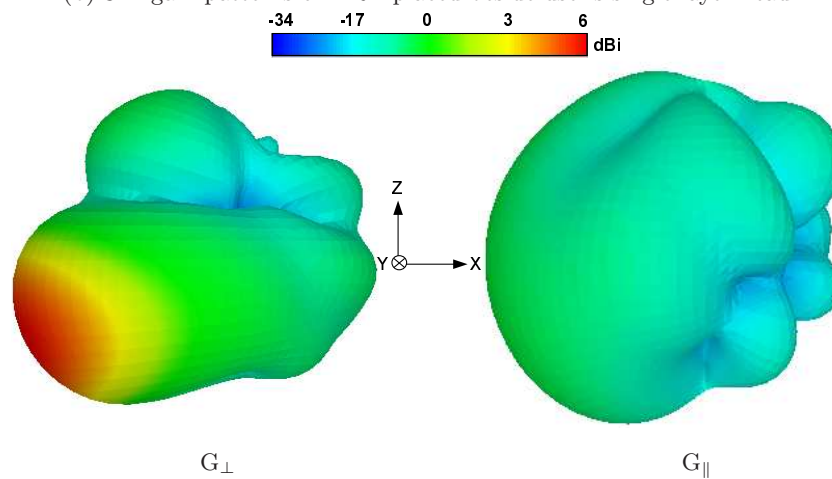
(c) 3-D gain patterns of helix placed beside user's single layer head

Figure 5.22: Simulated 3-D gain patterns for perpendicular and parallel polarisations of PIFA, DRA and helix GPS mobile terminal antennas placed beside user's homogeneous single layer head
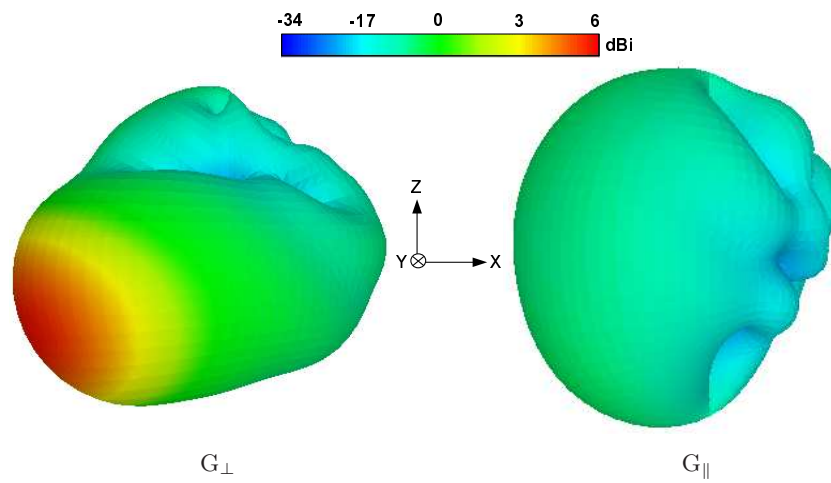
(a) 3-D gain patterns of PIFA placed beside user's multi-layer head
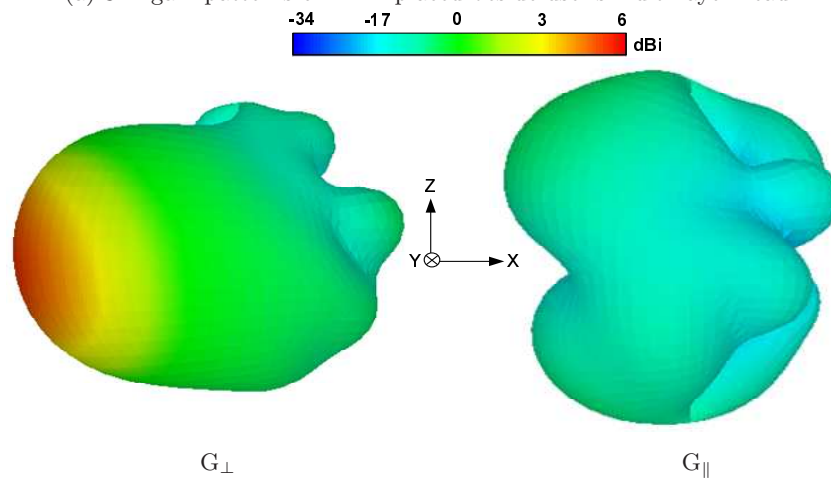
(b) 3-D gain patterns of DRA placed beside user's multi-layer head
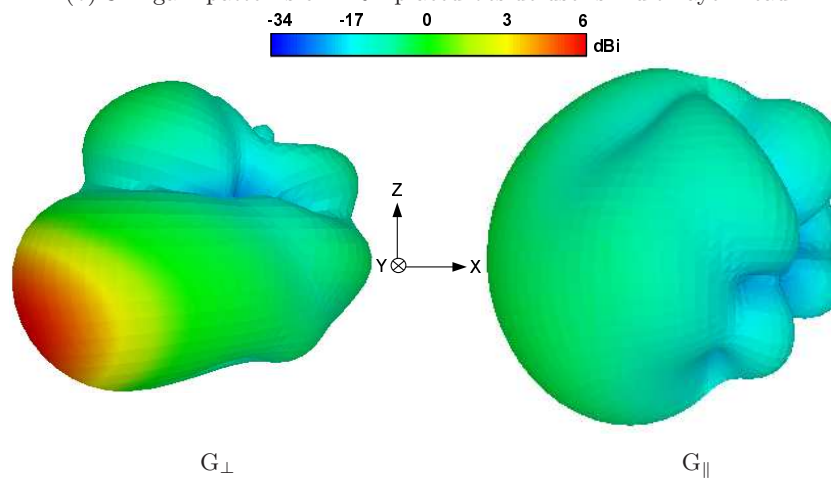
(c) 3-D gain patterns of helix placed beside user's multi-layer head

Figure 5.23: Simulated 3-D gain patterns for perpendicular and parallel polarisations of PIFA, DRA and helix GPS mobile terminal antennas positioned beside user's inhomogeneous multi-layer head

$G_\perp$ $\qquad\qquad\qquad\qquad\qquad\qquad\qquad\qquad\qquad$ $G_\parallel$

(a) 3-D gain patterns of PIFA held in user's hand and placed beside his single layer head

$G_\perp$ $\qquad\qquad\qquad\qquad\qquad\qquad\qquad\qquad\qquad$ $G_\parallel$

(b) 3-D gain patterns of DRA held in user's hand and placed beside his single layer head

$G_\perp$ $\qquad\qquad\qquad\qquad\qquad\qquad\qquad\qquad\qquad$ $G_\parallel$

(c) 3-D gain patterns of the helix held in user's hand and placed beside his single layer head
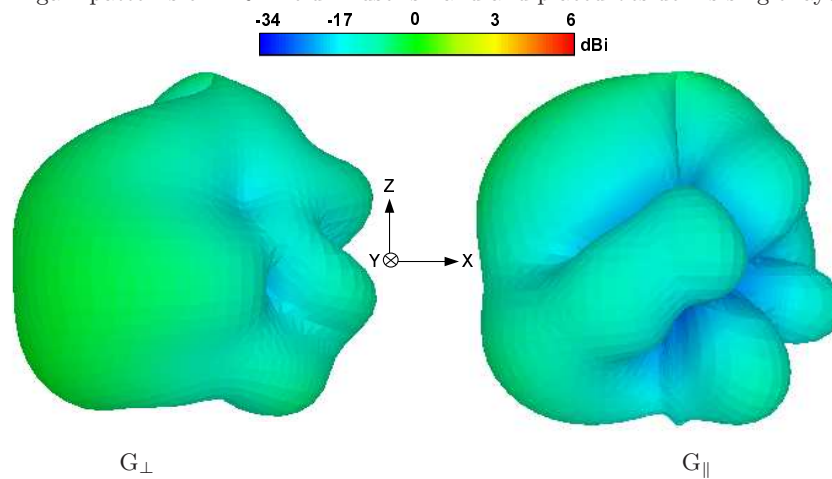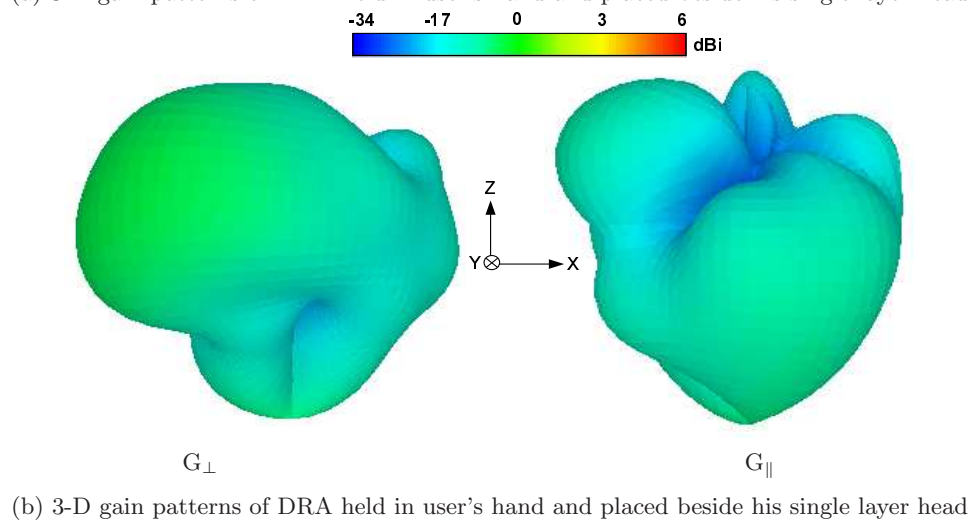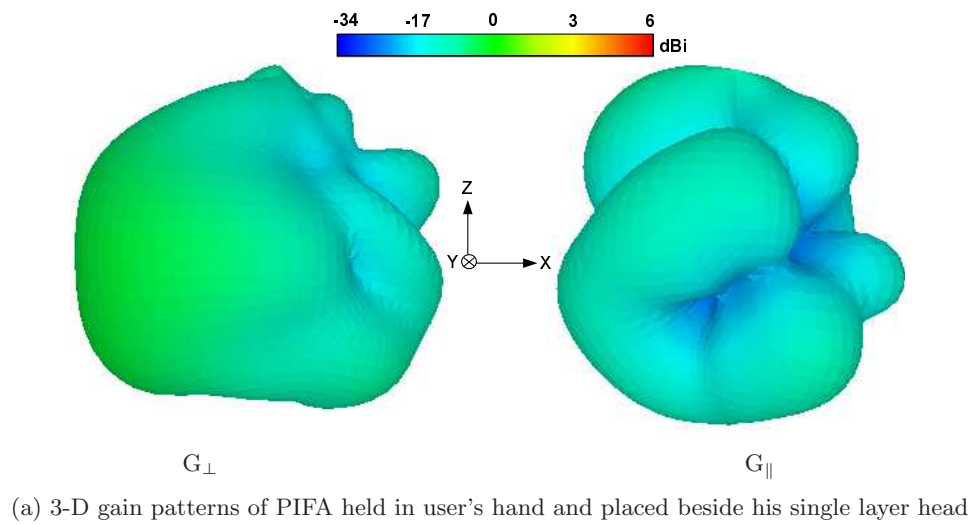
Figure 5.24: Simulated 3-D gain patterns for perpendicular and parallel polarisations of PIFA, DRA and helix GPS mobile terminal antennas held in user's hand and placed beside his homogeneous single layer head

(a) 3-D gain patterns of PIFA held in user's hand and placed beside his multi-layer head

(b) 3-D gain patterns of DRA held in user's hand and placed beside his multi-layer head

(c) 3-D gain patterns of helix held in user's hand and placed beside his multi-layer head
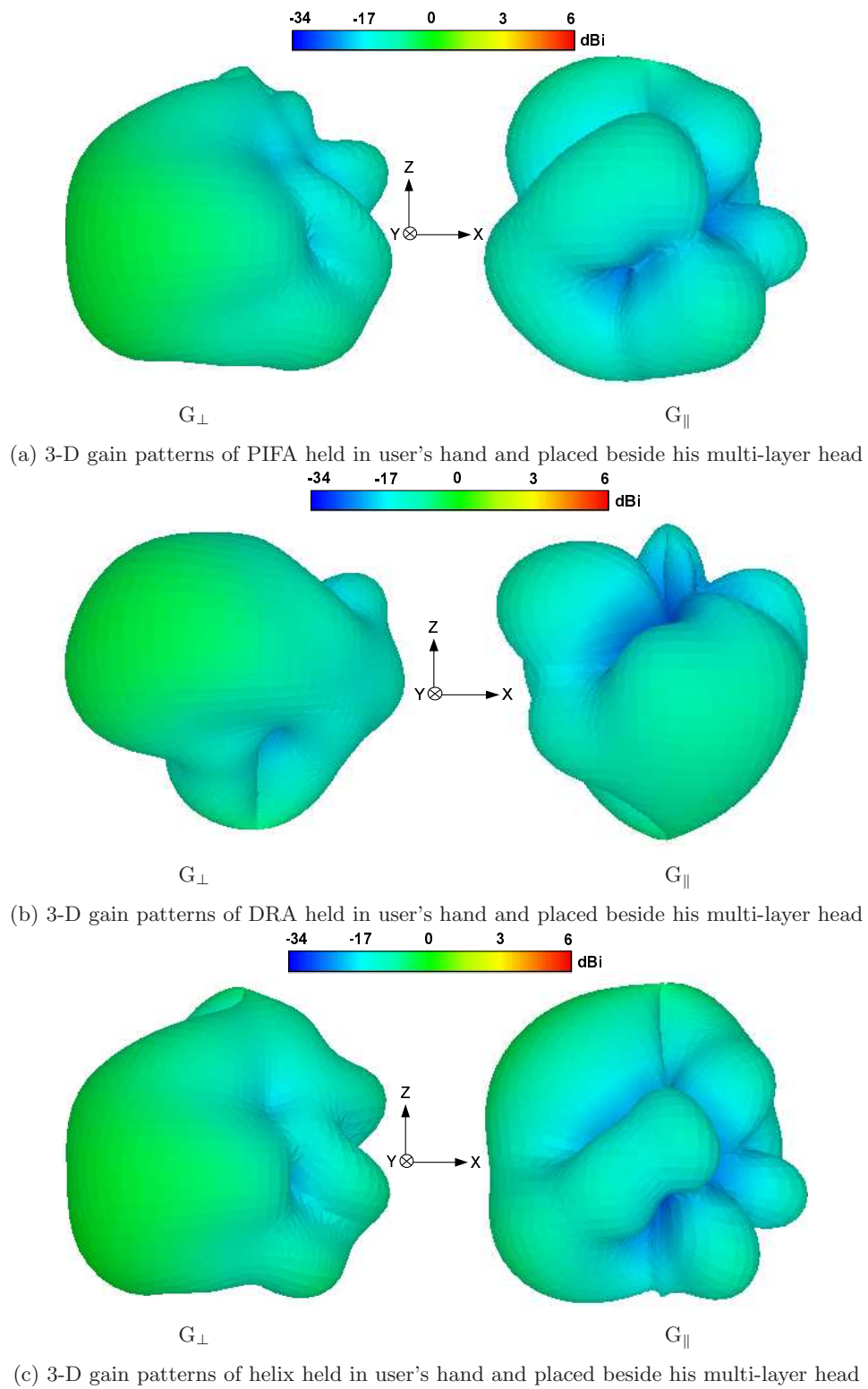
Figure 5.25: Simulated 3-D gain patterns for perpendicular and parallel polarisations of PIFA, DRA and helix GPS mobile terminal antennas held in user's hand and placed beside his inhomogeneous multi-layer head

less in the upper hemisphere as compared to the lower hemisphere. When the antenna is held in user's hand in talking position, presence of both the hand and head on the two sides of the antennas give rise to electromagnetic absorptions and reflected fields are minimum. It defragments the antenna radiation greatly and causes poor gain levels in all the directions, depicted in Figures 5.24-5.25.

The performance of the PIFA, DRA and helix GPS mobile terminal antennas in the multipath environment is evaluated using the discussed statistical model in terms of MEG_{GPS} and η_c. The simulated 3-D gain patterns of the designed antennas in different configurations, shown in Figures 5.20-5.24 are input to the model. The ground plane (earth) is considered as made of dry concrete with a relative permittivity of 4.5 [26, 27] to include the ground reflections.

Table 5-4: Calculated GPS Coverage Efficiency and GPS Mean Effective Gain of three mobile terminal GPS antennas operating at 1575.42 MHz in multipath environment in proximity of human body with effects of human hand and head

Test Set-up in Presence of Human Hand and Head	Model Calculations Using Simulated 3-D Patterns in Actual Reflection Multipath Environment					
	PIFA		DRA		Helix	
	η_c	MEG_{GPS}	η_c	MEG_{GPS}	η_c	MEG_{GPS}
	(%)	(dB)	(%)	(dB)	(%)	(dB)
Antenna without human body presence	92	-8.2	95	-5.7	88	-5.8
Antenna held in user's hand	89	-11.2	58	-10.6	78	-7.8
Antenna placed beside user's single layer head	75	-10.0	76	-8.2	66	-7.4
Antenna placed beside user's multi-layer head	74	-10.1	73	-8.4	65	-7.5
Antenna held in talking position beside user's single layer head	42	-15.9	36	-14.9	58	-11.0
Antenna held in talking position beside user's multi-layer head	41	-16.0	34	-15.2	57	-11.1

Table 5-4 summarises the calculated values of η_c and MEG_{GPS} for the three tested antennas in different near-body configurations. It has been noted that the presence of the lossy human body tissues causes significant degradation in the antenna performance due to electromagnetic absorptions in the tissues and field reflections from the surface of the human body. It results in the gain pattern deformations as compared to that without the presence of the human body, illustrated in Figures 5.21-5.25. This deterioration of the gain patterns reduces the coverage and MEG_{GPS} of the GPS antennas and their ability to pick up the GPS satellite signal suffers drastically.

It has also been noted that the reduction in η_c depends mainly on the extent of available clear sky view to the radiating element. The more the antenna radiating element is covered by the user, the lesser is its η_c. The amount of present body mass in the vicinity of the GPS antenna also plays a key role.

Figure 5.26(a) compares the coverage of the three antennas in the above described test configurations. In the case of the PIFA, the radiating element is in the negative x-direction. For the held in hand position, the radiating element (top edge of the PCB) is not covered by the palm or the gripping fingers. Only a small disturbance comes from the index finger resulting in η_c of 89% i.e. 3% lower than the free space value. When the antenna is placed beside the head, greater body volume produces larger detuning due to the surface reflections and energy absorptions and hence, η_c decreases to 75%. The antenna placement in the talking position shields its clear sky view on both sides by the user's holding hand and his head reducing the antennas's coverage to 42%.

On the contrary, the radiating DRA is in positive x-direction, located in the middle of the PCB and hence, affected more by the palm. The gripping fingers also cover most part of the radiating element, resulting in a reduced η_c value of 58% as compared to the free space value of 95%. Placing the antenna beside the head blocks its view only on one side resulting in η_c of 76% but the presence of both the hand and head shields most of the useful angles and hence, η_c becomes 36%.

C1: Antenna without human body presence
C2: Antenna held in hand
C3: Antenna placed beside single layer head
C4: Antenna placed beside multi-layer head

C5: Antenna in talking position with single layer head
C6: Antenna in talking position with multi-layer head

(a) Coverage efficiency of GPS antennas

C1: Antenna without human body presence
C2: Antenna held in hand
C3: Antenna placed beside single layer head
C4: Antenna placed beside multi-layer head

C5: Antenna in talking position with single layer head
C6: Antenna in talking position with multi-layer head

(b) MEG of GPS antennas

Figure 5.26: Multipath environment performance of three GPS mobile terminal antennas in free space and in different on-body positions with effects of human head and hand

For the helix, the radiating element is mounted on the top left of the ground plane, having the feed in negative x-direction. The index finger restricts the radiating element view on one side when held in hand. The palm of the holding hand and gripping fingers also disturbs the major radiation area as evident by comparing Figure 5.20(c) and Figure

5.21(c). It causes η_c to drop from 88% for free space to 78%. The placement of the antenna beside the head is affected from the surface reflections. The antenna experiences clear sky view on one side but the other half is completely blocked causing η_c to drop to 66%. The talking position with held in hand placed near head restricts the clear sky view of the antenna on both sides in similar fashion as noted for the PIFA and DRA, resulting in a poor η_c of 58%.

The loss due to the human body presence is also replicated in MEG_{GPS} values, shown in Figure 5.26(b). Since, MEG_{GPS} is the average performance of the antenna in the multipath environment, it depends on the overall gain pattern, taking into account both the power absorptions in the human body tissues and the antenna detuning, rather than the extent of the radiating element's clear sky view. Therefore, the three GPS antennas have been affected by the human head and hand presence in similar fashion. The performance degradation is less in held in the hand position and worst in held in the hand beside the head position as compared to the MEG_{GPS} value for antenna operating in multipath environment without human body presence. From Figure 5.20, it is clear that the three antennas have stronger radiation in azimuth plane with main lobes in negative y-direction. Therefore, when these antennas are held in the user's hand restricting most of the azimuth angles, gain values decrease sharply with almost equivalent levels in both the azimuth and elevation planes (Figure 5.21) resulting in decreased MEG_{GPS} values.

In the antennas placed beside the user's head configuration, the lossy human tissues are present on one side of the antennas. It produces reflected electromagnetic fields resulting in highly directive gain patterns as illustrated in Figure 5.22. This increase in directivity in certain azimuth angles fails to make a greater impact because of reduction in the gain levels in other directions, especially in the upper hemisphere. It lowers the overall performance of the antenna resulting in decreased MEG_{GPS}.

Finally, when the GPS antennas are placed in talking position, they are covered by the user's hand on one side and by his head on the other. The electromagnetic

absorptions in the lossy tissues and reflections from the head and hand surfaces cause greater degradation in the gain values causing MEG_{GPS} to reach its lowest (of the observed cases).

A reduction of 1.8-7.7 dB (in comparison to the MEG_{GPS} for no human body presence scenario) is observed in case of the PIFA antenna while this reduction is between 2.5-9.2 dB and 1.6-5.2 dB for the DRA and helix antenna, respectively.

The effects of the presence of a multi-layer head near the three GPS mobile terminal antennas for placed beside head with and without holding hand are also studied. The comparison of η_c and MEG_{GPS} obtained for these scenarios with that of the single layer head model, presented in Figure 5.26 clearly indicates that the internal organs have no significant effect on the antenna performance. The reduction in the values of η_c and MEG_{GPS} is between 1-3% and 0.1-0.3 dB respectively with varying permittivity and conductivity values of the internal head organs increasing the losses. However, the penetration depth is only slightly changed from 30.2 mm for single layer head model to 33.5 mm (average) for the multi-layer case at 1575.42 MHz. It minimises the increase in the power absorption resulting in little impact on MEG_{GPS} and η_c. It is therefore, concluded that study of the antenna performance in the multipath environment with single layer human body models containing electric properties of the muscle tissues provides reasonably accurate results and computational time could be saved by not employing multi-layer models.

Overall, the DRA antenna offers better performance in the multipath environment with no human body presence, in comparison to the PIFA and helix, with wider coverage and good MEG_{GPS}. However, performance of the helix antenna is good and more consistent in the presence of the human head and hand.

5.2.3 Effects of Complete Human Body Presence

The previous section has given an overview of the effects of the user's hand and head on the performance of the GPS mobile terminal antennas. However, in actual working scenarios, these antennas have to operate in the vicinity of the user's whole body that can further reduce their performance due to greater absorptions and reflections from the body surface. Therefore, it is pertinent to take into account the effects of the whole body presence on the working of the GPS mobile terminal antennas.
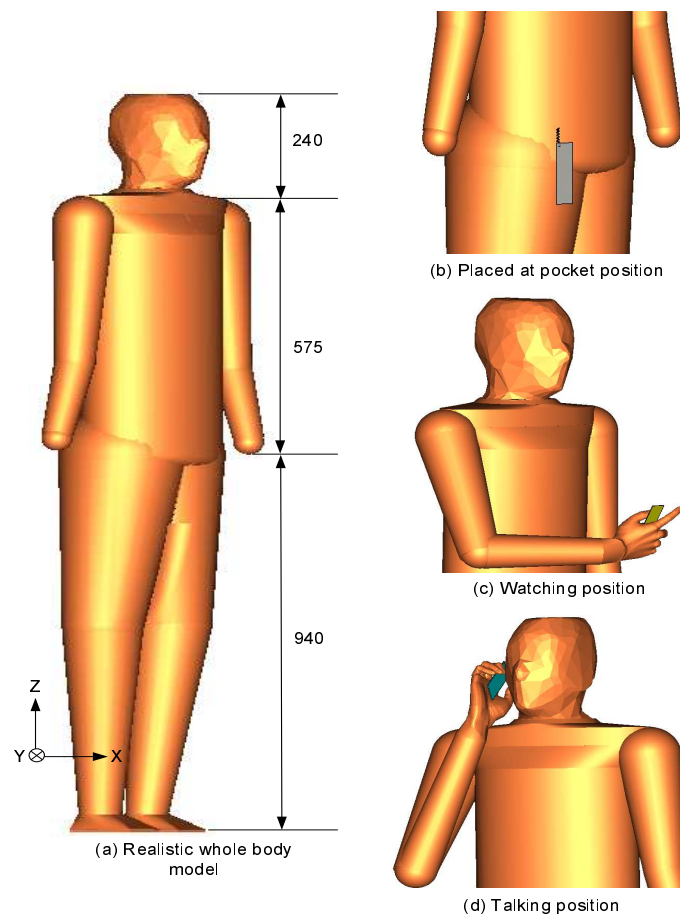
Figure 5.27: Medium resolution single layer homogeneous realistic human body model used to study effects of body presence on performance of GPS antennas with different placements of the antennas on-body (all lengths are in mm)

(a) Pocket position   (b) Watching position   (c) Talking position
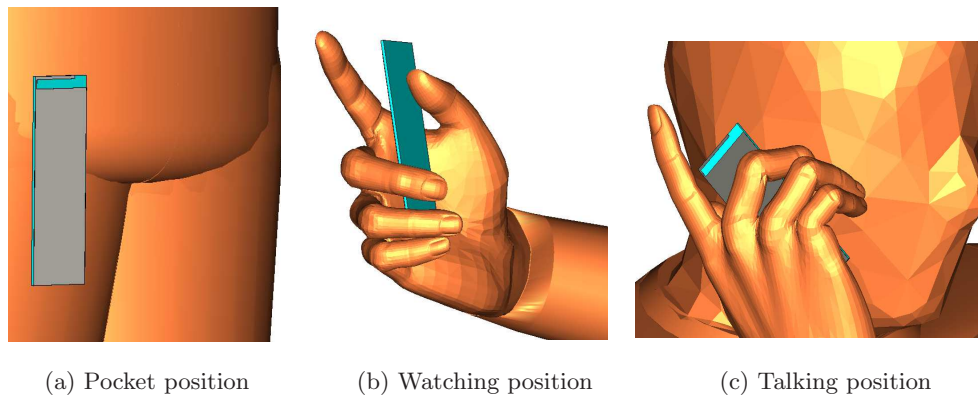
Figure 5.28: Various on-body placements of GPS mobile terminal PIFA

(a) Pocket position   (b) Watching position   (c) Talking position
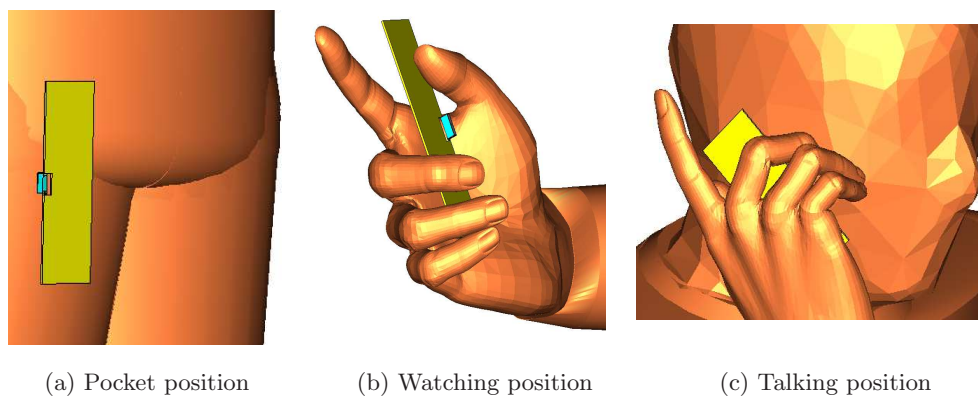
Figure 5.29: Various on-body placements of GPS mobile terminal DRA

(a) Pocket position   (b) Watching position   (c) Talking position
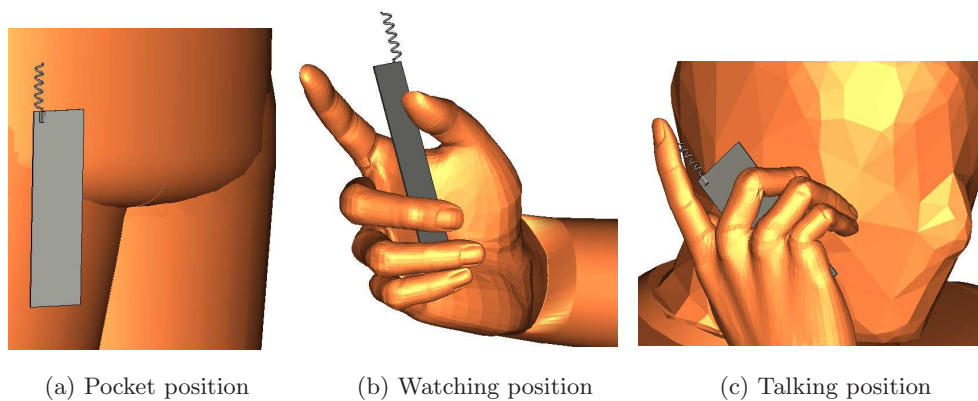
Figure 5.30: Various on-body placements of GPS mobile terminal helix

5.2.3.1 Test Set-up

In this study, the medium resolution realistic complete human body model, described in Chapter 3, is considered. The human body is modelled as a single layer homogeneous
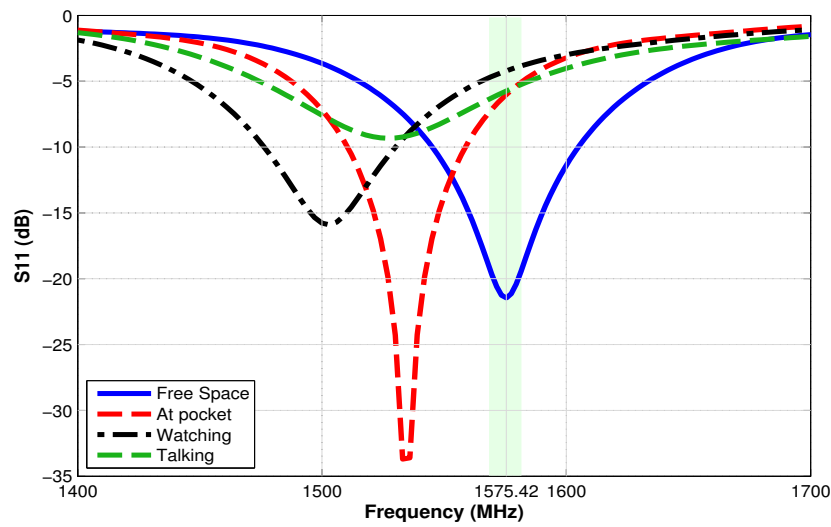
Figure 5.31: S11 response of PIFA operating in different on-body positions
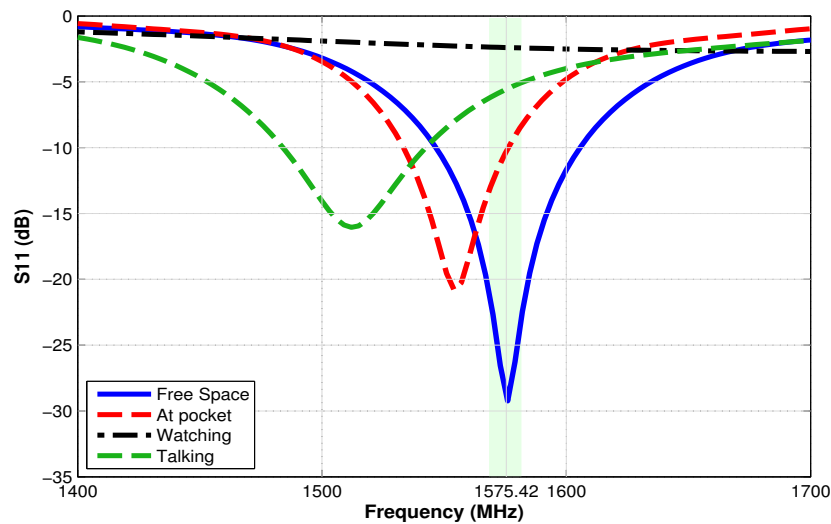
Figure 5.32: S11 response of DRA operating in different on-body positions

object, based on the observations made in the previous section for the single layer and multi-layer head models. This model offers not only faster computations as a result of reduced complexity but also gives flexibility in terms of re-positioning the body parts. It makes it easy to represent the talking-on-phone position and holding the phone positions. A high resolution hand is also added to realise the antenna held in hand scenarios, shown in Figure 5.27. The dielectric properties of the muscle tissue at 1575.42 MHz are used with permittivity of 53.86 and conductivity of 1.22 S/m [15–17].
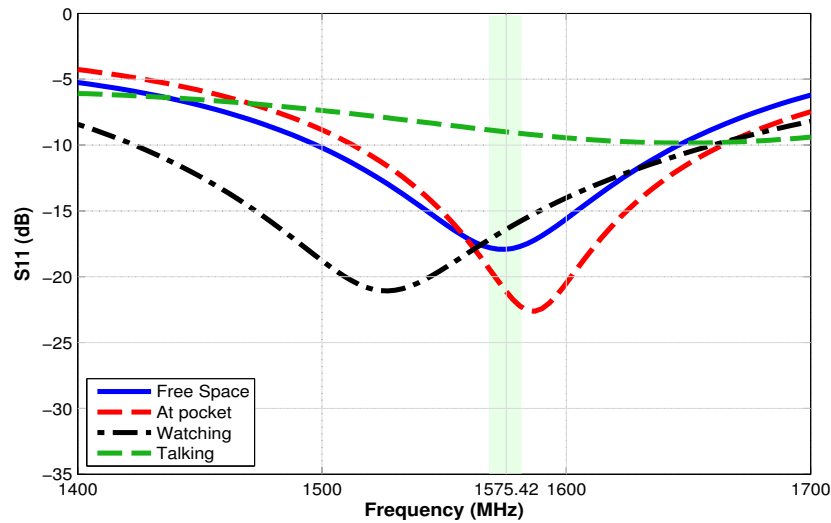
Figure 5.33: S11 response of helix operating in different on-body positions

The similar three types of the GPS antennas used in mobile terminals discussed in Section 5.2.1, PIFA, DRA and helix are used to analyse the effects of the human body presence in the multipath environment. Three possible scenarios of on-body placement of the GPS mobile terminal antennas are considered. For the device kept in the user's pocket, GPS antennas are placed on the left bottom torso at the pocket position on the body as shown in Figure 5.27(b). The separation between the antenna and the body is kept 10 mm to allow the clearance for the mobile casing. In the scenario where the GPS mobile terminal antenna is being watched by the user, the antennas are modelled to be held in the user's hand in front of the body, at a distance of 175 mm from the body surface, illustrated in Figure 5.27(c). Lastly, the effects of the presence of the human body on the GPS mobile terminal antennas are investigated for a common position of talking-on-the-phone. This configuration is modelled by re-positioning the human body in such a way that the antenna is being held in the user's hand beside the head, depicted in Figure 5.27(d). The separation is again kept at 10 mm between the antenna and the head to allow the covering assembly, whereas the antennas are inclined at 45° with respect to the z-axis. Figures 5.28-5.30 illustrate the details of position and orientation of the radiating elements of the three antennas in the considered on-body placements.

5.2.3.2 Performance of GPS Antennas

The S11 curves of the three antennas working in the on-body placements are plotted in Figures 5.31-5.33. The antenna detuning is evident from these results caused by the presence of the human body.

The PIFA is affected most as it has failed to exhibit the desired -10 dB impedance bandwidth of ±5 MHz in the three on-body configurations (Figure 5.31). The DRA antenna has also shown a poor performance as it completely detuned in the watching and talking position while achieving -10 dB impedance bandwidth of 5 MHz covering frequency range of 1570 MHz to 1575 MHz in the placed at pocket position, shown in Figure 5.32. The helix antenna has again shown a less sensitive behaviour to the detuning effects caused by the human body. It has fulfilled the ±5 MHz impedance bandwidth requirement in L1 band for placed at pocket and held in watching positions, while managed to attain a comparatively reasonable -8 dB impedance bandwidth of ±5 MHz when operating in the talking position (Figure 5.33). Overall, the three antennas has performed poorly in the talking position as compared to the other scenarios.

(a) Original watching position   (b) Modified watching position (d_z=40 mm)
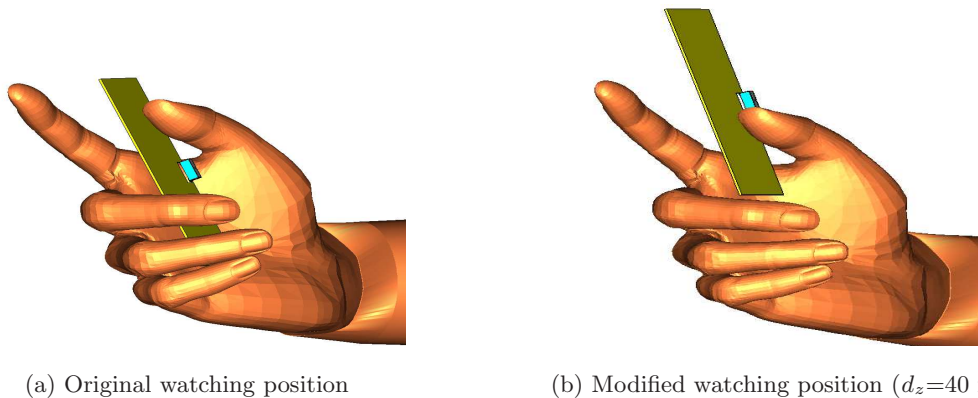
Figure 5.34: Modified watching position for GPS mobile terminal DRA to investigate S11 response

The greater detuning of the DRA in watching position and the helix in talking position is due to electromagnetic absorptions in the palm of the holding hand and the gripping fingers. The two antennas could perform better if the radiating element is

(a) Original talking position

(b) Modified talking position (d_z=40 mm)
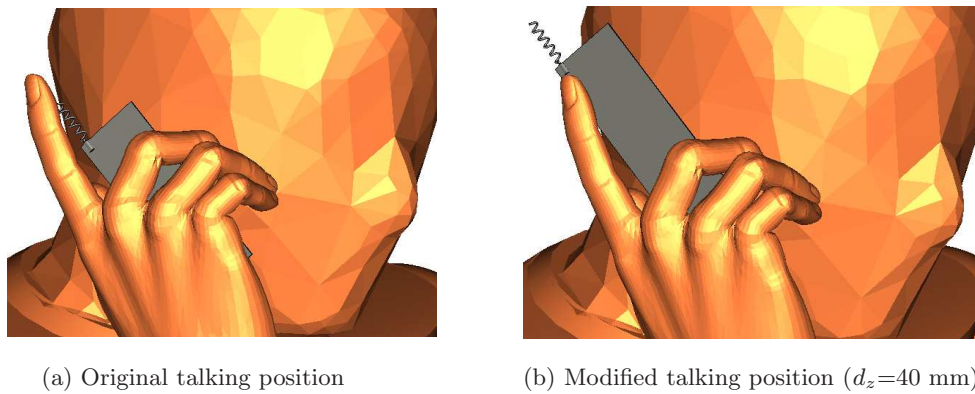
Figure 5.35: Modified talking position for GPS mobile terminal helix to investigate S11 response
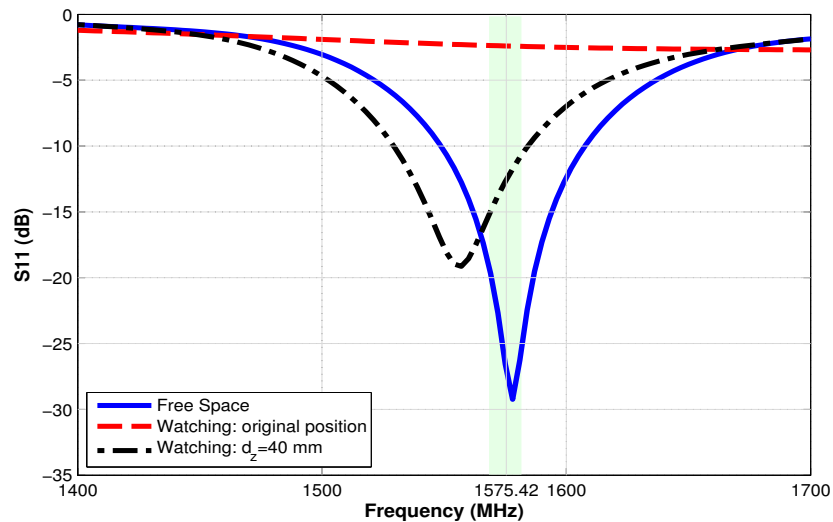
Figure 5.36: Comparison of S11 curves for DRA in original and modified watching positions

cleared from the palm of the hand and the gripping fingers. Therefore, the DRA in watching position and the helix in talking position are tested moving the antenna by 40 mm in z-direction (d_z). The two tested configurations are shown in Figures 5.34(b) and 5.35(b) in comparison to the original positions (Figures 5.34(a) and 5.35(a)).

The S11 responses of the DRA and helix in the modified watching and talking scenarios are plotted in Figures 5.36 and 5.37, respectively. It could be observed from these results that the two antennas exhibit better impedance matching when placed at d_z=40 mm as compared to the original positions. It is therefore, evident that the way a user
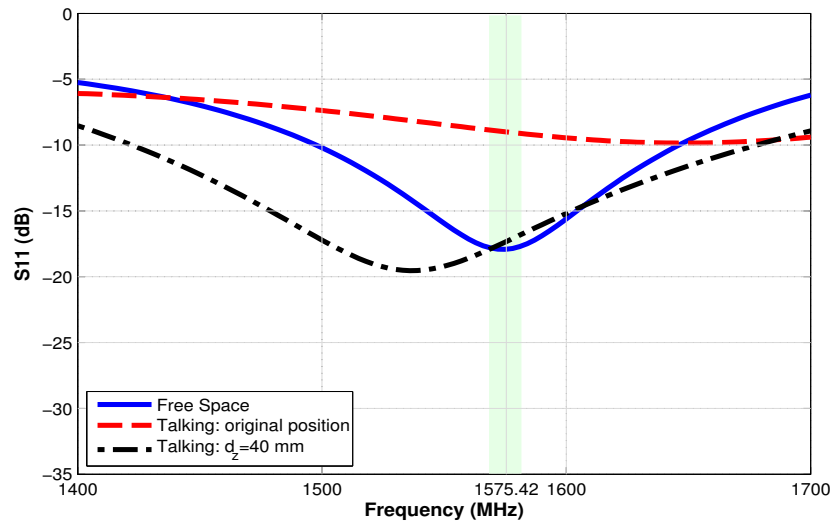
Figure 5.37: Comparison of S11 curves for helix in original and modified talking positions

holds the antenna plays a vital role to define the extent of antenna detuning.

The 3-D simulated gain patterns of the three antennas in different on-body positions are also observed and recorded, depicted in Figure 5.38-5.40. The proposed statistical model for the GPS multipath environment is used for the evaluation and comparison of the performance of the antennas in the three on-body configurations. The realised gain is used in the calculations of η_c and MEG_{GPS} to incorporate both the power absorption and detuning effects caused by the human body presence. Table 5-5 summarises these results in comparison to the values observed when the antennas operate without presence of the human body.

Figure 5.41 compares η_c and MEG_{GPS} for the three antennas. These results further strengthen the fact that the GPS mobile terminal antennas in the multipath environment undergoes performance degradations due to the presence of the lossy human body. The operation of the three antennas depends upon the factors discussed in the previous section including clear view of the sky, shielding body mass and antenna placement.

The human body presence causes a minimum drop of 3% in the GPS antenna's η_c and 1.5 dB in MEG_{GPS}. The three antennas perform reasonably well in the placed at pocket

(a) 3-D simulated gain patterns of PIFA at pocket position

(b) 3-D simulated gain patterns of DRA at pocket position

(c) 3-D simulated gain patterns of helix at pocket position
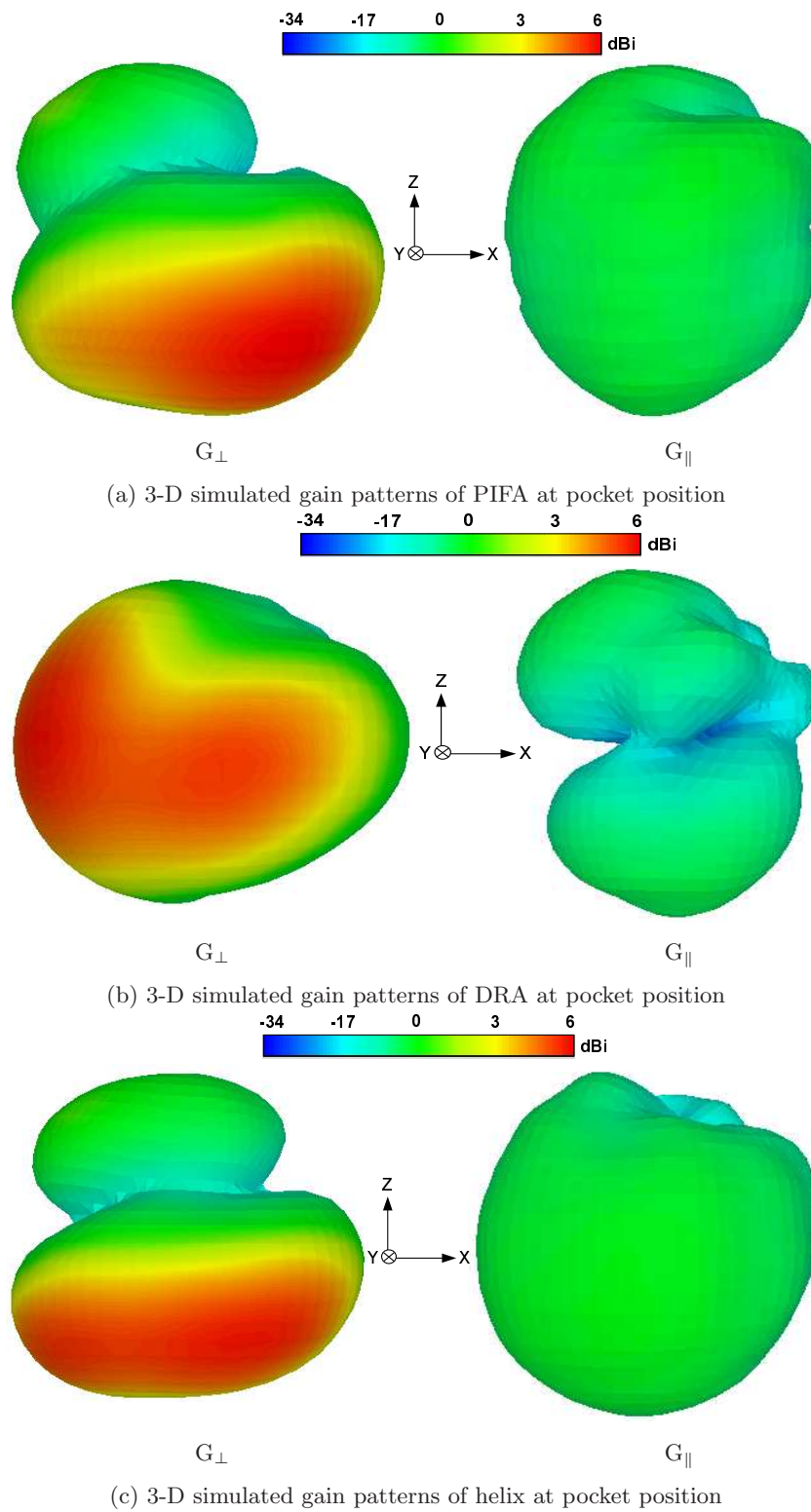
Figure 5.38: Simulated 3-D gain patterns for perpendicular and parallel polarisations of PIFA, DRA and helix GPS mobile terminal antennas placed at user's pocket position to evaluate effects of body presence on performance of the GPS antennas

(a) 3-D simulated gain patterns of PIFA in watching position

(b) 3-D simulated gain patterns of DRA in watching position

(c) 3-D simulated gain patterns of helix in watching position
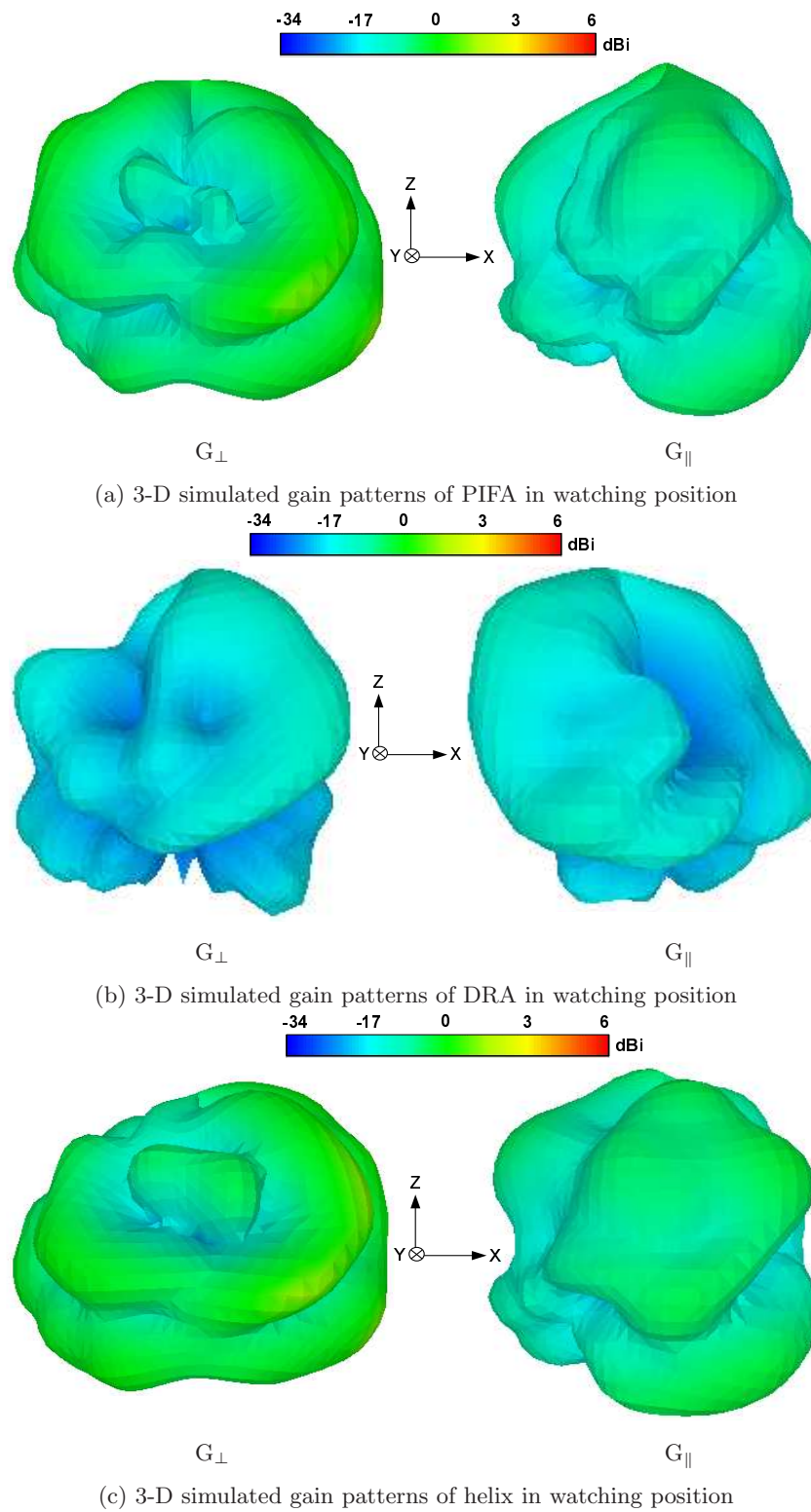
Figure 5.39: Simulated 3-D gain patterns for perpendicular and parallel polarisations of PIFA, DRA and helix GPS mobile terminal antennas held in user's hand at watching position to evaluate effects of body presence on the GPS antennas' operation
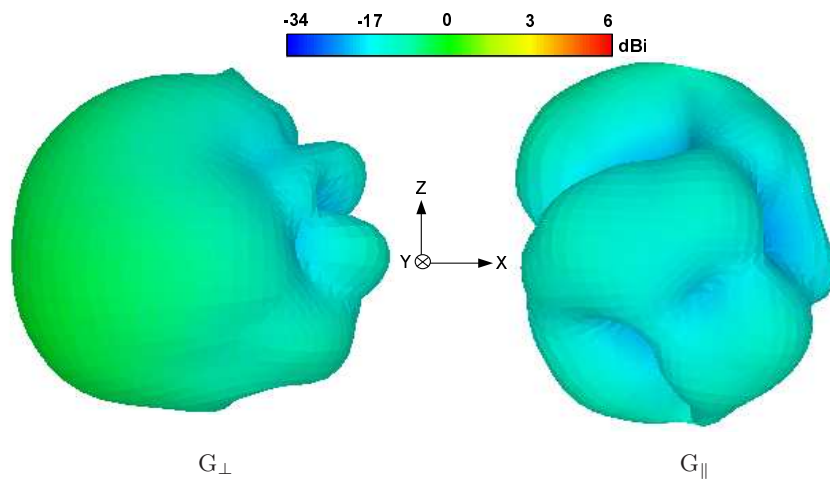
(a) 3-D simulated gain patterns of PIFA in talking position
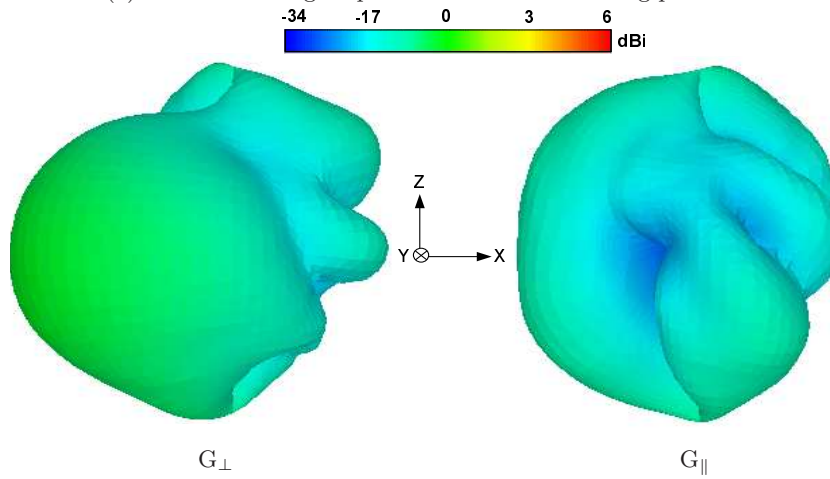
(b) 3-D simulated gain patterns of DRA in talking position
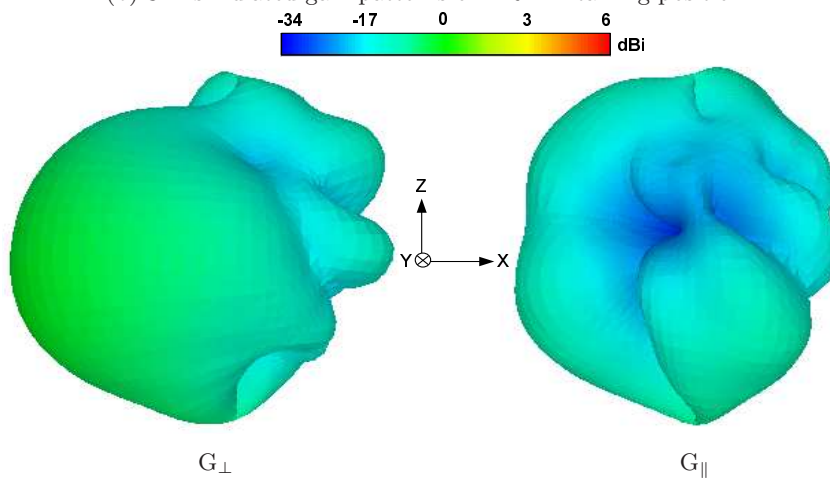
(c) 3-D simulated gain patterns of helix in talking position

Figure 5.40: Simulated 3-D gain patterns for perpendicular and parallel polarisations of PIFA, DRA and helix GPS mobile terminal antennas held in user's hand beside head in talking position for the GPS antenna performance evaluation near human body

Table 5-5: Calculated GPS Coverage Efficiency and GPS Mean Effective Gain of three mobile terminal GPS antennas working in the vicinity of human body in multipath environment with effects of whole human body presence

Test Set-up in Presence of Complete Human Body	Model Calculations Using Simulated 3-D Patterns in Actual Reflection Multipath Environment					
	PIFA		DRA		Helix	
	η_c	MEG_{GPS}	η_c	MEG_{GPS}	η_c	MEG_{GPS}
	(%)	(dB)	(%)	(dB)	(%)	(dB)
Antenna without human body presence	92	-8.2	95	-5.7	88	-5.8
Antenna placed at pocket position	52	-10.7	58	-7.2	53	-7.3
Antenna held in watching position	69	-13.2	3	-24.8	85	-8.0
Antenna held in talking position	34	-17.5	17	-18.5	20	-13.8

position. A greater clear view of the sky and enhanced gain levels in directions away from the body, owed to reflections from the surface of the body, constitute to minimise the degradations caused by the presence of the human body. The DRA antenna has shown best performance because of stronger radiation in upper hemisphere with η_c of 58% and MEG_{GPS} of -7.2 dB. In the watching position, larger gap between the torso and the antenna has lessened the tissue losses. The presence of the holding hand has proved the major source of degradation in this case. The PIFA and helix have exhibited an improved η_c of 69% and 85%, respectively, as a combined result of less shielded radiating element and increased gain in the upper hemisphere because of the reflections from the palm and arm. However, this increased coverage is made less effective by a reduced MEG_{GPS} of -13.2 dB and -8.0 dB, respectively, due to pattern deformations. On the other hand, the performance of the DRA has suffered greatly since, the radiating element is blocked to a larger extent by the palm and gripping fingers of the holding hand. It has reduced its η_c to just 3% and MEG_{GPS} to -24.8 dB.

The three antennas have again exhibited a poor performance in the talking position.

C1: Antenna without human body presence   C3: Antenna in watching position
C2: Antenna placed at pocket   C4: Antenna in talking position

(a) Coverage efficiency of GPS antennas

C1: Antenna without human body presence   C3: Antenna in watching position
C2: Antenna placed at pocket   C4: Antenna in talking position
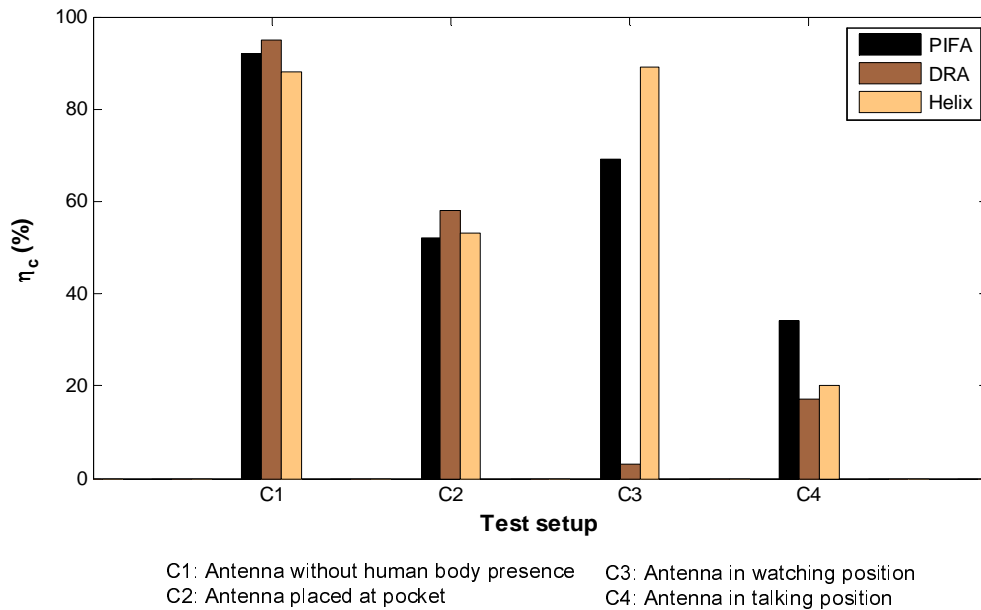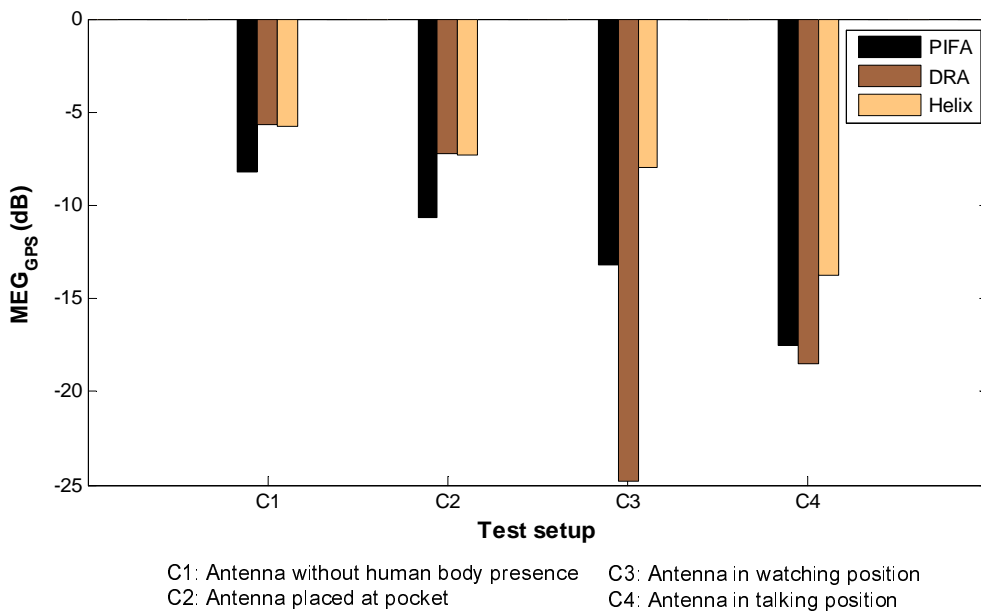
(b) MEG of GPS antennas

Figure 5.41: Multipath environment performance of GPS mobile terminal antennas in free space and in different on-body scenarios with effects of complete human body presence

The electromagnetic shielding by the lossy head and hand tissues on both sides has limited the reception of the signal from all directions. The η_c values are observed to be 34%, 17% and 20% for the PIFA, DRA and helix antenna, respectively. The MEG_{GPS}

is noted to be -17.5 dB, -18.5 dB and -13.8 dB for the three antennas, respectively. The ranking of the antenna performance is similar as observed in the previous section (in the presence of both the head and hand) whereas added losses have been introduced mainly by the shoulder and arm.

Overall, the helix has shown better capability to operate in the vicinity of the human body in the three tested scenarios, exhibiting reasonable level of MEG_{GPS} and η_c with lesser detuning in comparison to the PIFA and DRA. Therefore, it could be deduced that size and position of the radiating element also plays an important role to reduce the losses introduced by the human body tissues.

5.3 Summary

The demand of portable WPAN/WBAN devices with built-in navigation services has been rapidly increasing. The GPS receiving antennas have therefore been an essential part of such applications which necessitates the study of the function and behaviour of these antennas in the presence of the human body with very lossy tissues to realise the true extent of the performance degradation caused in actual working scenarios.

An investigative study on the performance of the GPS antennas operating near the human body has been presented in this chapter. The performance of a CP truncated corner microstrip patch antenna for the GPS operation in the vicinity of the human body has been studied using a low resolution human body model. The antenna performance is characterised in terms of S11 and radiation patterns, considering different on body scenarios including varying separation between the GPS antenna and the body, various on-body positions of the antenna and different held-in-hand situations.

The presence of the human body causes resonance shift, drop in antenna efficiency and radiation pattern deformations. It is observed that increasing separations between the body and the antenna, tends to reduce the detuning, improve the efficiency and

reduce the pattern deformations. Reduced amount of reflected (from the body) fields and shielding provided by the larger ground plane of the antenna dictates this behaviour. The shape of the lossy tissues and body mass present also affects the antenna performance. For example, the antenna placed at waist near belly has experienced greater degradations compared to the chest positions because of scattering caused by discontinuous edges towards legs and arms. Moreover, the deformation effects on the radiation performance of the antenna are more significant in YZ plane (body height) than XY plane (body width) due to the presence of greater body mass resulting in stronger reflecting fields.

A medium resolution human body model with realistic head and hand has been designed and employed to study the effects of the presence of the human body in the multipath environment on the operation of the GPS mobile terminal antennas. The antenna working is analysed first for only the human hand and head effects and then for the whole body presence in various practical scenarios. The proposed statistical model replicating the multipath environment with defined parameters of MEG_{GPS}, AoA_{GPS} and η_c is used to characterise the GPS mobile terminal antenna performances.

It has been noted that the presence of the human body lowers the operation of the GPS mobile terminal antennas due to the radiation pattern deformations. It limits the antenna coverage which influences less reception of the incoming GPS signal in the useful AoA_{GPS}. This pattern deformation also causes a decreased MEG_{GPS}. It is also noted that clear view of the sky observed by the antenna radiating element is necessary for a better η_c. A minimum loss of 3% in the GPS mobile terminal antenna coverage and 1.5 dB in its MEG_{GPS} is observed caused by the human operator. The reflections from and absorptions in the head and hand tissues on either side of the antenna in talking position forced the antennas to exhibit worst performance due to very limited coverage and poor radiation levels. It is therefore, concluded that in talking position, the size of the radiating element has a crucial role in the GPS mobile terminal antenna performance.

The presented results confirm that the multipath environment performance of the GPS mobile terminal antennas in the vicinity of the human user strongly depends on the

type of the antenna used, position of the antenna on-body and the human body posture. MEG_{GPS} provides a good figure of merit for the antenna performance as it describes the effects of polarisation state and directional response of the antenna while incorporating the impedance mismatch and total efficiency. Also, in such studies, acceptable results can be obtained using a single layer homogeneous model of the human body as maximum loss caused by the inner head organs with multi-layer inhomogeneous model is in the range of 2-3% for η_c and 0.1-0.3 dB for MEG_{GPS}.

References

[1] M. A. Jensen and Y. Rahmat-Samii, "EM interaction of handset antennas and human in personal communications," *IEEE Transactions on Antennas and Propagation*, vol. 83, no. 1, pp. 7–17, January 1995.

[2] J. Toftgard, S. Hornsleth, and J. B. Anderson, "Effects on portable antennas of the presence of a person," *IEEE Transactions on Antennas and Propagation*, vol. 41, no. 6, pp. 739–746, June 1993.

[3] M. Okoniewski and M. A. Stuchly, "A study of the handset antenna and human body interaction," *IEEE Transactions on Microwave Theory and Techniques*, vol. 44, no. 10, pp. 1855–1864, October 1996.

[4] P. A. Mason, W. D. Hurt, T. J. Walters, J. A. D'Andrea, P. Gajsek, K. L. Ryan, D. A. Nelson, K. I. Smith, and J. M. Ziriax, "Effects of frequency, permittivity and voxel size on predicted specific absorption rate values in biological tissue during electromagnetic field exposure," *IEEE Transactions on Microwave Theory and Techniques*, vol. 48, no. 11, pp. 2050–2058, November 2000.

[5] P. S. Hall and Y. Hao, "Antennas and propagation for body-centric wireless networks," *Artech House Publishers, (UK)*, 2006.

[6] J. Wang and O. Fujiwara, "EM interaction between a 5GHz band antenna mounted PC and a realistic human body model," *IEICE Transactions on Communications*, vol. E88-B, no. 6, pp. 2604–260, 2005.

[7] G. A. Conway and W. G. Scanlon, "Antennas for over-body-surface communication at 2.45ghz," *IEEE Transactions on Antennas and Propagation*, vol. 57, no. 4, pp. 844–855, April 2009.

[8] M. Sanad, "Effect of the human body on microstrip antennas," *IEEE Antennas and Propagation Society International Symposium (AP-S)*, vol. 1, pp. 298–301, June 1994.

[9] H. R. Chuang, "Human operator coupling effects on radiation characteristics of a portable communication dipole antenna," *IEEE Transactions on Antennas and Propagation*, vol. 42, no. 4, pp. 556–560, April 1994.

[10] J. S. Colburn and Y. Rahmat-Samii, "Human proximity effects on circular polarized handset antennas in personal satellite communications," *IEEE Transactions on Antennas and Propagation*, vol. 46, no. 6, pp. 813–820, Junuary 1998.

[11] "Considerations for the evaluation of human exposure to electromagnetic fields (EMFs) from mobile telecommunication equipment (MTE) in the frequency range from 30MHz-6GHz," *CENELEC, European Specification, Ref. No. ES-59005:1998 E*, 1998.

[12] L. Boccia, G. Amendola, and G. Di Massa, "Design of high precision antennas for GPS," *Penton Media, Inc.*, 2004.

[13] N. Padros, J. I. Ortigosa, J. Baker, M. F. Iskander, and B. Thornberg, "Comparative study of high-performance GPS receiving antenna designs," *IEEE Transactions on Antennas and Propagation*, vol. 45, no. 4, pp. 698–706, April 1997.

[14] R. B. Langley, "A primer on GPS antennas," *GPS World*, pp. 50–55, July 1998.

[15] C. Gabriel, "Compilation of the dielectric properties of body tissues at RF and microwave frequencies," *Brooks Air Force Technical Report, AL/OE-TR-1996-0037*, 1996.

[16] "Body tissue dielectric properties," *Federal Communication Commision (FCC), URL: http://www.fcc.gov/oet/rfsafety/dielectric.html.*

[17] "Caculation of the dielectric properties of body tissues," *Institute of Applied Physics, Italian National Research Council, URL:http://niremf.ifac.cnr.it/tissprop.*

[18] J. O. Nielsen and G. F. Pedersen, "Mobile handset performance evaluation using radiation pattern measurements," *IEEE Transactions on Antennas and Propagation*, vol. 54, no. 7, pp. 2154–2165, July 2006.

[19] J. Krogerus, C. Ichelun, and P. Vainikainen, "Dependence of mean effective gain of mobile terminal antennas on side of head," *European Conference on Wireless Technology (ECWT)*, pp. 467–470, October 2005.

[20] M. G. Douglas, M. Okoniewski, and M. A. Stuchly, "A planar diversity antenna for handheld PCS devices," *IEEE Transactions on Vehicular Technology*, vol. 47, no. 3, pp. 747–754, August 1998.

[21] K. Fujimoto and J. R. James, "Mobile antenna systems handbook (2nd edition)," *Artech House, Inc., (USA)*, 2001.

[22] G. F. Pedersen and J. B. Andersen, "Handset antennas for mobile communications: Integration, diversity, and performance," *Radio Science Review 19961999, Oxford University Press, UK*, 1999.

[23] K. Ogawa and T. Uwanao, "Mean effective gain analysis of a diversity antenna for portable telephones in mobile communication environments," *Electronics and Communication in Japan (Part I: Communications)*, vol. 83, no. 3, pp. 88–96, December 2000.

[24] *CST Microwave Studio*® *2010 User Manual*.

[25] C. Balanis, "Antenna theory analysis and design (2nd edition)," *John Wiley and Sons, Inc., (USA)*, 1997.

[26] J. Jemai, T. Kurner, A. Varone, and J. F. Wagen, "Determination of the permittivity of building materials through WLAN measurements at 2.4GHz," *IEEE International Symposium on Personal, Indoor and Mobile Radio Communications*, September 2005.

[27] G. Klysza, J. P. Balayssaca, and X. Ferriresb, "Evaluation of dielectric properties of concrete by a numerical FDTD model of a GPR coupled antennaparametric study," *NDT & E International*, vol. 41, no. 8, pp. 621–631, December 2008.

Chapter 6

Conclusions and Future Work

6.1 Summary

The evolution of user-centric communications systems based on the concept of being connected anytime and anywhere has brought a revolution in the field of wireless communications. This rapid growth of research and development has been promoted by the development of portable devices that provides multiple features in a small package guaranteeing mobility and ease of use. These devices have to operate in the vicinity of human users in cluttered environments.

The review of the open literature on studies regarding the operation of WPAN/WBAN antennas has ascertained that a degraded performance in on-body communication links is often associated to such antennas. The multipath arrival of the electromagnetic waves due to the presence of the reflectors and scatterers in the vicinity further reduces the antenna performance. It proved a need for a deeper insight into the physical mechanism involved in the on-body radio transmission and effective analysis of the multipath environment effects using statistical models. The main investigations and analyses presented in this thesis based on the reviewing process and background studies, are summarised as follows.

The on-body Bluetooth link between a mobile handset and Bluetooth headset has been analysed to study the physics behind the on-body transmission mechanism. The comparison of high, medium and low resolution human body models has indicated that in such studies, a low resolution human body model gives precise results with efficient computations. The human body presence has caused a loss of 10-15 dB in the Bluetooth path gain attributed to the blocking of line-of-sight between handset and headset antennas. The study has demonstrated that surface waves play an important role in the on-body Bluetooth transmission channel. The dependance of this on-body channel on the handset antenna orientation, handset antenna and human body separation and presence of the surface wave's blocking objects has also been analysed. A vertically oriented handset antenna has shown much stronger link due to excitation of stronger surface waves as compared to the horizontal orientation. Increasing separations of the handset antenna from the human body weakens the on-body Bluetooth link because of the reduction in the surface wave excitation. Blockage of the surface waves by the objects located nearer than half wavelength also results in severe degradation of the on-body link.

A statistical model has been presented with a novel GPS Angle of Arrival (AoA_{GPS}) distribution of the incident radio waves and a new concept of the GPS Mean Effective Gain (MEG_{GPS}) and GPS Coverage Efficiency (η_c). It has been demonstrated that the proposed model efficiently predicts and precisely ranks the GPS antenna performance with close agreement to open field measurements.

Characterisation of the GPS antenna performance in the multipath environment in terms of MEG_{GPS} and η_c has shown that these parameters depend strongly on AoA_{GPS} and antenna power gain patterns. The change in the antenna orientation with respect to the ground (earth) plays an important role in the navigation solution as it varies antenna gain patterns and inflicts η_c deviations. The horizontal orientation of the GPS antenna has appeared to be more efficient in the majority of the tested cases exhibiting high η_c due to greater clear sky view. Similarly, increased reception of the GPS signal

due to higher gain values, especially in the incident region, give rise to MEG_{GPS} for majority of the horizontally oriented antennas. Varying the position of the antenna radiating element on the PCB/ground plane has shown no significant improvement in MEG_{GPS} and η_c values as overall change in antenna radiation pattern is minimal. The dual-element mono-loop antenna has increased MEG_{GPS} by 1.4 dB and η_c by 23% as compared to the single-element antenna indicating that the diversity antennas could be used effectively to reduce the degrading effects of the multipath environment.

The dependence of truncated corner microstrip patch GPS antennas on the separation between the antenna and the human body, on-body position of the antenna and held-in-hand scenarios was investigated using numerical analysis. The study has shown that degradations in antenna input impedance, efficiency and radiation pattern depends upon the gap between the antenna and the body, physiological structure of the body and amount of present body mass. These effects are more stronger in YZ plane (height of the body) as compared to XY plane (width of the body) as the presence of greater body mass resulted in stronger reflecting fields. Increased separations has lessened these losses. The antenna placed at waist near belly has experienced more detuning as compared to the chest positions because of larger change in tissue shape giving rise to reflected fields.

The true extent of the performance degradation a WPAN/WBAN antenna faces in actual working scenarios has been realised by including the human body effects in the multipath model. The study has demonstrated that the operation of GPS mobile terminal antennas depends on the type of the antenna used, position of the antenna on-body and the human body posture. MEG_{GPS} is considered as a figure of merit due to its essential benefits of describing antenna performance taking into account effects of impedance mismatch, total efficiency, polarisation state and directional response of the radio environment. The radiation pattern deformations caused by the human operator has limited the antenna coverage influencing less reception of the incoming GPS signal in the useful AoA_{GPS}. In turn, MEG_{GPS} of the antenna also decreased. The presence of the human body has lowered the GPS antenna operation with a minimum loss of 3%

in η_c and 1.5 dB in MEG_{GPS}. The antenna held by the user in talking position has exhibited worst performance due to reflections from and absorptions in the head and hand tissues on either side of the antenna and restricted sky view resulted in a very limited coverage and poor radiation levels. A maximum loss caused by the inner head organs with multi-layer inhomogeneous model has been noted to be in the range of 1-3% for η_c and 0.1-0.3 dB for MEG_{GPS} showing that acceptable results could be obtained using a single layer homogeneous model of the human body in such studies.

6.2 Key Contributions

The major contributions in this thesis are detailed as follows:

- Establishing the role of the surface waves in the on-body Bluetooth link between two body-worn antennas. Antenna placements that excite stronger surface waves have developed stronger on-body channels. Based on the investigations carried out, the surface waves need an un-blocked space of at least half wavelength away from the human body to contribute efficiently in the on-body Bluetooth communication.

- A novel statistical model for the GPS multipath environment with parameters of GPS Angle of Arrival distribution, GPS Mean Effective Gain and GPS Coverage Efficiency. This model is an efficient tool for the analysis of the GPS mobile terminal antenna performance in the actual working scenarios eliminating the need of an open field measurement test.

- Identifying the dependence of the GPS mobile terminal antenna performance in the multipath environment not only on the orientation of the antenna with respect to the ground but also on the location of the radiating element on the chassis. Antenna MEG_{GPS} and η_c vary with change in the orientation due to varying radiation pattern and extent of clear sky view.

- Demonstrating the use of diversity antennas to enhance the performance of the

mobile terminal GPS antennas in the multipath environment. The potential of the diversity antennas has been shown achieving 40% increase in MEG_{GPS} and 23% in η_c employing a dual-element mono-loop antenna.

- Characterisation of human body effects on the performance of the GPS mobile terminal antennas operating in the multipath environment. The antenna operation depends on the type of the antenna used, position of the antenna on-body and the human body posture and clear sky view of the antenna. Identifying acceptability of the use of single layer homogeneous body model in such studies due to their precision and efficient computations.

6.3 Future Work

The WPAN/WBAN are experiencing greater advancements both in terms of research and development. The work presented in this thesis covers a small but important part of this area. In the light of the drawn conclusions and limitations of the accomplished work, further research could be carried out in the following aspects:

Numerical Modelling of Human Body

- A medium resolution efficient human body model with more realistic shape of the torso could be developed to further investigate the effects of varying shapes of body parts on the Bluetooth on-body transmission mechanism and performance of the on-body GPS antennas.

On-body Bluetooth Transmission Mechanism

- The on-body Bluetooth transmission mechanism has been studied for a single type of handset and headset antenna. The study could be expanded including other types of commercially used antennas. Different placements of the handset antenna on-body for example at back pocket or chest pocket position could be investigated.

Placement of the headset antenna at the other side of the head is also a factor that could be studied. Role of surface waves in the on-body link for different human body postures would also provide useful information.

Statistical Modelling of Multipath GPS Environment

- The proposed statistical model for the GPS multipath environment takes the GPS Angle of Arrival distribution as uniform in both the azimuth and elevation. A more realistic GPS Angle of Arrival distribution for elevation plane should be applied to suit the actual scenarios attained by the measurements. The Gaussian and elliptical distributions could be the potential contenders describing higher probability of arrival of the GPS signal near the zenith and lower near the horizon.

- Extending the proposed environment model to include effects of ground roughness and varying electric properties (permittivity and conductivity) of ground (earth) would also be of interest.

- More efficient diversity antennas with reduced level of mutual coupling should be designed to achieve increased performance in the multipath environment

Human Body Presence and GPS Antennas in Multipath Environment

- The presented investigations for human body effects on the GPS antennas in the multipath environment are based on simulation set-ups. Results based on open field and anechoic chamber measurements would be helpful to enhance the level of confidence in the presented data.

- It has been demonstrated in the thesis that the use of diversity antennas could enhance the operation of the GPS antennas in the multipath environment. New designs of the GPS mobile terminal antennas based on diversity techniques could also be explored. These designs could offer performance increase in the antenna stand alone operation as well as withstand the degrading effects of the human body presence.

Appendix A

Numerical Modelling Techniques

Numerical techniques calculate the solution to a problem based on a full-wave analysis. A number of numerical algorithms in the time and frequency domains have been widely used to solve electromagnetic problems, with each technique suitable for the analysis of a particular type of problem. In this thesis, time-domain methods are preferred over others due to their stability and strength in modelling complex inhomogeneous dispersive media [1].

A.1 Finite Difference Time Domain (FDTD)

Finite-Difference Time-Domain (FDTD) is a popular electromagnetic modelling technique. The basis of this method has been introduced in 1966 by K.S. Yee who introduced the FDTD method for solving Maxwell's equations in a discretised form [2]. Maxwell's equations are simply modified to central-difference equations, discretised, and implemented in software. The equations are solved in a leapfrog manner; i.e., the electric field is solved at a given instant in time, then the magnetic field is solved at the next instant in time and the process is repeated over and over again [3, 4].

Maxwell's curl equations can be expanded in their Cartesian vector component form
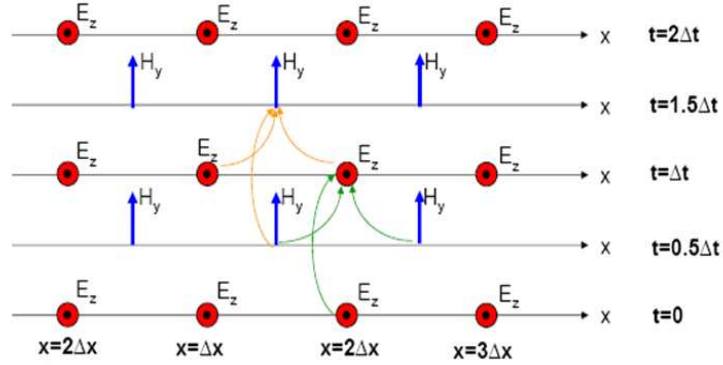
Figure A.1: Leapfrog scheme in space and time for FDTD [4]

for the general 3-D case as:

$$\frac{\partial H_x}{\partial t} = \frac{1}{\mu} \left(\frac{\partial E_y}{\partial z} - \frac{\partial E_z}{\partial y} - \sigma_m H_x \right) \tag{A.1}$$

$$\frac{\partial H_y}{\partial t} = \frac{1}{\mu} \left(\frac{\partial E_z}{\partial x} - \sigma_m H_y \right) \tag{A.2}$$

$$\frac{\partial H_z}{\partial t} = \frac{1}{\mu} \left(\frac{\partial E_x}{\partial y} - \frac{\partial E_y}{\partial x} - \sigma_m H_z \right) \tag{A.3}$$

$$\frac{\partial E_x}{\partial t} = \frac{1}{\varepsilon} \left(\frac{\partial H_z}{\partial y} - \sigma_e E_x \right) \tag{A.4}$$

$$\frac{\partial E_v}{\partial t} = \frac{1}{\varepsilon} \left(-\frac{\partial H_z}{\partial x} - \sigma_e E_y \right) \tag{A.5}$$

$$\frac{\partial E_z}{\partial t} = \frac{1}{\varepsilon} \left(\frac{\partial H_y}{\partial x} - \frac{\partial H_x}{\partial y} - \sigma_e E_z \right) \tag{A.6}$$

These six equations form the basis of the FDTD algorithm.

A.1.1 FDTD Method

This method uses a leapfrog scheme on staggered Cartesian grids where the electric field (E) is offset spatially and temporally from the magnetic field (H). This approach solves the "present" fields throughout the computational domain in terms of the past fields.
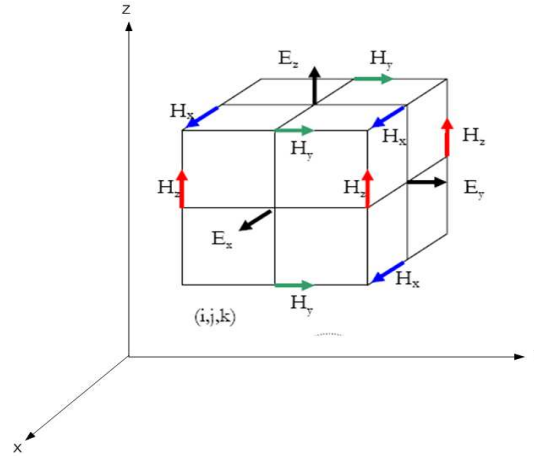
Figure A.2: Yee cell representation for spatial discretisation [2]

FDTD uses simple central-difference approximations to evaluate the space and time derivatives. The region being modelled is represented by two interleaved grids of discrete points. One grid contains the points at which the magnetic field is evaluated. The second grid contains the points at which the electric field is evaluated. Figure A.2 presents a basic element of the FDTD space lattice, where a space lattice point (i, j, k) is denoted as:

$$(i, j, k) = (i\Delta x, j\Delta y, k\Delta z) \tag{A.7}$$

While any function of space and time is evaluated as:

$$F^n(i, j, k) = F(i\Delta x, j\Delta y, k\Delta z, n\Delta t) \tag{A.8}$$

The simplified vector form of Maxwell's curl equations can be represented in the FDTD equations for EM waves by using the central finite difference approximation of space and time derivatives. To incorporate the element of time, each of the E and H components are evaluated at alternate half time-steps using an explicit finite difference approximation and represented as the following equations:

$$H_x^{n+\frac{1}{2}}(i, j, k) = H_x^{n-\frac{1}{2}}(i, j, k) + \frac{\Delta t}{\mu_x(i, j, k)} \left[\frac{E_y^n(i, j, k+1) - E_y^n(i, j, k)}{\Delta z(k)} - \frac{E_z^n(i, j+1, k) - E_z^n(i, j, k)}{\Delta y(j)} \right] \tag{A.9}$$

$$H_y^{n+\frac{1}{2}}(i,j,k) = H_y^{n-\frac{1}{2}}(i,j,k) + \frac{\Delta t}{\mu_y(i,j,k)} \left[\frac{E_z^n(i+1,j,k) - E_z^n(i,j,k)}{\Delta x(i)} \right. $$
$$\left. - \frac{E_x^n(i,j,k+1) - E_x^n(i,j,k)}{\Delta z(k)} \right] \qquad \text{(A.10)}$$

$$H_z^{n+\frac{1}{2}}(i,j,k) = H_z^{n-\frac{1}{2}}(i,j,k + \frac{\Delta t}{\mu_z(i,j,k)} \left[\frac{E_x^n(i,j+1,k) - E_x^n(i,j,k)}{\Delta y(j)} \right. $$
$$\left. - \frac{E_y^n(i+1,j,k) - E_y^n(i,j,k)}{\Delta x(i)} \right] \qquad \text{(A.11)}$$

$$E_x^{n+1}(i,j,k) = \frac{\varepsilon_x(i,j,k) - 0.5\Delta t.\sigma_x(i,j,k)}{\varepsilon_x(i,j,k) + 0.5\Delta t.\sigma_x(i,j,k)} E_x^n(i,j,k) + \frac{\Delta t}{\varepsilon_x(i,j,k) + 0.5\Delta t.\sigma_x(i,j,k)}$$
$$\left[\frac{H_z^{n+\frac{1}{2}}(i,j+1,k) - H_z^{n+\frac{1}{2}}(i,j,k)}{\Delta y(j)} - \frac{H_y^{n+\frac{1}{2}}(i,j,k+1) - H_y^{n+\frac{1}{2}}(i,j,k)}{\Delta z(k)} \right]$$
$$\text{(A.12)}$$

$$E_y^{n+1}(i,j,k) = \frac{\varepsilon_y(i,j,k) - 0.5\Delta t.\sigma_y(i,j,k)}{\varepsilon_y(i,j,k) + 0.5\Delta t.\sigma_y(i,j,k)} E_y^n(i,j,k) + \frac{\Delta t}{\varepsilon_y(i,j,k) + 0.5\Delta t.\sigma_y(i,j,k)}$$
$$\left[\frac{H_x^{n+\frac{1}{2}}(i,j,k+1) - H_x^{n+\frac{1}{2}}(i,j,k)}{\Delta z(k)} - \frac{H_z^{n+\frac{1}{2}}(i+1,j,k) - H_z^{n+\frac{1}{2}}(i,j,k)}{\Delta x(i)} \right]$$
$$\text{(A.13)}$$

$$E_z^{n+1}(i,j,k) = \frac{\varepsilon_z(i,j,k) - 0.5\Delta t.\sigma_z(i,j,k)}{\varepsilon_z(i,j,k) + 0.5\Delta t.\sigma_z(i,j,k)} E_z^n(i,j,k) + \frac{\Delta t}{\varepsilon_z(i,j,k) + 0.5\Delta t.\sigma_z(i,j,k)}$$
$$\left[\frac{H_y^{n+\frac{1}{2}}(i+1,j,k) - H_y^{n+\frac{1}{2}}(i,j,k)}{\Delta x(i)} - \frac{H_x^{n+\frac{1}{2}}(i,j+1,k) - H_x^{n+\frac{1}{2}}(i,j,k)}{\Delta y(j)} \right]$$
$$\text{(A.14)}$$

In the above equations, the superscripts represent the time index and the arguments represent the spatial sampling location.

To use the FDTD, a computational domain must be established. It is the physical region over which the simulation will be performed. The E and H fields are determined

at every point in space within that computational domain. The material of each cell inside the domain should be specified. Typically, the material is either free-space (air), metal, or dielectric. Any material can be used if the permeability, permittivity, and conductivity are mentioned [5].

After the computational domain and the grid materials are determined, the next step is the specification of a source. The type of the source depends upon the application. It may be a plane wave, a current on a wire, or an applied electric field [3].

The simulation gives usually the E or H field at a point or a series of points within the computational domain because the fields are determined directly.

A.1.2 Far-field Computations Using FDTD

In the FDTD method, the fields are computed in the near field region around the cell. In antenna modelling, it is desired to determine the far-field pattern. The near-field data can be transformed to obtain the far-field pattern by weighting it with the free space Green's function and integrating over a surface, S, surrounding the cell [5].

A.1.3 Numerical Error and Stability

Free space is dispersion-less medium as a wave propagating in the free space, propagates at the same phase velocity regardless of the direction of the propagation. However, phase velocity of the propagating wave is distorted and waves propagating in a discrete domain e.g. FDTD grid, suffer from numerical dispersion as a result of the discretisation. Numerical dispersion is a function of the number of cells used per wavelength and the direction of the wave propagation across the spatial grid. The variation of the phase velocity with wave-propagation angle tends to improve significantly when the number of cells used per-wavelength is increased.

Numerical stability is defined as a bounded input produces a bounded output, as

the iteration time progresses. For the Yee algorithm to produce a convergent result, its numerical stability must be ensured. One of the convergence factors is the Courant stability criterion that assumes that for stability to be maintained, the field must not change significantly from one point to another and a wave must not propagate more than one spatial field point in any one iteration of the algorithm This can be achieved by putting an upper limit on the time step that is used in the update equations [6].

In order to guarantee the numerical stability and to avoid the algorithm to be numerically instable, the time increment Δt should be bound relative to the lattice space increments Δx, Δy and Δz. Hence, the maximum allowable time step for the smallest cell size is expressed as:

$$\Delta t \leq \frac{1}{c\sqrt{\left(\frac{1}{\Delta x}\right)^2 + \left(\frac{1}{\Delta y}\right)^2 + \left(\frac{1}{\Delta z}\right)^2}} \tag{A.15}$$

Where c represents the speed of light. For an equilateral cubic volume cell this above stability criterion could be simplified to:

$$\Delta t \leq \frac{\Delta}{c\sqrt{3}} \tag{A.16}$$

Where, $\Delta = \Delta x = \Delta y = \Delta z$

For antenna analysis using the FDTD technique, several assumptions are made including that the electric or magnetic field must not change significantly from one field point to the next and the variation of the field between field points is linear. This imposes limits on the sizes of the cells that are used in the spatial domain so that the cells should not (normally) have a side length greater than $\lambda/10$.

A.1.4 Absorbing Boundary Conditions (ABCs)

To update the electric field strength in a cell in the FDTD grid, the central-difference discretised Maxwell's curl equations employed in FDTD needs the knowledge of the
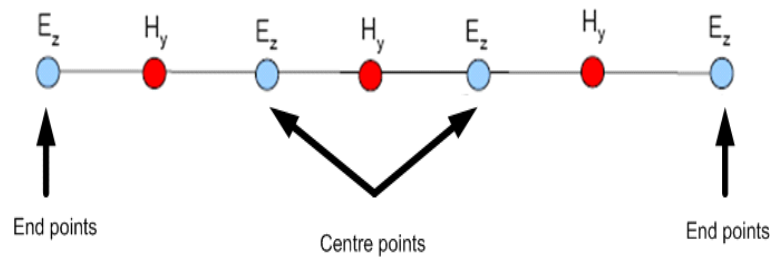
Figure A.3: Need of Absorbing Boundary Conditions in a FDTD grid

values of the locally neighbouring magnetic field points on either side of it.

Modelling an antenna using the FDTD in a finite volume of space makes it appear to a propagating wave that is continuous beyond the finite volume of the modelled space. Since, the field at inner cells of the grid can be modified easily but the field points at the edge of the spatial domain do not have all the necessary data to be updated. It makes the domain boundary vulnerable to non physical reflections of outgoing waves and special treatment is needed for the edge points to avoid these reflections. This special treatment is known as Absorbing Boundary Conditions (ABCs) that employs special update equations at the spatial grid boundaries to absorb outgoing waves. There have been many types of ABC developed over the time. The perfectly matched layer (PML) [7] has been known to be one of the most successful ABCs ever developed. The basic characteristic of the PML ABC is the splitting of the electric and magnetic fields in the absorbing boundary region to account for the individual losses to be assigned. This creates a non-physical absorbing medium that has its wave impedance independent of the frequency and angle of incident of the incoming wave [8]. The spatial domain is surrounded by layers of conducting material, several FDTD cells thick. These layers have a conductivity profile that increases with more penetration into the material to absorb any incoming wave. Reflection coefficients better than -100 dB can be achieved using the PML absorbing boundaries.

A.1.5   Advantages of FDTD

The FDTD method is the most direct possible solution of Maxwell's equations. It is complete and "full wave" i.e., there are no approximations that prevent a correct solution from being reached. Boundary conditions are automatically satisfied. Furthermore, it is easy to understand and easy to implement in software. Also, as it is a time-domain technique, it can cover a wide frequency range with a single simulation run [9].

A.2   Finite Integration Technique (FIT)

The Finite Integration Technique (FIT) is a time-domain numerical method for solving the integral forms of Maxwell's equations. It is a consistent formulation for the discrete representation of Maxwell's equations on numerical grids and was introduced in 1977 by Weiland [10]. It solves the electromagnetic problems in a manner equivalent to the FDTD method.

The matrix equations for the electromagnetic integral quantities obtained by FIT possess the inherent properties of Maxwell's equations with respect to charge and energy conservation and thus ensure an especially favourable stability and convergence behaviour in the numerical implementation. One of the great advantage of this formulation in comparison with other methods is that it represents a comprehensive theory which can be successfully used within the whole spectrum of electromagnetic applications [10, 11].

In FIT, for a three-dimensional problem, the volume is approximated by the tetrahedral cells and special set of basis functions. Definition of volume sizes of the discretisation of the computational domain is typically balanced between achieving numerical stability (e.g. ten lines per wavelengths) and the computation cost in terms of the memory and time [9].

New techniques such as non-orthogonal gridding, variable meshing and sub-gridding

have been introduced to the FIT to increase the flexibility of controlling the cell gridding/meshing in the problems. Errors which might exist due to stair-case approximations can be reduced by either creating denser mesh cells, or by introducing a scheme where only part of the cell is considered called Partial Cell Filling. The capability to take into account the sub-cellular information makes FIT an algorithm with second order accuracy for arbitrary shaped problems.

A.2.1 Advantages of FIT

A principal advantage of the FIT method is that the fields can be interpolated accurately inside a cell of almost arbitrary shape, eliminating the need for tight control on the cell shapes. This should also provide increased accuracy on irregular or non-uniform grids. Also, more accurate solutions are obtained due to enhanced meshing techniques. Furthermore, this method can solve problems associated to the whole spectrum of electromagnetic applications.

A.3 CST Microwave Studio$^{\textregistered}$

CST Microwave Studio$^{\textregistered}$ is a specialist tool for the fast and accurate 3-D electromagnetic simulation of high frequency problems using the Finite Integration Technique (FIT). It is designed for the accurate calculation of S-parameters and antenna parameters on a computer in a Windows based environment [12].

A.3.1 Features of CST Microwave Studio$^{\textregistered}$

CST Microwave Studio$^{\textregistered}$ simplifies the process of inputting the structure by providing a powerful solid modelling interface. Strong graphics feedback simplifies the definition of the device even further. After the component has been modelled, a fully automatic meshing procedure is applied before the simulation engine is started [12].

Since no method works equally well in all application domains, the software contains four different simulation techniques (transient solver, frequency domain solver, eigenmode solver, modal analysis solver) that best fit different particular applications.

The most flexible tool is the *transient solver*, normally used for on-body antenna simulations, which can obtain the entire broadband frequency behaviour of the simulated device from only one calculation run. This solver is very efficient for most kinds of high frequency applications such as connectors, transmission lines and antennas [12].

References

[1] P. Shubitidze, R. Jobava, B. R., I. Shamatava, R. Zaridze, and K. D., "Application of FDTD to dispersive media," *International Seminar/Workshop on Direct and Inverse Problems of Electromagnetic and Acoustic Wave Theory (DIPED)*, pp. 112–116, 1999.

[2] K. Yee, "Numerical solution of initial boundary value problems involving Maxwell's equations in isotropic media," *IEEE Transactions on Antennas and Propagation*, vol. 14, no. 3, pp. 302–307, May 1966.

[3] T. Hubing, "Survey of numerical electromagnetic modeling techniques," *University of Missouri-Rolla*, September 1991, *URL:http://www.emclab.umr.edu/pdf/TR91-1-001.pdf*.

[4] K. Heater, "The FDTD method: Computation and analysis," *MSc. Research*, May 2005, *URL:http://www.nmr.mgh.harvard.edu/adunn/papers/dissertation/node36.html*.

[5] A. Dunn, "FDTD method," *Chapter of Dissertation*, 1998, *URL:http://web.math.umt.edu/bardsley/students/KiraHeater/ProfPaper.pdf*.

[6] K. L. Shlager and J. B. Schneider, "A selective survey of the finite-difference time-domain literature," *IEEE Antennas and Propagation Magazine*, vol. 37, no. 4, pp. 39–57, August 1995.

[7] J. Berenger, "A perfectly matched layer for the absorption of electromagnetic waves," *Journal of Computational Physics*, vol. 114, no. 2, pp. 185–200, October 1994.

[8] A. Taflove, "Computational electrodynamics - the finite-difference time-domain method," *Artech House Publishers, (UK)*, 1995.

[9] S. Rao and G. Gothard, "Recent techniques in electromagnetic modeling and analysis," *International Conference on Electromagnetic Interference and Compatibility*,

pp. 131–137, December 1995.

[10] T. Weiland, "A discretization model for the solution of Maxwell's equations for six-components fields," *Electronics and Communications AEU*, vol. 31, no. 3, pp. 116–120, March 1977.

[11] M. Dehler, M. Dohlus, A. Fischerauer, G. Fischerauer, P. Hahne, R. Klatt, T. Propper, P. Schutt, and T. Weiland, "Status and future of the 3D MAFIA group of codes," *IEEE Transactions on Magnetics*, vol. 26, no. 2, pp. 751–754, March 1990.

[12] *CST Microwave Studio$^{\textregistered}$ 2010 User Manual.*

Appendix B

Reflection Coefficients for Incident Wave Components

B.1 Reflection of the Oblique Incidence Incoming Wave from the Ground Plane

To analyse the oblique incidence of a plane wave on an interface between two different dielectric mediums, as shown in Figure B.1, it is convenient to consider the perpendicular and parallel polarised wave components separately.

We can divide the incoming plane wave in the perpendicular and parallel components as shown in Figures B.2- B.3. Hence, we can express the incident wave as:

$$E_{inc} = E_{inc_{\perp}} + E_{inc_{||}} \tag{B.1}$$

The reflection angle at each smooth reflection point is equal to the incident angle.
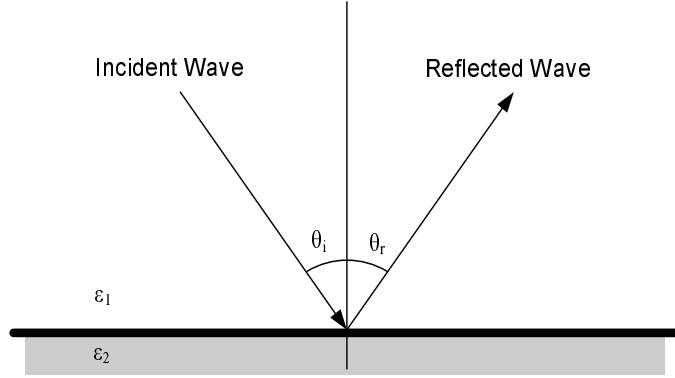
Figure B.1: Reflection of plane wave of oblique angles of incidence from the dielectric boundary
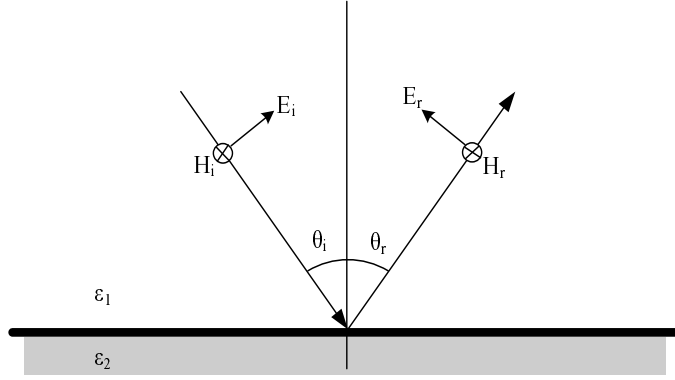

Figure B.2: Parallel polarised wave component

The reflection coefficients can be found as [1, 2]:

$$\Gamma_{\perp} = \frac{\cos\theta_i - \sqrt{(\varepsilon_2/\varepsilon_1) - \sin^2\theta_i}}{\cos\theta_i + \sqrt{(\varepsilon_2/\varepsilon_1) - \sin^2\theta_i}} \tag{B.2}$$

$$\Gamma_{\|} = \frac{(\varepsilon_2/\varepsilon_1)\cos\theta_i - \sqrt{(\varepsilon_2/\varepsilon_1) - \sin^2\theta_i}}{(\varepsilon_2/\varepsilon_1)\cos\theta_i + \sqrt{(\varepsilon_2/\varepsilon_1) - \sin^2\theta_i}} \tag{B.3}$$

Where, $\Gamma_{\perp}$ is the reflection coefficient for perpendicular polarised component and $\Gamma_{\|}$ is the reflection coefficient for parallel polarised component.

The reflected wave can also be separated in two components in the same fashion and expressed as:

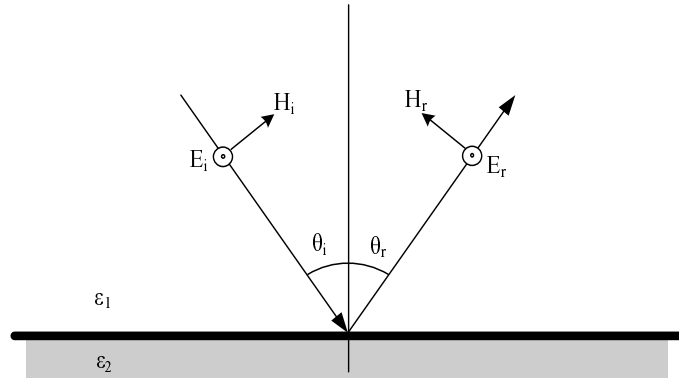$$E_{ref} = E_{ref_{\perp}} + E_{ref_{\|}} \tag{B.4}$$

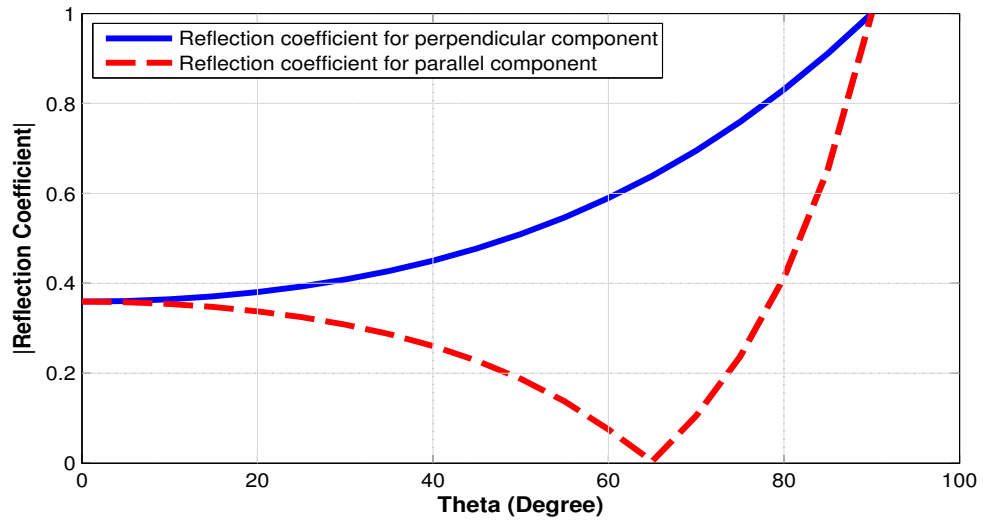Figure B.3: Perpendicular polarised wave component

Figure B.4: Graph between the incident angle and the reflection coefficients for perpendicular and parallel components

These two components can be computed by the following equations:

$$E_{ref_\perp} = \Gamma_\perp E_{inc_\perp} \tag{B.5}$$

$$E_{ref_{||}} = \Gamma_{||} E_{inc_{||}} \tag{B.6}$$

References

[1] D. K. Cheng, "Field and wave electromagnetics (2nd edition)," *Addison Wesley, Inc., (USA)*, 1989.

[2] U. Inan and A. Inan, "Electromagnetic waves," *Prentice-Hall, Inc., (USA)*, 1999.

Appendix C

GPS Gain Calculator

C.1 GUI based on Matlab Coding

The statistical model for the multipath operation of the GPS antenna has been implemented using MatLab. A graphical user interface (GUI) has also been developed to provide the ease of use. The main window of the GUI is illustrated in Figure C.1.

The working of this GUI is simple. Data files containing power gain data of the antenna is imported in .txt or .dat format using the "Import Data" button. The data can either be in dB or linear values. Name of the imported file will be displayed. Antenna efficiency can be selected from the drop down list with options of 100%, 75%, 50%, 25%, 2.5% and 1.25%. A number of coverage efficiency threshold levels are also available ranging from -6 dB to -25 dB under "CE Threshold" drop down list. The performance of the antenna in the multipath environment could be analysed by calculating Mean Effective Gain (MEG) and Coverage Efficiency (CE) by pressing the "Calculate" buttons.

The calculated values are compared with the values obtained from open field tests as well as values calculated using measured 3-D power gain patterns. The 3-D power gain patterns are measured in Satimo Stargate 64 anechoic chamber as shown in Figure C.2.
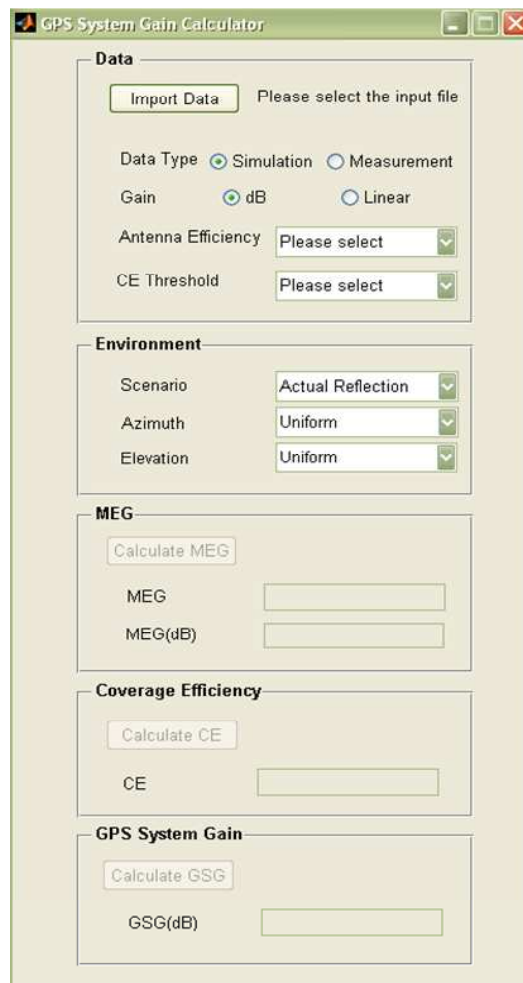
Figure C.1: GUI for the GPS System Gain calculator that implements the statistical model for GPS multipath environment
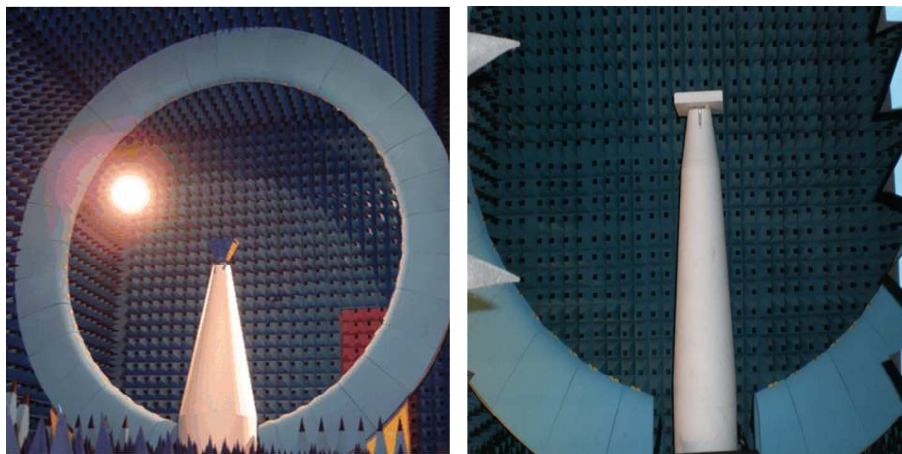

Figure C.2: Satimo Stargate 64 anechoic chamber used to measure 3-D power gain patterns of GPS antennas